UNIVERSITÀ DEGLI STUDI DI MESSINA

DIPARTIMENTO DI SCIENZE CHIMICHE, BIOLOGICHE, FARMACEUTICHE ED AMBIENTALI

DOTTORATO DI RICERCA IN SCIENZE CHIMICHE
XXIX CICLO

THE SUPRAMOLECULAR CHEMISTRY OF IONISABLE (OXA)CALIXARENES

Dott. Nadia Manganaro

Supervisor:
Prof. Giuseppe Gattuso

2014-2016

Index

Synopsis

My PhD studies have been focused on the synthesis and development of new supramolecular systems whose applications range from host molecules towards neutral and charged guest molecules, and building blocks for the construction of supramolecular polymers.

The first system that hereby describes is the tetraammonium-oxacalix[4]arene **66**·4HCl. This macrocycle, the first water-soluble member of its class, acts as 'molecular tweezers': despite being positively charged, when in the right protonation state it is able to overcome unfavourable repulsive effects and recognize and bind the dicationic guest, methyl viologen, in water.[1] Binding takes place in the π-rich cleft generated by the two facing resorcinol rings, despite the electrostatic repulsion between the positive charges on the macrocycle and those on the guest. In-depth NMR, UV-Vis and DFT studies allowed us to measure the four protonation constants of **66** and demonstrate that only the tricationic form is able to positively interact (at an acidic pH) with the guest with a K_a = 253 ± 50 M^{-1}.

As a follow-up,[2] we decided to test the versatility of this polycationic receptor towards a number of very different potential substrates. After several attempts, turned out that 2,7-dihydroxynaphtalene (DHN) is also recognized by our ionisable macrocycle. NMR coupled to semi-empirical calculations showed that, similarly the case of paraquat, the π-rich DHN guest nestles within the aromatic cleft generated by the resorcinol rings. In addition, it came out (again) that only the triprotonated form of the macrocycle (**66**·$3H^+$) is able to significantly recognize the guest, albeit now with a modest K_a of 44 ± 4 M^{-1}.

Interesting structural data were provided by the computational studies. Optimisation of the geometry of the receptor – with its three chloride counterions – and of the guest within a cluster of 200 explicit solvent molecules (H_2O) showed that the guest lies within the cavity of the receptor, with its hydroxyl groups pointing away from the oxacalixarene cavity, in order to hydrogen-bond with the surrounding solvating water molecules. These findings suggested that π-staking interactions are not the only driving force of this complexation event, but rather that the solvent plays a crucial role through hydrophobic and solvent effects.

---

[1] Manganaro, N.; Lando, G.; Gargiulli, C.; Pisagatti, I.; Notti, A.; Pappalardo, S.; Parisi, M. F.; Gattuso, G. *Chem. Commun.*, **2015**, *51*, 12657–12660.

[2] Manganaro, N.; Lando, G.; Pisagatti, I.; Notti, A.; Pappalardo, S.; Parisi, M. F.; Gattuso, G. *Supramol. Chem.*, **2016**, *28*, 493-498.

Encouraged by the results obtained with the tetraamino-derivative **66**, and aware that solubility somehow limited its general applicability, we turned our attention to compounds such as [4,6,16,18]tetra-amino[11,23]dihydroxy-tetraoxacalix[4]arene **68**·2H and [4,6,16,18]tetra-amino[25,27]dihydroxy-tetraoxacalix[4]arene **70**·2H. The introduction of two additional ionisable *exo*- or *endo*-cyclic phenolic groups on the oxacalixarene skeleton led to an increased water solubility.

We undertook a comparative (with respect to **66**) paraquat binding study with compound **70**·2H. Remarkably, the greater stability throughout the pH range of the new receptor – due to the introduction of the two additional (de)protonable sites (i.e., the OH groups) – allowed us to investigate host-guest association also at basic pH values, a range that remained unexplored in our previous study, given the limited solubility of $\mathbf{1}\cdot n\mathrm{H}^{+}$ at pH > 2.5. The apparent association constants for the $\mathbf{70}\cdot n\mathrm{H}^{(n-2)+}\supset\mathrm{PQT}^{2+}$ complex at low pH proceeds with a similar efficiency to that seen above for $\mathbf{66}\cdot n\mathrm{H}^{n+}\supset\mathrm{PQT}^{2+}$. Moreover, at basic pH, when oxacalixarene becomes negatively charged the stability of the $\mathbf{70}\cdot n\mathrm{H}^{(n-4)-}\supset\mathrm{PQT}^{2+}$ (n = 5,6) complexes is higher than in acidic media, as a consequence of additional electrostatic attractive interactions (e.g., K_{app} = 700 M^{-1} at pH 11.59).

Within the same frame, we also synthesised two molecular cages, **75** and **77**, with the goal of using them as cryptand-like receptors. Compounds **75** and **77** where characterized by ^{1}H and DOSY NMR techniques, whereas semiempirical calculations suggested that, while **75** does not appear to posses a well-defined cavity, cage **77** presents a roughly spherical inner space, that may potentially accommodate small guest molecules.

Where the first part of my work was devoted to 'basic' (i.e., amino-bearing) macrocycles, the second part dealt with 'acidic' (i.e., carboxyl-bearing) ones. Our research group has focused, for several years, on the development of new supramolecular systems based on classical calix[5]arene building blocks. Within this frame, we recently focused on a solid state investigation on the recognition properties of tetraester-calix[5]arene carboxylic acid **98**·H, which was found to be able to form capsular or *quasi*-capsular complexes with α,ω-diaminoalkanes ($H_2N[CH_2]_nNH_2$) as their ammonium dications, generated after a double host-to-guest proton transfer event.[3]

The solid state structure of the $\mathbf{98}^{-}\supset H_3N(CH_2)_{10}NH_3^{+}\subset\mathbf{98}^{-}$ and $\mathbf{98}^{-}\supset^{+}H_3N(CH_2)_{11}NH_3^{+}\subset\mathbf{98}^{-}$ complexes reveals that the proton-transfer-mediated

[3] Brancatelli, G.; Gattuso, G.; Geremia, S.; Manganaro, N.; Notti, A.; Pappalardo, S.; Parisi, M. F.; Pisagatti, I. *CrystEngComm*, **2015**, *17*, 7915–7921.

encapsulation has taken place, and that the diprotonated guest is nestled within the confined space defined by two calix[5]arene units.

The guest adopts a fully extended zigzag conformation, spanning the space between the bottoms of the receptor cavities, whereas the calixarenes adopt a cone-out conformation, mandatory for ammonium *endo*-cavity inclusion. The complex is held together by a number of concomitant interactions: the hydrogen bonds between ammonium ions and three oxygen atoms belonging to three different phenolic rings and an ester carbonyl oxygen atom, CH-π interactions between the α and β-CH_2 groups at the two ends of the ammonium guest and the calixarene aromatic rings. In addition, the wider rim *tert*-butyl moieties are in van der Waals contact providing, at the same time, sealing of the *endo*-capsular space and additional weak attractive interactions. The solid state structure of **98**$^-$⊃$^+H_3N(CH_2)_{12}NH_3^+$⊂**98**$^-$ showed many differences with respect to the other two systems, due to the longest guest chain that fails to fit within a capsule formed by two calix[5]arene units. Although $^+H_3N(CH_2)_{12}NH_3^+$ adopts a single highly compressed conformation, the two calixarene molecules do not come into van der Waals contact, giving rise to a *quasi*-capsular assembly.

Willing to test the efficiency of our capsule design beyond the proof-of-concept stage, we decided to move forward and pit calix[5]arene carboxylic acid **99**·H against potential guests with a mismatched number of protonable sites. To this end, the biogenic polyamines, spermine (Spm) and norspermine (Nspm), were selected as tetraamino-containing guests.[4]

Contrary to the low affinity seen in solution, solid-state structure analyses of the two complexes revealed an altogether different picture. The structure of the norspermine capsular complex (**99**$^-$⊃Nspm·2H$^+$⊂**99**$^-$), shows that encapsulation of the dicationic form of the guest –within two facing carboxylate-calix[5]arene cavities – takes place as a result of an initial acid-base host-to-guest proton transfer. The two calix[5]arene molecules, as generally seen in the case of alkylammonium *endo*-cavity inclusion complexes in the solid state, are arranged in a typical (approximately C_S-symmetric) *cone-out* conformation. A similar picture is seen for the solid-state structure of the spermine capsular complex (**99**$^-$⊃Spm·2H$^+$⊂**99**$^-$). Again, regioselective acid-base proton-transfer generates a three-component salt-bridged supramolecular complex very similar to the one just described.

[4] Brancatelli, G.; Gattuso, G.; Geremia, S.; Manganaro, N.; Notti, A.; Pappalardo, S.; Parisi, M. F.; Pisagatti, I. *CrystEngComm,* **2016**, *18*, 5012–5016.

This recognition motif was harnessed for the self-assembly of internally-ion-paired AABB-type supramolecular polymers.[5] DOSY NMR investigations reveal that bis-calix[5]arene-bis-carboxylic acids **106**·2H–**108**·2H, upon exposure to α,ω-diaminoalkanes self-assemble by iterative proton-transfer-mediated recognition, ultimately producing overall neutral aggregates. DLS and AFM allowed to discover that **108**·2H, when mixed with 1,12-diaminododecane gives cyclic oligomeric assemblies, whose morphology (i.e., cyclic vs. linear) can be controlled by means of external chemical stimuli.

A further macrocycle investigated during my PhD is based on a dithia[3.3]paracyclophane framework, attractive materials that can be used as comonomers in the preparation of a wide range of π-conjugated copolymers. The synthesis of some of these derivatives proceeds with complete stereoselection, resulting in the exclusive formation of the *meso*-diastereoisomers. We undertook a theoretical study on the mechanism underlying the formation of dithia[3.3]paracyclophane *S*,*S*'-dioxide (*R*,*S*)-**125** and a density functional study on the transition state of the cyclisation was carried out, to examine the pathways that could lead to (*R*,*S*)-**125** or to the diastereomeric racemic mixture (*R*,*R*)/(*S*,*S*)-**125** discovering that the exclusive formation of the *meso*-(*S*,*R*)-**125** proceeds under kinetic control.[6]

[5] Gattuso, G.; Manganaro, N.; Notti, A.; Pisagatti, I.; Pappalardo, S.; Parisi, M. F. *Curr. Org. Chem.*, **2015**, *19*, 2271–2280.

[6] Barattucci, A.; Bonaccorsi, P.; Papalia, T.; Manganaro, N.; Gattuso, G. *Tetrahedron Lett.*, **2014**, *55*, 5096–5100.

Chapter 1

1.1. Introduction

Supramolecular chemistry has been the field where the most important advancements in chemistry have been shaped over the past few years, as finally demonstrated by the award of the 2016 Nobel Prize in Chemistry to Jean-Pierre Sauvage, Sir J. Fraser Stoddart and Bernard L. Feringa for the "*Design and synthesis of molecular machines*".
Relying on self-assembly,[1] i.e. the mutual recognition between complementary building block *via* noncovalent weak interactions, a multitude of nano-sized, interlocked supramolecular architectures has been developed.[2] The key players in this game have been macrocyclic receptors. Macrocycles, owing to the constant improvement of synthetic procedures, have been in fact providing unique platforms for the construction and development of supramolecular arrays. That is why the synthesis and design of new functional macrocyclic molecules still draws the attention of the chemical community, as demonstrated by the presence in the literature of several reports on, among many, crown ethers,[3] cryptands,[4] cyclodextrin derivatives[5] spherands[6] and so on.[7]
More recent examples include calixarenes,[8] the aromatic macrocycles composed of a number of *p*-substituted phenol moieties bridged by methylene units. They are considered the third generation of synthetic receptors (after crown ethers and cyclodextrins) and heteracalixarenes,[9] where the conventional methylene linkage

between the aromatic rings are replaced by heteroatoms, can be regarded as the natural evolution of their carbon-bridged ancestors (**Fig. 1**).

The inherent nature of the heteroatoms bestows upon the heteracalixarenes different properties in terms of conformation and recognition ability[10] with respect to the traditional calixarenes.[11]

The rich molecular diversity, unique conformational behaviour, and tunability of the cavity provide ample freedom in the design of multicomponent molecular self-assembling systems. Moreover, the synthesis of enantiopure, inherently chiral heteracalixaromatics may provide important applications in asymmetrical catalysis and chiral recognition.

All this features make them an invaluable addition to the toolbox of supramolecular chemistry researchers.

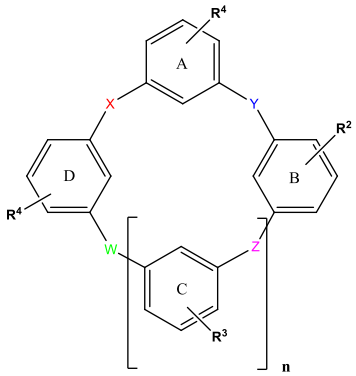

Figure 1. Representation of a general heteracalixarene X, Y, Z, W = heteroatoms; A, B, C, D = heteroaromatic rings.

The easy availability of thiacalixarenes from phenol and elemental sulfur and the similarities with the more familiar calixarenes, makes them[12] the first and most studied of the heteracalixarene family, while the oxacalixarenes and azacalixarenes homologues, due to their low-yielding synthetic procedures and poor solubility, despite their

discovery dates back to 1960s,[13] only recently have been recognized as a new generation of macrocycles.

In fact, until a few years ago, their supramolecular properties and extraordinary potential as host molecules were still unexplored, although the literature was full of heteracalixarene examples[14] differing in the nature of the connecting atom –sulfur, oxygen, nitrogen more recently, selenium or combination thereof– and incorporating, as aromatic moieties, either hydrocarbons (e.g. benzene, naphthalene and trypticene) or heteroaromatic units, such as pyridines, pyrazines, pyrimidines, triazines or naphthyridines.

The historical background of this compounds starts in 1966 when Sommer and Staab synthesized, in the course of their studies on conjugation in aromatic ethers, the first oxygen-bridged calixarene-type macrocycle **3** by a S_NAr reaction of 1,3-dichloro-4,6-dinitrobenzene **1** and resorcinol **2** in the presence of K_2CO_3 and using DMF as the solvent (**Scheme 1**).

The yield of this one-pot reaction was as low as 13%. In 1974 Lehmann was able to improve the yield to 46%, using a more reactive 1,3-difluoro-4,6-dinitrobenzene (but still a one-pot procedure) as the electrophilic component and triethylamine as the base.[15]

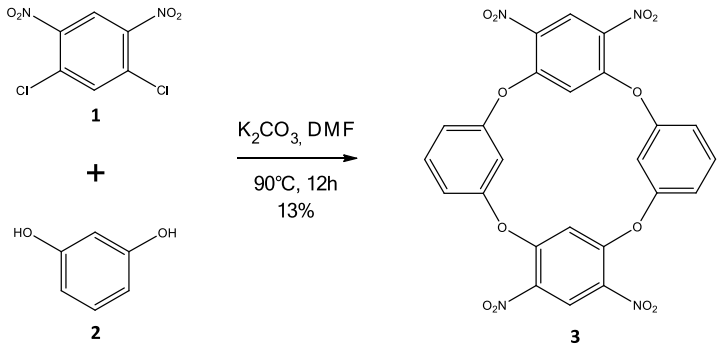

Scheme 1. First oxacalix[4]arene synthesized by Sommer and Staab.[13]

After these pioneering papers, very few attempts at improving the modest yields and harsh reaction conditions were done, and these macrocycles were put aside for almost 40 years.

The one-pot approach gave modest results for the synthesis of nitrogen-bridged derivatives, i.e. the azacalixarenes. Therefore, a stepwise fragment-coupling approach was adopted.

The first step was performed using 1,3-diaminobenzene **4** and 2,6-dibromopyridine **5** by a two-directional nucleophilic aromatic substitution, thus obtaining the linear tri-aryl product **6**. Subsequent treatment with methyl iodide produced an intermediate that, by means of a palladium-catalysed cross-coupling reaction, led to the azacalix[2]arene[2]pyridine **8** (**Scheme 2**). The yield was 26% and, in addition, larger macrocyclic ring homologues were also produced.[16]

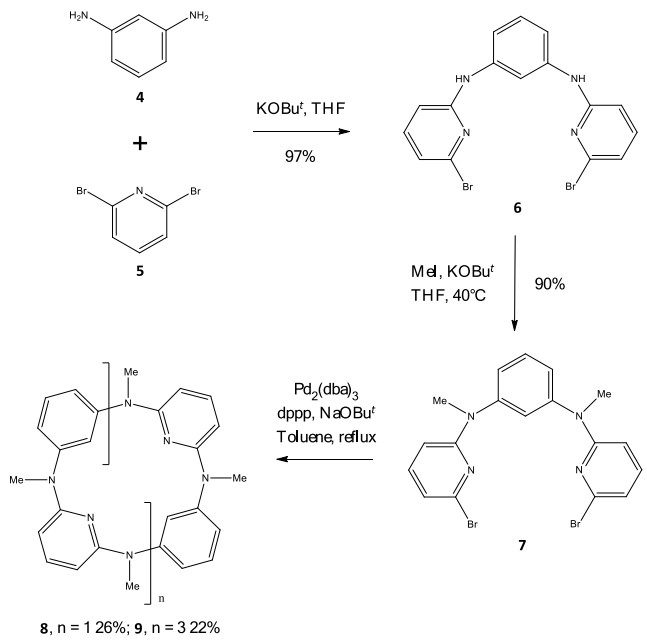

Scheme 2. Synthesis of azacalix[2]arene[2]pyridine performed by Wang *et al.*.[16]

Following the same synthetic route, and optimizing the experimental conditions, Wang and co-workers succeeded in the selective synthesis of azacalix[4]pyridine and azacalix[8]pyridine, in 36% and 20% yield respectively,[17] obtaining also different macrocyclic azacalix[*n*]pyridines containing both odd and even numbers of pyridine units (**12**-**17**, **Scheme 3**).[18]

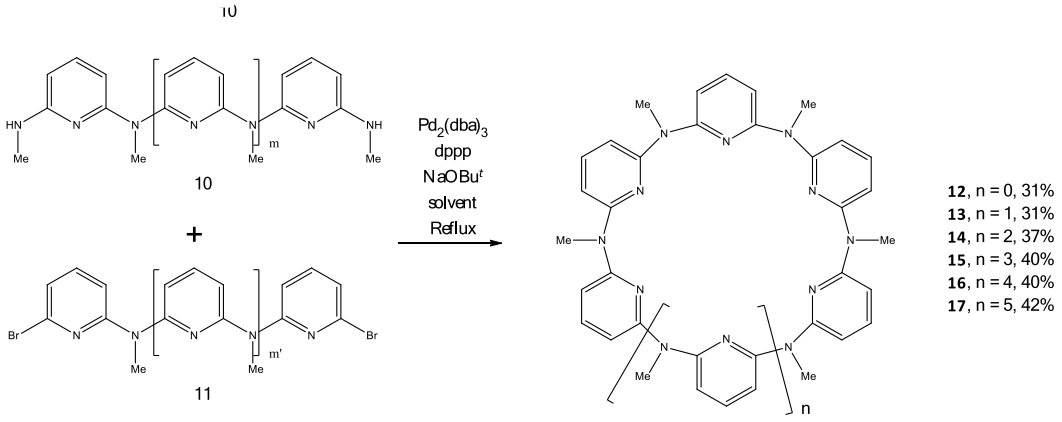

Scheme 3. Azacalix[*n*]pyridines (*n* = 5-10) synthesized by a cross coupling reaction.

The attractive features, synthetic accessibility and the complexation abilities of these novel azacalixarene macrocycles made again oxacalixarenes a sought after species. It was then in 2005 that Katz and co-workers envisaged an old-fashioned but very versatile and flexible S_NAr-based route to obtain these compounds in multi-grams scale[19] (**Scheme 4**).

The high yield of the synthesis and the absence of larger oxacalix[*n*]arenes and related acyclic oligomers, suggested that the oxacalix[4]arene might be the thermodynamic product of a dynamic reversible process involving ring opening and cyclization.[20]

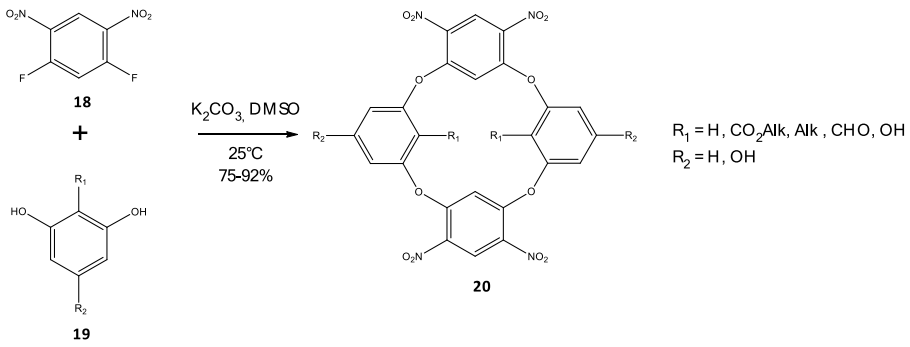

Scheme 4. Oxacalix[4]arene obtained by a one-step approach (Katz *et al.*).[19]

Given that the reaction did not require high dilution condition, and tolerated a wide range of substituents on the nucleophilic component, selected either to increase the solubility or to pursue specific structural modifications and allow for further derivatizations, other research groups followed up. For instance, Vincente and co-workers[21] synthesized symmetrical and non-symmetrical oxacalix[4]arene-porphyrins derivatives (**Fig. 2**) using Katz's reaction conditions or a '3 + 1' fragment coupling approach, respectively. More recently, the same group reported a new system based on a porphyrin connected with two opposing *meso*-oxacalix[4]arene groups that has shown remarkable photophysical properties.[22]

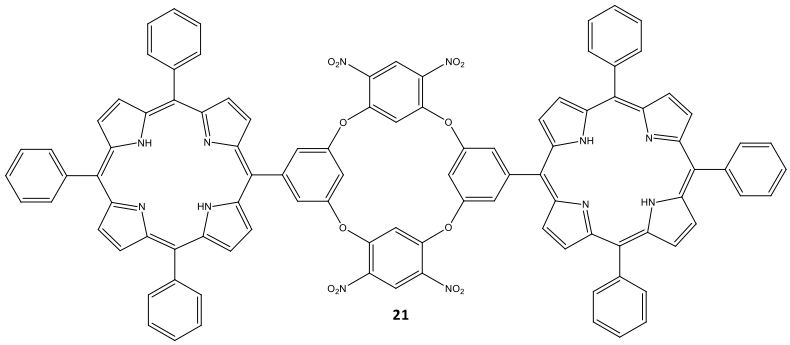

Figure 2. Oxacalix[4]arene-locked bis-porphyrin (Vincente *et al.*).[21]

Following the same strategy, using a 2,7-dihydroxytripticene building block as the nucleophilic component, Zhang and Chen synthesized an enlarged-cavity trypticene-based oxacalix[4]arene[23] (**Fig. 3**). Owing to the rigid 3D structure of the triptycene moiety, a mixture of two diastereomers **22a,b** was obtained. These compounds were found to assemble in tubular structures and other porous architectures in the solid state.

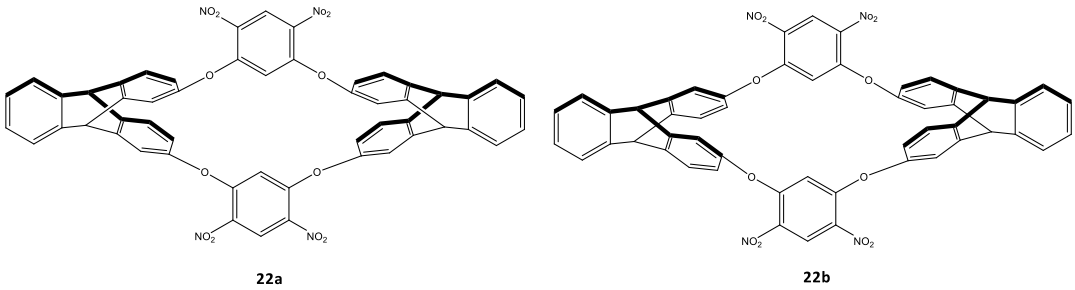

Figure 3. Oxacalix[4]arene-triptycene derivatives (Zhang and Chen).[23]

A new synthetic route based on Ullmann coupling has been developed by You *et al.*, providing new macrocycles susceptible to be functionalized at the intra-annular positions.[24] The reaction between 1,3-dihydroxybenzene **2** and 3,5-dibromo-4-nitrotoluene **23** using *N*,*N*-dimethylglycine as the catalyst, lead to an oxacalix[4]arene with a intra-annular nitro group (**Scheme 5**).

The synthesis of oxacalix[4]arenes by S_NAr route prompted some research groups to employ polyhalogenated compounds as electrophilic building blocks for the construction of macrocycles in which the presence of additional heteroatoms would make subsequent modifications possible.

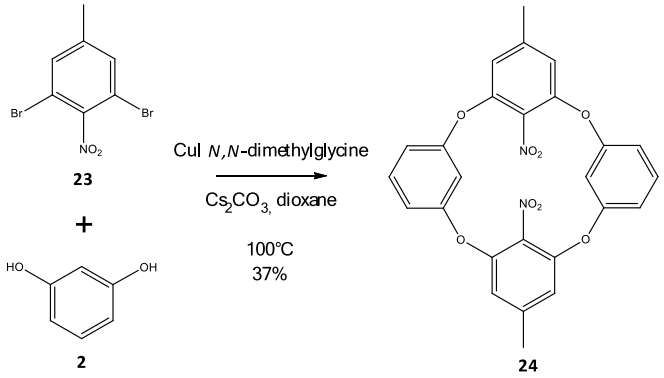

Scheme 5. Oxacalix[4]arene derivatives synthesized by You *et al.*[24]

For instance, Chambers and co-workers prepared polyhalogenated heteracalix[2]arene[2]pyridines derivatives by using polyfluoropyridine **25** building blocks and bis-trimethylsilyl orcinol **26** under desilylating conditions, to get a tri-aryl derivative **27**, that, after cyclization with a second molecule of **26**, afforded oxacalix[4]arene **28** (**Scheme 6**).[25]

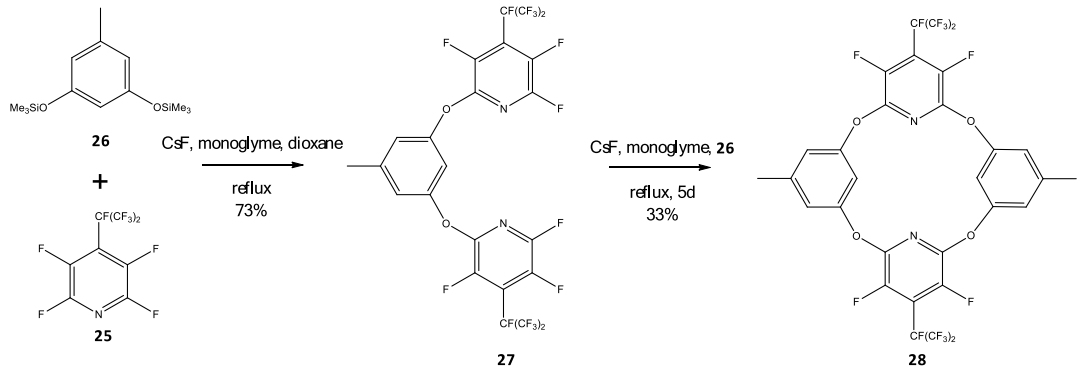

Scheme 6. Oxacalix[2]arene[2]pyridine (Chambers *et al.*).[25]

Furthermore, Katz *et al.* described a simple (DMSO, rt, Cs_2CO_3), high-yielding (up to 95%) procedure for the synthesis of bicyclooxacalixarenes by nucleophilic aromatic substitution between phloroglucinol and suitable electron-deficient *meta*-dihalogenated

aromatics. The incorporation of nitro-, cyano- and chloro- groups at the oxacalixarene extra-annular positions and nitrogen atoms at the internal ones, make them potentially powerful building blocks for construction of covalent supramolecular systems.[26]

The fragment coupling approach has proved to be useful for the synthesis of heteracalixtriazine derivatives[27] and azacalix[4]pyrimidines.[28] Triazine is a valuable unit in molecular recognition because of its proclivity to act as both hydrogen bond acceptor and as a π-acceptor in anion-π recognition. As a result, it has been widely employed as a building block for selective hosts for a number of different guests including carbohydrates, cyanuric acid and uracil derivatives.[29]

In 2005, Wang *et al.* reported the first heteracalix[2]arene[2]triazine obtained in a good yield by means of a reaction between resorcinol **2** and cyanuric chloride **29** in THF at 0 °C using diisopropylethylamine as the base, then followed by a cyclization reaction with a second equivalent of resorcinol (**Scheme 7**).[27]

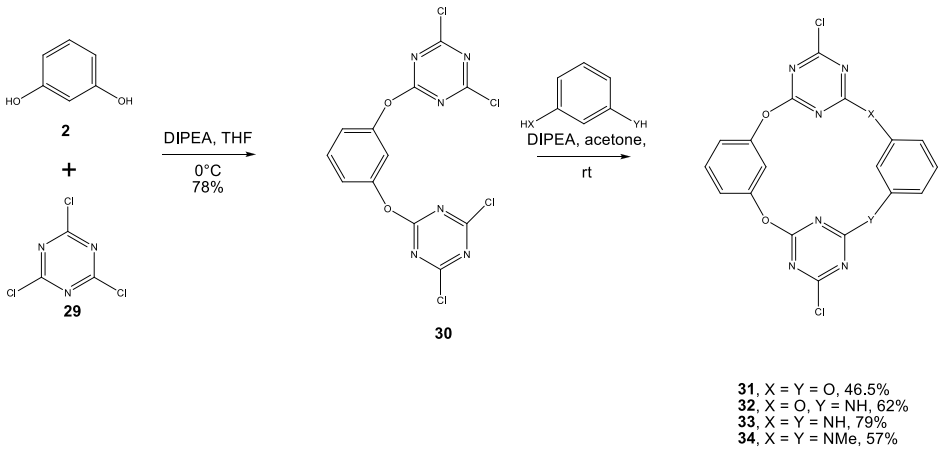

Scheme 7. Heteracalix[2]arene[2]triazine (Wang *et al.*).[27]

More recently, they synthesized 1,3-alternate oxacalix[2]arene[2]triazine-azacrowns by a condensation reaction of ethylene glycol linkers and dichlorinated

oxacalix[2]arene[2]triazine.[30] Because of the conjugation of amino groups with the triazine rings, tetraoxacalix[2]arene[2]triazine-azacrowns (**Fig. 4**) existed in a mixture of *syn-* and *anti*-isomeric forms. Both fluorescence titration and ^{1}H NMR spectroscopic study showed that this species recognized fluoride anions.

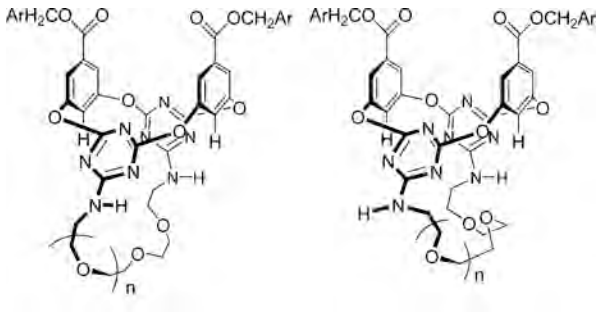

Figure 4. Tetraoxacalix[2]arene[2]triazine-azacrowns (Wang *et al.*).[30]

Following this route, chiral oxacalixcrowns derivatives – as pairs of diastereomers – were synthesized.[31]

The versatility of oxacalix[*m*]arene[*n*]pyrimidines for supramolecular applications drew the attention of several research groups, and in 2006 Katz *et al.* synthesized a oxacalix[2]arene[2]pyrimidine in a single step by nucleophilic aromatic substitution of *meta*-dichlorinated azaheterocycles with *meta*-diphenols, even though with a disappointing yield of just 12%.[32] Meanwhile, Dehaen and co-workers demonstrated that, depending on the S_NAr conditions, a mixture of oxacalix[*n*]arenes ranging from oxacalix[4]- up to oxacalix[12]arene (**35**-**38**) can be prepared (**Fig 5**).[33]

Oxacalix[4]arene may selectively be obtained as well, by careful control of the experimental conditions. The same group performed a Liebeskind-Srogl cross-coupling reaction[34] on the pyrimidine moiety of the oxacalixarene scaffold, introducing a functionalized aryl group in which O-, S-, N-, and C-nucleophiles were attached by S_NAr reactions.

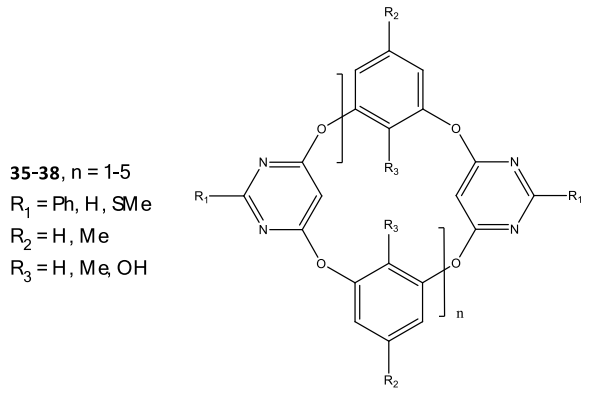

Figure 5. Oxacalix[*m*]arene[*n*]pyrimidines (Dehaen *et al.*).[33]

During these studies, it was noted that when the S_NAr reaction was performed under kinetic control, enlarged oxacalix[*n*]arenes (*n* > 4) were obtained as secondary – often unwanted – products.[30,31]

It was only recently that some research groups have actively investigated the routes to access enlarged oxacalixarenes, envisaging the opportunity to produce potential host molecules for larger guests.

The yields of larger oxa-bridged cyclooligomers, which are not always easy to purify, heavily depend on the reaction conditions employed. For example Dehaen *et al.*[34] reported a synthesis of oxacalix[*m*]arene[*n*]pyrimidines (*m,n* = 2–6, **Fig. 6**) starting from orcinol and 4,6-dichloro-2-phenylpyrimidine under non-equilibrating conditions, with yields ranging from 8 to 10%, whereas Gibb and co-workers[35] synthesized symmetrical and asymmetrical oxacalix[8]arene derivatives using resorcinarenes as templates, considerably increasing the yields (up to 85%).

But what makes this family of compounds so attractive? A deeper insight into their structural features obtained by the combination of X-ray diffraction studies in the solid state and NMR analysis in solution, reveals the peculiarities that make them unique.

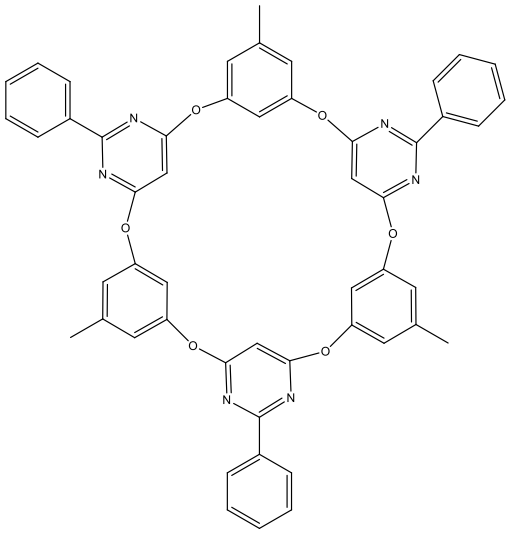

Figure 6. Oxacalix[3]arene[3]pyrimidines (Dehaen *et al.*).[34]

Differently to their calix[4]arene parents that are seen to adopt four major different conformations,[36] the heteracalix[4]aromatic investigated so far, show only two stable conformations: the 1,3-*alternate*[19,25,27,30,31] and the flattened *partial cone*[38,39] (**Fig. 7**).

The introduction of the heteroatom in the bridging position, being it oxygen or nitrogen, makes so that the abovementioned conformations are adopted as a result of heteroatom-aromatic moiety conjugation, given also the lack of the intramolecular hydrogen-bonding that exists in classical calix[4]arenes.[37]

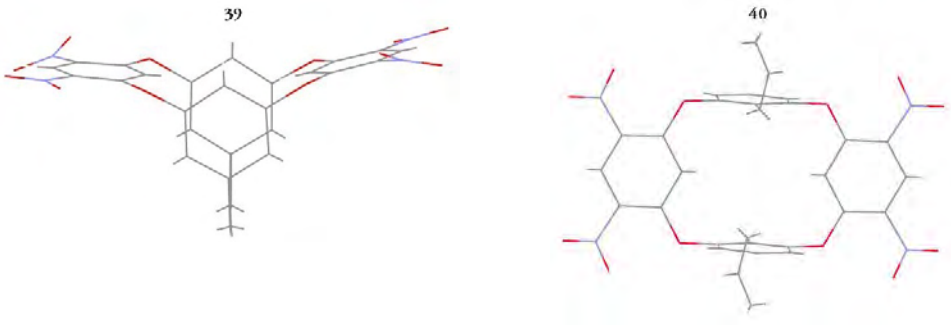

Figure 7. X-ray diffraction structures of oxacalix[4]arenes : **39**, 1,3-*alternate* conformation (Katz *et al.*);[19] **40**, *partial cone* conformation (Konishi *et al.*).[38]

The structural data gathered so far have shown that the aromatic rings of the electrophilic components approach coplanarity, or are anyways oriented to maintain conjugation with the bridging oxygen (or nitrogen) atoms, whereas the nucleophilic component electron-rich rings are generally eclipsed and nearly parallel.

The ^{1}H NMR spectra of this family of compounds is characterized by high-field resonance for the intra-annular aromatic hydrogen atoms of the electrophilic moieties, due to the diamagnetic shielding arising from the flanking aromatic rings, whose intensity strongly depends on the overall conformation.

In addition, variable-temperature NMR experiments on oxacalixarene mixtures revealed that in all cases only one set of sharp signals was observed, even at very low temperature, data in agreement with a single conformation or a very rapid conformational interconversion on the NMR time scale.

Interestingly, the nature of the aromatic rings and the presence of substituents dictate the fine-tuning of macrocyclic conformation and of the cavity size.

In general, the replacement of nitrogen atoms by oxygen atoms influences the interplanar angle between the two facing aryl rings, decreasing also the interplanar distance, as a consequence of the lower proclivity of the oxygen atom to share its lone pairs.

Recently, the groups of Konishi[38] and Wang[39] independently, reported rare examples of oxacalixarenes in which the saddle-shape conformation (thermodynamically favoured) is flanked by a flattened *partial cone* one (kinetically favoured). This was observed by the introduction of sterically demanding groups which are unable to rotate though the central annulus (**Fig. 8**).

Despite the huge potential of this promising family of compounds (that have already been the subject of several papers), examples of their supramolecular applications are still dismayingly few.

Aside from rare exceptions,[40] only the tetraoxacalix[2]arene[2]triazine and the azacalix[*n*]pyridine families have been investigated in depth for their host-guest properties.

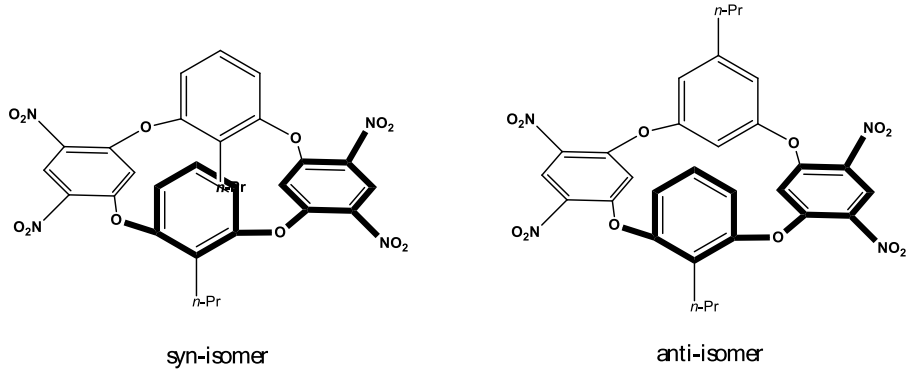

Figure 8. Schematic representation of two conformational isomer of an oxacalix[4]arene derivative (Konishi *et al.*).[38]

For example, during their study on polyfluorinated oxacalix[2]arene[2]pyridine, Chambers and co-workers described the properties of this macrocycle as molecular receptor towards halide anions, while no coordination with metal cations was noticed.[25] The same oxacalixarene was also found to be efficient for the extraction of sodium picrate from an aqueous phase into dichloromethane solution.

Oxacalix[4]crown ligands have been studied by Bitter *et al.*[41] as complexing agents for metal cation extraction in biphasic chloroform-aqueous alkali picrate mixtures.

In contrast to analogous thiacalix[4]arene species, no appreciable cation extraction was observed for oxacalix-crowns, an inability data that may be explained by the lack of cation-π interactions of the electron-poor 1,3-*alternate* aromatic rings.

Wang *et al.*[42] reported some calix[2]arene[2]triazines in which a few chelating groups had been introduced at the extra-annular position of the triazine rings through a straightforward and very convenient aromatic nucleophilic displacement of the

chlorine atoms **42**,**43** (**Fig. 9**). These oxacalix[2]arene[2]triazines species with pending bidentate pyridine ligands exhibited excellent selectivity in the complexation of metal ions in an acetonitrile/water mixture (4:1 v/v), forming 1:1 complexes with Cu^{2+} ions.

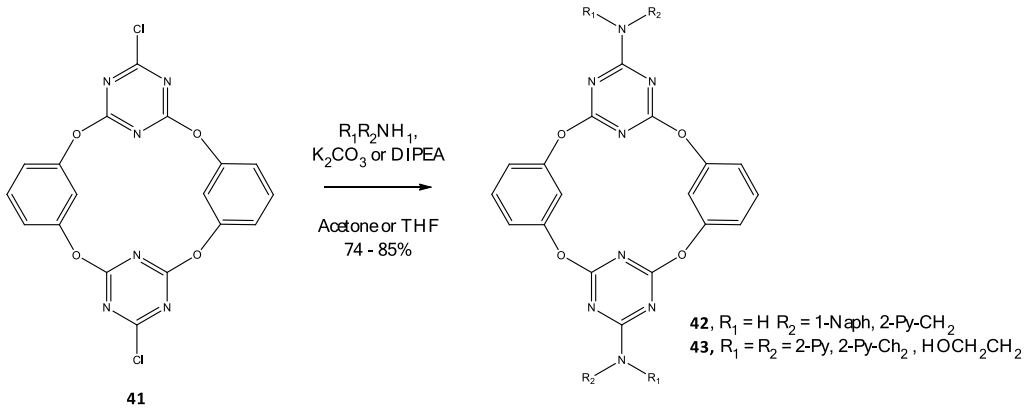

Figure 9. Calix[2]arene[2]triazines with chelating groups (Wang *et al.*).[42]

Recently, Katz and co-workers[43] employed oxacalix[2]naphthalene[2]naphthyridine **46** with an increased cavity size, to bind neutral guests through a combination of π-π interactions and hydrogen bonding. Additionally, the inner-cavity naphthyridine nitrogen atoms are able to impart substrate selectivity to the recognition event (**Scheme 8**).

Notably, some of the larger azacalix[6]- and azacalix[8]arene derivatives have been shown to recognise and efficiently bind fullerenes both in solution and in the solid state, with association constants in toluene in the 10^4–10^5 M^{-1} range.[44]

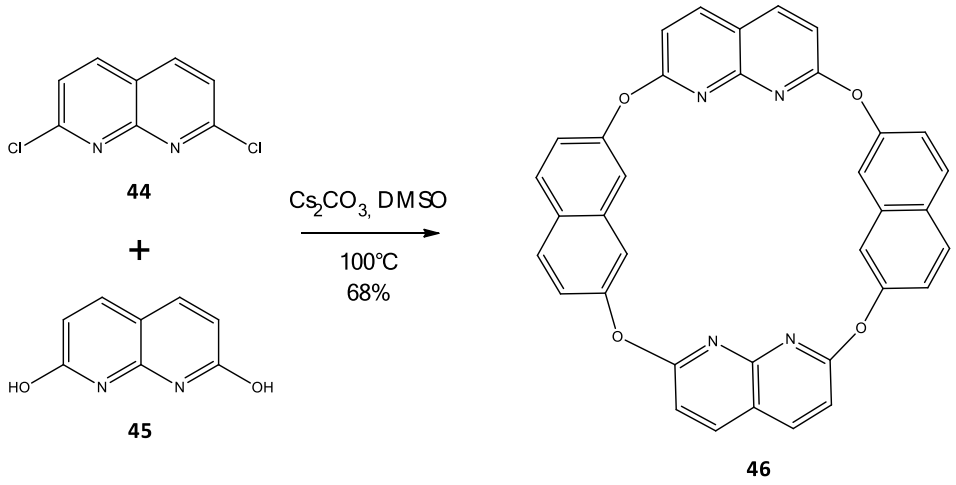

Scheme 8. Synthesis of oxacalix[2]naphthalene[2]naphthyridine (Katz *et al.*).[43]

All these reports, however, prove the hosting abilities of this family of compounds only when the process takes place in the solid state or in organic solvent solutions.

It is only recently that the first papers on water-soluble derivatives have appeared: De-Xian Wang and co-workers[45] showed that amphiphilic oxacalix[2]arene[2]triazines assembled in water into vesicles and micelles, still retaining their host-guest affinity to inorganic anions. Modulation of the self-assembled aggregates from vesicles to micelles was obtained by regulating the hydrophilicity and polarity of the substituents attached to the larger rim of triazine rings.

Foreseeing the non-conventional ability of the oxacalix[4]arenes to recognize a wide range of molecules in the π-rich cleft generated by the two electron-rich nucheophilic component aromatic moieties, and knowing their proclivity for π -stacking, our ambitious aim was to transfer this charming system in water envisaging the possibility to use it as molecular tweezers toward suitable neutral or charged guest molecules .

1.2. Oxacalixarenes

1.2.1. Oxacalixarenes: a brief overview on our background

Our investigations on oxacalix[4]arenes started in 2009. The first studies were focused on the synthesis of a number of tetra-N-(1-octyl)ureido-oxacalix[4]arenes **57–61**. The experimental procedure relied on the synthesis of tetranitro-oxacalix[4]arenes precursors **47–51**, that were subsequently reduced to the corresponding tetraamino derivatives **52–56** and finally converted in the ureido-oxacalixarene derivatives by treatment with an excess of 1-octyl isocyanate in dry DMSO (for **57** and **59–61**) or $CHCl_3$ (for **58**, **Scheme 9**).[46]

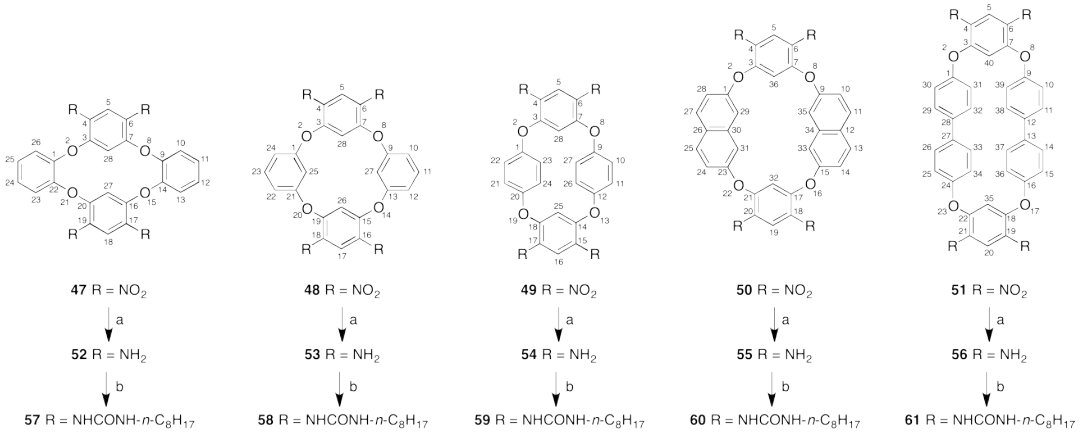

Scheme 9. Synthesis of tetraureido-oxacalix[4]arenes **57–61** starting from tetranitro-derivatives **47–51**. Reagents: (a) H_2, Raney-nickel, THF or DMF; (b) $CH_3(CH_2)_7NCO$, $CHCl_3$ or DMSO (Pappalardo *et al.*).[46]

The ^1H NMR spectra of the oxacalix[4]arenes **47–61** are characterized by high field resonances for the intra-annular aromatic protons of the electrophilic component (δ =

5.12–6.72 ppm), owing to the diamagnetic shielding arising from the flanking aromatic rings, which in turn depends on the molecular conformation. This suggests that compounds **57**, **58**, **60** adopt a saddle-shaped (1,3-alternate) conformation in solution, while **59** and **61** derivatives – because of the geometric features of the nucleophilic components – can adopt boat or chair conformations equally (**Fig. 10**).

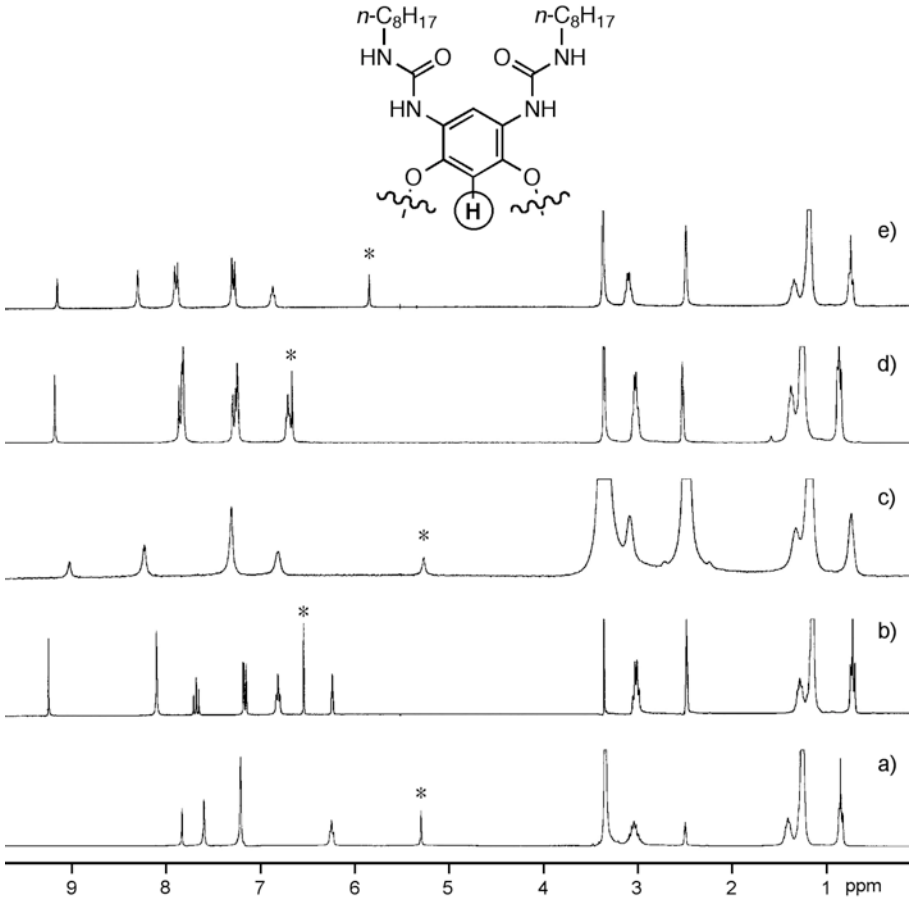

Figure 10. ^{1}H NMR spectra (300 MHz, DMSO-d_6, 22 °C) of tetra-*N*-(1-octyl)ureido-oxacalix[4]arenes **57**–**61** (traces a) to e), respectively). The asterisks indicate the peaks for the intra-annular hydrogen atoms (Pappalardo *et al.*).[46]

In order to gather information about the geometry of the ureido-oxacalix[4]arenes **57–61**, so as to evaluate the stereoelectronic matching potential (poly)anionic guests, *ab initio* calculations were performed by using the Hartree-Fock method with the 6-31G(d) basis set.[47]

To decrease the degrees of freedom, and simplify the calculations, the *n*-octyl moieties were replaced by methyl groups (compounds **Me-57–Me-61**).

It turned out that all the structures adopt a boat-like conformation, with the ureido-bearing aryl groups in a *syn* relationship with respect to the mean plane generated by the four bridging oxygen atoms.

In the compounds **Me-59** and **Me-61** the bis-ureido aryl rings are seen in a wide-open and slightly twisted arrangement, the angles between the rings being 124.9° and 124.2°, respectively.

The distances between the centroids of these rings vary considerably according to the length of the spacer. Compounds **Me-57**, **Me-58** and **Me-60** on the other hand, present the ureido-aryl rings facing each other in a slightly divergent arrangement and the angles formed by the mean planes of these aryl rings are in the 30–40° range (**Fig. 11**).

The results of the optimized molecular geometries indicated that tetraureido-oxacalix[4]arenes **57**, **58**, and **60** could be the best candidates for an initial screening of the anion-complexation abilities.

It was deemed likely that, as a result of the relatively small angle formed by the aryl groups, the ureido moieties could have the correct geometry to act cooperatively for a tweezers-type complexation of suitably-sized anions. However, test experiments gave modest results.

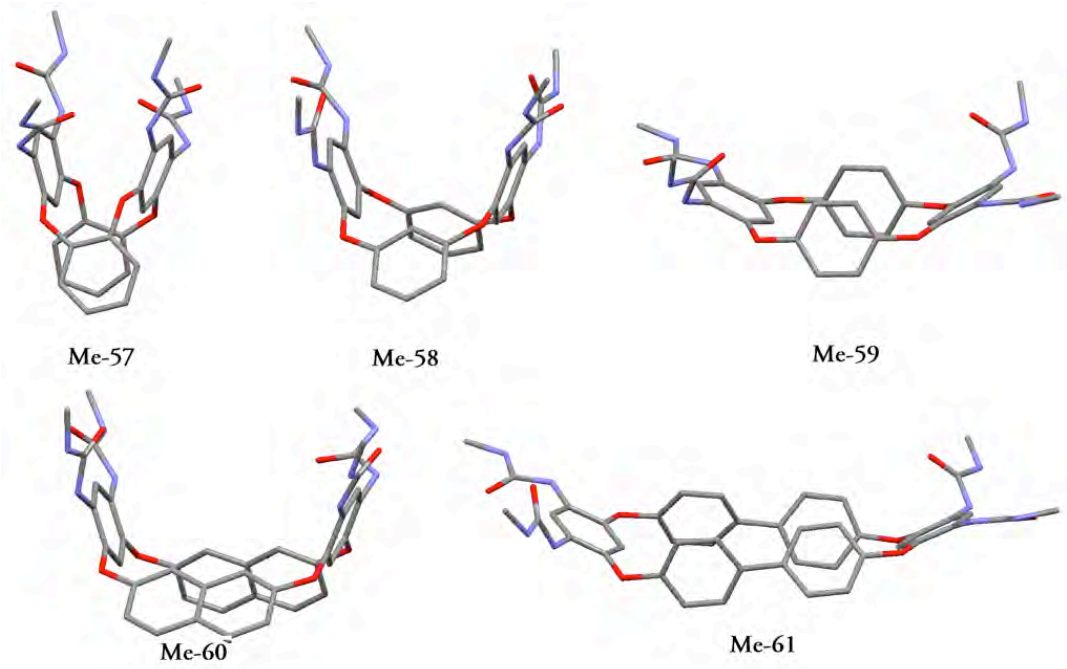

Figure 11. Optimized ground-state geometries for model compounds **Me-57**–**Me-61** (derived from ureido-oxacalix[4]arenes **57**–**61** by replacement of the *n*-octyl moieties with methyl groups), obtained by HF/6-31G(d) *ab initio* calculations. Hydrogen atoms omitted for clarity (Pappalardo *et al.*).[46]

Following that, in 2011 my research group reported one of the first examples of chiral oxacalixarene, derivative **62**, in which chirality was introduced in the oxacalixarene skeleton by using a (±)-**1,1'-bi-2-naphthol** (BINOL) as the nucleophilic component.[48] From the reaction between (±)-BINOL and difluorodinitrobenzene, two different oxacalix[4]arenes were formed, a C_{2h}-symmetric *meso* form, containing both a (*R*)- and a (*S*)-BINOL moiety, and a racemic mixture of D_2-symmetric (*R,R*)- and (*S,S*)-oxacalix[4]arene (**Scheme 10**).

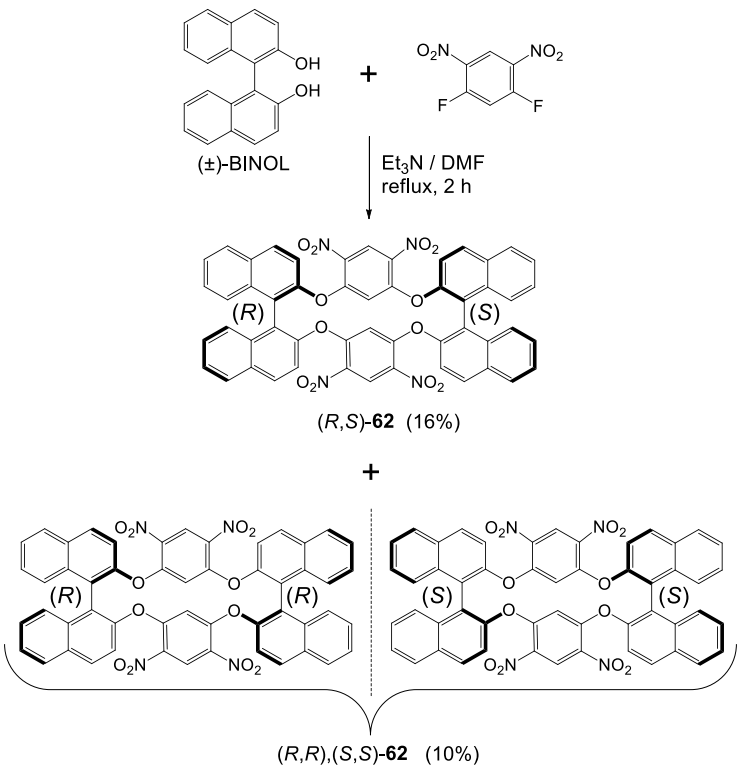

Scheme 10. Synthesis of *meso* (*R,S*)-**62** and racemic (*R,R*),(*S,S*)-**62** oxacalix[4]arenes (Gattuso *et al.*).[48]

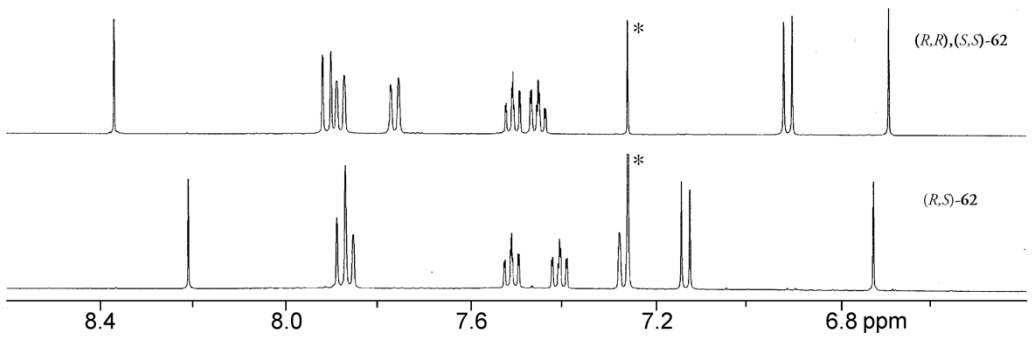

Figure 12. ^{1}H NMR spectra (500 MHz, 25 °C, 5 mM, $CDCl_3$) of the oxacalix[4]arenes (*R,S*)-**62** and (*R,R*),(*S,S*)-**62**. ∗Residual solvent peak.

Analysis of the ^{1}H NMR spectra, however, does not allow discrimination between the two sets of diastereoisomers, X-ray analysis was then employed for the elucidation of the stereochemistry of the products.

Oxacalix[4]arene (*R,S*)-**62** in the solid-state adopts a fairly distorted conformation and the two dinitrobenzene rings are arranged in an antiparallel fashion with respect to the ideal axis intersecting the cavity of the macrocycle. Interestingly, in the crystal, pairs of (*R,S*)-**62** molecules are held together by intermolecular π–π stacking between a dinitrobenzene ring and a naphthyl unit of an adjacent molecule.

The two nitro groups of ring A lie out of the C27–C32 mean plane, pointing in opposite directions (N3 0.270(2) and N4 0.355(2) Å), as a result of the buttressing effect[49] of the sterically congesting naphthyl ortho-substituents. One of the NO_2 groups of ring B, was found to be disordered over two orientations (see **Fig. 13**).

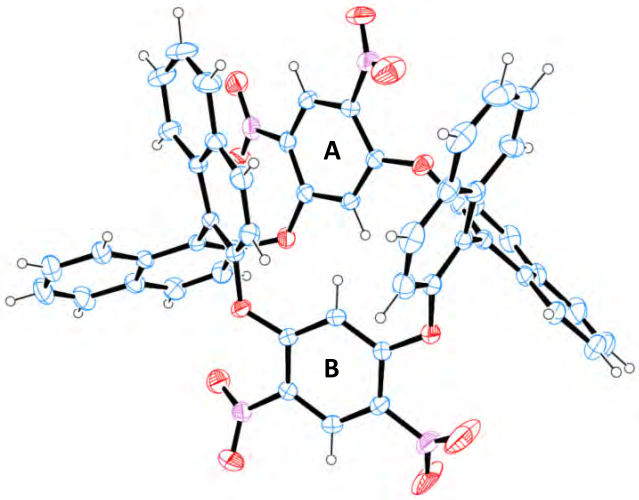

Figure 13. ORTEP drawing of the X-ray crystal structure of oxacalix[4]arene (*R,S*)-**62**·$CHCl_3$ (the chloroform molecule is omitted for the sake of clarity). C: light blue, H: white, O: red, N: magenta. Probability of the ORTEP ellipsoids is set to 30%, whereas H size is arbitrary (Gattuso *et al.*).[48]

Additional experiments revealed that the reaction does not proceed under thermodynamic control. To this end, both meso (*R,S*)-**62** and racemic (*R,R*),(*S,S*)-**62** were separately heated (160 °C, DMSO-d_6) in the presence of 1 equiv. of CsF and then monitored by ^{1}H NMR over a period of 12 h. Under these conditions, if the reaction was thermodynamically controlled, compounds should have equilibrated (via aromatic unit exchange) and eventually produced identical mixtures.[50] However, both experiments yielded oligomeric materials, without the formation of (the other) macrocyclic species, thus indicating that, under these experimental conditions, (*R,S*)-**62** and (*R,R*),(*S,S*)-**62** do not equilibrate.

Within this frame, we followed up in 2012, reporting the first example of photo-responsive azobenzene-containing oxacalixarenes **63**,**64**.[51]

Knowing the ability of azobenzene species to undergo reversible *E/Z* photoisomerization,[52] we decided to introduce this moiety on the calixarene skeleton by a ″3+1″ condensation reaction (using precursors **65** and **66**) to see if a selective capture and/or controlled release of a specific substrate could be achieved.

The triaryl compounds were in turn reacted with either (*E*)-4-phenylazoresorcinol or (*E*)-4-(40-nitrophenylazo)resorcinol according to **Scheme 11** to give oxacalixarenes (*E*)-**63a** and (*E*)-**63b** in a 61% and a 91% yield, and (*E*)-**64a** and (*E*)-**64b** in an 17% and a 87% isolated yield, respectively.

^{1}H NMR spectra of these compounds suggest that in all the cases a common 1,3-alternate saddle-shaped conformation is adopted (**Fig. 14**).

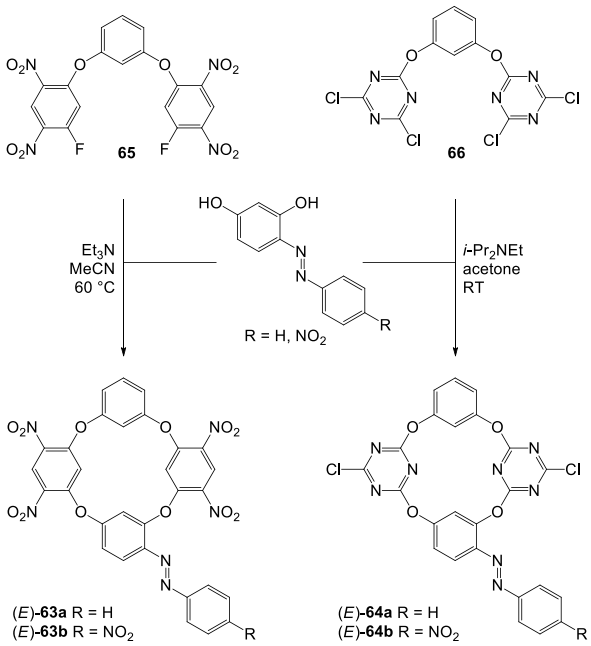

Scheme 11. Synthesis of oxacalixarenes (*E*)-**63a,b** and (*E*)-**64a,b** (Gattuso *et al.*).[51]

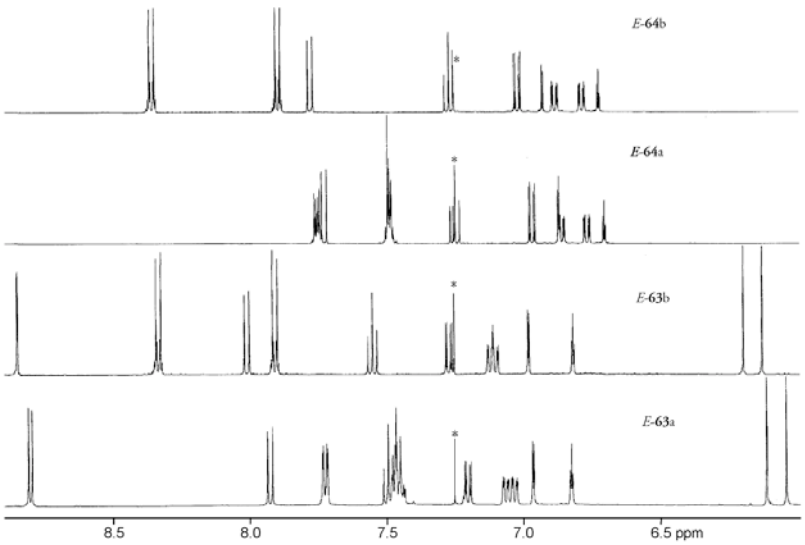

Figure 14. ^{1}H NMR spectra (500 MHz, $CDCl_3$, 25 °C, 5 mM) of oxacalix[4]arenes (*E*)-**63a,b** and oxacalix[2]arene[2]triazines (*E*)-**64a,b**.

Additional evidence in favour of such 1,3-alternate saddle-shaped conformation for derivatives (*E*)-**63a,b** and (*E*)-**64a,b** was also collected carrying out molecular modelling calculations[53] at the density functional level of theory (B3LYP/6-31G(d).[54]

The absorption spectra of all four compounds are characterized by a weak band in the visible region, and an intense one in the near UV region, owing to the azobenzene moiety.

Remarkably, for the nitro derivatives an additional band at 267 nm due to π-π electronic transitions have been observed (**Fig. 15**).

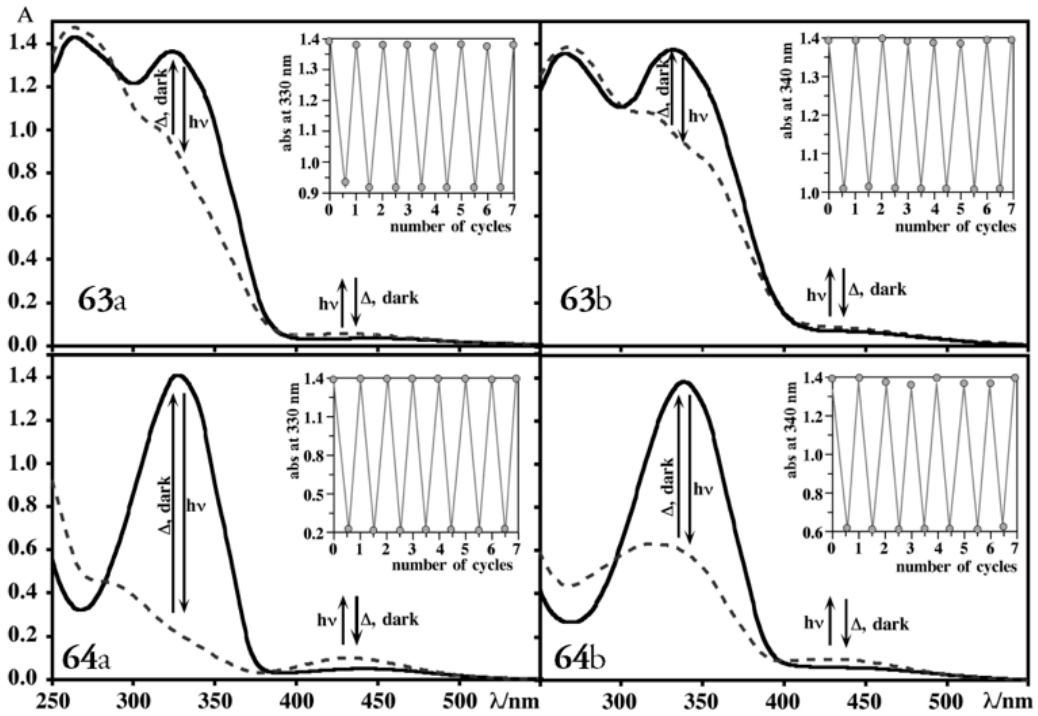

Figure 15. Absorption spectra (5.5×10^{-5} M, CH_2Cl_2, 25 °C) of **63a,b** and **64a,b** in the *E*-form (solid line) and in the photo-stationary state (dashed line) reached after 1 h irradiation at λ= 334 nm. Insets show the fatigue-cycle plots (Gattuso *et al.*).[51]

The dependence of the isomerization process on the nature of the macrocycle was investigated by a combination of NMR and UV-vis techniques.

The NMR spectra of the irradiated sample showed that all compounds undergo photoisomerization producing mixtures of *E*- and *Z*-isomers.

The absorption spectra in CH_2Cl_2 solutions of **63a,b** and **64a,b** were found to partially overlap (**Fig. 15**) and, as a consequence, upon irradiation at λ = 334 nm a stationary state was reached.

Irradiation at λ = 432 nm induces the quantitative reverse isomerization to the *E*-isomer. The photoequilibrium conditions can repeatedly be reached in a cyclic manner with no evidence of product degradation. Moreover we observed that *E*→*Z* photoisomerization process becomes less efficient when the *p*-nitro-substituent is present on the azobenzene moiety. In line with the known process of thermal reverse isomerization of (*Z*) azobenzene derivatives[‡‡] to the corresponding *E*-isomers, in the dark, oxacalixarenes (*Z*)-**63a,b** and (*Z*)-**64a,b** (CH_2Cl_2, 25 °C) were found to revert back to their *E*-isomers with first-order kinetics and because *p*-nitro group stabilizes more efficiently the *E*- rather than the *Z*-isomers, oxacalixarenes **63b** and **64b** display higher $k_{Z\rightarrow E}$ values than the corresponding phenylazo derivatives (**Fig. 16**).

It was then concluded that the nature of the oxacalixarene framework affects the excited states involved in the thermal isomerization process of the azobenzene moieties, with the dinitroaryl rings —more than the chlorotriazine ones— exerting a stabilizing effect on the *E*-isomers. Additional investigations on the photoswitching behaviour and on the molecular recognition properties are currently in progress.

[‡‡] Thermal *Z*-*E* isomerization of diphenyldiazene is a first-order process that proceeds with an activation energy value close to 24 kcal mol^{-1} (Ciminelli, C.; Granucci, G.; Persico, M. *Chem.–Eur. J.* **2004**, *10*, 2327–2341).

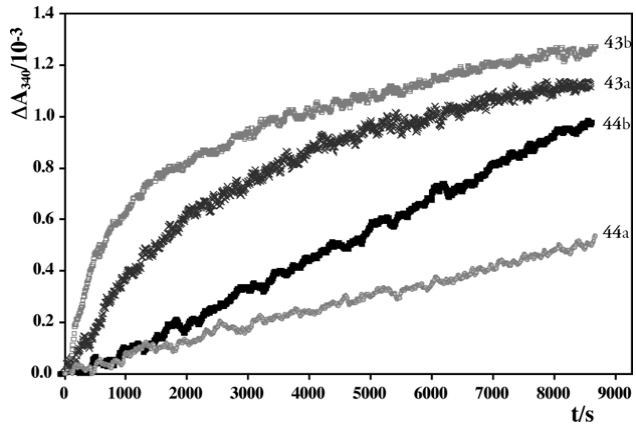

Figure 16. Absorption variations at 340 nm for the thermal *Z*→*E* reactions in the dark at 25 °C in CH_2Cl_2 (Gattuso *et al.*).[51]

1.2.2. Tetrammonium-tetraoxacalix[4]arene tetrachloride: characterization

During my PhD in the research group of Professor Gattuso, I began a study on oxacalixarene species in 2014. The goal of my research was to obtain water-soluble oxacalixarene derivatives, and then to investigate their scarcely-explored host-guest properties in water.

To this end, we turned to synthesis of ionisable oxacalixarenes.

4,6,16,18-Tetraamino-2,8,14,20-tetraoxacalix[4]arene **66** was prepared by Raney-Ni-catalysed reduction of the tetranitro precursor **65**, according to the procedure we reported in 2009.[46]

Treatment of a THF solution of **66** with an aqueous 0.1 M HCl led to the formation of the tetra-hydrochloride salt **66**·4HCl, that showed a modest solubility in plain water that significantly increases upon lowering the pH.

Its ^{1}H NMR spectrum, recorded at pH = 2.0 (10^{-2} M DCl in D_2O) suggests that **66**·4HCl adopts a saddle-like conformation typical of oxacalix[4]arenes, as indicated

by the high field resonance of the intra-annular aromatic hydrogen atoms of the electrophilic component (δ = 6.55 ppm, see Fig. **17**), owing to the mentioned diamagnetic shielding provided by the flanking aromatic rings (see above, section 1.1).[55]

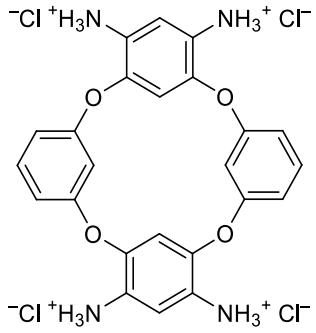

66 4HCl

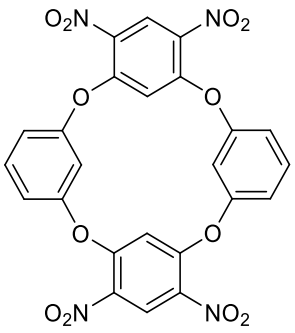

65

Solubility in acidic media, along with a strong dependence of the ^{1}H NMR spectrum on pH (**Fig. 18**), confirmed that prior to any investigation on the binding potential of this oxacalixarene derivatives, it was necessary to gain a clear picture of the distribution of the different protonated species (i.e., **66**·nH$^+$ with n = 0–4) over a wide range of pH (1.0 < pH < 10.0).[56]

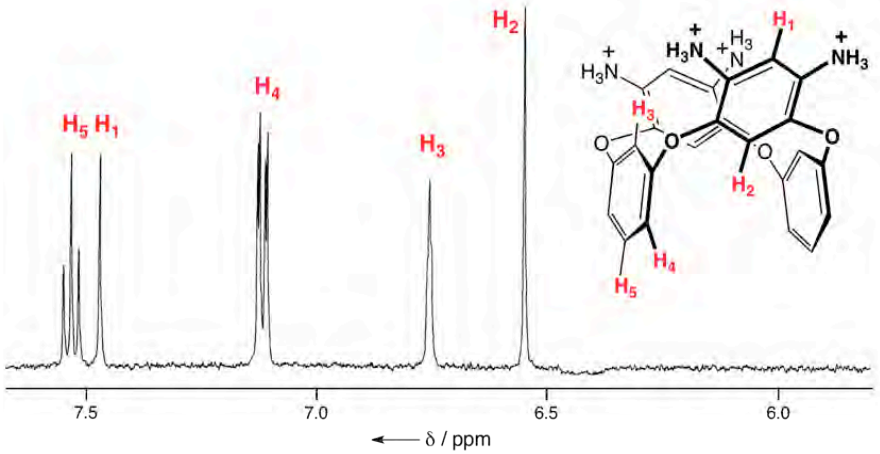

Figure 17. ^{1}H NMR spectrum (500 MHz, 298 K, D_2O/DCl, pH = 2) of oxacalix[4]arene **66**·4HCl.

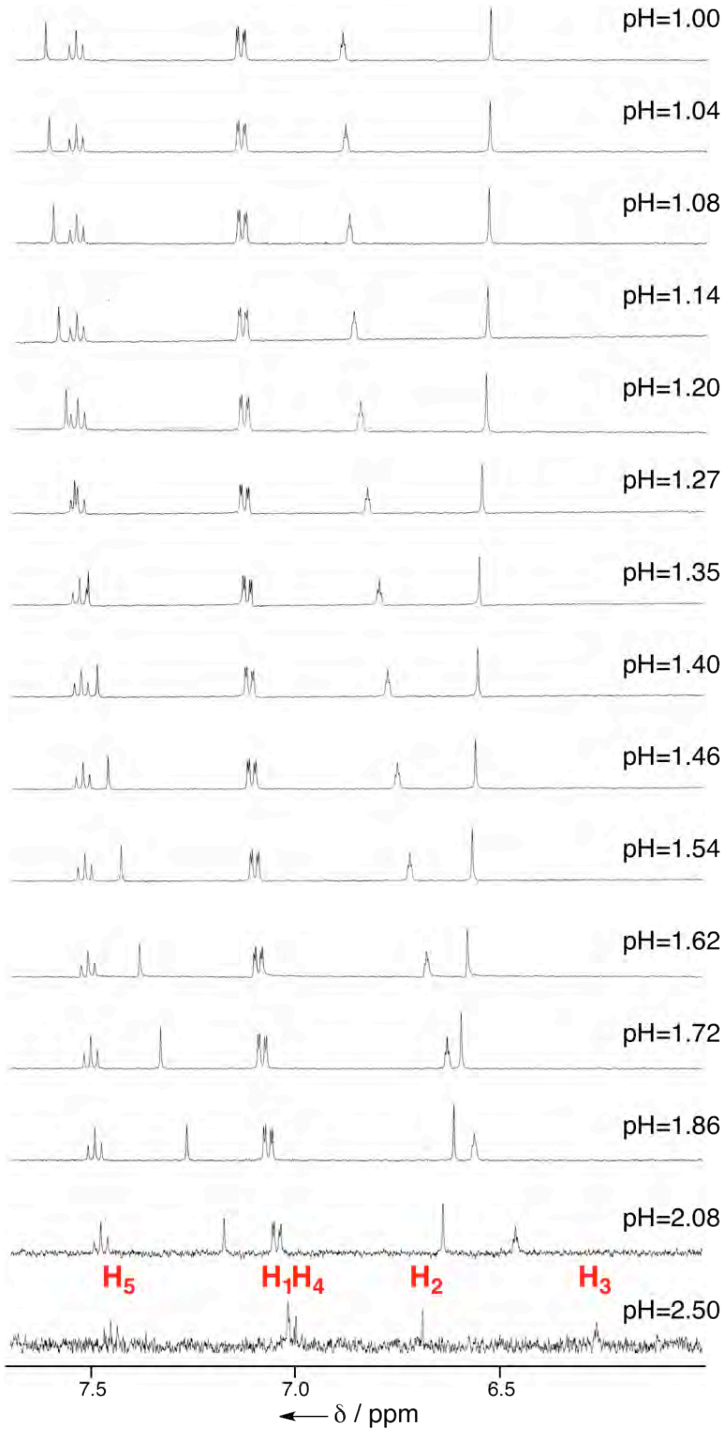

Figure 18. ^{1}H NMR spectra (500 MHz, 298 K, D_2O/DCl) for the titration of **66** with DCl (1 M).

Given the limited solubility of **66**·4H$^+$ at pH > 2.5, UV-Vis spectroscopy was selected for the determination of the four protonation constants of tetraamine **66**.

To this end, solutions of the tetraammonium tetrachloride salt in 0.1 M HCl ([**66**·4HCl] in the $3 \times 10^{-5} - 5 \times 10^{-6}$ M range) were titrated with a 0.1 M NaOH solution.

Sets of spectra recorded at different pH were analysed with the HypSpec[57] software, to determine the values of the four protonation constants. Typical absorbance spectra of aqueous solutions of **66**·nH$^+$, recorded at different pH values, are shown in **Fig. 19**.

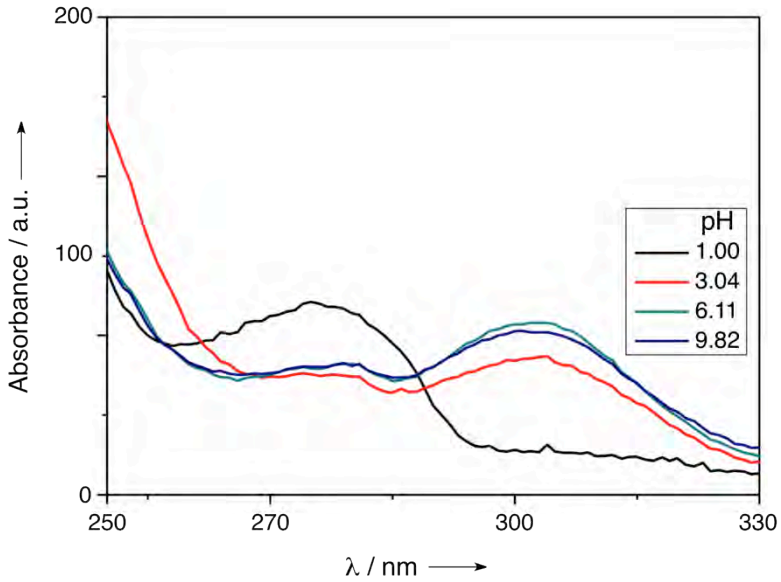

Figure 19. Absorbance spectra of **66**·nH$^+$ at selected different pH values (inset); [**66**·4HCl] = 3.0×10^{-5} M, (T = 298.15 K).

The spectrum recorded at pH>9 was confidently assigned to the tetra-amino oxacalixarene **66** and consequently, in the following calculations, the molar extinction coefficient at any given wavelength was obtained from the corresponding absorbance value of a solution of known concentration.

Extinction coefficients of the other protonated species (**66**·nH$^+$), on the hand, were calculated by the HypSpec software after the optimization of the protonation constants.

In this manner, once the percentage of formation of a given protonated species has been determined, it is then possible to calculate the absorbance of each species. In the case under study here, the fully-protonated **66**·4H$^+$ species displays a characteristic band centred at λ = 276 nm, whereas all the other **66**·nH$^+$species (with n = 0–3) show absorbance maxima at λ = 302 nm (**Fig. 19**).

HypSpec analysis of the data recorded at different pH values gave the following protonation constants values: log K^{H}_{1} = 4.39 ± 0.04, log β^{H}_{2} = 8.19 ± 0.04, log β^{H}_{3} = 10.74 ± 0.06, log β^{H}_{4} = 12.58 ± 0.06 according to eq. (1) and log K^{H}_{1} = 4.39 ± 0.04, log K^{H}_{2} = 3.80 ± 0.04, log K^{H}_{3} = 2.55 ± 0.06, log K^{H}_{4} = 1.84 ± 0.06 according to eq. (2) (see **Table 1**)

nH$^+$ + **66** = **66**·nH$^+$ $\quad\quad$ β^{H}_{n} (overall) $\quad\quad$ (1)

H$^+$ + **66** (n - 1) H$^+$ = **66**·nH$^+$ $\quad\quad$ K^{H}_{n} (stepwise) $\quad\quad$ (2)

Table 1. Protonation constants (T = 298.15±0.1 K, I = 0.1 M) of oxacalix[4]arene **66**·4HCl.

	n = 1	n = 2	n = 3	n = 4
log β^{H}_{n}	4.39±0.04	8.19±0.04	10.74±0.06	12.58±0.06
log K^{H}_{n}	4.39±0.04	3.80±0.04	2.55±0.06	1.84±0.06

Once the protonation constants are known, the **66**·nH$^+$ species distribution as a function of the pH can be calculated by using the HySS[58] software.

The distribution diagram of the different **66**·nH$^+$ protonated species formed, in the 1–7 pH range at T = 298.15 K, from a 10^{-5} M aqueous solution of **66**·4HCl is shown in **Fig. 20**.

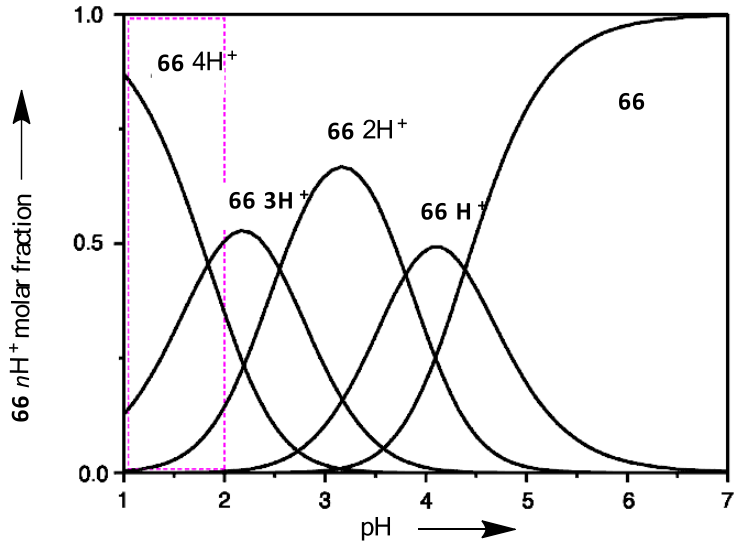

Figure 20. Distribution diagram of the **66**·nH$^+$ protonated species at [**66**·4HCl] = 10^{-5} M, I = 0.1 M and T = 298.15 K.

1.2.3. Recognition of dicationic methyl viologen: overcoming electrostatic repulsion

A preliminary screening was carried out to gain information on the affinity of the oxacalixarene for a range of different neutral and charged guests. The ^{1}H NMR of [**66**·4HCl] = 10^{-3} M in D_2O/DCl at pH = 1.6 showed, rather surprisingly, that upon addition of dicationic methyl viologen (paraquat) dichloride [PQT^{2+}·$2Cl^-$], the resonances belonging to the positively charged macrocycle (H_5 and H_1, in particular) underwent small but significant, guest concentration-dependent shifts.

A 2D ROESY spectrum, carried out on a 1:4 host-to-guest solution, shed light on the topological features of this complexation event, showing NOE cross-peaks between the H_α and H_β of the paraquat unit and the H_1, H_4 and H_5 hydrogen atoms of the receptor, indicating that the guest molecule nests within the cleft generated by the two π-rich aromatic units of **66**·nH$^+$ (**Fig. 20**).

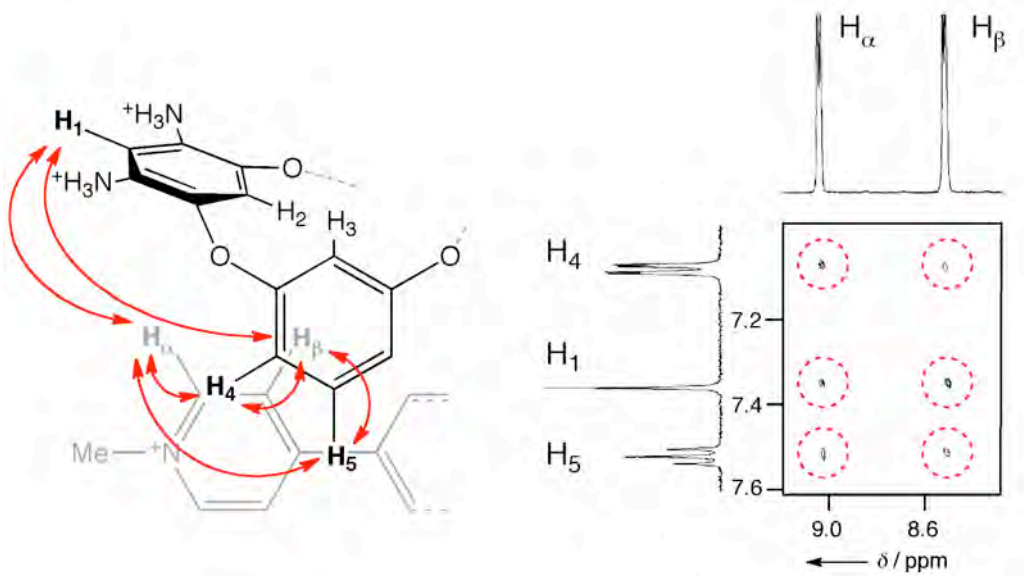

Figure 20. Section of the 2D ROESY spectrum (500 MHz, 298 K, D_2O, pH = 1.6) of the PQT^{2+}⊂**66**·nH$^+$ complex: [**66**·4HCl] = 10^{-3} M; [PQT·2Cl] = 4×10^{-3} M.

The host-guest system was found to be in fast exchange regime on the NMR timescale. Being aware that at pH = 1.6 there are no less than three protonated forms of **66**, and that as a result the observed resonances are the weighted averaged of up to six species (the 'free' receptors **66**·4H$^+$, **66**·3H$^+$ and **66**·2H$^+$, along with PQT^{2+}⊂**66**·4H$^+$, PQT^{2+}⊂**66**·3H$^+$ and PQT^{2+}⊂**66**·2H$^+$), five ^{1}H NMR titrations at different fixed pH values (in the 1.0 < pH < 2.0 range) were carried out, with the aim of gathering sufficient data to unravel the multiple equilibrium and quantify all the microconstants relative to the individual host-guest events (**Fig. 21**).

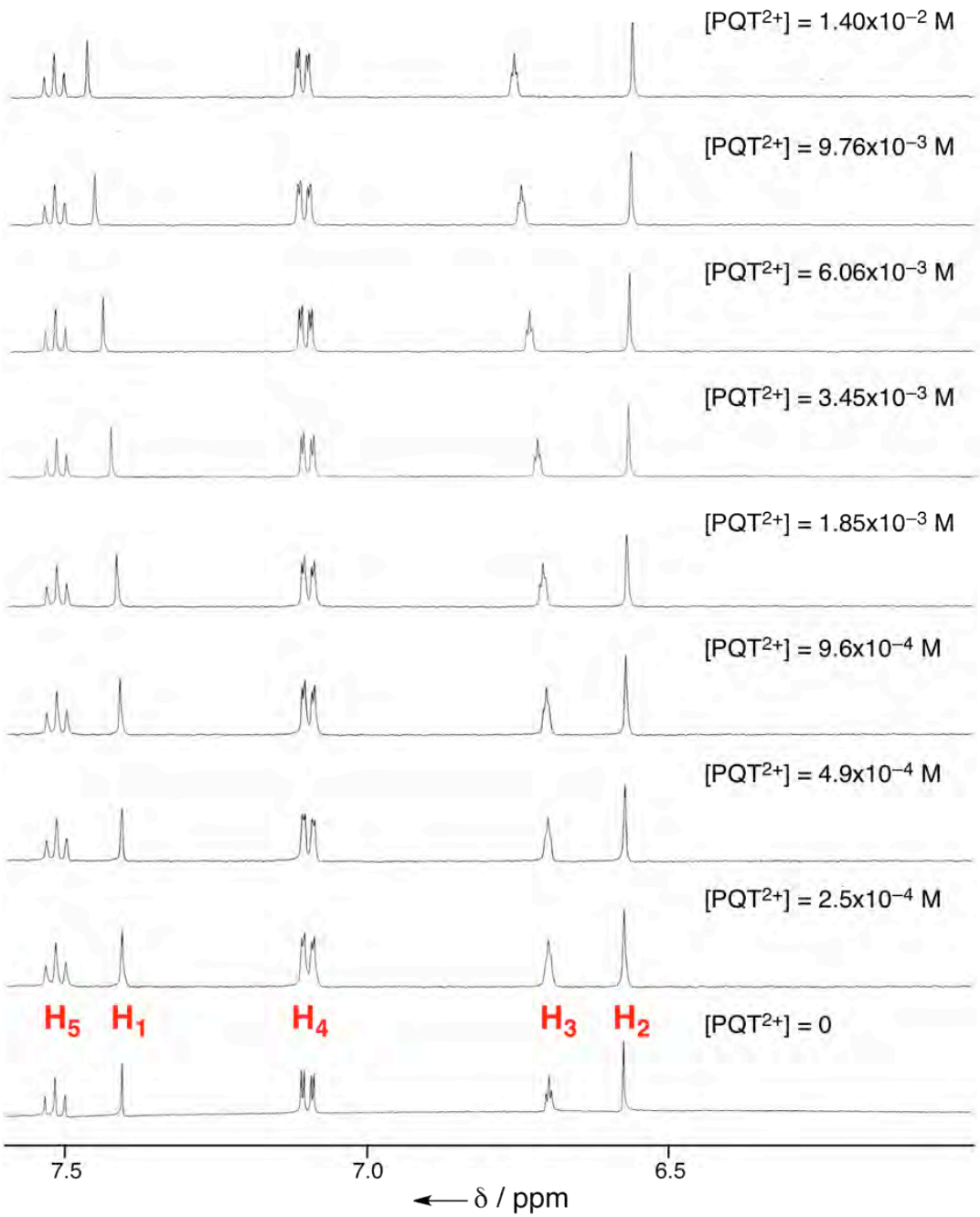

Figure 21. ^{1}H NMR spectra (500 MHz, 298 K, D_2O/DCl, pH = 1.59) for the titration of **66**·4HCl (10^{-4} M) with PQT·2Cl (2.5×10^{-2} M).

The association process of **66**·nH$^+$ with PQT^{2+} is expressed by eqs. (3) and (4) For an easier comparison with the UV-Vis data, given that deuterated chemicals were used throughout the NMR measurements, pH values were recalculated from pD measurements by applying the appropriate correction.[§§]

$$n\mathrm{H}^+ + \mathbf{66} + \mathrm{PQT}^{2+} = [\mathrm{PQT}^{2+}\subset\mathbf{66}\cdot n\mathrm{H}^+] \qquad \beta^{\mathrm{H}}_{\mathrm{n}}\ \text{(overall)} \qquad (3)$$

$$\mathbf{66}\cdot n\mathrm{H}^+ + \mathrm{PQT}^{2+} = [\mathrm{PQT}^{2+}\subset\mathbf{66}\cdot n\mathrm{H}^+] \qquad K^{\mathrm{H}}_{\mathrm{n}}\ \text{(stepwise)} \qquad (4)$$

Data analysis was carried out with the HypNMR[59] software.

Given that titrations were run at fixed pH values, the protonation constants of the **66**·nH$^+$ species can be ignored during the determination of the apparent host-guest formation constant (K_{app} eq. 5). K_{app} is pH-dependent, as its value depends on the percentage of formation, at given pH, of the different protonated species of the host and their relative affinity for the guest considered.

$$K_{app} = \frac{[\mathrm{PQT}^{2+}\subset\mathbf{66}\cdot n\mathrm{H}^+]}{[\mathrm{PQT}^{2+}]\,[\mathbf{66}\cdot n\mathrm{H}^+]} \qquad (5)$$

In this eq. [**66**·nH$^+$] and [PQT^{2+}⊂**66**·nH$^+$] account for the total concentration of all the species at a different protonation state that may participate to the equilibrium.

Data in **Table 2** and **Fig. 22** as well, show that the contribution of the **66**·2H$^+$ specie to the binding of PQT^{2+} is negligible, as the value of K_{app} rapidly drops to zero soon

[§§] pH values were obtained from pD measurements by applying the appropriate correction factor. See: Bates, R.G., *Determination of pH: Theory and Practice*, John Wiley & Sons: New York, **1973.**

after this species begins to form. This is likely to be caused by a precipitation process observed at pH>2.

Table 2. Dependence on pH of the log K_{app} of the interaction between **66**·4HCl and PQT·2Cl at T = 298.15 K.[a]

[DCl]	pH	log K_{app} [a]	% **66**·4H$^+$	% **66**·3H$^+$	% **66**·2H$^+$	% **66**·H$^+$	% **66**
0.100	0.97	n.d.[b]	87.06	12.58	0.35	–	–
0.075	1.35	1.44±0.03[c]	74.40	24.08	1.41	0.01	–
0.050	1.48	2.29±0.02	67.85	29.62	2.52	0.01	–
0.025	1.59	1.70±0.04	61.56	34.62	3.80	0.02	–
0.010	1.99	n.d.[b][d]	34.97	50.55	14.25	0.23	–

[a] Average of two measurements. [b] n.d.: not detected

[c] Confidence interval (C.I.). [d] Precipitation of the oxacalixarene did not allow to measure log K_{app}.

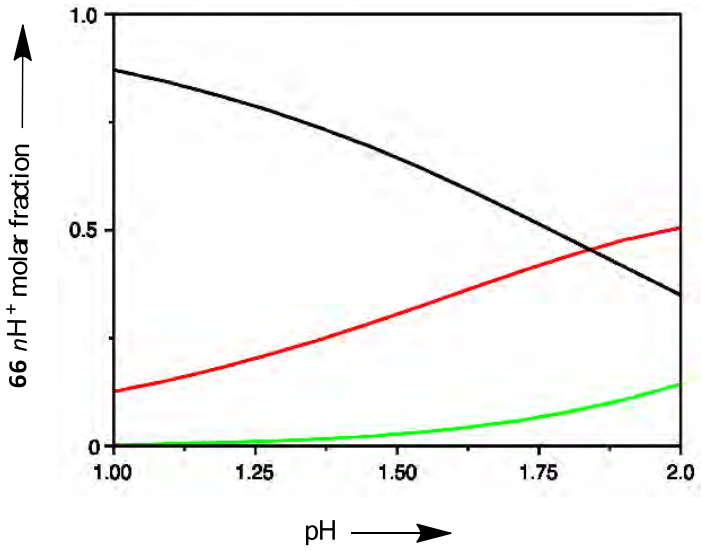

Figure 22. Distribution diagram of the **66**·nH$^+$ protonated species at [**66**·4HCl] = 1 × 10^{-5} M, I = 0.1 M and T = 298.15 K, in the range 1.0 < pH < 2.0.

If only [PQT^{2+}⊂**66**·3H^+] and [PQT^{2+}⊂**66**·4H^+] species are considered, given that PQT^{2+}does not undergo acid-base equilibria and knowing the mass balance eq. of **66**·*n*H^+, the eq. 5 can write as follows :

$$K_{app} = \frac{[PQT^{2+}\subset\mathbf{66}\cdot 3H^+ + PQT^{2+}\subset\mathbf{66}\cdot 4H^+]}{[PQT^{2+}]\,[\mathbf{66}\cdot 3H^+ + \mathbf{66}\cdot 4H^+]} \quad (6)$$

Calculating [PQT^{2+}⊂**66**·3H^+] and [PQT^{2+}⊂**66**·4H^+] from the formation constants of eq. (4) we have :

$$K_{app} = \frac{[PQT^{2+}]\,\{K_3[\mathbf{66}\cdot 3H^+] + K_4[\mathbf{66}\cdot 4H^+]}{[PQT^{2+}]\,[\mathbf{66}\cdot 3H^+ + \mathbf{66}\cdot 4H^+]} \quad (7)$$

Simplifying and calculating [PQT^{2+}⊂**66**·3H^+] and [PQT^{2+}⊂**66**·4H^+] from the formation constants of eq. (1)

$$K_{app} = \frac{K_3\,\beta^{H}_{3}\,[H]^3\cdot[\mathbf{66}] + K_4\,\beta^{H}_{4}\,[H]^4\cdot[\mathbf{66}]}{\beta^{H}_{3}\,[H]^3\cdot[\mathbf{66}] + \beta^{H}_{4}\,[H]^4\cdot[\mathbf{66}]} \quad (8)$$

Equation (8) can be simplified as follows:

$$K_{app} = \frac{K_3\,\beta^{H}_{3}\,[H]^3 + K_4\,\beta^{H}_{4}\,[H]^4}{\beta^{H}_{3}\,[H]^3 + \beta^{H}_{4}\,[H]^4} \quad (9)$$

Knowing the K_{app} at different pH value (**Table 2**) as well as the protonation constants of the **66**·nH$^+$ species, the formation constants of the different host-guest species can be easily calculated by non-linear least square treatment (the LIANA[60] software was used for this study).

Accordingly, K_3 and K_4 were found to be 253 ± 50 and <1 M^{-1}, respectively.

This evidence, along with the marked log K_{app} decrease observed on lowering the pH, indicates that in the 0.97–1.48 range –where the only two oxacalixarene species present are the tetra- and tri-protonated forms (**Fig. 22**)– only the tricationic macrocycle **66**·3H$^+$ is able to significantly interact with the methyl viologen dication.

A deeper insight into the structural features of **66**·nH$^+$ – and its proclivity to act as molecular tweezers towards paraquat – was gathered by means of a geometry optimization study carried out at the density functional level of theory (B3LYP functional, 6-31G(d) basis set). All the possible protonation states were examined (**Fig. 23**), with the added care of considering two different isomers for **66**·2H$^+$ (i.e., a C_2 and a C_S symmetric one, depending on the protonation pattern on opposite amino-bearing rings).

All protonated species possess the typical oxacalix[4]arene saddle-shaped conformation. Progressive protonation, however, has a dramatic effect on the interplanar angles between the pairs of aromatic rings facing each other. The free base **66** is seen with almost coplanar amino-bearing rings (30.8°) and spread-apart dioxaphenylene rings (76.0°).

The first protonation step has almost no effect on the overall conformation of **66**·H$^+$, but once the second proton comes into play (**66**·2H$^+$), electrostatic repulsion drives the two ammonium-bearing rings away from each other, forcing a marked narrowing of the interplanar angle between the electron-rich rings.

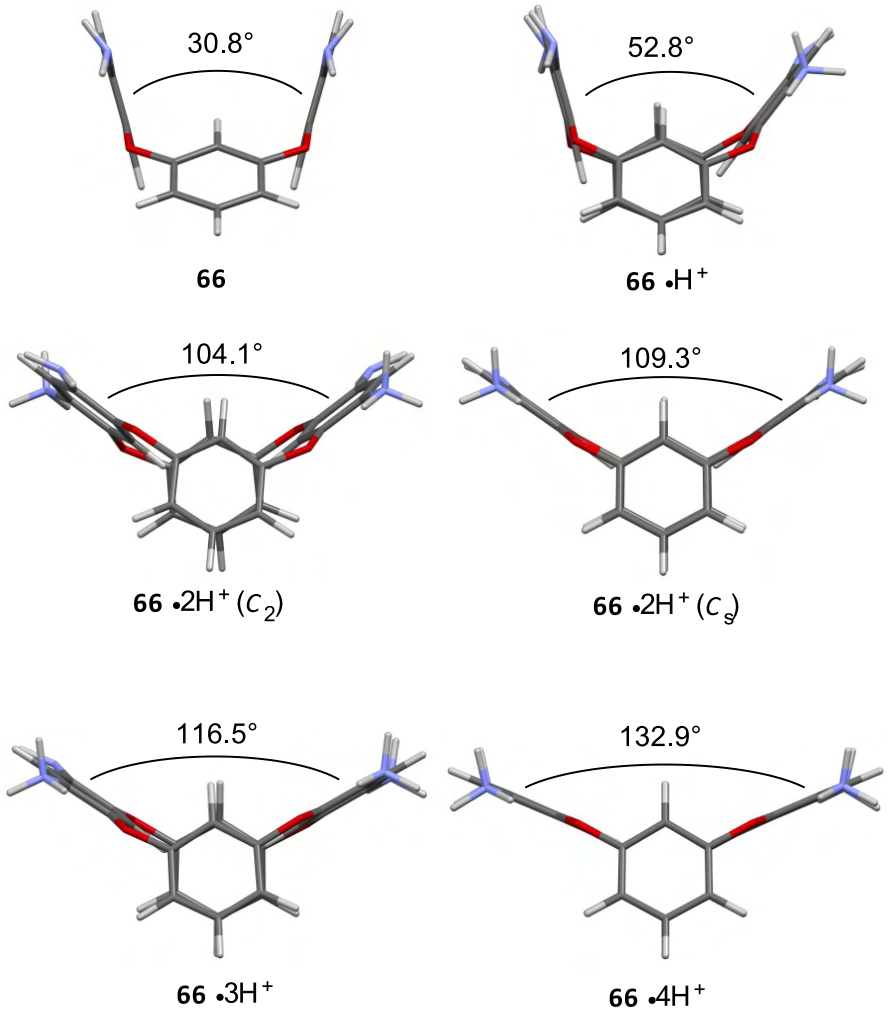

Figure 23. Calculated gas-phase geometries (DFT, B3LYP/6-31G(d)) of oxacalixarene **66**·nH$^+$ (n = 0–4).

Repulsion increases with additional protonation, resulting in a further narrowing of the interplanar angle (37.8° and 34.7° for **66**·3H$^+$ and **66**·4H$^+$, respectively) that effectively preorganises the molecular tweezers for paraquat complexation (in the case of **66**·3H$^+$ a cleft with a edge-to-edge distance of 6.6 Å allows for a close-to-ideal match with the *ca.* 3.4 Å thick paraquat guest).

However, even though **66**·2H$^+$, **66**·3H$^+$, and **66**·4H$^+$, all appear to be a suitable receptors for paraquat, only **66**·3H$^+$ is able to efficiently recognize the dication guest, thus finding the best trade-off between host-guest positive charge repulsion and π-π interaction (**Fig. 24**): **66**·2H$^+$ is not soluble enough, whereas in the case of **66**·4H$^+$ – even in the presence of the highest chloride concentration– repulsion clearly overcomes attractive interactions.

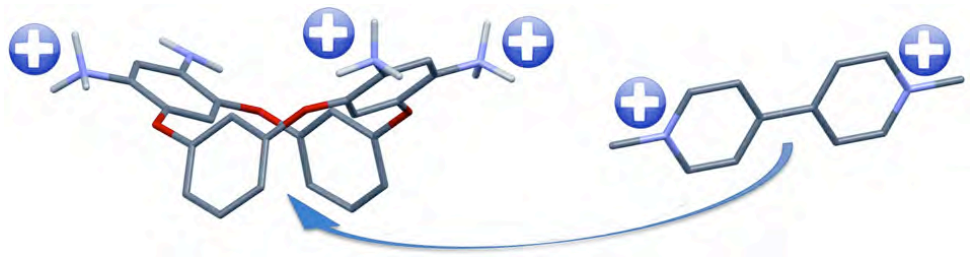

Figure 24. Representation of interaction between **66**·3H$^+$ and PQT^{2+}

1.2.4. Recognition of 2,7-dihydroxynaphtalene: hydrophobic effect

Intrigued by the unusual properties of the macrocycle **66**·4HCl, with the aim to gathering further information on its binding behaviour we tested its affinity towards neutral guests ranging from neutral aromatic hydrocarbons (i.e., naphthalene, anthracene, pyrene) to acidic (naproxen[61]) and anionic (sodium tosylate) species but all to no avail.

Based on ^{1}H NMR analysis, none of the three neutral hydrocarbons dissolved in a D_2O/DCl solution (pH = 1.91) containing **66**·4HCl (10^{-4} M), even upon extensive sonication, while binding of naproxen and sodium tosylate to **66**·4HCl (10^{-4} M in D_2O/DCl, pH = 1.91) was ruled out because there were no detectable complexation-induced shifts (CISs) of the oxacalixarene resonances upon excess guest addition (50

equiv.). Surprisingly, though, given the supposedly π-rich nature of the recognition cleft – which is composed of two facing resorcinol rings – addition of 2,7-dihydroxynaphthalene (henceforth referred to as DHN) to a 10^{-4} M solution of **66**·4HCl in D_2O/DCl (pH = 1.91) showed small but significant CISs of the ^1H NMR resonances of the receptor.[***]

Similar to the case of paraquat mentioned above, the new host–guest system was found to be in a fast exchange regime on the NMR timescale. Progressive addition of the DHN guest to an oxacalixarene solution resulted in concentration-dependent CISs of the key probe resonances belonging to the intra-annular hydrogen atoms of the macrocyclic receptor (i.e., H_2 and H_3), indicative of an interaction between the DHN guest and the aromatic cleft of the oxacalixarene.

Contrary to the case of the $PQT^{2+}\subset$**66**·nH$^+$ complex, where the two probe resonances were seen to undergo downfield shifts, upon titration with the π-rich DHN molecule the resonances of **66**·nH$^+$ underwent upfield shifts (**Fig. 25**).

Given that H_2 and H_3 belong to different aromatic moieties of the macrocycle – H_3 to the resorcinol rings, H_2 to the ammonium-bearing rings – it is likely that the observed CISs on these two probe resonances are not a consequence of π-stacking alone. These resonances are known to be particularly sensitive to tiny conformational modifications, H_2 and H_3 being shielded by the adjacent resorcinol and *m*-phenylenediammonium moieties, respectively. It is reasonable to envisage that the oxacalixarene may slightly rearrange its conformation, depending on the electronic nature of the guest, to fit within its cleft either an electron-deficient or an electron-rich substrate.

[***] Preliminary experiments showed that, upon addition to an oxacalixarene solution, isomeric 1,5-dihydroxynaphthalene also induces small CISs to the receptor resonances. Given the structural similarity between the two substrates, we decided to focus our attention on 2,7-dihydroxynaphthalene only. However, this observation seems worth mentioning, as it provides further evidence of the significant role played by hydroxyl groups in the complexation process.

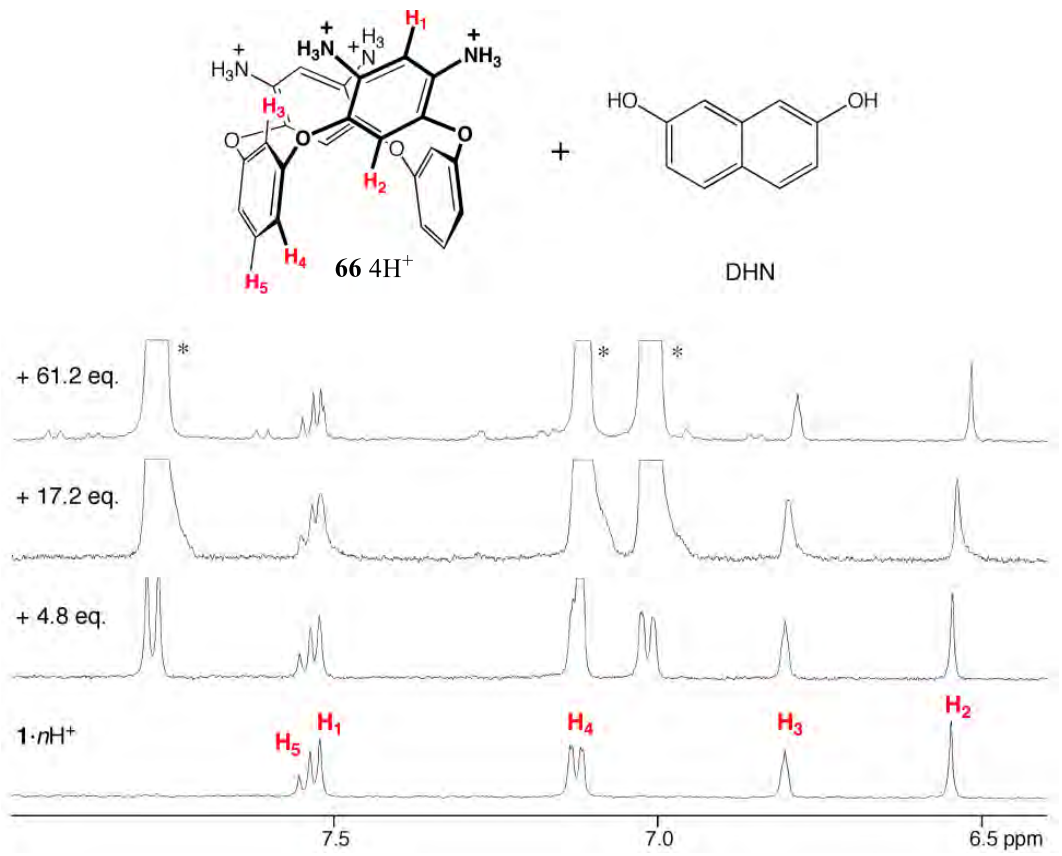

Figure 25. Selected ^{1}H NMR spectra (500 MHz, 25 °C, D_2O/DCl) recorded upon titration of [**66**·nH$^+$] = 10^{-4} M with 2,7-dihydroxynaphthalene at pH = 1.91. Asterisks indicate guest resonances.

As a consequence of the fast-exchange regime, resonances are the weighted average of all the species present at a given concentration and pH, and individual titration experiments may only yield a K_{app} (eq. (5), replacing PQT^{2+} with DNH) that account for the overall equilibrium involving all the free and complexed species.

Combining K_{app} with the four protonation constants of tetraamino-oxacalixarene **66** (see eq. (1) and (4)) and extracting [DHN⊂**66**·2H$^+$], [DHN⊂**66**·3H$^+$] and [DHN⊂**66**·4H$^+$] from the individual association constants (K_n) of equation (4), we obtain eq. (10) that in turn can be simplified in eq. (11)

$$K_{app} = \frac{[DHN]\ \{ K_2[\mathbf{66}\cdot 2H^+] + K_3[\mathbf{66}\cdot 3H^+] + K_4[\mathbf{66}\cdot 4H^+]\}}{[DHN]\ \{[\mathbf{66}\cdot 2H^+]+[\mathbf{66}\cdot 3H^+]+[\mathbf{66}\cdot 4H^+]\}} \quad (10)$$

$$K_{app} = \frac{K_2\,\beta^H{}_2\,[H]^2 + K_3\,\beta^H{}_3\,[H]^3 + K_4\,\beta^H{}_4\,[H]^4}{\beta^H{}_2\,[H]^2 + \beta^H{}_3\,[H]^3 + \beta^H{}_4\,[H]^4} \quad (11)$$

Assuming a 1:1 binding mode, the combination of the K_{app} values at different pHs (see **Table 3**) with the protonation constants of the **66**·nH$^+$ species (see above) provides the association constants of the different host–guest species.

Accordingly, the association constants for the DHN⊂**66**·2H$^+$, DHN⊂**66**·3H$^+$ and DHN⊂**66**·4H$^+$ complexes (i.e., K_2, K_3 and K_4) were found to be 16 ± 15, 44 ± 4 and <1 M^{-1}, respectively.

A comparison between the association constants of DHN⊂**66**·nH$^+$ with those reported for the binding of paraquat dichloride lead to some interesting observations. First, and most evident, of all the possible protonated receptors, the triprotonated **66**·3H$^+$ species is again the only one able to significantly act as a receptor towards an aromatic guest molecule, albeit with an association constant of just 44 ± 4 M^{-1}. The tetracationic species **66**·4H$^+$ does not show any significant affinity, possibly as a consequence of a less favourable resorcinol–resorcinol interplanar angle. The latter, in fact, progressively narrows upon increasing the number of positive charges on the amino-ammonium-bearing rings, making the aromatic cleft less and less available for complexation.

Table 3. pH dependence of the log K_{app} of the interaction between **66**·nHCl and 2,7-dihydroxynaphthalene (DHN) at T = 25 °C.[a]

			% of formation				
[DCl] (M)	pH	log K_{app} [a]	**66**·4H$^+$	**66**·3H$^+$	**66**·2H$^+$	**66**·H$^+$	**66**
0.099	1.00	0.21±0.15 [b]	87.06	12.58	0.35	0.00	0.00
0.063	1.33	0.26±0.15 [b]	75.32	23.28	1.40	0.00	0.00
0.024	1.62	1.11±0.12 [b]	59.59	36.11	4.27	0.03	0.00
0.012	1.91	1.49±0.07 [b]	41.02	47.92	10.92	0.14	0.00
0.006	2.24	1.40±0.06 [b]	21.07	52.61	25.62	0.70	0.00

[a] Average of two measurements. [b] 95% confidence interval (C.I.).

As for the dicationic receptor **66**·2H$^+$, the analysis of our titration data provided a rather small association constant value with a large margin of error (K_2 = 16 ± 15 M^{-1}), which should be cautiously treated as merely indicative of a very weak interaction. It should be noted, however, that in our previous study, **66**·2HCl was found to precipitate when titration with paraquat dichloride was attempted at a pH > 2.0, most probably as a result of the increase in ionic strength – and in Cl^- concentration – deriving from titrating with a saline guest.

Structural data on the binding of the DHN guest to oxacalixarene **66**·3H$^+$ came from computational studies. Preliminary attempts at obtaining an optimised geometry for the DHN⊂**66**·3H$^+$ complex *in vacuo* failed, as the DHN guest would be extruded from the receptor binding cleft.

It was therefore envisaged that placement of the receptor – with its three chloride counterions – and the guest within a cluster of 200 explicit solvent molecules (H_2O) would provide a more accurate description of the binding event. PM6 semiempirical calculations yielded a minimum energy geometry of the DHN⊂**66**·3H$^+$ complex,

providing indirect evidence of the nature of the interaction holding the complex together in aqueous solution (**Fig. 26**). Within the water cluster, the guest is seen lying askew within the cavity of the receptor, with the hydroxyl groups pointing away from the oxacalixarene cavity to take advantage of hydrogen bonding interactions with the surrounding water molecules. In addition, the resorcinol rings of the receptor open up (interplanar angle: 71.8°) to accommodate the hydrophobic portion of the DHN guest. Interestingly, such a widening of the interplanar angle is consistent with the CIS observed during the ^{1}H NMR titrations described above.

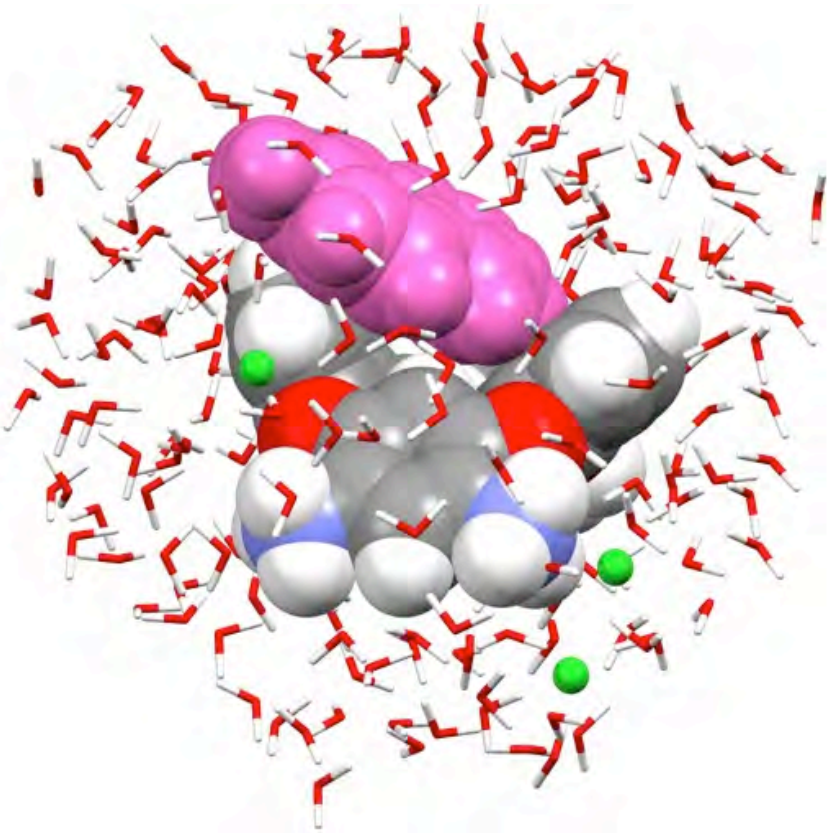

Figure 26. Optimised geometry (PM 6) of the complex between DHN (coloured in pink) and **66**·3HCl in a cluster containing 200 explicit water molecules.

The geometry obtained suggests that π-stacking may not be the only – or the main – interaction responsible for the formation of DHN⊂**22**·3H^{+}, but that hydrophobic[62]

and solvent effects[63] most probably play a key role in stabilising the host–guest complex. Further studies are in progress to define the enthalpic and entropic contributions to the binding free energy, which may provide further – and definitive – evidence of the nature of the interaction involved in the formation of the complex under investigation.

1.2.5. Tetraamino-dihydroxy-oxacalix[4]arenes: improving water-solubility

From the beginning, our research was guided by the tempting idea of water-soluble oxacalixarenes. Encouraged by the results obtained with the tetraamino-derivative **66**, we turned our attention to similar compounds such as [4,6,16,18]tetra-amino[11,23]dihydroxycalix[4]arene **68**·2H and [4,6,16,18]tetra-amino[25,27]dihydroxycalix[4]arene **70**·2H, in which the introduction of two ionisable phenolic groups on the oxacalixarene skeleton could lead to an increased water solubility.

Taking advantage of the procedures reported by Katz,[19] a S_NAr reaction between 1,5-dichloro-2,4-dinitrobenzene and pyrogallol (1,2,3-trihydroxybenezene) in DMSO, using K_2CO_3 as the base, yielded the tetra-nitro precursor **67**, that after a Raney-Ni-catalysed reduction was converted in the corresponding tetra-amino macrocycle **68**·2H (**Scheme 12**).

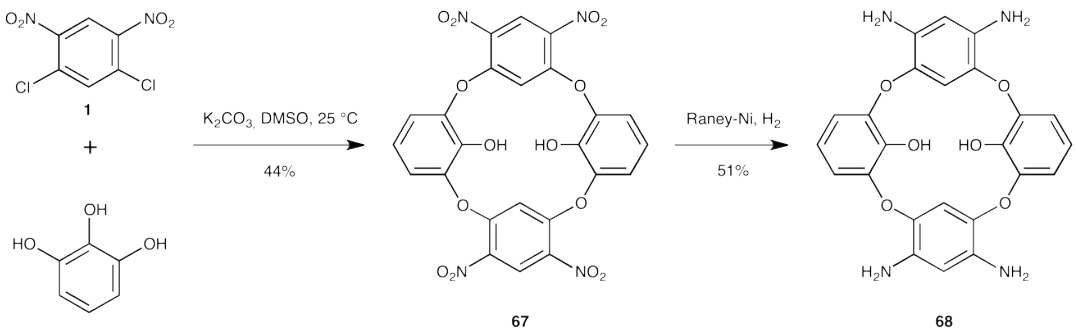

Scheme 12. Synthesis of [4,6,16,18]tetra-amino[11,23]dihydroxycalix[4]arene **68**·2H.

The same synthetic route was employed for the synthesis of **70**·2H, replacing pyrogallol with phloroglucinol (1,3,5-trihydroxybenezene, **scheme 13**) even though this latter reaction afforded the product in a lower yield (26% *vs.* 44%), as a consequence of a competitive macrobicyclization reaction.

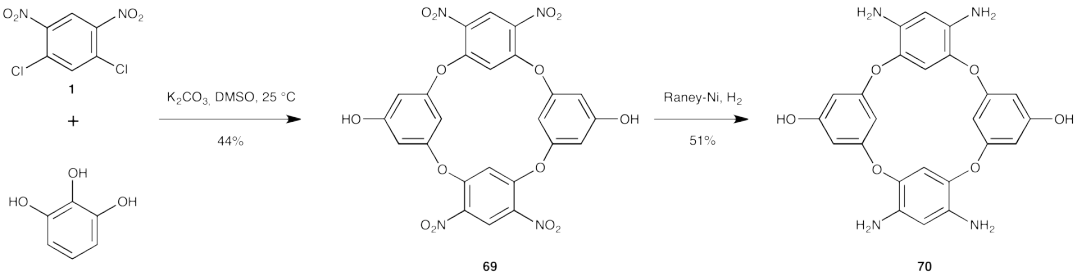

Scheme 13. Synthesis of [4,6,16,18]tetraammino[25,27]dihydroxycalix[4]arene **70**·2H.

Again, to gather a full picture in water on the distribution of the different protonated species **68**·nH$^{(n-2)+}$ and **70**·nH$^{(n-2)+}$ (in these cases, n = 0-6) across the full pH range (1.0 < pH < 10.0), we followed the same approach we used for the compound **66**, performing several UV-Vis titrations.

We started from acid conditions (pH<1) of a solution of macrocycle (either **68**·2H or **70**·2H) in a concentration range between 1.39×10^{-5} M and 6.4×10^{-5} M, and adding to it fixed aliquots of 0.1 M NaOH solution.

Analysis of absorption spectra sets recorded at different pH values provided the protonation constants of all the possible species generated by subsequent protonation of compounds **68**·2H and **70**·2H, according to eqs. (1) and (2), noting tough that these macrocycles possess six ionisable sites (two phenolic OH groups on top of the four NH_2 groups).

Table 4. Protonation constants (T = 298.15 K, I = 0.1 M) of **68**·nH$^{(n-2)+}$.

	n = 1	n = 2	n = 3	n = 4	n=5	n=6
log k^{H}_{n}	10.13±0.01	6.50±0.03	5.69±0.02	3.91±0.06	2.80±0.06	1.85±0.01
log β^{H}_{n}	30.88±0.01	20.75±0.03	14.25±0.02	8.56±0.06	4.65±0.06	1.85±0.01

Table 5. Protonation constants (T = 298.15 K, I = 0.1 M) of **70**·nH$^{(n-2)+}$.

	n = 1	n = 2	n = 3	n = 4	n=5	n=6
log k^{H}_{n}	10.75±0.02	8.71± 0.01	5.99±0.02	4.63±0.02	2.73±0.04	1.89±0.07
log β^{H}_{n}	34.70±0.02	34.70±0.02	15.24±0.02	9.25±0.02	4.62±0.04	1.89±0.07

The protonation constants obtained after a refining with the HypSpec software are reported in **Tables 4** and **5**. **Fig. 27** and **28** detail the species distribution for **68**·nH$^+$ and **70**·nH$^+$ obtained with the HySS software (see above).

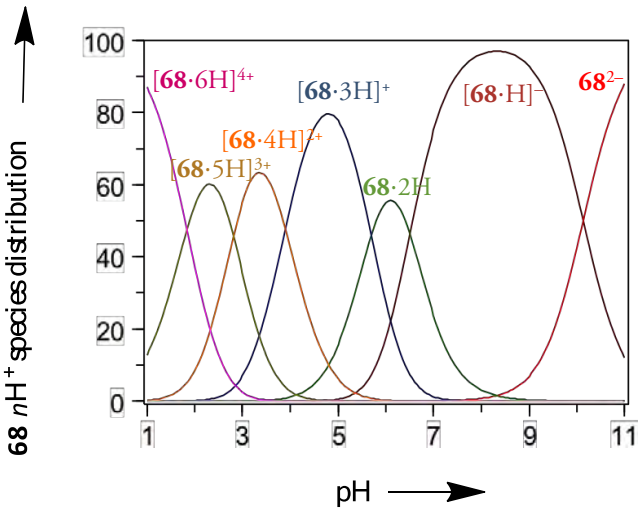

Figure 27. Distribution diagram of the **68***n*H$^{(n-2)+}$ protonated species at [**68**·2H] = 10^{-5} M, I = 0.1 M and T = 298.15 K.

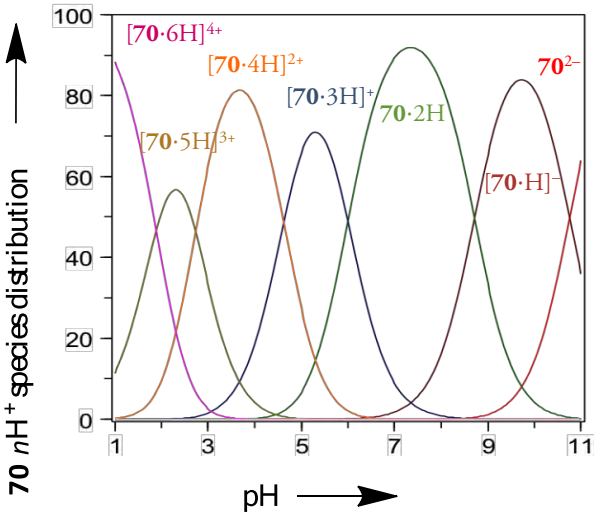

Figure 28. Distribution diagram of the **70**·*n*H$^+$ protonated species at [**70**·2H] = 10^{-5} M, *I* = 0.1 M and T = 298.15 K.

Remarkably, the solubility of **68**·2H and **70**·2H is slightly higher than the parent oxacalix[4]arene **66**, and they are soluble also in a basic pH interval.

Protonation constants of **70**·2H are slightly higher than those of **68**·2H, in agreement with the behaviour of the corresponding starting materials phloroglucinol and pyrogallol, while the better stability – much higher permanence range – of the monoprotonated derivative **68**·H^- (see **Fig. 27**) could be ascribed to a hydrogen bonding interaction between the two oxygen atoms in the intra-annular positions, that hampers further deprotonation.

A conformational analysis was carried out using the Spartan'10 software (DFT, B3LYP/6-31G(d) level of theory), providing a clear picture of the structural features *in vacuo* of the main protonated species for compound **68**·2H and **70**·2H, that is, only the fully deprotonated (i.e., X^{2-}), the neutral (X·2H) and fully-protonated species (X·$6H^{4+}$) were calculated.

Again the 1,3-alternate conformation, with the two electron rich aromatic rings in an eclipsed position, resulted the favourite one.

These optimized geometries show that upon protonation of the neutral **68**·2H and **70**·2H, the hexa-protonated forms **68**·$6H^{4+}$ and **70**·$6H^{4+}$ see a widening of the angle between the two electrophilic rings, as a consequence of an enhanced electrostatic repulsion between the charged ammonium moieties. This causes also a shortening of the interplanar distance between the two nucleophilic rings.

Conversely, the optimized structures of the fully deprotonated dianionic species, $\mathbf{68}^{2-}$ and $\mathbf{70}^{2-}$, highlighted interesting differences. In the case of $\mathbf{70}^{2-}$ the presence of two negative charges on the intra-annular positions, leads to an outwards twist of the two charged oxygen atoms that makes the rings they are attached to almost parallel to each other. In the case of $\mathbf{68}^{2-}$ on the other hand, the extra annular position of the two negative charges causes an opening of the "tweezers" angle described by the two electron-rich rings, stabilizing this rather unusual pinched-cone conformation (**Fig. 29**).

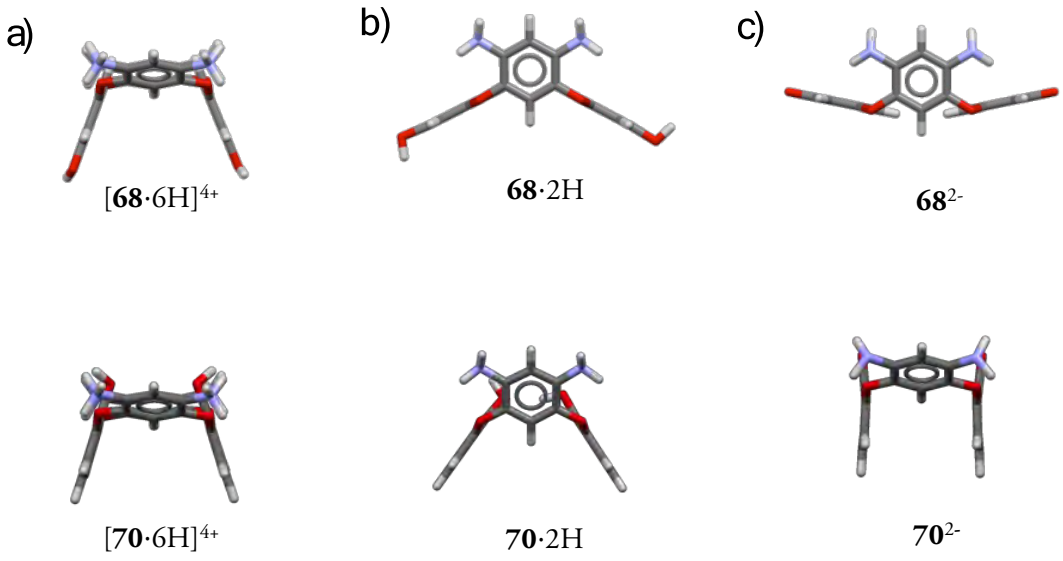

Figure 29. Calculated gas-phase geometries (DFT, B3LYP/6-31G(d)) of: a) **68**·6H^{4+}, **70**·6H^{4+}, b) **68**·2H, **70**·2H c) **68**$^{2-}$, **70**$^{2-}$.

1.2.6. Interaction with methyl viologen at a basic pH

Driven by the success of our previous work in which oxacalix derivative **66** was proved able to interact and bind efficiently the paraquat dication,[64] we undertook a similar study with compound **70**·2H.

Following the same approach, five ^{1}H NMR titrations at different pH values (1.59, 2.0, 11.0, 11.5 and 12.0) were carried out, adding increasing aliquots of PQT·2HCl to an acidic or basic solution of **70**·2H (**Fig. 30**).

As in the case of compound **66**,[64] the host-guest system was found to be in fast exchange regime on the NMR timescale. However, while the ^{1}H NMR set of spectra recorded at low pH showed a downfield shift of the probe resonances of macrocycle **70**·2H, at high pH values an upfield shift was observed.

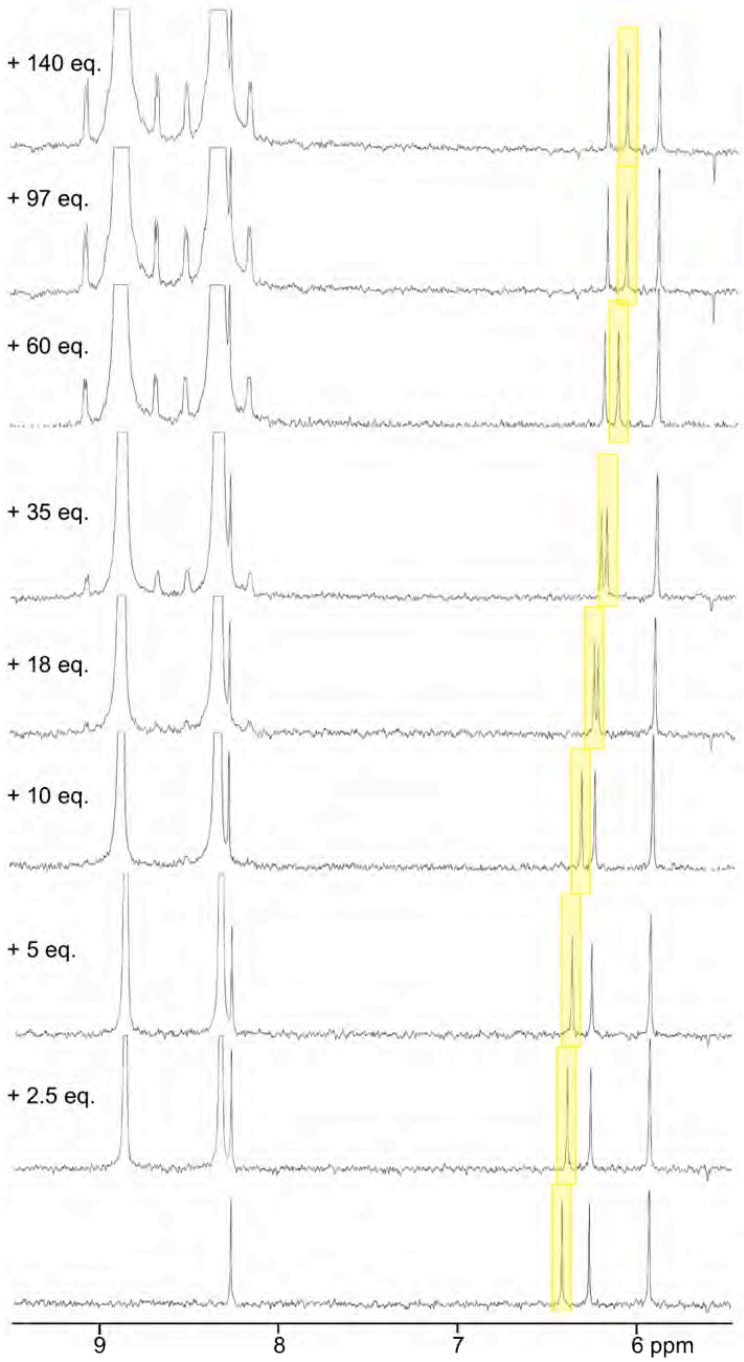

Figure 30. Sections of ^{1}H NMR spectra (500 MHz, 298 K, pH = 11.59) for the titration of **70**·2H (10^{-4} M) with PQT·2Cl (2.5×10^{-2} M).

Using eq. (5)(see above), and replacing macrocycle **66** with **70**·2H, K_{app} at all pH values was obtained, and assuming a 1:1 binding mode, through the combination of the K_{app} values with the protonation constants of the **70**·nH$^{(n-2)+}$ species (see **Table 5**), the association constants of the different host–guest species were extracted.

Remarkably, the greater stability throughout the pH range of the new receptor – due to the introduction of the two additional deprotonable sites (OH moieties) – allowed us to evaluate host-guest association also at basic pH, a range that remained unexplored in our previous study,[64] given the limited solubility of **66**·nH^{+} at pH > 2.5.

Data in **Table 6** highlighted that the apparent association constants of **70**·nH$^{(n-2)+}$⊂PQT^{2+} system in acidic conditions proceeds with a similar efficiency to that seen above for **66**·nH^{+}⊂PQT^{2+}. Moreover, at high pH values, when **70**·2H becomes negatively charged, the stability of the **70**·nH$^{(n-2)-}$⊂PQT^{2+} (n = 0,1) complexes is higher than in acidic media, as a consequence of additional electrostatic attractive interactions.

Table 6. Apparent association constants of **70**·nH$^{(n-2)+}$⊂PQT^{2+} (n = 1–6) at fixed pH values (T = 298.15 K, I = 0.1 M).

pH	log K_{app}
1.59	1.33±0.12
2.00	1.42±0.11
11.00	2.63±0.11
11.59	2.84±0.05
12.00	2.37±0.12

The host-guest interactions between **70**·2H and PQT·2Cl have been also investigated by isothermal titration calorimetry. Microcalorimetry allowed us to obtain the standard enthalpy changes, stoichiometry, equilibrium constants, standard Gibbs

energy changes and the entropy effect of the complexation processes, based on the directly calorimetric data.

To evaluate the standard enthalpy of formation for **70**·nH$^{(n-2)+}$⊂PQT^{2+} system, apparent equilibrium constants $\beta^{H}_{n\ i}$ for overall reactions have been defined as in eq. (4) (see above). Thermodynamic parameter ΔH_i at pH 11.59 were obtained by calorimetric titration showed in **Fig. 31**.

According to the thermodynamic formula:

$$\Delta G° = - R\,T \ln K \qquad (12)$$

standard changes of Gibbs free energy (ΔG°) of the complexes can be derived from apparent association constants values (K_{app}) at fixed pH.

Knowing ΔG° and ΔH°, applying eq. (13), TΔS° values can be extracted.

$$\Delta G° = \Delta H° - T\Delta S° \qquad (13)$$

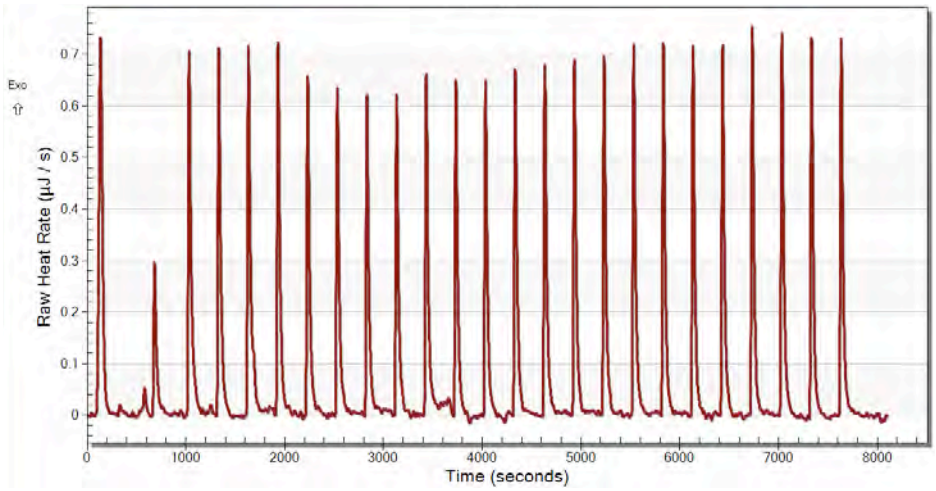

Figure 31. Variation of Raw Heat Rate as a function of time t, (pH = 11.59) for the titration of **70**·nH$^{(n-2)+}$ (10^{-4} M) with PQT·2Cl (2.5×10^{-2} M).

In **Fig. 32** the histogram detailing ΔG, ΔH° and *T*ΔS° values at pH 11.59 is reported, from which it can be concluded that the complexation event is driven mainly by hydrophobic interactions and by the release of 'high energy water' molecules from the cavity.

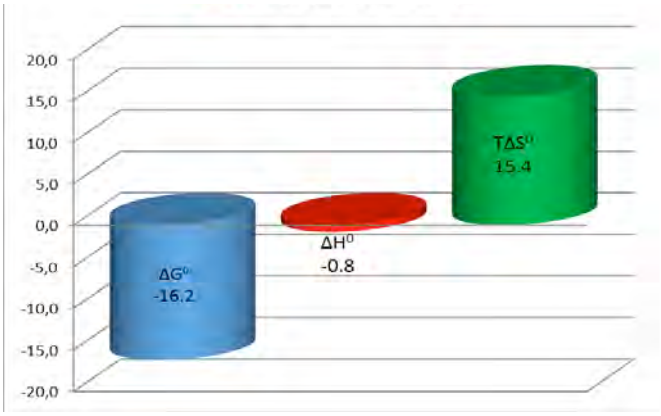

Figure 32. Histogram of **70**·nH$^{(n-2)+}$⊂PQT (pH= 11.59) system in kJ/mol.

1.2.7. Molecular cages

The design of new molecular cages has often fascinated the community of supramolecular chemists, owing to their recognition abilities as highly selective host molecules, a consequence of their strict steric requirements for host-guest matching.

Recently, Wang and co-workers reported the first example of oxygen-bridged bicyclocalixaromatics, starting from phloroglucinol as the nucleophilic component and cyanuric chloride or 2,6-dihalopyridine derivatives as the electrophilic counterpart,[65] with the aim of exploiting the aromatic cavity of the macrobicycle for selective

molecular recognition applications. The resulting cavity, however, was found too small to incorporate any guest molecule.

In 2011 the same group synthesized the first triangular prism **74** based on electron rich and electron poor building-blocks connected by triazine rings (**Scheme 14**) that, having a larger cavity, may be used in selective host-guest recognition.[66]

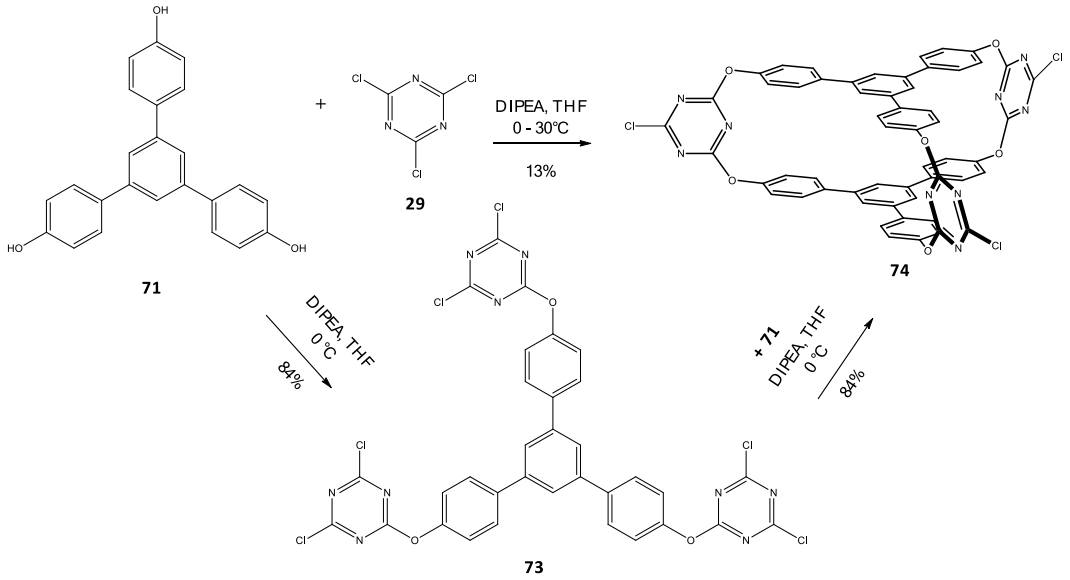

Scheme 14. Synthesis of the first triangular prism **74** (Wang *et al.*).[65]

A one-pot approach gave the product in very low yields (<13%), whereas a stepwise route, in the presence of DIPEA and TPHPB at 0°C, lead to the desired product with a final yield of 84%.

Having developed a procedure to make this macrocycles easily available even on multi-gram scale, Wang *et al.* managed to construct the first asymmetrical prism-derivatives, using 1,3,5-triphenylbenzene as electron rich building block (on the top) and 2,4,6-triphenyltriazine as electron-deficient part (on the bottom).

Inspired by the beauty of this system we designed two different kind of supramolecular cages (**75** and 77).

Compound **75** was synthesized starting from 1,5-dichloro-2,4-dinitrobenezene **1** and 1,3,5-tris(4-hydroxyphenyl)benzene **71** in 1.5 to 1 molar ratio, using Et_3N as the base and DMSO as the solvent (**Scheme 15**), performing the reaction at 80°C.

Even though the ^1H NMR spectrum (**Fig. 33**) of the final mixture gave encouraging evidence, showing the presence of diagnostic peaks indisputably assignable to the desired product, purification led to a disappointing yield of just 7%.

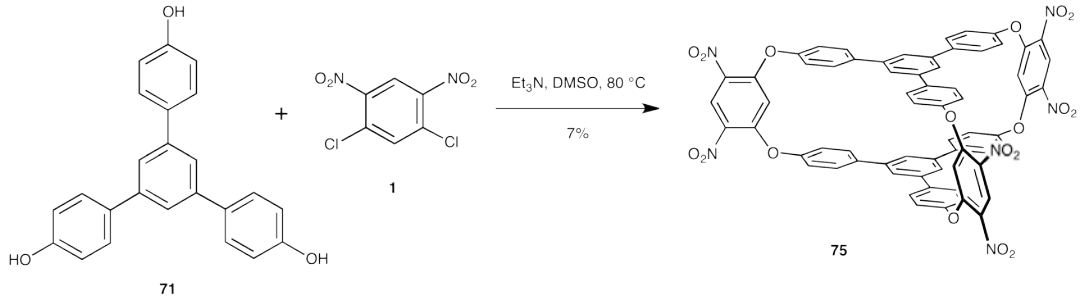

Scheme 15. Synthesis of the molecular cage **75**.

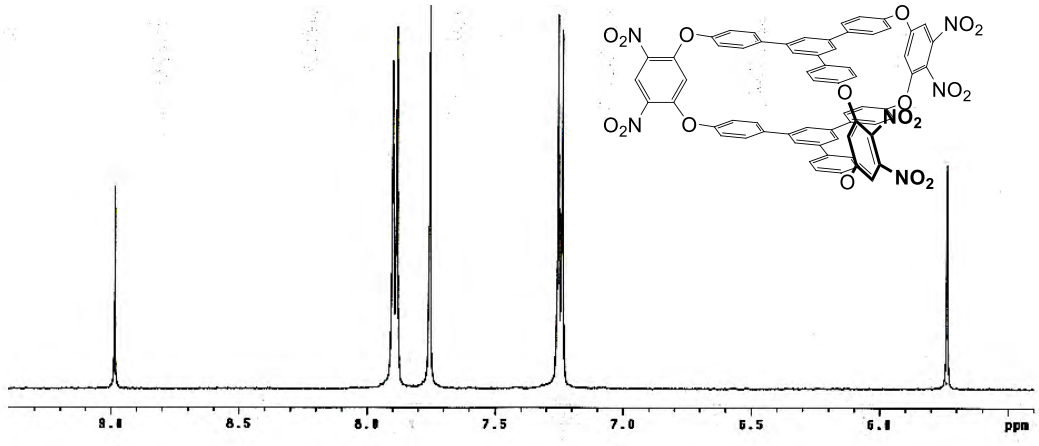

Figure 33. ^1H NMR spectrum (500 MHz, DMSO-d_6, 25 °C) of cage **75**.

The molecular cage was further characterized by DOSY NMR. The diffusion information in DOSY spectra is used, as a rule, only qualitatively because of the laboured relationship between diffusion coefficients and molecular structure.

The correlation is described by the Stokes-Einstein equation (14), which relies on the assumption that molecules have a spherical shape with a hydrodynamic radius r and are moving through a continuum fluid, characterized by the viscosity η (size of solvent molecules negligible compared to the solute one), at temperature T. K_B is the Boltzmann constant and f the friction factor unity for a hard sphere.

$$D = \frac{K_B\, T}{6\,\pi\,\eta\, r\, f} \quad (14)$$

A simple model to extract MW from the diffusion coefficient have been proposed by Morris *et. al.*, [67] in which ρ_{eff}, the effective density of a small molecule, allowing for packing effects, geometry, solvation, and flexibility, together with the viscosity η, the molecular weight MW_s of the solvent used, and N_A, the Avogadro number, were considered (eq. (15)).

$$D = \frac{K_B\, T\,(3a/2 + 1/\,1+a)}{6\,\pi\,\eta\,\sqrt[3]{3MW/4\pi\rho_{eff}N_A}} \quad (15)$$

Where $a = \sqrt[3]{MW_s}/MW$. Applying this model to our system it turned out that the real MW for the product and the precursors is comparable to the calculate one (MW_c, see **Table 7**).

Table 7. Formula weight estimation from DOSY NMR experiments.

	D_{obs} ($\times 10^{-10}$ m^2/s)	MW	MW_c[a]
1	1,40 ± 0,02	1201	1320
70	4,06 ± 0,01	237	147
75	1,98 ± 0,01	354	543

[a] MW_c were calculate following Evans *et al.*[67]

Diffusion coefficient extracted from the resonances of **75** indicate that the cage is moving slower than the precursors as a consequence of its increased size, thus confirming the success of the experiment (**Fig. 34**).

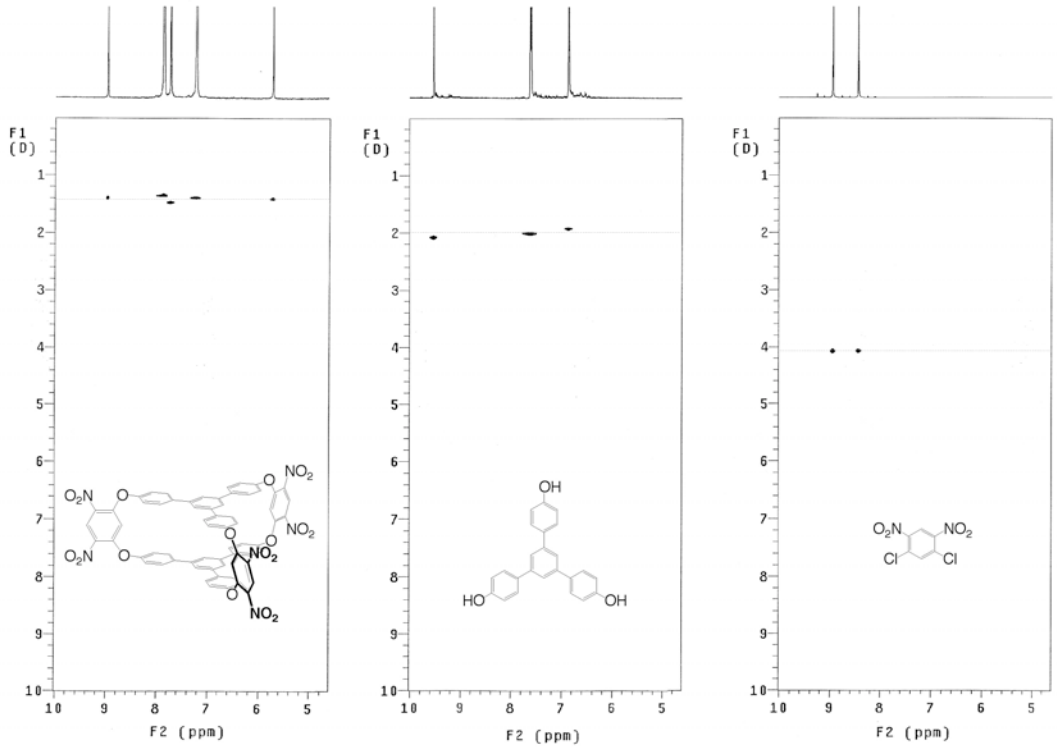

Figure 34. DOSY spectra (500 MHz, DMSO-d_6, 25 °C) of cage **75**, precursors **70** and **1**.

Molecular cage **77** was synthesized from tris(*p*-hydroxyphenyl)methane **76** and 1,5-dichloro-2,4-dinitrobenezene **1** under the same experimental conditions described for compound **75** (**Scheme 16**). The ^{1}H NMR spectrum of the crude mixture suggests the presence of the desired product in solution but at the time of writing this thesis, purification has not been achieved yet.

The optimized structures of the two molecular target, obtained by a semiempirical calculations (PM3), showed that both cages possess a D_{3h}-symmetric structure (**Fig. 35**).

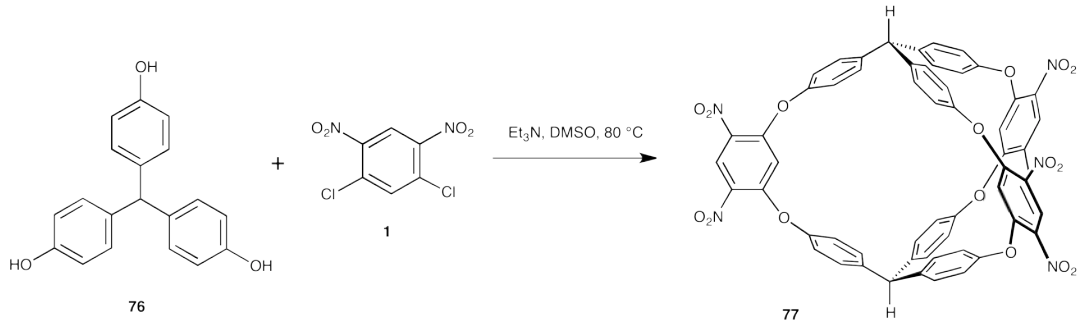

Scheme 16. Synthesis of the molecular cage **77**.

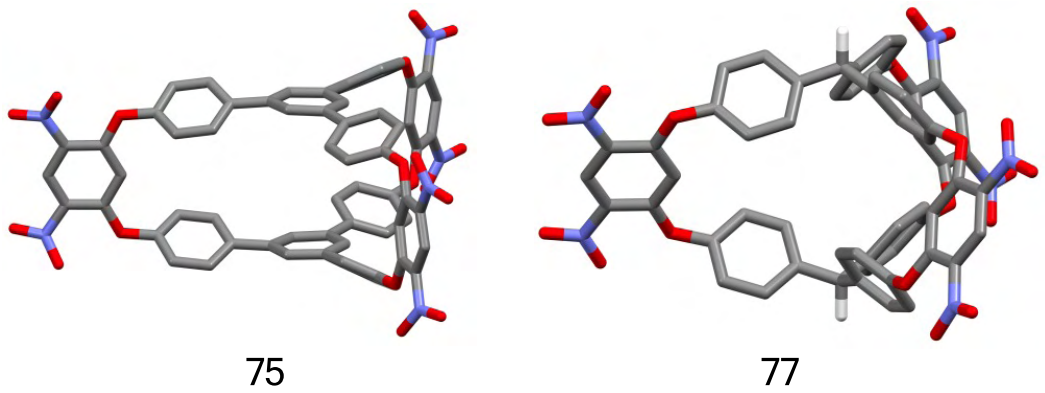

Figure 35. Calculated gas-phase geometries (PM3) of molecular cage **75** and **77**.

However, while the **75** does not appear to posses the correct steric requirements to trap suitable aromatic guests (e.g., PQT or halides) because of the tight internal cavity – the two central annular rings just 5.5 Å away from each other – the optimized geometry of cage **77** evidenced a more spherical inner space, that may accommodate small guest molecules such as, possibly, inorganic anions. Investigations on these compound are currently in progress.

1.3. Experimental section

General

All chemicals were purchased from Sigma-Aldrich and were used as received. Solvents were dried according to standard procedures.[68] ^{1}H and ^{13}C NMR spectra were recorded at 500 and 125 MHz, respectively, on a Varian Vnmrs-500 instrument. Chemical shifts are reported in ppm and are referenced to the residual solvent peak or, in D_2O, to 1,4-dioxane (δ_H 3.75 ppm, δ_C 67.19 ppm) added as an internal standard.

UV/Vis absorption spectra were recorded with a Varian Cary 50 UV-Visible spectrophotometer with an optic fibre probe having a fixed 1 cm path length, using spectrophotometric grade water.

1.3.1 Synthesis

4,6,16,18-Tetranitro-2,8,14,20-tetraoxacalix[4]arene (65)

A stirred solution of 1,5-difluoro-2,4-dinitrobenzene (204 mg, 1 mmol, 1 equiv.), 1,3-dihydroxybenzene (110,1 mg, 1 mmol, 1 equiv.), and TEA (0.3 mL, 2.2 equiv.) in dry DMF (10 mL) was refluxed for 2 h, under N_2 atmosphere. The solvent was removed under reduced pressure. The solid was triturated with $CHCl_3$ and collected by suction filtration to afford **65** as yellow powder, which analysed correctly for the desired macrocycle (200 mg, 73% yield); M.p. > 350 °C (lit.4,5,9, Mp > 350 °C); ^{1}H NMR ∂ 8.93 (s, 2 H, 5,17-Ar*H*), 7.57 (td, *J* = 1.5, 8.2 Hz, 2 H, 11,23-Ar*H*), 7.21 (t, *J* = 2.0 Hz, 2 H, 25,27-Ar*H*), 7.19 (dd, *J* = 2.0, 8.2 Hz, 4 H, 10,12,22,24-Ar*H*), 6.72 (s, 2 H, 26,28-Ar*H*) ppm; ^{13}C NMR ∂ 155.1, 154.5, 134.2, 132.6, 124.8, 117.9, 110.5, 108.9 ppm.

4,6,16,18-Tetraamino-2,8,14,20-tetraoxacalix[4]arene (66)

A suspension of **65** (1.89 g, 3.45 mmol) and Raney-nickel in THF (150 mL) was stirred under H_2 (1 atm) at room temperature for 2 days, and then filtered on celite. The solvent was evaporated under reduced pressure, and the residual solid was triturated with acetone and collected by suction filtration to afford **66** (1.13 g, 76% yield); M.p. 287–290 °C (dec); ^{1}H NMR ∂ 7.24 (t, *J* = 8.2 Hz, 2 H, 11,23-Ar*H*), 6.71 (dd, *J* = 2.3, 8.2 Hz, 4 H, 10,12,22,24-Ar*H*), 6.14, 6.28 (s, 1:1, 4 H, 5,17-Ar*H,* 26,28-Ar*H*), 5.95 (t, *J* = 2.3 Hz, 2 H, 25,27-Ar*H*), 4.51 (br s, 8 H, N*H*2) ppm; ^{13}C NMR ∂ 160.3, 138.2, 130.3, 130.1, 114.8, 110.2, 102.3, 98.8 ppm. MALDI-TOF, *m/z* 428.6 [M]+. *Anal.* Calcd. for C24H20N4O4·1/2H2O: C 65.90; H 4.84; N 12.81. Found: C 65.72; H 4.98; N 12.68.

4,6,16,18-Tetraammonium-2,8,14,20-tetraoxacalix[4]arene tetrachloride (66·4HCl)

Aqueous HCl (0.1 M, 5 mL) was added to a stirred solution of tetraamino-oxacalix[4]arene **66** (130 mg, 0.300 mmol) in THF (10 mL). After 10 minutes, the solvents were removed under reduced pressure. The resulting residue was triturated with Et_2O and collected by suction filtration to yield **66**·4HCl as a dark brown solid (164 mg, 0.285 mmol); M.p. > 280 °C; ^{1}H NMR (D_2O/DCl, pH 1.6) ∂ 7.52 (t, *J* = 8,3 Hz, 2 H, H_5), 7.43 (s, 2 H, H_1), 7.10 (dd, *J* = 2Hz, 8.3 Hz, 4 H, H_4), 6.72 (t, *J* = 2.2 Hz, 2 H, H_3), 6.57 (s, 2 H, H_2) ppm; ^{13}C NMR (D_2O/DCl, pH 1.6) ∂ 156.3, 147.7, 132.0, 120.7, 116.6, 116.1, 108.4, 107.6 ppm. ESI-MS: 429.0 (**66**·H$^+$).

[4,6,16,18]tetranitro[11,23]dihydroxycalix[4]arene (67)

A solution of 1,5-difluoro-2,4-dinitrobenzene (974 mg, 4 mmol, 1 equiv.), 1,3,5-trihydroxybenzene (504 mg, 4 mmol, 1 equiv.), and K_2CO_3 (1.38 g, 10 mmol, 2.2 equiv.) in dry DMSO (20 mL) was stirred under N_2 atmosphere, for 24h. After this time, 50ml of AcOEt and 40ml of HCl 1M solution, were added to the reaction

mixture. The organic layer was collected and put aside. The aqueous solution was washed with AcOEt (3 × 20 mL). The combined organic layers were dried with $MgSO_4$, filtered, and the solvents were removed under reduced pressure, to afford the a solid residue that was finally purified by column chromatography (AcOEt : Cyclo-Hex 1:4 v/v), yielding **67** as a yellow powder. 574 mg, 44% yield , M.p. > 380°C ^{1}H NMR (300 MHz, DMSO-d_6) ∂ 10.57 (s, 2H, O*H*), 8.91 (s, 2H, 5,17-Ar*H*), 7.18 (d, 4H, 4 *J* = 8.2 Hz, 10,12,22,24-Ar*H*), 6.95 (t, 2H, 4 *J* = 8.2 Hz, 11,23-Ar*H*), 5.62 (s, 2H, 26,28-Ar*H*) ppm.

[4,6,16,18]tetraamino[11,23]dihydroxycalix[4]arene (68·2H)

A suspension of **67** (574 mg, 0.98 mmol) and Raney-nickel in THF (150 mL) was stirred under H_2 (1 atm) at room temperature for 24 h, and then filtered on celite. The solvent was evaporated under reduced pressure, and the residual solid was triturated with acetone and collected by suction filtration to afford **68**·2H in 44% yield, ^{1}H NMR (300 MHz, DMSO-d_6) ∂ 8.07 (sb, 2H, O*H*), 7.40 (s, 2H, 26,28-Ar*H*), 6.80–6.90 (m, 4H, 10,12,22,24-Ar*H*), 6.92–7.0 (m, 2H, 11,23-Ar*H*), 5.54 (s, 2H 5,17-Ar*H*) ppm.

[4,6,16,18]tetranitro[25,27]dihydroxycalix[4]arene (69)

A solution of 1,5-difluoro-2,4-dinitrobenzene (974 mg, 4 mmol, 1 equiv.), 1,2,3-trihydroxybenzene (504 mg, 4 mmol, 1 equiv.), and K_2CO_3 (1.38 g, 10mmol, 2.2 equiv.) in dry DMSO (20 mL) was stirred under N_2 atmosphere, for 24 h. After this time, 50 mL of AcOEt and 40 mL of aqueous 1M HCl were added to the reaction mixture. The organic layer was collected and put aside. The aqueous solution was washed with AcOEt (3 × 20 mL). The organic layer was collected, joined with the other organic layer, dried with $MgSO_4$, filtrate, and dried under reduce pressure, to

afford a solid residue. The crude compound was purified by chromatography (AcOEt : Cyclo-Hex 1:2 v/v), and the product was obtained as yellow powder (370 mg, 26% yield), ^{1}H NMR (300 MHz, DMSO-d_6): ∂ 10.48 (bs, 2H, O*H*), 8.87 (s, 2H, 5,17-Ar*H*), 6.74 (s, 2H, 26,28-Ar*H*), 6.56-6.57 (m, 6H, 10,12,22,24,25,27-Ar*H*) ppm.

[4,6,16,18]tetraammino[25,27]dihydroxycalix[4]arene (70·2H)

A suspension of **69 (**574 mg, 0.98 mmol) and Raney-nickel in THF (150 mL) was stirred under H_2 (1 atm) at room temperature for 24 h, and then filtered on celite. The solvent was evaporated under reduced pressure, and the residual solid was triturated with acetone and collected by suction filtration to afford **70**·2H, 321 mg 23% yield, ^{1}H NMR (500 MHz, DMSO-d_6): ∂ = 9.56 (bs, 2H, O*H*), 6.22 (s, 2H, 5,17-Ar*H*), 6.13 (d, 4H, 4 *J* = 2.1 Hz, 10,12,22,24-Ar*H*), 6.08 (s, 2H, 8,26-Ar*H*), 5.39 (t, 2H, 4 *J* = 2.1 Hz, 25,27-Ar*H*) ppm.

1,3,5-tris(4-hydroxyphenyl)benzene (71)

To a solution of 4-hydroxyacetophenone (1,94 g, 14,34 mmol, 1 equiv.) in dry ethanol (40 ml), at 0°C, was added slowly $SiCl_4$(8,4ml, 71,7 mmol, 5 equiv.). The reaction mixture was stirred at RT for 20 h, under N_2 atmosphere. After this time, 10 mL of H_2O were added and the resulting mixture was extracted with CH_2Cl_2 (3 × 20 mL). The organic layer was collected, dried with $MgSO_4$, and the solvent was removed under reduce pressure. The crude mixture was purified by column chromatography (AcOEt : *n*-hexane 1:4 v/v) yield 22%, M.p. > 230°C. ^{1}H NMR (CD_3CN, 500 MHz): ∂ = 7.62 (s, 3H, Ar-*H*), 7.55 (d, 6H, J = 8.4 Hz, Ar-*H*), 6.92 (d, 6H, = 8.4 Hz, Ar-*H*), 7.41 (br s, 3H, -*OH*) ppm; ^{13}C NMR (CD_3CN, 125 MHz): ∂ = 156.5, 141.8, 132.8, 128.3, 128.2, 115.7 ppm.

Synthesis molecular cage 75

A stirred solution of 1,5-dichloro-2,4-dinitrobenzene (544 mg, 2.3 mmol, 2 equiv.), 1,3,5-tris(4-hydroxyphenyl)benzene (514 mg, 1.14 mmol, 1 equiv.), and Et_3N (714 μL, 5.13 mmol, 5 equiv.), in dry DMSO (20 mL), was refluxed for 12 h, under a N_2 atmosphere. After this time, 50ml of AcOEt and 40ml of HCl 1M solutions, were added to the reaction mixture. The organic layer was collected and put aside. The aqueous solution was washed with AcOEt (3 × 20 mL). The organic layer was collected, joined with the other organic layer, dried with $MgSO_4$, filtrate, and the solvents were evaporated under reduce pressure. Cage **75** was obtained after precipitation in acetone. 50 mg, 7 % yield, M.p. > 230 °C. ^{1}H NMR (500 MHz, DMSO-d_6) ∂ = 8,98 (s, 3H), 7,89 (d, *J* = 8.4 Hz, 6H) 7,75 (s, 6H), 7,24 (d, *J* = 8.4 Hz, 6H), 5,74 (s, 3H) ppm; ^{13}C NMR (125 MHz, DMSO-d_6) ∂ = 157.41, 152.41, 138.10, 131.04, 128.93, 125.97, 123.32, 121.89, 105.63 ppm.

Synthesis of tris(*p*-hydroxyphenyl)methane (76)

Phenol (1 g, 10,6 mmol, 5 equiv.) and 4-hydroxybenzaldeide (0.26 g, 2.1 mmol, 1 equiv.), were heated at 45 °C until a homogeneous solution was obtained.$ZnCl_2$ (28.8 mg, 0.215 mmol, 0.1 equiv.) and *p*-toluenesulfonic acid (36.5 mg, 0.215 mmol, 0.1 equiv.) were then added and the formation of a red precipitate was immediately observed. The reaction mixture was kept at 45 °C for 8 h. After this time, CH_2Cl_2 (50 mL) was added and the precipitate was filtered and washed with hot water, yielding **76**, 300 mg, 13% yield, ^{1}H NMR (500 MHz, acetone-d_6) ∂ = 8.15 (s, 3H, -*OH*), 6.94 (d, 6H, Ar-*H*), 6.76 (d, 6H, Ar-*H*), 5.33 (s, 1H, CH) ppm; ^{13}C-NMR (125 MHz, acetone-d_6) ∂ = 155.5, 136.4, 130.1, 114.7, 54.3 ppm.

Synthesis molecular cage 77

A stirred solution of 1,5-dichloro-2,4-dinitrobenzene (243 mg, 1.03 mmol, 1.5 equiv.), tris(*p*-hydroxyphenyl)methane (200 mg, 0.684 mmol, 1 equiv.), and Et_3N (322 μL, 2.4 mmol, 4 equiv.), in dry DMSO (20 mL), was refluxed for 12 h, under a N_2 atmosphere. After this time, 50 mL of AcOEt and 40 mL of aqueous 1M HCl were added to the reaction mixture. The organic layer was collected and put aside. The aqueous solution was washed with AcOEt (3 × 20 mL). The organic layer was collected, joined with the other organic layer, dried with $MgSO_4$, filtrate, and evaporated under reduce pressure. The ^1H NMR spectrum of the crude suggests the presence of the desired product in solution but at the time of writing this thesis, purification has not been achieved yet.

1.3.2. Determination of the protonation constants by UV-Vis spectroscopy

The protonation constants of **66**·4HCl, **68**·2H and **70**·2H were determined by means of UV-Vis spectrophotometric titrations. Solutions of **66**·4HCl, **68**·2H and **70**·2H in the 3×10^{-5} – 5×10^{-6} M concentration range were prepared by dissolving the stipulated amount of solid **66**·4HCl **68**·2H and **70**·2H in aqueous 0.1 M HCl.

The pH of the resulting solutions was recorded with a ISE-H^+ combined electrode (Metrohm, 6.032.100 model), calibrated with buffer solutions immediately before the titration. 25 mL of **66**·4HCl, **68**·2H and **70**·2H solutions were placed in a thermostatted cell (T = 298.15±0.1 K), and titrated with standard 0.1 M NaOH (typically 10–20 aliquots) to vary the pH in the 1.0 – 12.0 range.

UV-Vis spectra were recorded for each addition in the λ = 250–330 nm spectral window, with baseline subtraction (0.1 M HCl).

1.3.3. ^{1}H NMR titrations

The association of **66**·*n*H$^+$and **70**·2H with paraquat (PQT^{2+}), expressed as in eqs. (3)-(4), were investigated by ^{1}H NMR, carrying out titrations at different pH values. Given that deuterated chemicals were used, pH values were obtained from pD measurements by applying the appropriate correction.

For **66**·4HCl five titrations were carried out, in two replicates, at pH = 0.97, 1.35, 1.48, 1.59, 1.99, respectively.

For **70**·2H , five titrations were performed at pH = 1.59, 2.00, 11.00, 11.59, 12.00.

Stock solutions of [**66**·4HCl] = 10^{-4} M were prepared by dissolving solid **66**·4HCl in DCl/D_2O solutions ([DCl] = 0.1, 0.075, 0.050, 0.025, 0.010 M, respectively). Paraquat dichloride guest solutions ([PQT·2Cl] = 0.025 M), were, in turn, prepared by using as solvent the above mentioned **66**·*n*HCl stock solutions so that, upon addition of the titrant, both the host concentration and the pH of the solution would remain constant over the entire titration experiment.

The same procedure was used for **70**·2H. For the experiments at acid pHs, stock solutions [**70**·2H = 10^{-4} M] were prepared dissolving the solid **70**·2H in DCl/D_2O solutions ([DCl] = 0.025 and 0.010 M)

Stock solution of NaOD (1 M) was prepared dissolving the solid NaOH in D_2O.

For the experiments at basic pHs stock solutions [**70**·2H = 10^{-4} M] were prepared dissolving the solid **70**·2H in NaOD/D_2O solutions. ([NaOD] = 0.001, 0.0038, 0.01 M).

Typically, data were collected in the 1:0.25 to 1:140 host/guest ratio interval, by adding 12 aliquots of the above mentioned PQT·2Cl solution to a given stock solution of the host.

The interaction between **66**·*n*HCl and 2,7-dihydroxynaphtalene DHN was investigated by NMR as well.

To this end, five NMR titrations experiments were carried out, in two replicates, at pH = 1.00, 1.33, 1.62, 1.91, 2.24, respectively.

Stock solutions of [**66**·4HCl] = 10^{-4} M were prepared by dissolving solid **66**·4HCl in DCl/D_2O solutions ([DCl] = 0.099, 0.063, 0.024, 0.012, 0.006 M).

DHN guest solutions ([DHN] = 0.0125 M), were prepared by using as solvent the above mentioned **66**·*n*HCl stock solutions, again, to maintain constant the concentration of both host concentration and pH value, over the entire titration experiment.

1.3.4. Molecular Modelling

The conformational analysis of the oxacalix[4]arenes **66**·*n*H^+, **68**·2H, **70**·2H, molecular cages **75** and **77**, were carried out with the classical molecular mechanics force field (MMFF) by using the Monte Carlo method to randomly sample the conformational space. The equilibrium geometries were then calculated at the density functional level of theory (DFT, B3LYP functional) using the 6-31G(d) basis set. Computational data of DNH⊂**66**·3HCl complex in a water cluster consisting 200 explicit solvent molecules was carried out with the classical molecular mechanics force field (MMFF), using the Monte Carlo method. The 2,7-dihydroxynaphtalene guest was placed at a short distance from the oxacalix[4]arene, and both components were placed within the solvent cluster.

The system was then left free to relax without constraints. The conformer obtained was further refined by semiempirical methods at the PM6 level.

All calculations were performed using Spartan'10 (Wavefunction, Inc., Irvine, CA, USA).

1.3.5. Calorimetric measurements

Calorimetric experiments were performed on the paraquat-oxacalix system using a nano-ITC low volume calorimeter (TA Instruments) equipped with a reference and sample cell (0.943 cm^3), following the recommended procedures reported elsewhere.[69] Measurements were run in the overfilled mode which does not require any correction for liquid evaporation and/or for the presence of the vapour phase.[70] All titrations were carried out at T = 298.15 K using a 0.250 cm^3 syringe with a stirring rate of 250-350 rpm. The reference cell was always filled with ultra pure water (R = 18 MΩ cm). All solutions were degassed for 15 minutes before starting the experiments to eliminate air bubbles. The experimental conditions used for the determination of the association constants of the PQT/**70**·2H species, the sample cell was filled with **70**·$2H_{(aq)}$ (0.1 mmol dm^{-3}) and $HCl_{(aq)}$ (in order reach pre-established pH values) and the syringe with PQT (11.8 mmol dm^{-3}) and standard $HCl_{(aq)}$ at the same concentration of the sample cell. For each calorimetric titration dilution measurements (used as blank) were performed. In these runs **70**·2H and acid were not present in the sample cell whereas the titrant was the same of the measurement.

Chapter 2

2.1. Introduction

Over the past decades, supramolecular polymers[71] have attracted considerable attention because of their unique properties, such us stimuli-responsiveness, adaptive behaviour or shape memory,[72] which endow them with a broad range of potential applications as smart, self-healing materials, as well as building-block in the construction of higher level molecular arrays and delivery carriers.

Differently to the conventional polymers, where monomeric units are covalently and almost always irreversibly bound to each other, in supramolecular polymers individual repeating units are held together by reversible, directional, non-covalent interaction.

As a result of the intrinsic difference between covalent and non-covalent bonds, this latter class of compounds turns out to be easier to employ and more prone to recycling, may show self-healing, and is capable to act as shape memory materials in combination with covalent cross-linking.[73]

After the pioneering work by Jean-Marie Lehn,[74] reporting in 1990 the first example of supramolecular polymer based on the hydrogen bonding between uracil- and 2,6-diacylaminopyridine-bearing complementary units, a lot of papers focused on a variety of self-assembly supramolecular polymers, have been reported.

So far, to construct supramolecular entities exploiting self-assembly mechanism, hydrogen bonding, metal-ligand coordination, π-π stacking or combination of them have been widely used.

Along with these strategies, host-guest complexation has emerged over the years as an efficient method to drive polymerization process. This approach to the non-covalent linking of monomers offers the possibility of building two different types of aggregates that can be defined – borrowing the terminology from classical polycondensation polymers – AA/BB- and AB-type polymers. The former consist of homoditopic complementary monomer pairs, e.g., a bis-receptor unit (AA) paired to a bis-guest unit (BB), whereas the latter are built from heteroditopic monomers simultaneously bearing a host (A) and a guest (B) moiety on the same molecule. Both types of polymers, however, display similar self-assembly behaviour, their chain-growth proceeds generally under thermodynamic control, and their number-average degree of polymerization (DP) can generally be described (or predicted) by the Carothers' equation (16):[75]

$$DP = \frac{1 + r}{1 + r - 2\,r\,p} \quad (16)$$

where r is the molar ratio between monomers, in the case of AA/BB type polymers (r is equal to one in the case of AB monomers, where host and guest components are part of the same molecule), and p represents the degree of 'reaction' (complexation, in this case) of the end-groups.

Given the possibility to choose among a variety of building-blocks as host-guest pairs for the design of polymeric species, then to generate supramolecular materials that posses the most different properties, the host-guest approach can be considered the most versatile approach over the other methods. Furthermore, the simultaneous use of different host-guest recognition motifs allows easy access to multicomponent copolymeric systems whose self-assembly and self-sorting is regulated by orthogonal recognition processes.[76]

Crown ethers, cryptands, cyclodextrins, curcubiturils, and more recently pillararenes, have found applications in this field.[77]

In this thesis, however, following up on previous studies reported by my research group, we focused on supramolecular polymers based on calix[5]arene framework.

Calix[*n*]arenes are [1$_n$] cyclophanes consisting of *n* phenolic units (*n* ≥ 4) linked together, in their *ortho* position, by methylene bridging groups (**Fig. 35**).

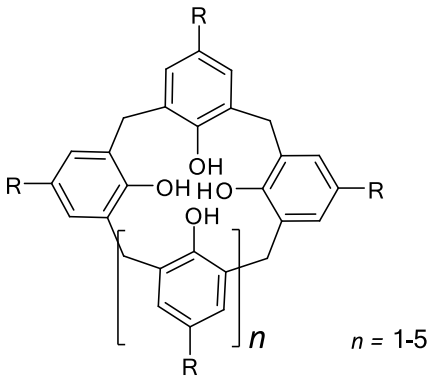

Figure 35. Schematic representation of a general calix[*n*]arene.

The first calixarene was synthesized by Zinke and Zigler[78] in the '40s using a one-pot approach, and this strategy is still the method of choice for the preparation of calixarenes composed of only one type of phenolic units.

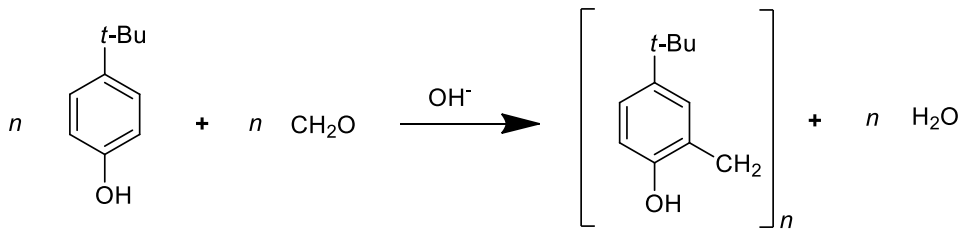

Scheme 17. Synthesis of calix[*n*]arene by one-pot reaction (Zinke and Zigler).[78]

However, the most significant advances in this field can be ascribed, above others, to the group of C. D. Gutsche that in the '70s re-interpreted the results reported by Zinke and planned the synthesis of the three distinct cyclic oligomers (a tetramer, a hexamer and an octamer).[79]

As an alternative to the one-pot synthesis, multiple step synthetic procedures have been described but given the large number of synthetic steps needed to produce the linear precursor, overall yields are generally low.[80]

Calixarenes are characterised by a marked conformational mobility, as a result of the rotation of the aryl residues around the CH_2ArCH_2 σ bonds. This motion may occur via two different pathways, generally termed '*lower-rim-through-the-annulus*' and '*upper-rim-through-the-annulus*'.

VT NMR studies on calix[4]- and calix[5]arenes showed that, at higher temperatures, the topologically non-equivalent protons of the bridging methylenes resonate as a singlet, and that upon cooling, the singlet evolves to an AX system. This has been explained assuming a fast interconversion at higher temperature between two equivalent cone conformations.[81]

Conversely, in the solid state, as well as in solution at lower temperatures, calix[4]- and calix[5]arenes[82] adopt a cone conformation stabilized by intramolecular hydrogen bonds between the phenolic hydroxyl groups (**Fig. 36**).

Figure 36. Solid state structure of *p-tert*-butylcalix[5]arene

When hydrogen *p*-substituent are replaced by bulking group such as *tert*-butyl groups, the rotation of the aryl moieties through the macrocycle ring is not allowed any more, and the NMR spectrum at low temperature highlighted that the preferred conformation for *p-tert*-butylcalix[5]arene is the regular cone, being it the most stable structure, owing to the formation of intramolecular hydrogen bonds between the phenolic hydroxyl groups.

The main target of upper and lower rim functionalization is to lock the calixarenes in a particular conformation and, moreover, to give them specific receptor characteristics connected to the intrinsic nature of the functional groups.

Among the so-called conventional calix[*n*]arenes (*n* = 4–8 and thus excluding the 'giant' ones that can be as high as 20[83]), the odd-numbered members (i.e., *n* = 5 and 7) have enjoyed less attention than their even-numbered analogues, most likely as a result of their lower-yielding syntheses.[84] However, the intriguing and multifaceted binding behaviour of calix[5]arenes has tickled the curiosity of some in connection with the potential use of this macrocycle as a building block for the construction of more complex supramolecular architectures. Leaving aside those cases where the macrocyclic framework has just been used as a molecular scaffold to arrange different functional groups in the tri-dimensional space, calix[5]arenes display remarkable affinity for structurally different substrates, as they can recognize guests by means of i) π-π stacking interactions, ii) *endo*-cavity hydrogen bonding formation or –when present as *p*-sulfonate derivatives– iii) electrostatic attraction.

In the early 90's, independent reports from the groups of Atwood[85] and Shinkai[86] showed that *p-tert*-butylcalix[8]arene can be efficiently used to separate fullerene mixtures.

Solid state analysis[87] revealed that the calix[8]arene octol forms a 3:3 complex with C_{60} with a cloverleaf-shaped micelle-like structure, held together by π-interactions between

the π-rich cavity of the macrocycle and the electron-deficient C_{60} molecule. The receptors adopt an 'eight-shaped' conformation, where the two halves of a given calix[8]arene molecule were seen to independently interact with two different C_{60} units. Most remarkably, the four *p-tert*-butylphenol moieties forming the 'bay' where C_{60} docked adopt interplanar angles very similar to those seen in the solid-state structure of *p*-tert-butylcalix[5]arene **78**.[88] (**Fig. 36**)

In 1997, Fukazawa and co-workers reported on the formation of the first host-guest complexes between calix[5]arenes and C_{60}.[89] They observed that a series of calix[5]arene derivatives (**79**–**81**) –bearing at their wider rim methyl, iodine or hydrogen substituents– in low-polarity solvents such as toluene, benzene, carbon disulfide or *o*-dichlorobenzene, would recognize fullerene with association constants in the 200–2000 M^{-1} range. This remarkable result was ascribed to a favourable stereoelectronic matching between the convex surface of C_{60} and the concave cavity of the receptor. (**Fig. 37**)

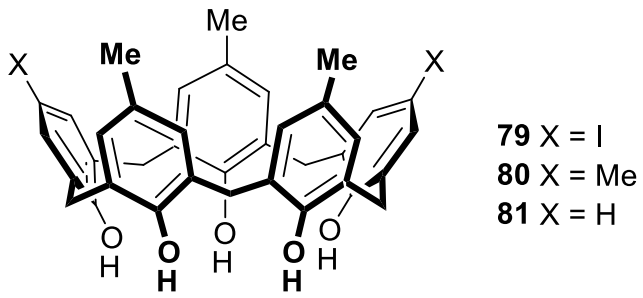

Figure 37. Calix[5]arene derivatives synthesized by Fukazawa *et al.*.[89]

X-ray crystallographic studies[90] revealed that, although in solution the three calix[5]arenes form complexes with a 1:1 stoichiometry, in the solid state only calixarenes **80** and **81** form complexes with the same stoichiometry, whereas **79** gave a 2:1 capsular complex (**Fig. 38**).

The discovery that suitably modified calix[5]arenes could give encapsulation complexes,[91] led to the development, in the following year[92], of a series of convergent-cavity covalently-linked bis-calix[5]arenes able to bind C_{60} even more efficiently (K_as up to 76000 M^{-1}). Even though these receptors were found to prefer C_{70} over C_{60}, they became the key building-blocks for the construction of polymeric networks, owing to their high affinity to fullerenes (in agreement with Carothers equation's predictions).

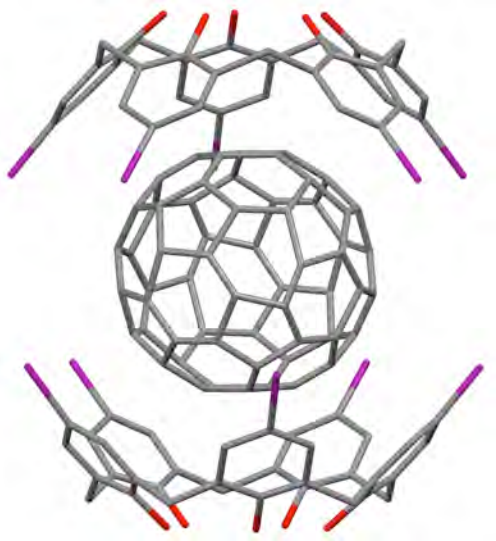

Figure 38. Solid state structure of **79**⊃C_{60}⊂**79**. Owing to positional disorder of the iodine atoms over the *para* position, the complex displayed an apparent D_{5d} symmetry in the solid-state.[90]

In 2005 Haino and co-workers synthesized a ditopic calix[5]arene host **82**, able to assemble with a bis-C_{60} dumbbell complementary monomer **83** to yield supramolecular oligomers[93](**Fig. 39**).

Pulsed field gradient NMR experiments (BPPSTE pulse) showed that in chloroform, at a 2×10^{-4} M concentration, the average DP was *ca*. 3. However, once deposited on surfaces, upon evaporation the oligomers gave spider-web fibres of nano-sized thickness (**Fig. 40**).

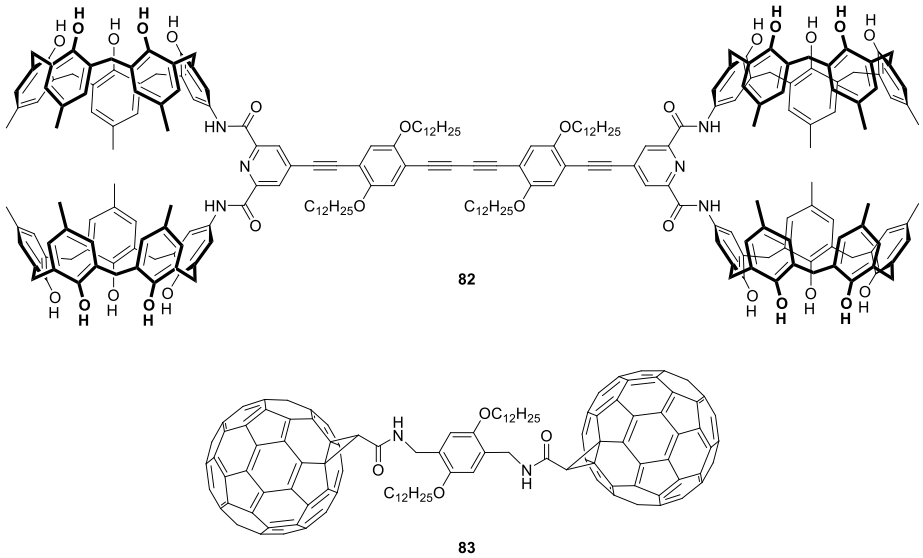

Figure 39. Ditopic calix[5]arene host and bis-C_{60} dumbbell complementary monomer (Haino *et al.*).[93]

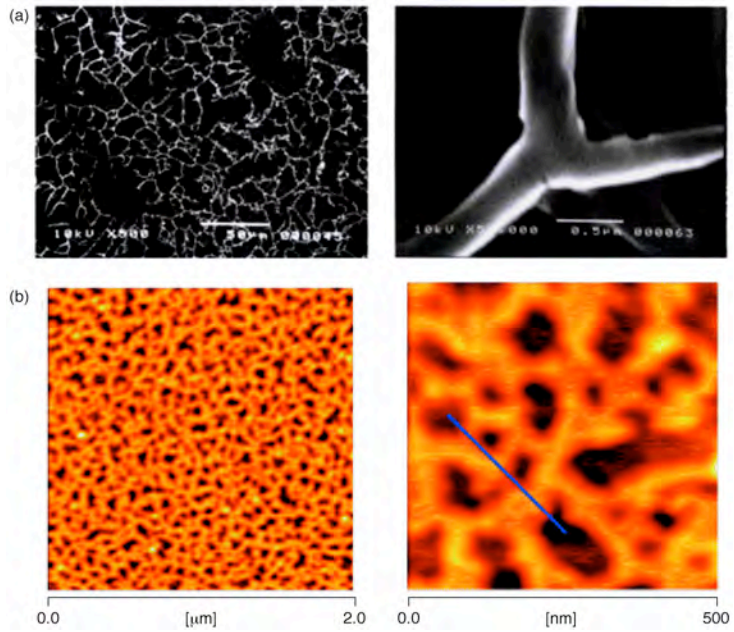

Figure 40. a) Scanning electron micrograph of the cast-film of a mixture of **82** and **83** on glass plate. b) AFM images of drop-cast of the **82** and **83** solution in chloroform on mica (Haino *et al.*).[93]

The same tetra-calixarene **82** was later employed in experiments on supramolecular crosslinking of the C_{60}-decorated phenylacetylene polymer[94] **84** and in this case, rather than a linear supramolecular polymer, a 3D-network was generated.

The resulting material was studied by size-exclusion chromatography, showing that the addition of increasing amounts of tetra-calixarene **82** (0.25 and 0.5 equiv.) to a toluene solution of **84** led to a progressive increase in the average molecular weight, from M_n = 18000 to 25000 and then 32000, respectively, with a corresponding increase of the polydispersity index (PDI) from 1.38 to 2.80 and 2.81(**Fig. 41**). No molecular weight increase was observed in the case of more competitive solvents (*o*-dichlorobenzene, chloroform), leading the Authors to conclude that supramolecular cross-linking in this system can be regulated by solvating effects.

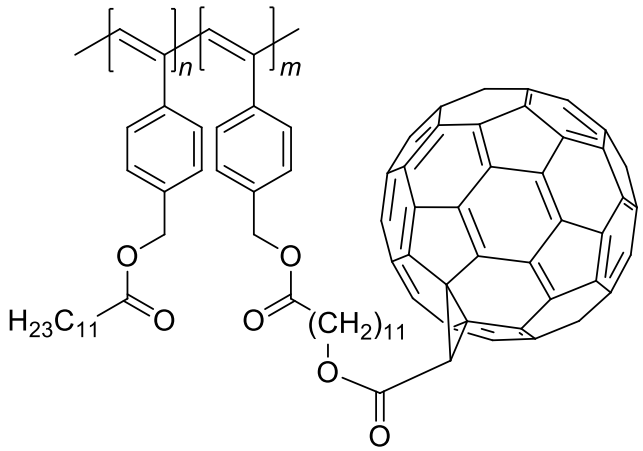

84 x = 0.93; y = 0.07

Figure 41. C_{60}-decorated phenylacetylene polymer **84** synthesized by Haino *et al.*[94]

More intriguing results were obtained by Haino and co-workers when they employed the extended bis-C_{60} dumbbell-shaped guest **86**, in conjunction with the tetra-calixarene **82** and the new tritopic hexa-calix[5]arene monomer **85**.[95]

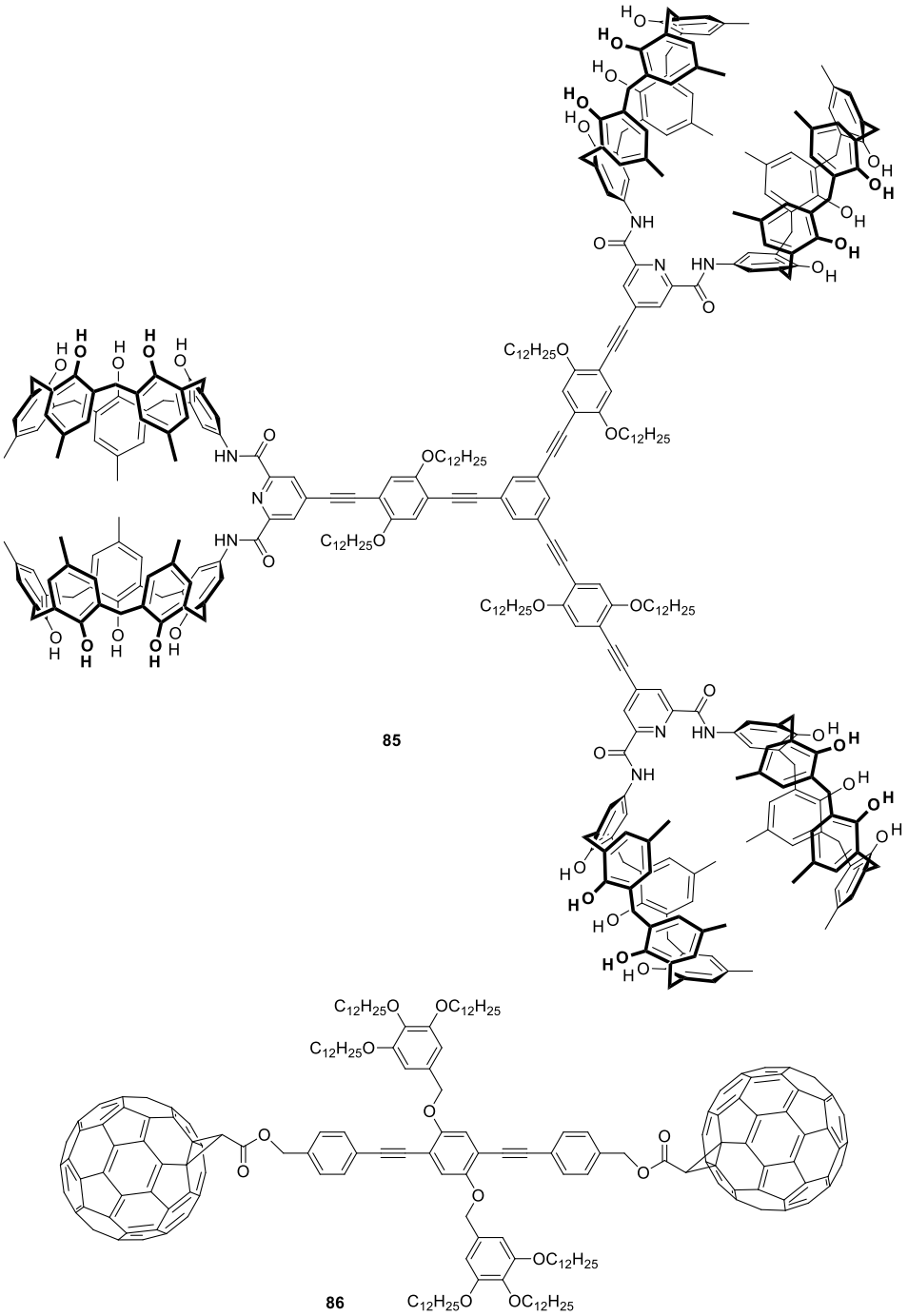

Figure 42. Extended bis-C_{60} dumbbell-shaped guest **86**, and the new tritopic hexa-calix[5]arene monomer **85** (Haino *et al.*).[96]

Diffusion-ordered ^{1}H NMR (DOSY) studies showed that, in the 10 mM range (chloroform solution), the homoditopic monomers **82** and **86** (1:1 equiv.) produce linear supramolecular polymers displaying an estimated average DP of 85, whereas the tritopic/ditopic pair **85**/**86** (2:3 equiv.) yields a polymeric material with a DP as high as 135. Interesting observations came from viscometry studies carried out at different temperature.

The **85**/**86** mixture showed a much stronger dependence of the viscosity on both concentration and temperature than **82**/**86**, with high concentration and low temperature increasing more significantly the viscosity of the former pair rather than the latter. This effect was ascribed to the different morphology of the polymeric assemblies. The ditopic monomers **82**/**86** form rigid rod-like aggregates that may affect viscosity –in the semi-diluted regime– only to a limited extent, as a result of a progressively hindered molecular rotation. Conversely, the tritopic/ditopic monomer pair **85**/**86** forms tri-dimensional networks which, upon increase of the concentration (or temperature decrease), rapidly grow as a result of a supramolecular cross-linking process.

It is worth mentioning that no AB-type supramolecular polymers have been built exploiting the calix[5]arene-C_{60} recognition motif. A calix[5]arene bearing a C_{60}-terminated pendant group at its upper rim has been described, but no evidence of its behaviour as a potential monomer was reported.[96]

Sulfonatocalixarenes **87**, a family of water-soluble calixarene derivatives, show strong binding affinity and high molecular selectivity towards the most diverse cationic guests, ranging from metal cations to alkylammonium- or pyridinium-derived organic ions, by the synergistic effect of additional anchoring points donated by sulfonate groups together with the intrinsic cavities. (**Fig. 43**)

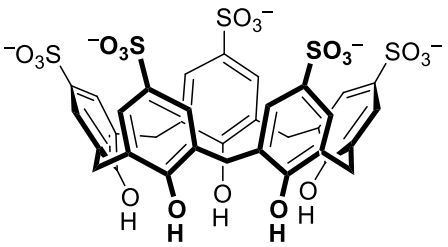

87

Figure 43. *p*-Sulfonatocalix[5]arene **87**.

Inspired by the desired inclusion property of sulfonatocalixarenes, Liu and coworkers designed 2:1 capsular complexes with a range of suitably-sized bis-pyridinium dicationic guests, using calixarene derivative **87**[97] (the complex with 1,4-bis-pyridiniumbutane BPDB is shown in **Fig. 44**), thus paving the way for the subsequent attainment of supramolecular polymers.

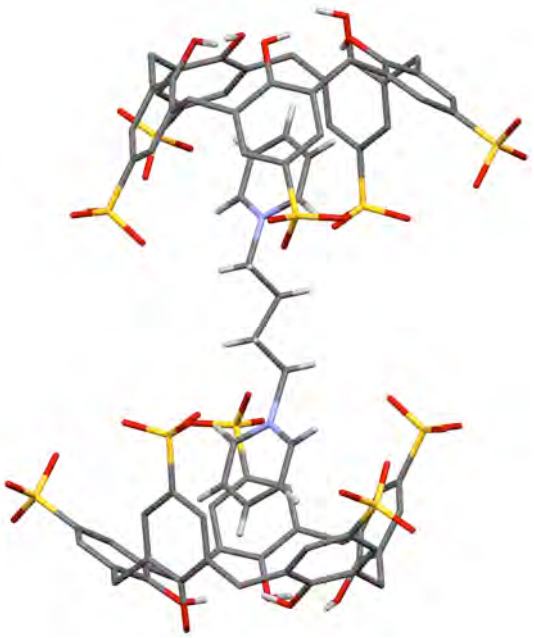

Figure 44. Solid state structure of the complex **87**⊃BPDB⊂**87** (Liu *et al.*).[97]

In fact, following this way, employing the homoditopic bis-(*p*-sulfonatocalix[5]arene) **88,** two highly complex supramolecular polymers with 2D netlike and 1D linear topological structures were constructed by employing tetracationic and dicationic porphyrins (**90** and **89** respectively) as model guests.(**Fig. 45**)[98]

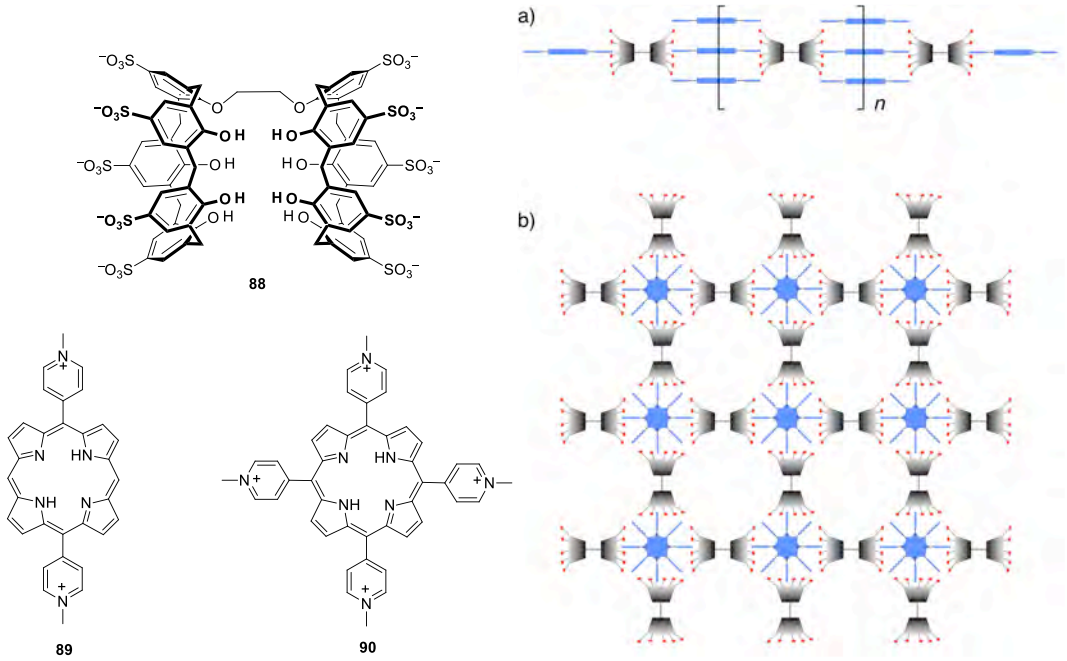

Figure 45. Schematic representation of supramolecular aggregates formed from: a) 1D polymer from bis-calixarene **88** and porphyrin **89**, b) 2D network from bis-calixarene **88** and porphyrin **90**.

Given that the complexation exceeds the conventional 1:1 molar ratio, while 2:5 and 1:5 complexes with tetracationic and dicationic porphyrins (respectively) were formed, the Authors stated that host–guest stoichiometry results from charge matching, with the number of negative sulfonate groups on the calixarenes equalling the number of the positive charges on the porphyrins.

Interestingly, these supramolecular framework, was found to be a good photo-sensitive system, in which calixarenes and porphyrins act as electron donor–acceptor pairs, and an unambiguous photo-induced electron transfer was observed.

More recently, Liu and co-workers employed *p*-sulfonatocalixarene **87** derivatives to build supramolecular polymers through aggregation with perylene bisimides.[99]

In detail, upon addition of calixarene **87** (n = 4, 5), electrostatic and host-guest interactions both boosted the π-π staking interaction between BPTA-PBI molecules, driving perylene backbone aggregation with a high degree of polymerization. Notably, the network formed by using calixarene **87**, shows a better defined structure than the oligomeric one that is shaped from the free discotic BPTA-PBI molecules.

Following this route, very different supramolecular networks were assembled from *p*-sulfonatocalixarene derivatives **87** and **88**.[100]

In fact, while supramolecular binary vesicles (22-247 nm range distribution) were obtained when using **87**, calixarene **88** induced the formation of 1D nanorods in the 200 nm range (**Fig. 46**).

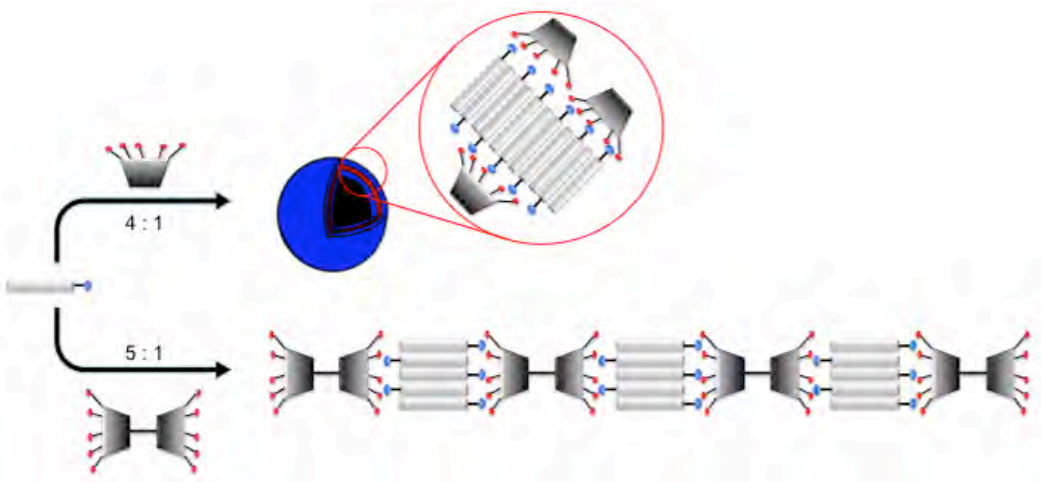

Figure 46 Schematic representation of the assembly modes of PMA in the presence of *p*-sulfonatocalix[5]arene **87** (top) and bis-*p*-sulfonatocalix[5]arene **88** (bottom) (Liu *et al.*).[100]

According to the Authors, the different stoichiometric ratio employed and the different conformational rigidity of the two calixarenes, play a vital role in the morphology of the two supramolecular structures generated, as a result of different host-guest complexation events, the electrophilic interaction between the upper rim sulfonates and the ammonium moieties, and π-π stacking between the aromatic surfaces of the pyrene groups.

2.2. Carboxyl-calix[5]arenes

2.2.1. Our contribution to ionisable calix[5]arene chemistry

Shortly after Fukazawa's communication on fullerene recognition, my research group reported that calix[5]arenes locked in a cone conformation[101] may act, with remarkable efficiency and selectivity, as *endo*-cavity receptors for linear primary alkylammonium ions.[102] Having found that a preorganized and permanent *cone* conformation – tuned by changing the nature and bulkiness of substituents on both the upper and lower rims – lead to more powerful receptors, they synthesized penta-O-alkyl- or penta-O-alkoxycarbonylmethyl-calix[5]arenes (such as, among many, **89** and **90**) that were found able to bind *n*-butylammonium ions with association constants in excess of 10^6 M^{-1}, and with a selectivity with respect to isomeric branched alkylammonium ion of *ca*. 10^3 (**Fig. 47**).

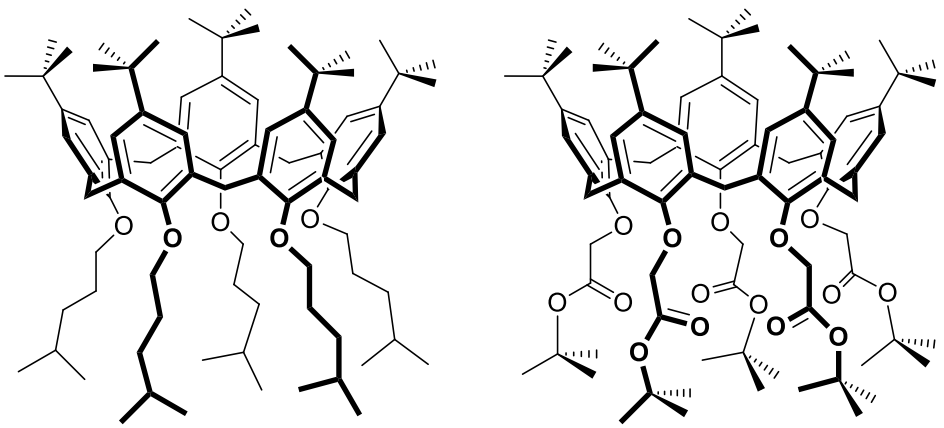

89 **90**

Figure 47. Representation of calix[5]arenes derivatives **89** and **90**.

Differently from C_{60} recognition, though, which is based solely on π-π interactions, alkylammonium recognition by calix[5]arenes involves a simultaneous and concerted set of concomitant interactions such as hydrogen bonding and CH-π interactions, as it is demonstrated by the solid state structures reported for some inclusion complexes (**Fig. 48**): the guest nests within the cavity of the calixarene, bringing the ammonium hydrogen atoms within H-bond distance with the phenolic oxygen atoms and, in addition, the α and β-methylene hydrogen atoms of the guest alkyl chain are involved in CH-π interactions with four distinct aromatic rings of the host.[103]

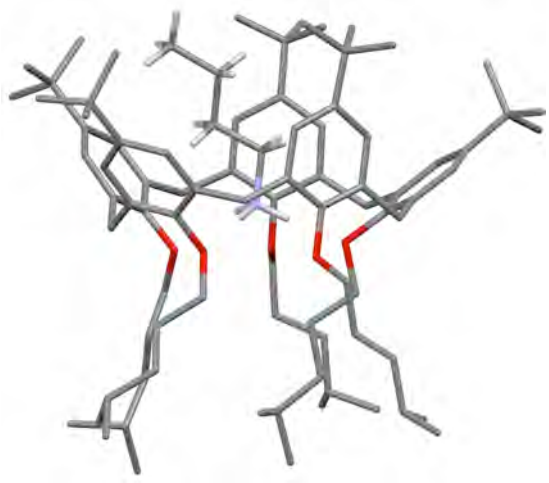

Figure 48. Solid-state structure of **89**⊃*n*-$BuNH_3^+$ (Gattuso *et al.*).[103]

During our studies we developed a new synthetic approach to achieve two different kinds of supramolecular polymers, namely AB- and AA/BB-type polymers.

The unlimited possibilities of functionalization offered by calixarene chemistry led to the preparation of the first AB-type calix[5]arene-containing monomer, the aminododecyloxy derivative **91**.[104]

Exposure of **91** to organic or inorganic acids (HCl, HBr, picric acid) triggered an iterative intermolecular *endo*-cavity inclusion process, leading to the formation of

supramolecular oligo/polymers (**Fig. 49**). The use of different acids demonstrated a key feature of these systems: the efficiency of the self-assembly, and hence the average DP, was seen to strongly depend on the nature of the counterion employed. In line with the Hofmeister trend,[105] anions that give rise to tight $RNH_3^+\cdots X^-$ ion-pairs hamper polymer formation, halting the growth of the chain to few monomer units. In other words, the counterion was found to effectively compete with the calixarene cavity for the alkylammonium guest moiety determining a progressive attenuation of the polymer-monomer association constant.

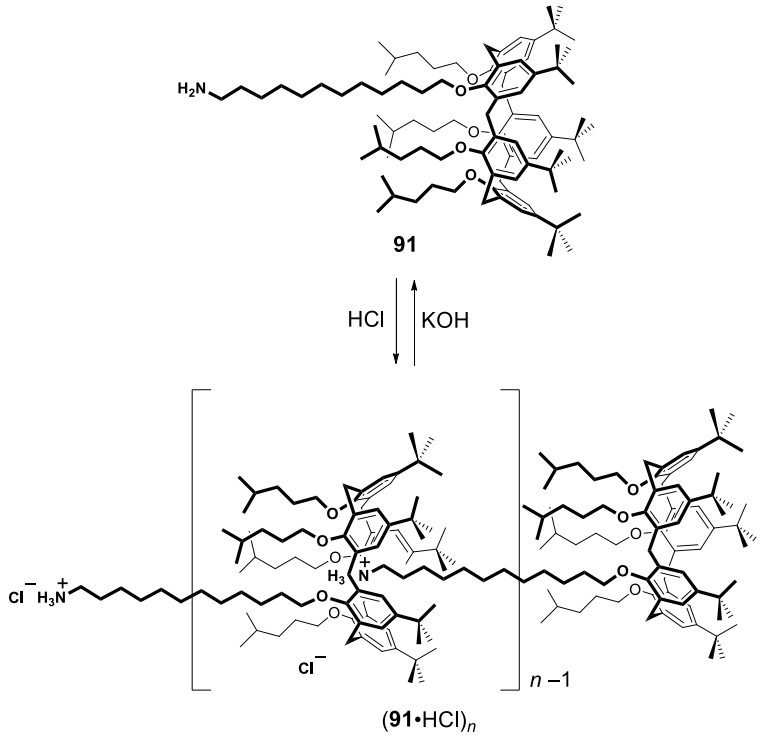

Figure 49. Reversible assembly-disassembly of AB-type supramolecular polymer (**91**·HCl)$_n$ (Gattuso *et al.*).[104]

Nonetheless, the most efficient of the systems investigated, **91**·HOPic (average DP = 20 at 40 mM), formed fibres up to 100 μm long and about 800 nm wide upon evaporation (**Fig. 50**).

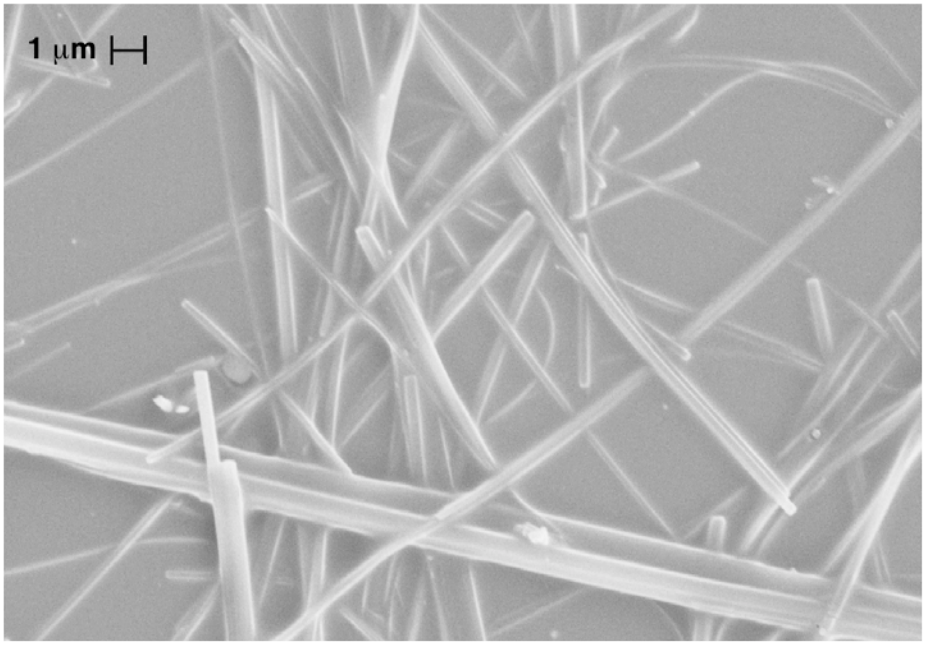

Figure 50. Scanning electron micrograph of fibres formed by slow evaporation of a chloroform solution of **91**·HOPic (Gattuso *et al.*).[104]

In a following paper, it was also demonstrated that for similar AB-type polymers, chain length was feasibly regulated by the use of A- or B-type orthogonal monotopic chain terminators, e.g. a competitive host (penta-*O*-*tert*-butoxycarbonylmethyl-calix[5]arene **90**) or a competitive guest (*n*-$BuNH_3^+PF_6^-$).[106]

Encouraged by the greater chain-length control ascertained in the above mentioned systems, as a natural evolution of this work, we designed an elegant strategy to enhance the degree of polymerization by synthesizing calixarene-derivative **92**.

This heteroditopic[107] AB-type monomer is able to simultaneously recognize and bind both the cation, within the calixarene cavity, and the pertinent counterion, by hydrogen-bond anchorage to the ureido site, ultimately overcoming the ion-pairing adverse effects connected with the recognition of a charged guest by a neutral receptor in low polarity solvents.[108]

Monomer **91** was therefore equipped with an auxiliary upper-rim *n*-butyl-ureido group, and the resulting monomer **92** was tested for self-assembly upon treatment with a range of different acids (**Fig. 51**).

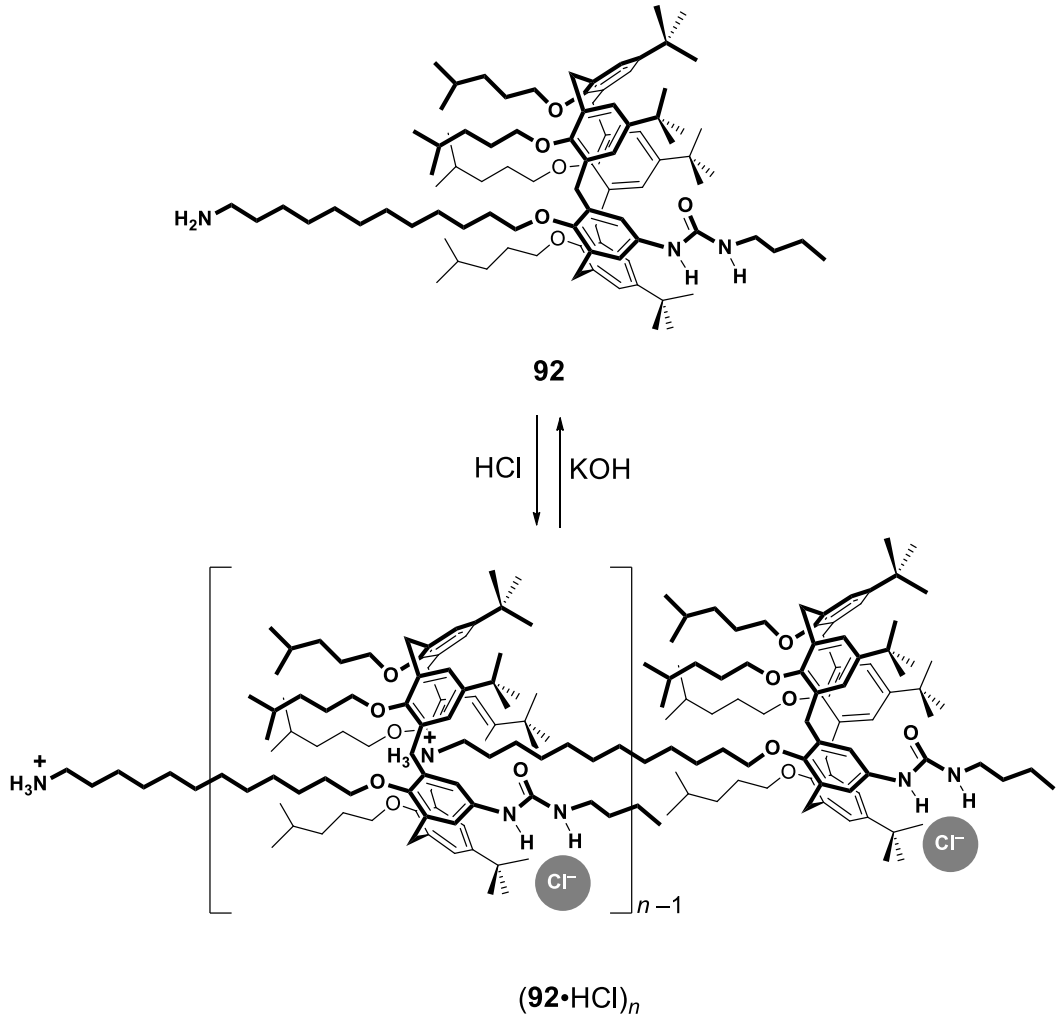

Figure 51. Reversible assembly-disassembly of AB-type supramolecular polymers (**92**·HCl)$_n$ (Gattuso *et al.*).[108]

The approach proved to be successful, with an approximate threefold increase of the DP value of (**92**·HCl)$_n$ (with respect to (**91**·HCl)$_n$), as shown by a combined ^{1}H and diffusion NMR study. Moreover, the polymer was found to be thermally stable over a

wide temperature range (–60 to 100 °C). Additional light scattering investigations showed that this supramolecular polymer assembles according to a rather unusual mechanism whereby, the monomers would first assemble into concentration-independent random-coiled strands, and the resulting oligomers would then form concentration-dependent clusters with radii as high as 150 nm in the semidilute regime ([**92**·HCl] = 0.1 g/cm^3).[109]

Envisaging this way as a smart route to generate chiral supramolecular polymers, we proceeded with a treatment of **92** with either (*R*)- or (*S*)-mandelic acid (henceforth referred to as MandH) and supramolecular polymers with opposite helical chirality, as shown from the induced circular dichroism traces with opposite sign, successfully, were assembled.[108] Additional experiments were performed aimed at revealing whether such aggregates could manifest 'chiral memory': treatment of (**92**·(*R*)-MandH)$_n$ –or the corresponding enantiomer (**92**·(*S*)-MandH)$_n$– with a stronger acid such as CF_3CO_2H led to the replacement of the backbone-docked counterion (i.e., trifluoroacetate instead of mandelate), but did not erase the chirality of the polymer (see the persistence of a CD signal in **Fig. 52**). In other words, the polymer assembled in a chiral fashion as a result of protonation with a chiral acid, and then kept (up to some extent) its own asymmetry even after replacement of the chiral docked anion with an achiral one.

The finding that paved the way to the use of the calix[5]arene-alkylammonium ion recognition motif for the self-assembly of supramolecular polymers was also the discovery of the ability to form of capsular assemblies.[110] In fact, in the presence of α,ω-alkanediyldiammonium dications of appropriate length ($^+H_3N(CH_2)_nNH_3^+$, n = 10, 12), both **89** and **90** were able to form 1:1 and 2:1 complexes (**Fig. 53**),[111] depending on the host-to-guest ratio.

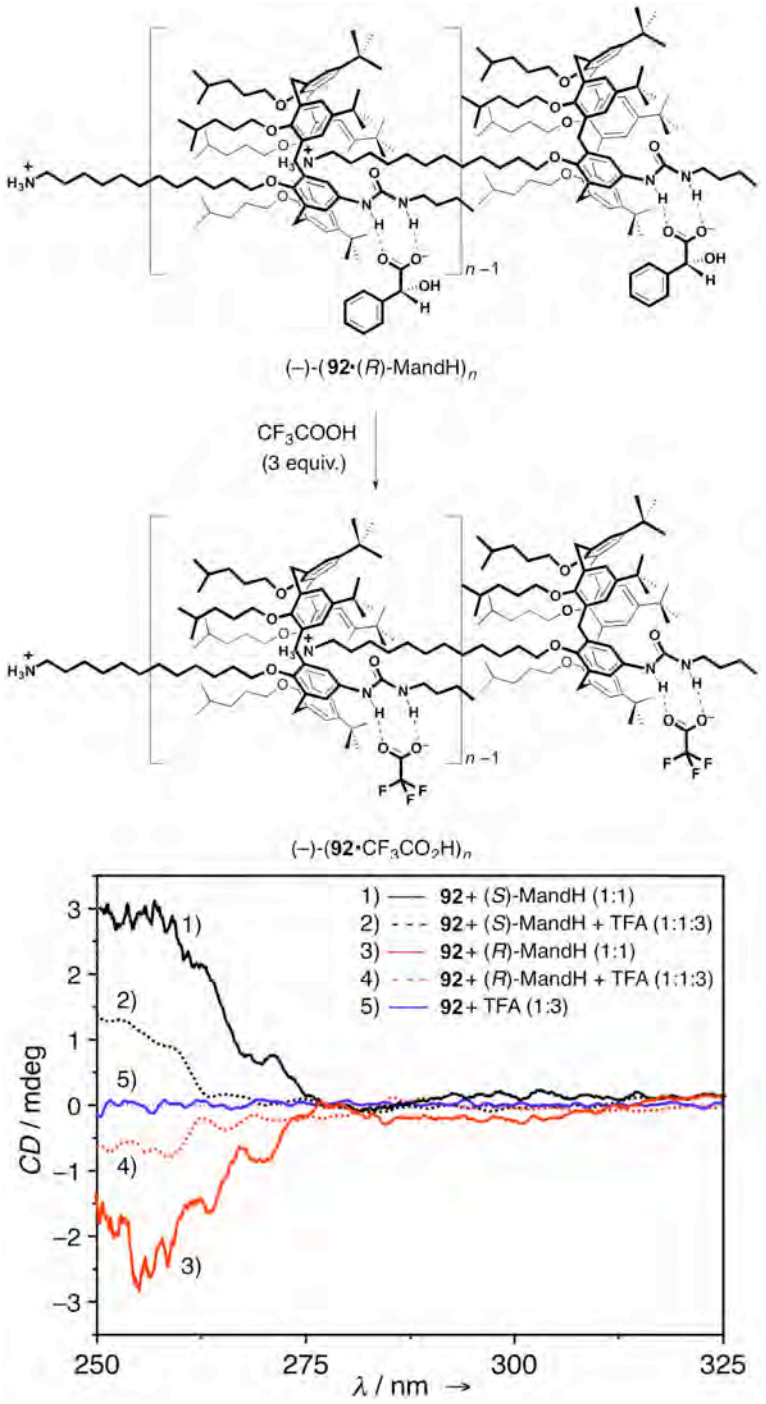

Figure 52. Chiral memory displayed by (**92**·(*R*)-MandH)n and (**92**·(*S*)-MandH)$_n$ (structures refer to (**92**·(*R*)-MandH)$_n$) (Gattuso *et al.*).[108]

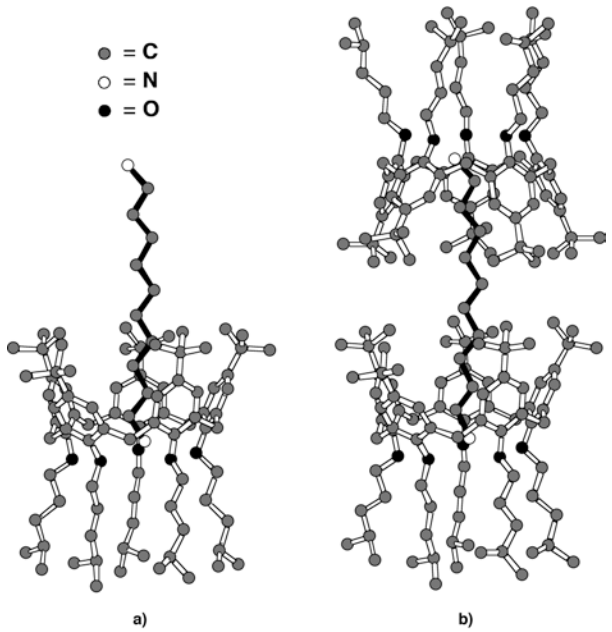

Figure 53. Molecular models of a) the 1:1 inclusion complex and b) the 2:1 capsular assembly between calix[5]arene **89** and 1,10-decanediyldiammonium ion (Parisi *et al.*).[111]

The divergent-cavity bis-calix[5]arenes **93–95** (**Fig. 54**) were then synthesized by using *p*-, *m*- or *o*-xylene spacers, and their self-assembly behaviour in the presence of 1,10-decanediyldiammonium dipicrate was studied in depth by ^{1}H NMR titration/dilution and diffusion NMR techniques.[112]

Four different types of supermolecules at will were formed : a 1:1 endo-cavity complex $^+H_3N(CH_2)_{10}NH_3^+\subset$**93**, a 1:2 bis-endo-cavity complex $^+H_3N(CH_2)_{10}NH_3^+\supset$**93**$\subset{}^+H_3N(CH_2)_{10}NH_3^+$, a monocapsular complex **93**$\supset{}^+H_3N(CH_2)_{10}NH_3^+\subset$**93**, and an oligomeric polycapsular assembly **93**$\supset[{}^+H_3N(CH_2)_{10}NH_3^+\subset$**93**$]_p\supset{}^+H_3N(CH_2)_{10}NH_3^+$ ($p > 1$) (referred to, in **Fig. 55**, as types A–D, respectively).

The latter, the type-D polycapsular species, was found to grow over the concentration range employed in these experiments (max 50 mM) up to an 8-mer.

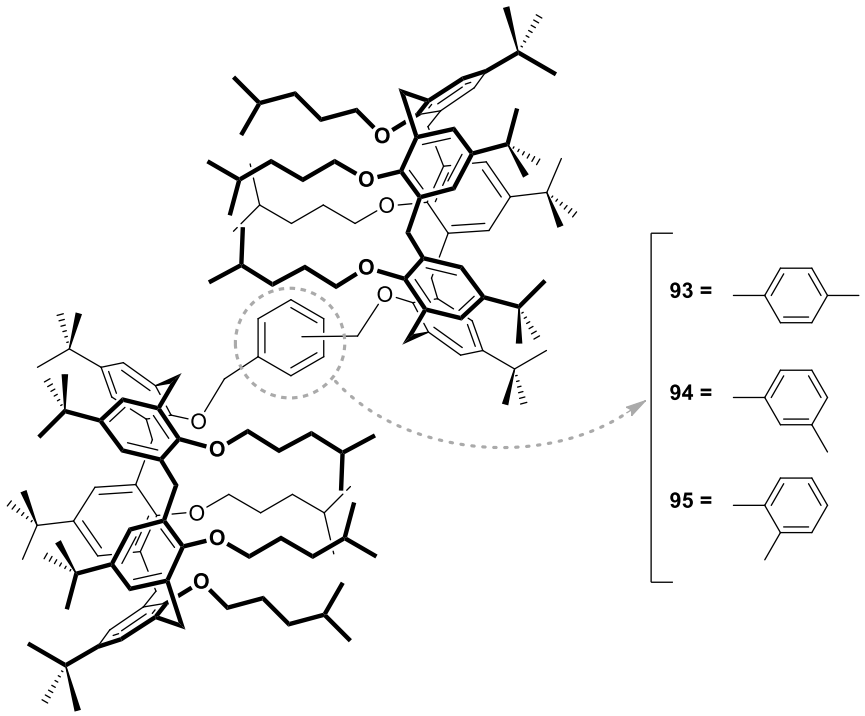

Figure 54. Divergent-cavity bis-calix[5]arenes **93–95** (Parisi *et al.*).[112]

The complementary host-guest pairs display a spontaneous and reversible tendency to self-assembly in supramolecular polymers through a mechanism strongly dependent on the geometry of the spacer, the molar ratios of the host/guest system, and the length of the connector employed.

As showed in **Fig. 55**, addition of a defect of guest ≤ 0.5 equiv. to a solution of **93** produced almost the monocapsular complex (type C). Upon increasing guest concentration (up to 1:1 molar ratio) the microequilibria shifted towards the oligomeric species (type D) that, after dilution, affords the 1:1 *endo*-cavity complex (type A).

Addition of an excess of guest solution to complex A lead to a bis-*endo*-cavity complex (type B) that can be reconverted to the type C by addition of host solution.

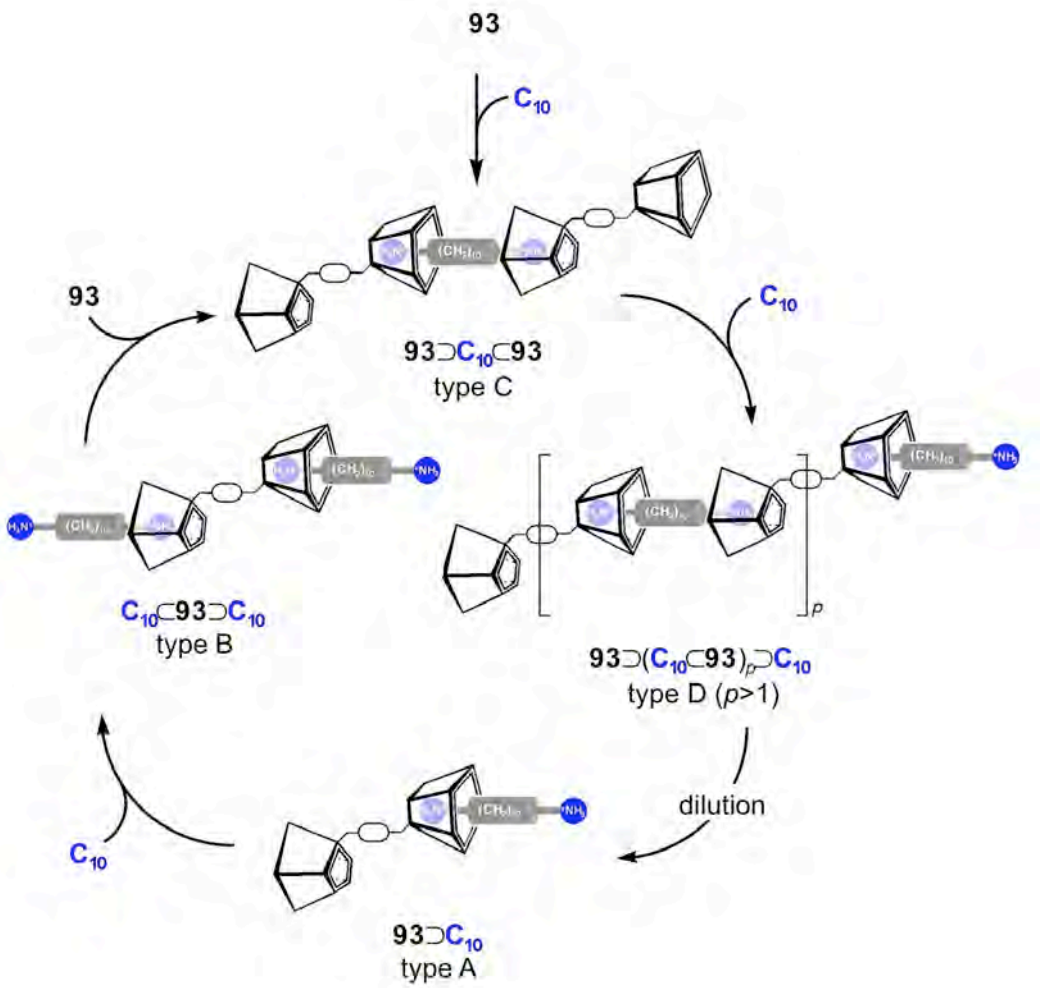

Figure 55. Cyclic reversible self-assembly dynamics of bis-calix[5]arenes **93** and $^{+}H_3N(CH_2)_{10}NH_3^{+}$ (C_{10}) monomers.[112]

According to microequilibria studies on the assembly of these complexes, growth-limitation was ascribed to the formation of type-B subunits (i.e., a bis-calixarene with both cavities filled by alkanediyldiammonium ions) suffering from electrostatic repulsion effects. Moreover, the geometry of the xylene spacer was found to influence the self-assembly efficiency (*para* > *meta* >> *ortho*) of these systems, probably as a result of both an increased steric crowding and a reduced guest-to-guest distance.

The strategy of pairing cation and anion binding sites was transferred from the AB-type to the AA/BB-type systems, however, placing in this case the ureido moiety at the lower rim, connecting two calix[5]-bis-crown-3 derivatives by means of a 1,4-bis-ureido-phenylene.[113] The resulting divergent bis-calixarene **96** (**Fig. 56**), in the presence of the complementary 1,8-octanediyldiammonium dichloride, gave rise to supramolecular oligomers including, at a monomer concentration of 25 mM, three bis-calixarene and three diammonium guest molecules.

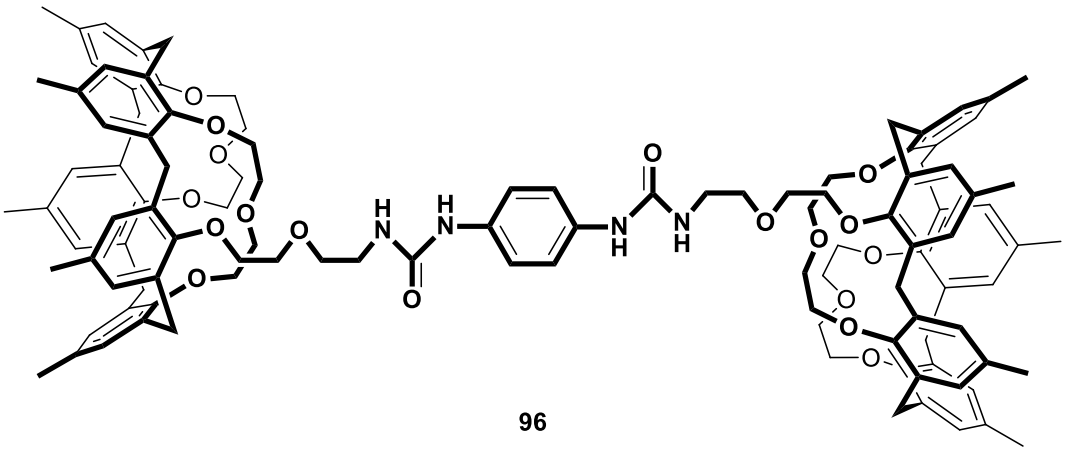

96

Figure 56. Divergent bis-calixarene **96** (Gattuso *et al.*).[113]

A set of ^{1}H NMR experiments demonstrated the ability of the ureido moieties of **96** to efficiently bind chloride ions thus providing additional stabilization of the supramolecular aggregates.

Pappalardo and co-workers reported on a poly(*p*-phenyleneethynylene) polymer **97** (**Fig. 57**), featuring two *cone*-like calix[5]arene cavities connected to a rigid *p*-phenyleneethynylene spacer, synthesized by using a Pd-catalyzed cross-coupling approach.[114]

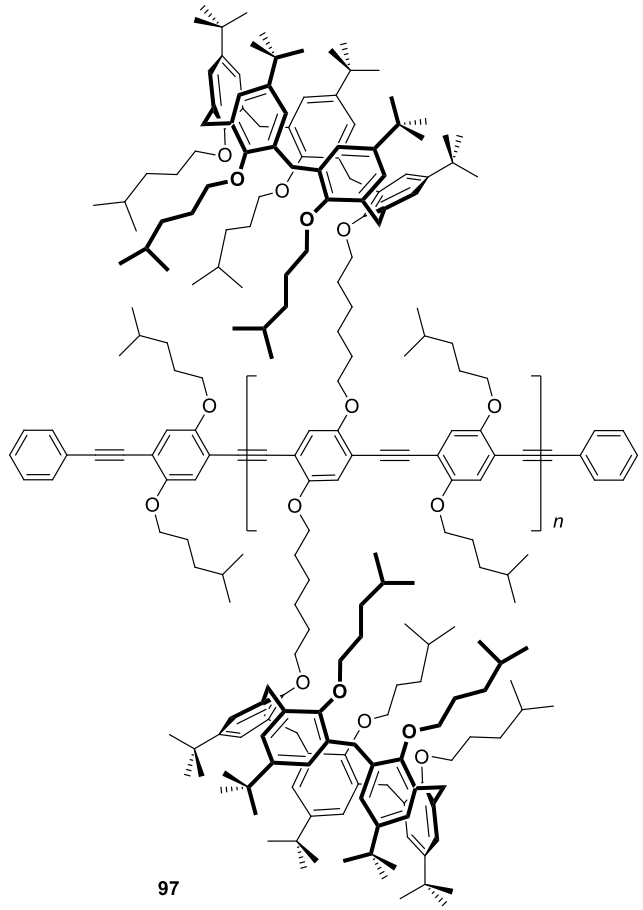

Figure 57. Poly(*p*-phenyleneethynylene) polymer **97** (Pappalardo *et. al.*).[114]

Treatment of **97** with 0.5 equiv. of 1,10-decanediyldiammonium dipicrate led to the formation of the polycapsular polymeric network $\mathbf{97}_{\mathbf{network}}$, whereas saturation of the calixarene cavities by addition of an excess of guest led to 'isolated' strands of bis-endo-cavity complexed $\mathbf{97}_{\mathbf{capped}}$ (**Fig. 58**).

Additions of Et_3N followed by TFA demonstrated the reversibility of the 'assembly-disassembly' process. Also, AFM analysis showed a homogeneous and very regular continuous, polycapsular network on surface, a feature that makes this system interesting for electronic and analyte sensing applications.

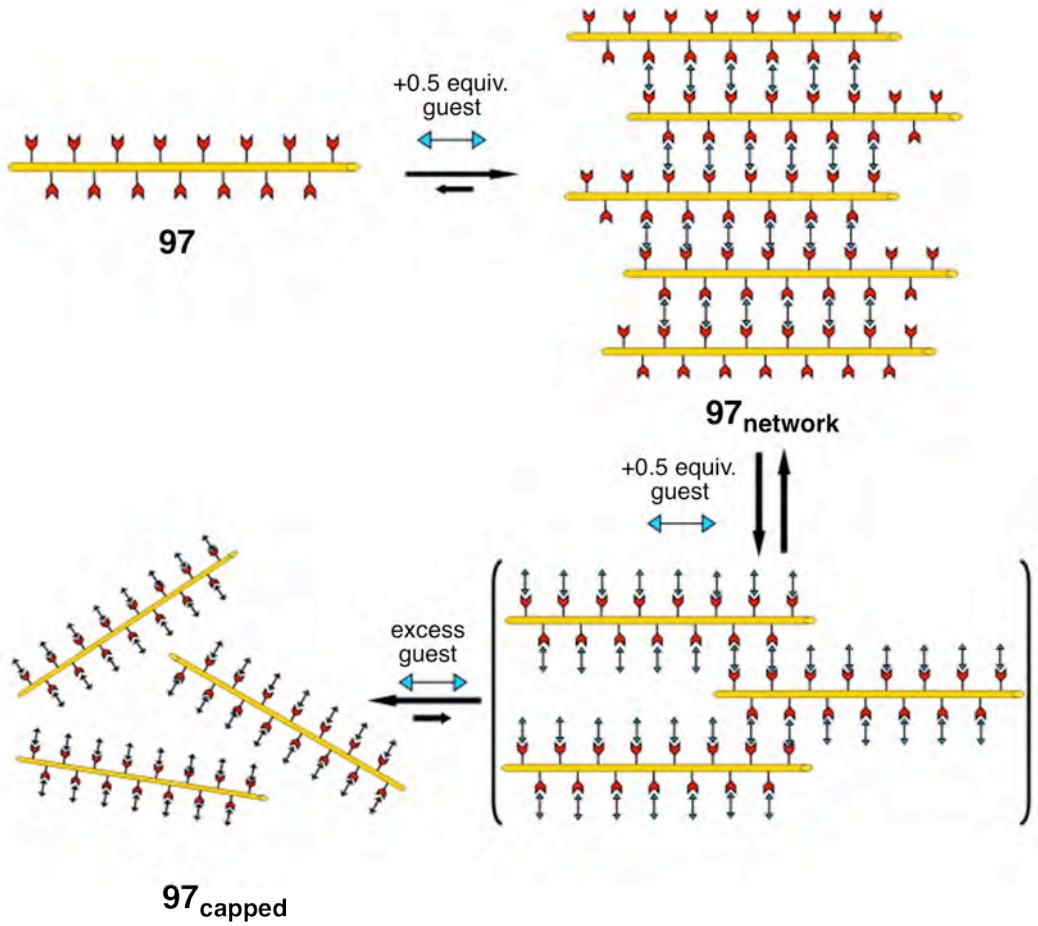

Figure 58. Schematic representation of the polycapsular polymer network assembly (**97**$_{network}$ and **97**$_{capped}$) obtained from **97** and 1,10-decanediyldiammonium dipicrate (Pappalardo *et al.*).[114]

2.2.2. Design and synthesis of carboxyl-calix[5]arenes: smart receptors for amines

Knowing the affinity of calix[5]arene for linear alkyammonium[110] ions, in 2012 my research group developed a new synthetic strategy to overcome ion-pair association that – particularly in low polarity solvents, where both receptor and counterion compete for the same ionic species – has a detrimental effect on host-guest association. To this end, calix[5]arene **98**·H and **99**·H – bearing a carboxyl group at the narrow rim– were selected as synthetic targets, as they formally descend from the two most efficient receptors for linear alkylammonium, i.e., calix[5]arenes **89** and **90**.

The replacement of a lower-rim substituent with a carboxyl group, capable of undergoing acid-base reaction with an amine guest, and so taking advantage of the additional stabilization provided by electrostatic ion-pairing interactions, was demonstrated to be an advantageous route, leading to increased apparent host-guest association constants (K_a = 3.21 ± 0.3 × 10^4 and K_a = 1.13 ± 0.1 × 10^4 M^{-1}, corresponding to *ca*. 84 and 74% complexation for *n*-$BuNH_3^+$⊂**98**$^-$ and *n*-$BuNH_3^+$⊂**99**$^-$, respectively).[110]

Carboxyl-calix[5]arenes **98**·H and **99**·H were synthesized from penta-*tert*-butyl-tetrakis-(4-methylpentyloxy)calix[5]arene[107b] **100** and penta-*tert*-butyl-(benzyloxy)calix[5]arene[101] **102**, respectively, as depicted in **Scheme 18**.

Accordingly, alkylation of tetra-O-ether **100** with tert-butyl bromoacetate, in the presence of K_2CO_3 as a base, provided mono-ester derivative **101** (92% yield). Removal of the tert-butyl group by TFA treatment yielded **98**·H (66%). Calix[5]arene **99**·H, on the other hand, was synthesized in four steps starting from mono-O-ether **102**, which was exhaustively alkylated with tert-butyl bromoacetate in the presence of K_2CO_3 to afford tetra-ester **103** in 81% yield. Catalytic hydrogenolysis (Pd/C) of the

benzyl protecting group provided hydroxy-calix[5]arene **104** (89%), which was alkylated with benzyl bromoacetate/K_2CO_3 to yield mixed penta-ester **105** (80%). Finally, debenzylation with H_2 and Pd/C provided the acid derivative **90**·H in 94% yield.

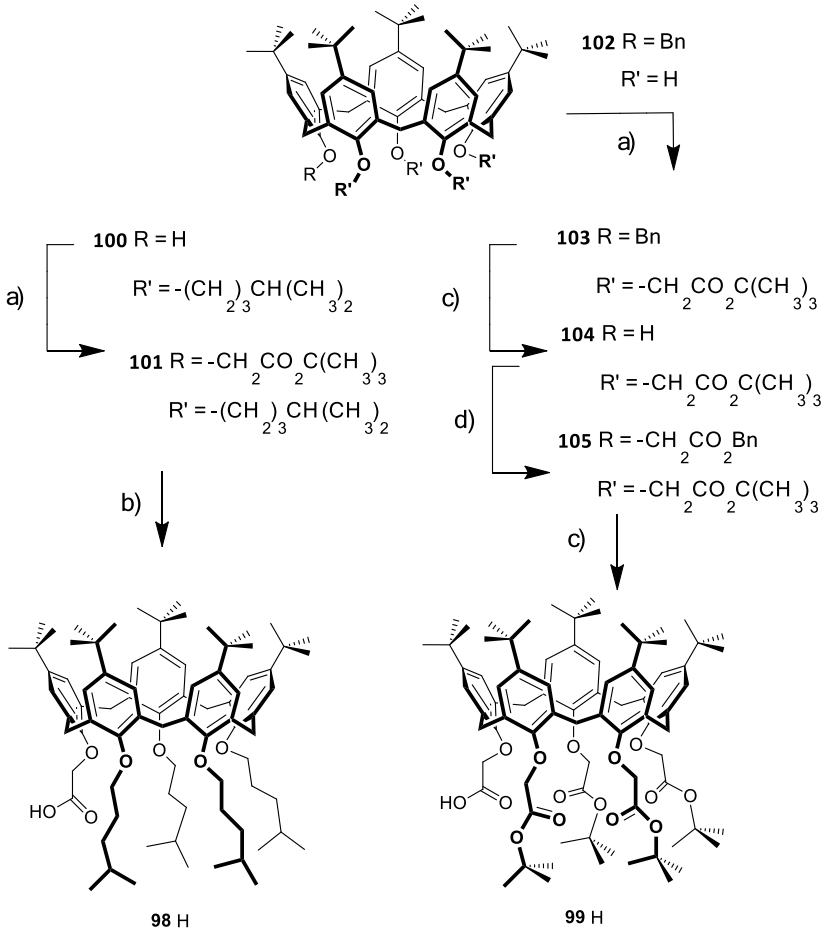

Scheme 18. Synthesis of calix[5]arenes **98**·H and **99**·H: a) $BrCH_2CO_2C(CH_3)_3$, K_2CO_3, CH_3CN, reflux, 24 h; b) TFA, $CHCl_3$, rt, 4 h; c) H_2, Pd/C, AcOEt, rt, 5-6 h; d) $BrCH_2CO_2Bn$, K_2CO_3, CH_3CN, reflux, 24 h.

A combination of NMR and XRD studies displays that both molecules possesses a C_S-symmetric cone-out conformation.[115] This non-regular cone conformation[101] is

substantiated by down-field resonances for the hydrogen atoms of the *tert*-butylphenoxy ring bearing the carboxyl moiety (relative to those of the remaining aryl units) which, together with the presence of a carboxyl hydrogen peak (δ = 10.2 and 10.1 ppm for **98**·H and **99**·H, respectively), suggest the likely presence of an intramolecular hydrogen bonding between the carboxyl group and the phenolic oxygen atoms of **98**·H and **99**·H.

Single-crystal X-ray analyses confirms that in the solid state both derivatives adopt similar cone-out conformations, wherein three tert-butylphenoxy rings are leaning outward with respect to the cavity of the macrocycle, whereas the remaining two (namely, B and B' for **98**·H and C and B' for **99**·H) are nearly perpendicular to the calixarene reference plane passing through the five bridging methylene groups.

In both cases, the calixarene aromatic cavity is filled by an acetonitrile solvent molecule, held inside the macrocycle by a number of CH···π interactions. The four pendant groups at the narrow rim take on an extended conformation and the carboxyl OH group points in, toward the bottom of the aromatic cavity. Close comparison of the two structures reveals that ring A of **98**·H is more markedly tilted away from the axis of the cavity than the corresponding ring of **99**·H (151.4(1) and 132.68(6)° for **98**·H and **99**·H, respectively). This conformational difference is associated with a different H-bond pattern involving the carboxyl group (**Fig. 59b**). While in **98**·H the carboxyl group forms a strong three-centre intramolecular hydrogen bond with the phenolic oxygen atoms linked to rings B and C (O···O distances, 2.625(9) and 2.874(9) Å), in the case of **99**·H a weaker two-centre hydrogen bond, between the corresponding carboxyl group and the phenolic oxygen of ring B (O···O 2.995(3) Å), is observed (**Fig. 59b**). The different H-bond strength and consequently the closer proximity of the oxymethylenecarboxyl moiety to the bottom of the cavity and the wider outward inclination of ring A, may reflect a superior H-bond acceptor ability of

the phenolic oxygen atoms present in **98**·H with respect to those of **99**·H (linked to 4-methylpentyl and *tert*-butoxycarbolylmethyl pendant moieties, respectively). The distance of the hydroxyl oxygen atom from the calixarene reference plane of –1.712(8) and –2.614(2) Å for **98**·H and **99**·H, respectively, quantifies the major conformational difference between the two macrocycles.

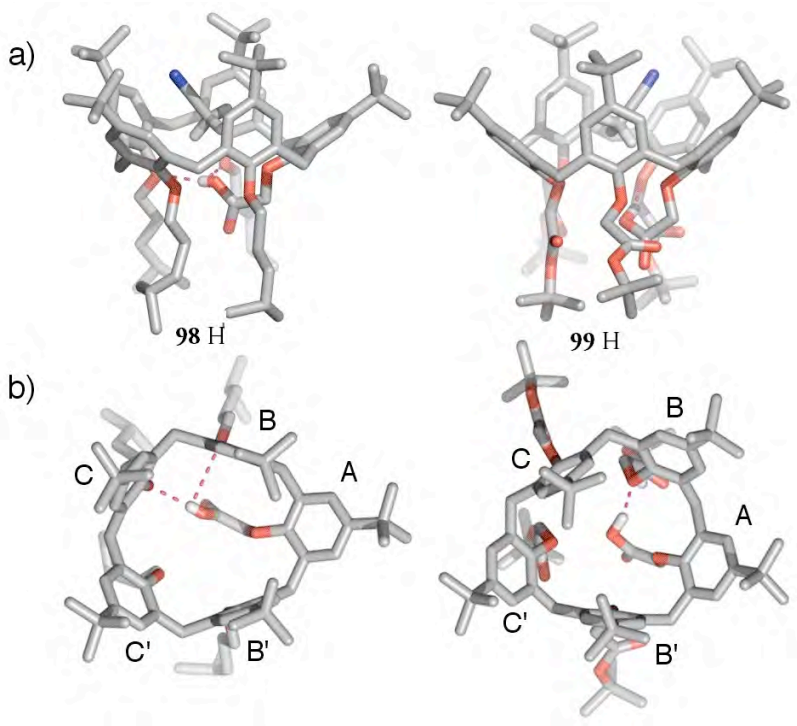

Figure 59. Solid-state structures of calix[5]arenes **98**·H and **99**·H: a) side views showing the presence of an acetonitrile solvent molecule filling the cavity and b) top views displaying the presence of intramolecular H-bond(s) between the carboxyl group and the phenolic oxygen atom(s) (the acetonitrile molecule has been omitted for clarity).

Early observations on the formation –in solution– of 2:1 capsular complexes,[111] allowed us to define the minimum length of the dicationic guest necessary to efficiently achieve capsule assembly, and we subsequently managed to harness this recognition motif to produce polycapsular oligomeric aggregates.[112,113]

2.2.3. Carboxyl-calix[5]arenes and α,ω-diaminoalkanes: making capsules

When the tetraether-calix[5]arene carboxylic acid **99**·H was exposed to α,ω-diaminoalkanes ($H_2N(CH_2)_nNH_2$, n = 10–12), proton-transfer-mediated recognition took place, leading to the formation of salt-bridged 2:1 capsular and quasi-capsular complexes (**Fig. 60**).[110b]

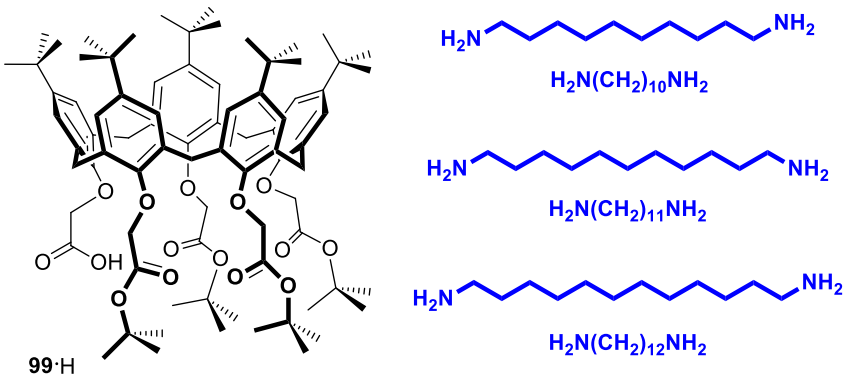

Figure 60. Tetraether-calix[5]arene carboxylic acid **99**·H and α,ω-diaminoalkanes ($H_2N(CH_2)_nNH_2$, n = 10–12).

Given the solubility of **99**·H in CF_3CH_2OH (TFE), co-crystallization experiments were successfully carried out with the vapour diffusion method using the sitting drop technique. Routinely, sample solutions were prepared by mixing 32 μL of **99**·H TFE solutions (34 mM) with 28 μL TFE solutions of a given $H_2N(CH_2)_nNH_2$ (n = 10–12) guest (20 mM) and well solutions (reservoir solutions) were prepared by mixing the precipitating agent, polyethylene glycol (PEG) 300, with TFE in the 15–40% range (v/v). A 4 μL aliquot of the sample solution was deposited on a micro-bridge inserted in a well of the Linbro box and mixed with an equal volume of the reservoir solution. The 8 μL drops were set to equilibrate by vapour diffusion with 1 mL reservoir

solutions in sealed wells at 20°. Single spearhead-shaped crystals suitable for X-ray analysis by synchrotron radiation were obtained after 3 months.

The **99**$^{-}\supset{}^{+}H_3N(CH_2)_{10}NH_3^{+}\subset$**99**$^{-}$ solid-state structure reveals that proton-transfer-mediated encapsulation has taken place, and that the diprotonated 1,10-decanediammine is nestled within the confined space defined by two calix[5]arene units (**Fig. 61**).

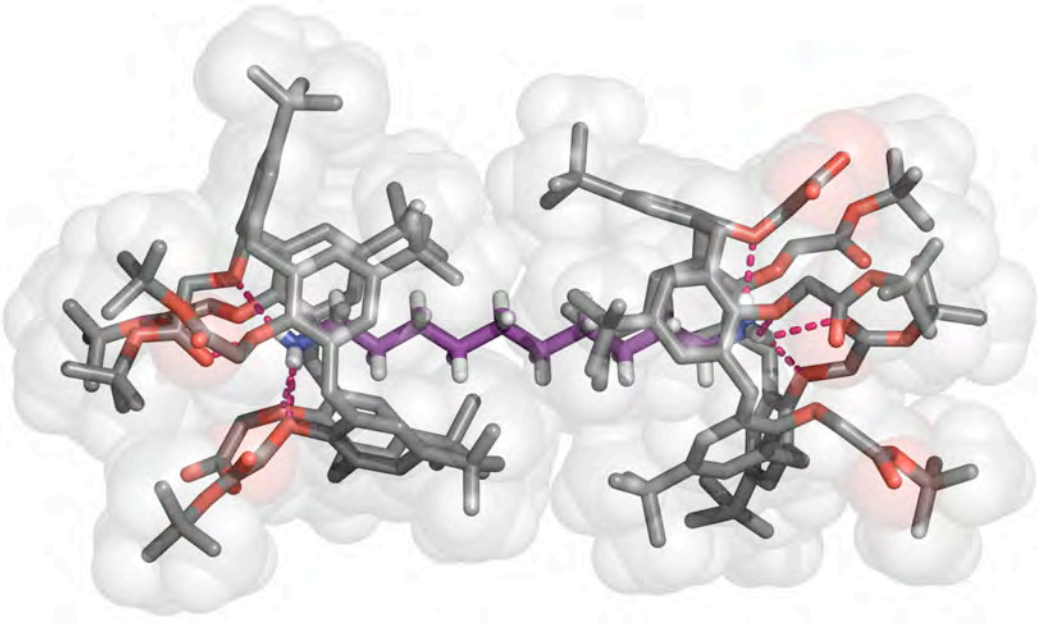

Figure 61. Solid-state structure of **99**$^{-}\supset{}^{+}H_3N(CH_2)_{10}NH_3^{+}\subset$**99**$^{-}$. Values of selected H-bonds, C-H···π and van der Waals interactions: N···O_{Ar} = 2.81(1)–2.87(1) Å; α-, β-CH_2···Ar = 3.47(1)–3.64(1) Å; C(CH_3)$_3$···C(CH_3)$_3$ = 3.74(2)–3.94(2) Å.

The guest adopts a single fully extended ziz-zag conformation, spanning the space between the bottoms of the two receptor cavities. The mean planes of the two calixarene molecules –defined by the bridging methylene carbon atoms– lie roughly parallel to each other (174.7(2)°) and the two facing cavities are seen offset (by 5.2 Å) to better accommodate the diammonium guest, as optimum host-guest interaction

(i.e., hydrogen bond formation) takes place when the C–N bond of the guest is almost perpendicular to the mean plane of the phenolic oxygen atoms.

A closer inspection shows that the two calixarene bowls adopt a *cone*-out conformation (**Table 9**), which is mandatory for *endo*-cavity inclusion of linear primary ammonium ions.

Table 9. Tilting angles (°) between the aromatic rings and the calixarene mean plane for the capsular complexes **99**$^-$⊃$^+H_3N(CH_2)_{10}NH_3^+$⊂**99**$^-$, **99**$^-$⊃$^+H_3N(CH_2)_{11}NH_3^+$⊂**99**$^-$ and **99**$^-$⊃$^+H_3N(CH_2)_{12}NH_3^+$⊂**99**$^-$.

	A	**B**	**B'**	**C**	**C'**
99$^-$⊃$^+H_3N(CH_2)_{10}NH_3^+$⊂**99**$^-$	127.0(2)	95.6(3)	122.0(2)	140.3(4)	93.0(2)
99$^-$⊃$^+H_3N(CH_2)_{11}NH_3^+$⊂**99**$^-$	126.9(2)	118.6(2)	92.8(2)	99.0(2)	135.2(2)
99$^-$⊃$^+H_3N(CH_2)_{12}NH_3^+$⊂**99**$^-$	92.7(1)	134.6(1)	138.4(1)	121.6(1)	93.3(1)

The aromatic rings of **99**$^-$ are labelled as shown in **Fig. 62** (the *tert*-butyloxycarbonylmethyl chains are omitted for the sake of clarity).

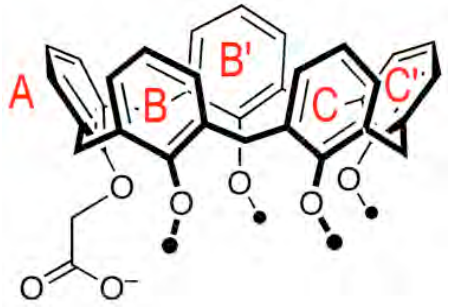

Figure 62. Labelling of aromatic rings of **99**$^-$.

This encapsulation complex is held together by a number of non-covalent interactions of a different nature. Each ammonium group forms four hydrogen

bonds (**Table 10**), three of which are with the oxygen atoms belonging to the A, B' and C phenolic rings, while the fourth is with the carbonyl oxygen atom of the ester pendant moiety attached to the C ring (whose *tert*-butyl group fills the space under the calixarene cavity).

Table 10. H···O distances (Å) for the H-bond interactions detected in the crystal structures of the three capsular complexes **99**$^{-}$⊃$^{+}H_3N(CH_2)_{10}NH_3^{+}$⊂**99**$^{-}$, **99**$^{-}$⊃$^{+}H_3N(CH_2)_{11}NH_3^{+}$⊂**99**$^{-}$ and **99**$^{-}$⊃$^{+}H_3N(CH_2)_{12}NH_3^{+}$⊂**99**$^{-}$.

Compound	N–H···O	
99^{-}⊃$^{+}H_3N(CH_2)_{10}NH_3^{+}$⊂**99**$^{-}$	N(6a)-H(6a2)···O(4l)	2.81(1)
	N(6a)-H(6a2)···O(4g)	2.83(1)
	N(6a)-H(6a1)···O(2g)	2.83(1)
	N(6a)-H(6a3)···O(1g)	2.87(1)
99^{-}⊃$^{+}H_3N(CH_2)_{11}NH_3^{+}$⊂**99**$^{-}$	N(6aa)-H(6a5)···O(3g)	2.72(2)
	N(6aa)-H(6a5)···O(3la)	2.93(3)
	N(6aa)-H(6a3)···O(1g)	2.96(3)
	N(6aa)-H(6a1)···O(5g)	3.11(2)
	N(6ab)-H(6a5)···O(3g)	3.01(2)
	N(6ab)-H(6a5)···O(3la)	2.76(3)
	N(6ab)-H(6a6)···O(1g)	2.66(3)
	N(6ab)-H(6a4)···O(5g)	2.65(2)
99^{-}⊃$^{+}H_3N(CH_2)_{12}NH_3^{+}$⊂**99**$^{-}$	N(6a)-H(6a3)···O(5l)	2.799(6)
	N(6a)-H(6a3)···O(5g)	2.825(5)
	N(6a)-H(6a1)···O(4g)	2.929(5)
	N(6a)-H(6a2)···O(2g)	2.737(6)

In addition, CH-π interactions are in play between the α- and β-CH_2s at each end of the diammonium guest and the calixarene B,C' and A,B' aromatic rings, respectively. The wider rim *tert*-butyl groups are in van der Waals contact, providing at the same time sealing of the *endo*-capsular space and additional weak

attractive interactions. Remarkably, the carboxylate groups are seen pointing away from the ammonium-containing calixarene cavity, in a similar fashion to what had previously been observed in the solid-state structure of the *n*-$BuNH_3^+$⊂**99**$^-$ *endo*-cavity complex. The wider rim *tert*-butyl groups are in van der Waals contact, providing at the same time sealing of the endo-capsular space and additional weak attractive interactions. Remarkably, the carboxylate groups are seen pointing away from the ammonium-containing calixarene cavity.

As in that case, the carboxylate group prefers to hydrogen-bond with CF_3CH_2OH crystallization molecules rather than fold back to ion-pair with the ammonium counterion.[110a]

In the case of the **99**$^-$⊃$^+H_3N(CH_2)_{11}NH_3^+$⊂**99**$^-$ complex, the overall picture is quite similar to that observed with the shorter $^+H_3N(CH_2)_{10}NH_3^+$ guest (**Fig. 63**).

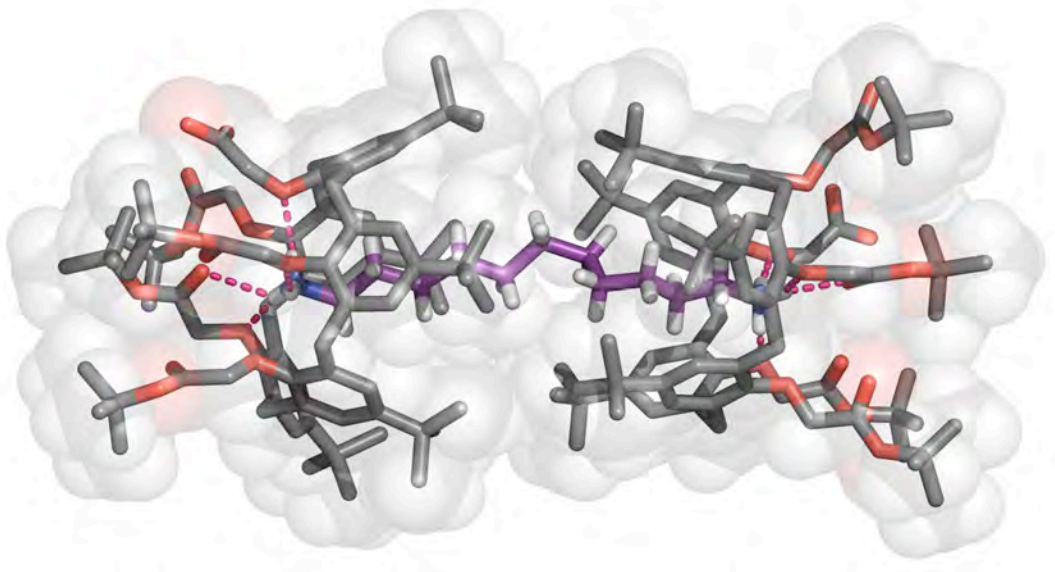

Figure 63. Solid-state structure of **99**$^-$⊃$^+H_3N(CH_2)_{11}NH_3^+$⊂**99**$^-$. Values of selected H-bonds, C-H···π and van der Waals interactions: N···O_{Ar} = 2.65(2)–3.11(2) Å; α-, β-CH_2···Ar = 3.55(1)–3.81(1) Å; C(CH_3)$_3$···C(CH_3)$_3$ = 3.91(2)–4.00(3) Å.

A crystallographic two-fold symmetry axis relates the two halves of the capsule. Again, the two calix[5]arenes fully envelop the $^{+}H_3N(CH_2)_{11}NH_3^{+}$ dication, bringing their wider-rim *tert*-butyl groups into van der Waals contact. The slightly longer guest, on the other hand, has to adjust its conformation to fit within the capsular space, by making one *gauche* turn. Owing to the mismatch between the guest conformation and the crystallographic symmetry, the guest is seen disordered over two equivalent positions. The two calixarenes are seen again offset, but to a lesser extent (4.2 Å), with their mean planes lying roughly parallel (175.1(1)°). The macrocycles adopt their customary *cone*-out conformation, and the ammonium heads of the guest are once again involved in four H-bonds, although in this case the three phenolic oxygen atoms belong to rings A, B and C', with the fourth H-bond donor this time being the pendant ester group linked to ring C'. CH-π and van der Waals interactions are again in play.

The solid state structure of the **99**$^{-}$⊃$^{+}H_3N(CH_2)_{12}NH_3^{+}$⊂**99**$^{-}$ complex demonstrates that the $^{+}H_3N(CH_2)_{12}NH_3^{+}$ dication, lying in this case on a crystallographic inversion centre, is far too long to fit within a capsule formed by two calix[5]arene units (**Fig. 64**).[110b]

In fact, although the $^{+}H_3N(CH_2)_{12}NH_3^{+}$ guest adopts a single highly compressed conformation (two *gauche* turns), the two calix[5]arene molecules do not come into van der Waals contact (macrocyclic mean plane-to-mean plane angle: 178.1(1)°; cavity offset: 2.5 Å). This *quasi*-capsular complex, however, is held together by the same concert of *endo*-cavity non covalent interactions, with the ammonium groups H-bonded to the phenolic oxygen atoms of rings B, B', C and with the carbonyl oxygen atom of the ester pendant group attached to ring B.

α-CH_2 and β-CH_2 are within CH-π interaction distance of rings A,C' and B,C, respectively. Yet again, no salt bridges between host and guest molecules are

observed.[110b] As mentioned above, we have recently described the solid state structure of a family of capsular and *quasi*-capsular complexes, composed of the same α,ω-diaminoalkanes ($H_2N(CH_2)_nNH_2$, n = 10–12) used in the present study, and a different receptor, namely tetrakis-(4-methylpentyloxy)-calix[5]arene carboxylic acid **98**·H (see above), closely related to **99**·H (i.e., 4-methylpentyloxy substituents rather than *tert*-butoxycarbonylmethoxy ones at the narrow rim).[110e]

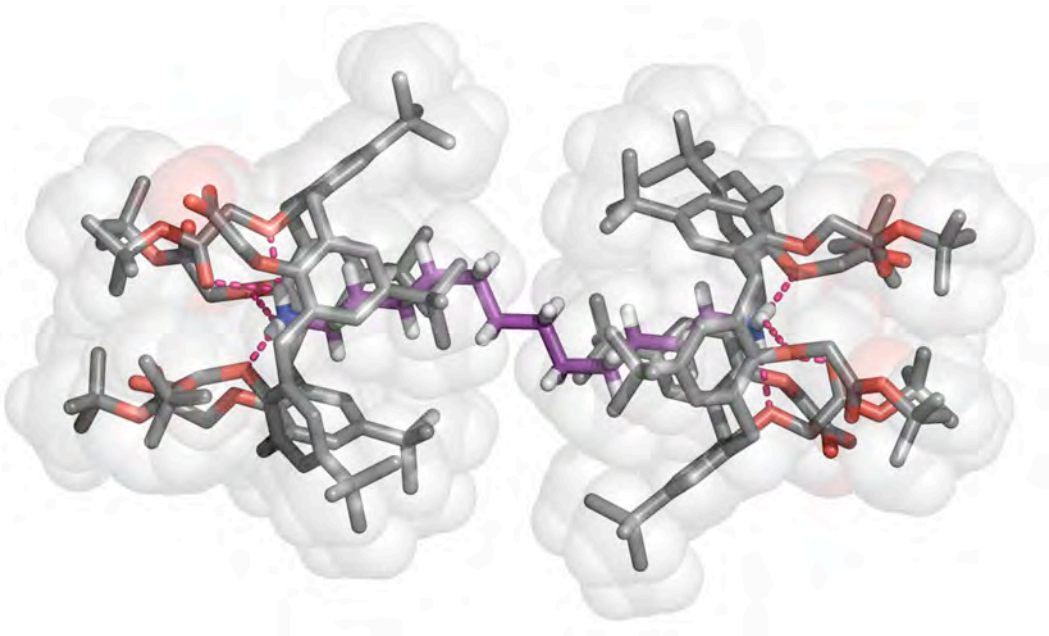

Figure 64. Solid-state structure of $\mathbf{99}^{-}\supset{}^{+}H_3N(CH_2)_{12}NH_3^{+}\subset\mathbf{99}^{-}$. Values of selected H-bonds and C-H···π: N···O_{Ar} = 2.737(6)–2.929(5) Å; α-, β-CH_2···Ar = 3.449(5)–3.933(5) Å.

Although in that case a similar general trend was observed, with the formation of sealed encapsulation complexes with $H_2N(CH_2)_{10}NH_2$ and $H_2N(CH_2)_{11}NH_2$, and a *quasi*-capsular one with $H_2N(CH_2)_{12}NH_2$, there are some remarkable differences that are worth discussing. The first, and possibly the most evident, is that in the previously

reported complexes all the carboxylate moieties were involved in endohedral salt bridge interactions with their respective *endo*-cavity-included guest ammonium ions. In the **99**$^{-}\supset{}^{+}H_3N(CH_2)_nNH_3^{+}\subset$**99**$^{-}$ complexes, no salt bridges are formed in analogy with the differences seen for the same receptors (**99**·H and **98**·H) in the solid state structures of their *n*-$BuNH_2$ *endo*-cavity complexes.[103c]

The carboxylate moiety, in the present cases, prefers an outward orientation, the ammonium heads forming their fourth H-bond with one of the carbonyl oxygen atoms of the ester pendant groups rather than with the carboxylate anion moiety. The second difference concerns the depth/position of the diammonium ion inside the cavities. In the previously reported encapsulation complexes, the nitrogen atom was seen above the reference mean plane described by the phenolic oxygen atoms at a distance of 0.474 to 1.051 Å, whereas in the **99**$^{-}\supset{}^{+}H_3N(CH_2)_nNH_3^{+}\subset$**99**$^{-}$ capsules it lies further away from the corresponding plane (0.71(3) to 1.136(9) Å). This lower degree of penetration may be the consequence of the exohedral orientation, adopted by the carboxylate group, which prevents salt-bridge formation. As a result, the complexes lack the attractive carboxylate-ammonium electrostatic interactions that would have pulled the ammonium moieties deeper inside the calixarene cavity. This behaviour is in line with that detected in the case of the *n*-$BuNH_2$ complexes (albeit to a lesser extent, 0.296 vs. 0.586 Å), but surprisingly in contrast with the *n*-$BuNH_3^{+}$ complexes of the parent neutral calix[5]arene receptors, where the ammonium guest penetrates deeper inside the cavity of pentakis-*tert*-butoxycarbonylmethoxy-calix[5]arene **90** than it does into the cavity of pentakis-(4-methylpentyloxy)-calix[5]arene **89.**[103a]

This effect was reasonably attributed to the ability of receptor **90** to establish a fourth hydrogen bond interaction with the ammonium moiety thanks to the

presence of the C=O hydrogen bonding acceptors from the ester groups at the lower rim.

With respect to the previously reported capsular complexes belonging to the **98**$^{-}\supset{}^{+}H_3N(CH_2)_nNH_3^{+}\subset$**98**$^{-}$ family, some differences were observed in the orientation of the receptor molecules in each complex (**Fig. 65**), particularly in the case of the capsule hosting the undecanediammonium guest.

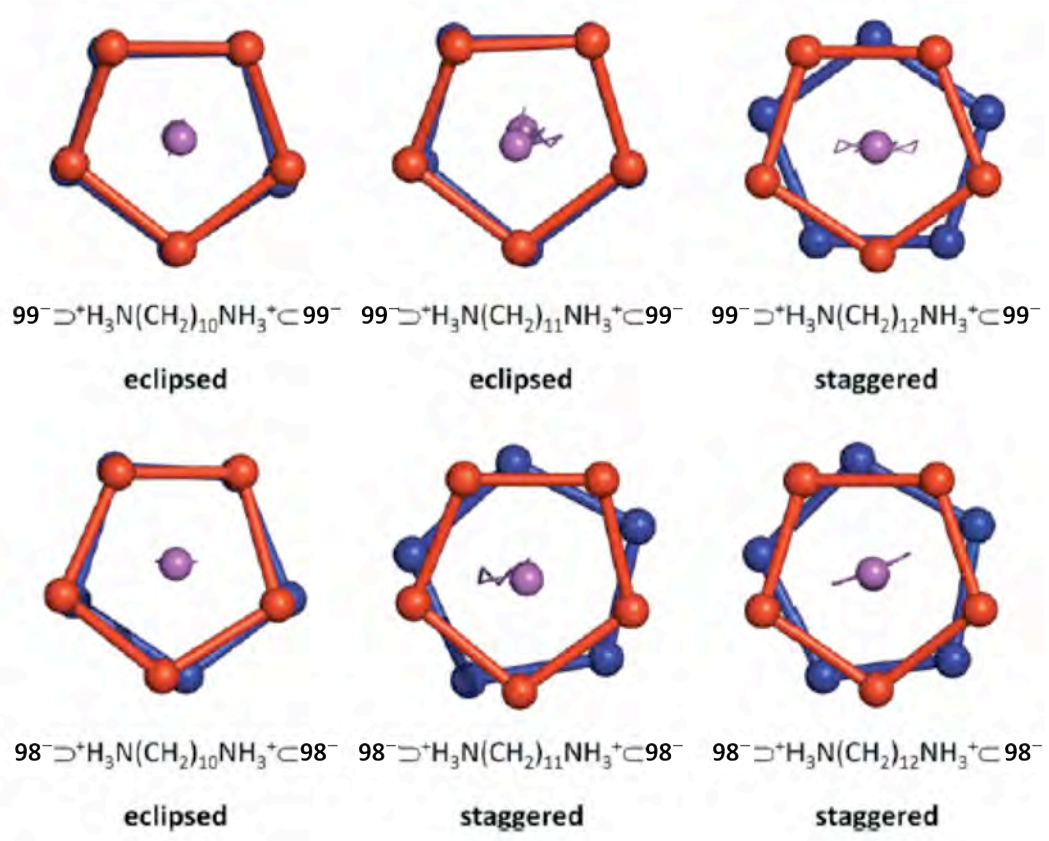

Figure 65. Schematic representation of the solid-state capsular structures displaying the relative orientation of the polygons formed by the five phenolic oxygen atoms belonging to the two calix[5]arene units. Red and blue spheres: phenolic oxygen atoms; purple spheres: nitrogen atoms.

Indeed, in **99**$^{-}\supset{}^{+}H_3N(CH_2)_{10}NH_3^{+}\subset$**99**$^{-}$ and **99**$^{-}\supset{}^{+}H_3N(CH_2)_{11}NH_3^{+}\subset$**99**$^{-}$, as well as in **98**$^{-}\supset{}^{+}H_3N(CH_2)_{10}NH_3^{+}\subset$**98**$^{-}$, the receptor molecules are mutually rotated by 3.4, 4.3 and 4.4°, respectively, yielding an eclipsed conformation of the facing calixarene macrorings, whereas in **99**$^{-}\supset{}^{+}H_3N(CH_2)_{12}NH_3^{+}\subset$**99**$^{-}$, **98**$^{-}\supset{}^{+}H_3N(CH_2)_{11}NH_3^{+}\subset$**98**$^{-}$ and **98**$^{-}\supset{}^{+}H_3N(CH_2)_{12}NH_3^{+}\subset$**98**$^{-}$ they are rotated by 36.0, 24.1 and 29.0°, respectively, resulting in an overall staggered conformation. Inspection of the internal volume of the capsular assemblies, and comparison with the volume taken up by the guests, provides a deeper insight into the efficiency of the encapsulation process. Rebek and Mecozzi[116] have studied the packing coefficients in a number of capsular systems in the solid state, concluding that stability peaks when 70% of the available space is taken up by the guest (this figure goes down to 55% when considering encapsulation complexes in solution).

Remarkably, in **99**$^{-}\supset{}^{+}H_3N(CH_2)_{10}NH_3^{+}\subset$**99**$^{-}$, 65% of the available space (299.4 Å^3, **Table 11**) is occupied by the fully extended decanediammonium guest (195.3 Å^3), whereas in the case of **99**$^{-}\supset{}^{+}H_3N(CH_2)_{11}NH_3^{+}\subset$**99**$^{-}$ the packing coefficient goes up to ca. 69% (307.3 Å^3 available space, 211.3 Å^3 guest volume). In the case of **99**$^{-}\supset{}^{+}H_3N(CH_2)_{12}NH_3^{+}\subset$**99**$^{-}$ the volume occupied by the guest (224.9 Å^3) drops to 61% of the available space. In this last case, however, it should be mentioned that for this *quasi*-capsular aggregate the value of the packing coefficient is overestimated (6–10%) as a direct consequence of the use of a rolling probe with a larger radius (1.7 instead of 1.4 Å) necessary to assess the internal volume of the capsular cavity. A comparison of the packing coefficient data calculated for the capsular complexes obtained for calixarene **99**·H and those previously reported for the structurally related derivative **98**·H (**Table 11**) reveals noticeable similarities for the $^{+}H_3N(CH_2)_{10}NH_3^{+}$ and $^{+}H_3N(CH_2)_{12}NH_3^{+}$ complexes, along with remarkable differences for the 1,11-diaminoundecane-containing capsules. The inner volume of the

99$^{-}\supset{}^{+}H_3N(CH_2)_{11}NH_3^{+}\subset$**99**$^{-}$ capsule is significantly smaller than that of the **98**$^{-}\supset{}^{+}H_3N(CH_2)_{11}NH_3^{+}\subset$**98**$^{-}$ one. The reasons for this difference can be ascribed to the relative orientation of the two facing calixarene units: while **99**$^{-}\supset{}^{+}H_3N(CH_2)_{11}NH_3^{+}\subset$**99**$^{-}$ is sealed and locked in an eclipsed conformation, in the **98**$^{-}\supset{}^{+}H_3N(CH_2)_{11}NH_3^{+}\subset$**98**$^{-}$ capsular complex the orientation of the two receptors is staggered. In other words, the reciprocal orientation of the two calixarene molecules significantly affects the shape –and size– of the internal capsular volume available.

Table 11 Calculated volumes of the guest (V_G), the capsular inner space (V_C) and packing coefficients (***PC***) of the capsular complexes **99**$^{-}\supset{}^{+}H_3N(CH_2)_nNH_3^{+}\subset$**99**$^{-}$ and **98**$^{-}\supset{}^{+}H_3N(CH_2)_nNH_3^{+}\subset$**98**$^{-}$ (n = 10–12).

	V_G (Å^3)	V_C (Å^3)	***PC*** (%)
99$^{-}\supset{}^{+}H_3N(CH_2)_{10}NH_3^{+}\subset$**99**$^{-}$	195.3	299.4	65.2
99$^{-}\supset{}^{+}H_3N(CH_2)_{11}NH_3^{+}\subset$**99**$^{-}$	211.3	307.3	68.8
99$^{-}\supset{}^{+}H_3N(CH_2)_{12}NH_3^{+}\subset$**99**$^{-}$	224.9	368.4[a]	61.0
98$^{-}\supset{}^{+}H_3N(CH_2)_{10}NH_3^{+}\subset$**98**$^{-}$	196.5	297.2	66.1
98$^{-}\supset{}^{+}H_3N(CH_2)_{11}NH_3^{+}\subset$**98**$^{-}$	209.3	338.0	61.9
98$^{-}\supset{}^{+}H_3N(CH_2)_{12}NH_3^{+}\subset$**98**$^{-}$	223.0	358.3[a]	62.2

Fig. 66 highlights the shape of the volume available inside the capsular complexes belonging to both families. When the calixarenes are seen in an eclipsed conformation, the internal volume of the capsule appears to be approximately cylindrical, whereas when the two receptors adopt a staggered conformation, additional room is available around the main cylindrical body (see the C–shaped surface of **98**$^{-}\supset{}^{+}H_3N(CH_2)_{11}NH_3^{+}\subset$**98**$^{-}$). When a 30° rotation between the two facing calixarenes is reached (see the Z–shaped

surfaces of **99**$^{-}\supset{}^{+}H_3N(CH_2)_{12}NH_3^{+}\subset$**99**$^{-}$ and **98**$^{-}\supset{}^{+}H_3N(CH_2)_{12}NH_3^{+}\subset$**98**$^{-}$) the capsular volume increases even further.

According to our data, the packing coefficients of these capsular complexes are affected not only by the relative proximity of the two receptors – depending on the length of the linear guest – but also by the reciprocal orientation of the receptors which influences, to some extent, the opening of the capsule seal. The facing calixarene units are seen to rotate with respect to each other to secure a sort of hydrophobic 'bayonet-mount' fastening of the capsule, which seals the space available for encapsulation.

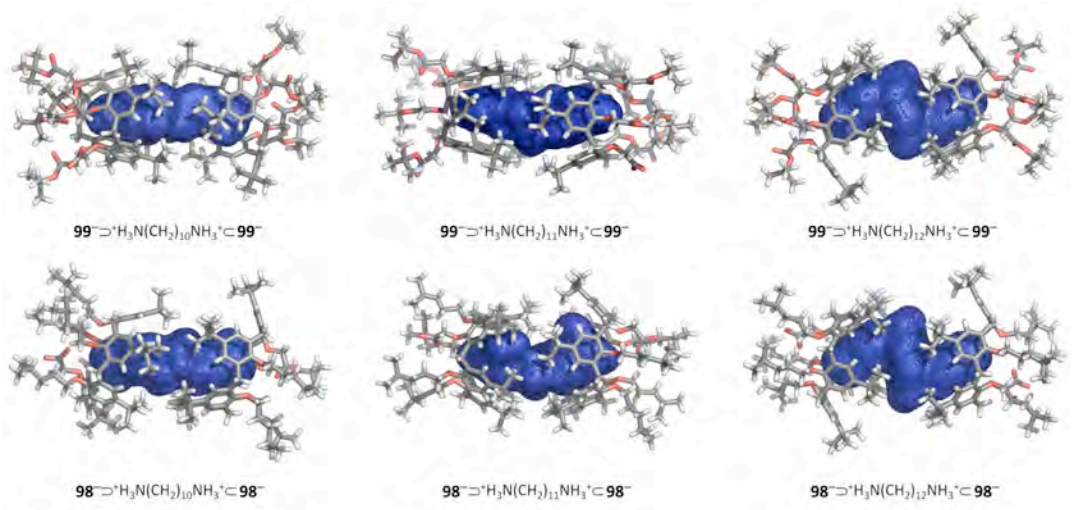

Figure 66. Surfaces of the inner space available in the solid-state structures of the **99**$^{-}\supset{}^{+}H_3N(CH_2)_nNH_3^{+}\subset$**99**$^{-}$ and **98**$^{-}\supset{}^{+}H_3N(CH_2)_nNH_3^{+}\subset$**98**$^{-}$ (n = 10–12) capsular complexes.

^{1}H NMR spectra of the 2:1 host-to-guest solutions ($CDCl_3/CD_3OD$ 9:1, v/v) provide additional evidence on the geometry of the complexes (**Fig. 67**). Leaving aside the low-intensity peaks assigned to the 1:1 host-guest complexes, the complexation-induced shifts determined by the bis-*endo*-cavity inclusion can be employed as a convenient tool for assessing the position of the ammonium moiety within the

aromatic cavity of the calixarene. For a given set of *endo*-cavity hydrogen atoms, the shielding effect of the aromatic rings increases to a maximum and then decreases, on moving from the top to the bottom of the cavity.[117]

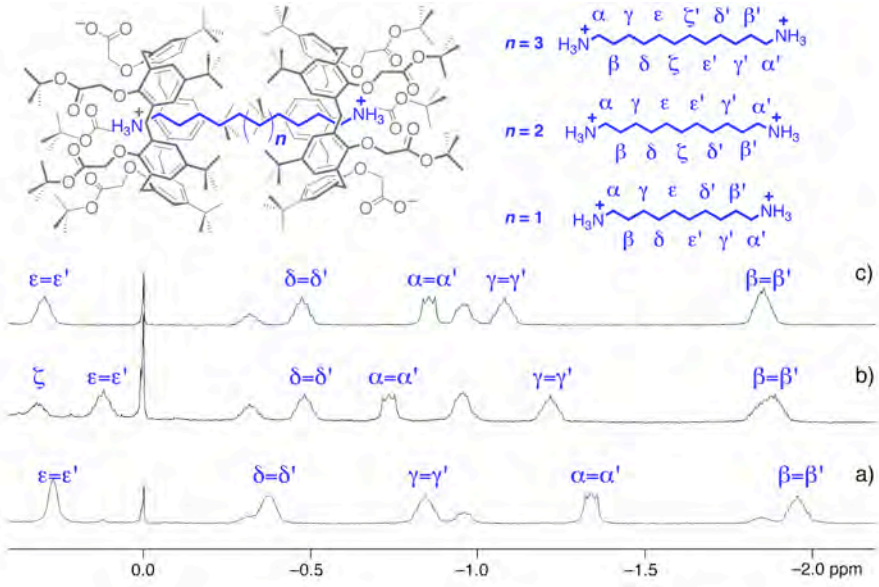

Figure 67. High-field regions of the ^{1}H NMR spectra (500 MHz, 298 K, $CDCl_3/CD_3OD$ 9:1, v/v) of a) [**99**·H] = 5 mM and $[H_2N(CH_2)_{10}NH_2]$ = 2.5 mM; b) [**99**·H] = 5 mM and $[H_2N(CH_2)_{11}NH_2]$ = 2.5 mM; c) [**99**·H] = 5 mM and $[H_2N(CH_2)_{12}NH_2]$ = 2.5 mM

In these cases, as often happens with calix[5]arene/alkylammonium complexes, it is the β-CH_2 that resides roughly in the area of maximum shielding (δ–1.9 ppm; $\Delta\delta$ = 3.22–3.35 ppm), whereas the α-CH_2 is located deeper beyond this point. Hence, for these hydrogen atoms, the more downfield the chemical shift, the deeper they are positioned within the cavity. In the case of **99**$^-$ $\supset{}^+H_3N(CH_2)_{10}NH_3^+\subset$**99**$^-$, the fact that the α-$CH_2$s resonate at δ = –1.34 ppm indicates that the ammonium moieties, at the two extremities of the guest are

not able to reach the edges of the capsule simultaneously (which is to be expected, given the shorter length of the dication), whereas the guest that fully bridges the capsular cavity is $^{+}H_3N(CH_2)_{11}NH_3^{+}$ (δ = –0.74 ppm), in agreement with the observations on the solid state structures of these complexes.

2.2.4. Carboxyl-calix[5]arenes and polyamines : a biological application

Inspired by the beauty of the biogenic polyamine-enzyme complexes and willing to test the efficiency of our capsule design beyond the proof-of-concept stage, we decided to move forward and pit calix[5]arene carboxylic acid **98**·H against potential guests with a mismatched number of protonable sites. To this end, spermine (Spm) and norspermine (Nspm) were selected as tetraamino-containing guests (**Fig. 68**),[118] in consideration of their size and shape similarity to the 1,12-diaminododecane and 1,11-diaminoundecane guests previously studied.

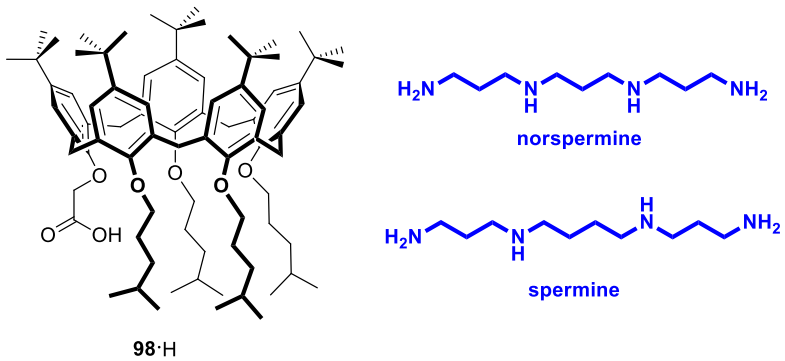

Figure 68. Tetraether-calix[5]arene carboxylic acid **98**·H, and spermine and norspermine guests.

Preliminary ^{1}H NMR experiments (500 MHz, 25 °C, $CDCl_3/CD_3OD$ 9:1 v/v) revealed that, in solution, calixarene **98**·H has a modest affinity for the two tetraamino

guests. Addition of Spm or Nspm (0.5 equiv.) to a 5 mM solution of the host resulted – leaving aside the 1:1 host-guest complexes – in the formation of just 6% and 4% respectively of the corresponding capsular complexes, indicating that the host-to-guest proton transfer process proceeds less efficiently than in the case of α,ω-diamines of similar length. (**Fig. 69** and **70**)

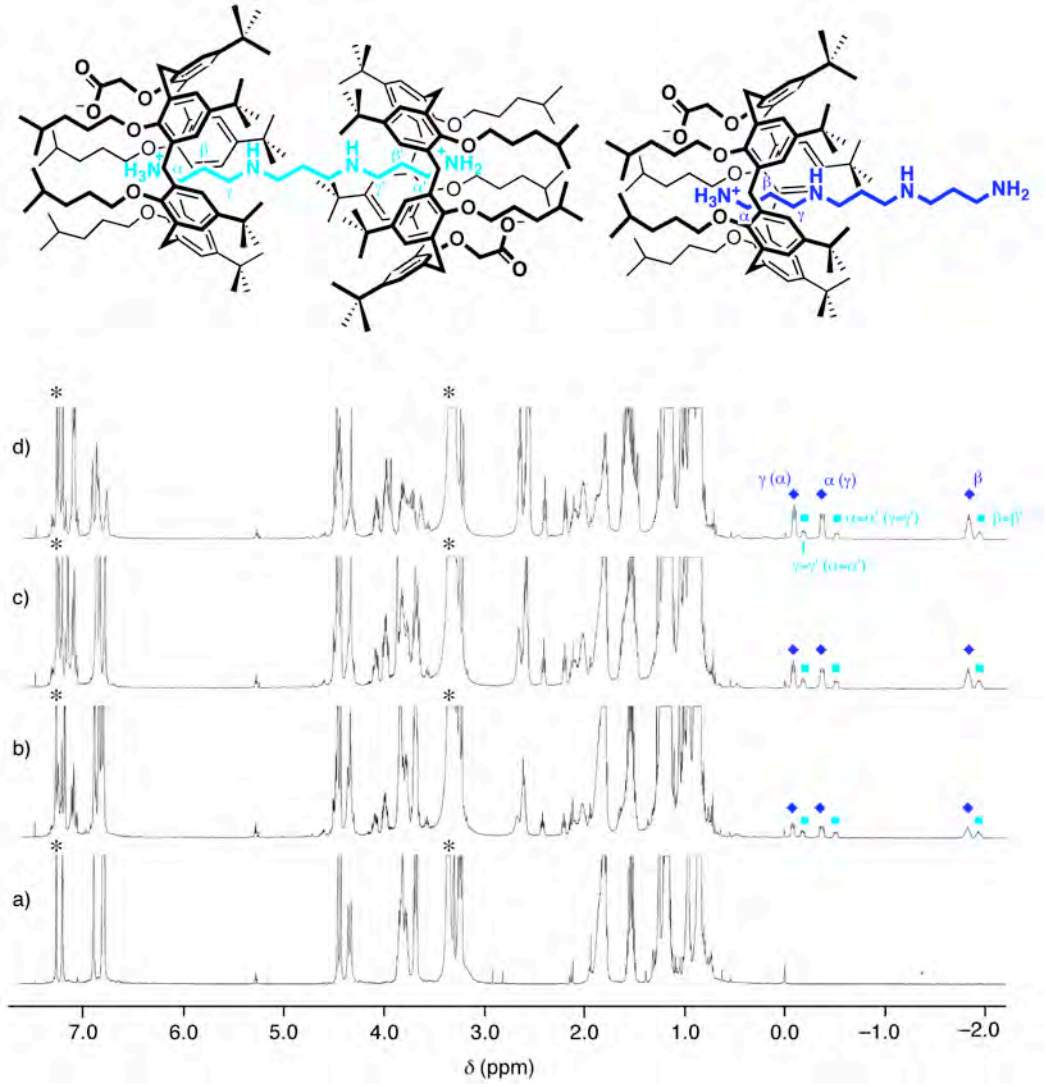

Figure 69. ^{1}H NMR spectra (500 MHz, 25 °C, $CDCl_3/CD_3OD$ 9:1, v/v) of a) [**98**·H] = 5 mM; b) [**98**·H] = 5 mM and [Nspm] = 1.25 mM; c) [**98**·H] = 5 mM and [Nspm] = 2.5 mM; d) [**98**·H] = 5 mM and [Nspm] = 5 mM. * Residual solvent peaks

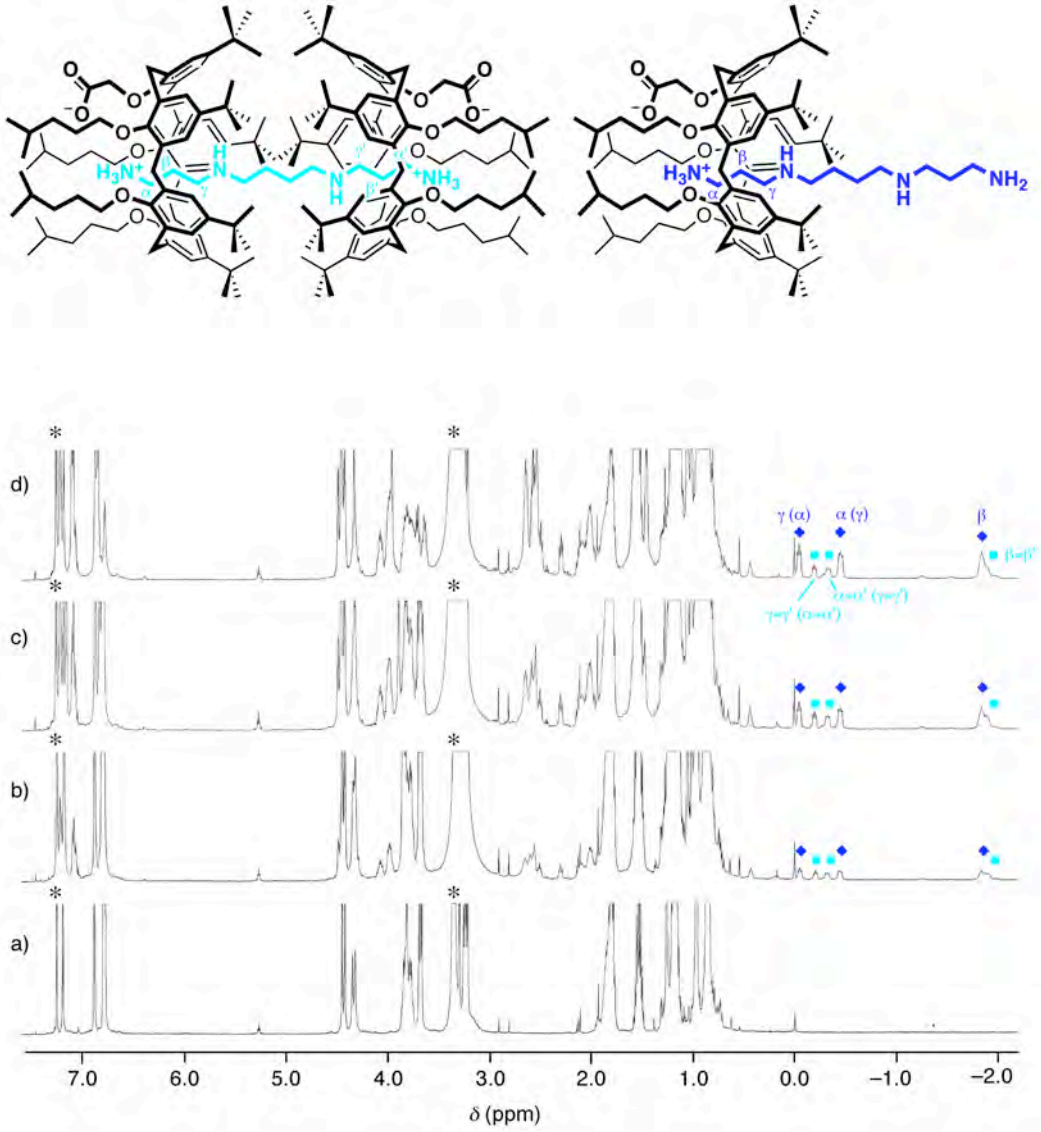

Figure 70. ^{1}H NMR spectra (500 MHz, 25 °C, $CDCl_3/CD_3OD$ 9:1, v/v) of a) [**98**·H] = 5 mM; b) [**98**·H] = 5 mM and [Spm] = 1.25 mM; c) [**98**·H] = 5 mM and [Spm] = 2.5 mM; d) [**98**·H] = 5 mM and [Spm] = 5 mM. * Residual solvent peaks.

In comparison, proton-assisted encapsulation of $H_2N(CH_2)_nNH_2$ had previously been seen to reach to a more satisfying 45% and 38% for n = 12 and 11, respectively.[110e] This, however, did not come entirely as a surprise, since earlier studies on

calix[5]arene/spermidine (used as the tri-hydrochloride salt, Spmd·3HCl) complexation had shown that, when faced with this asymmetric guest (too short to form capsules), the calix[5]arene cup would toposelectively include the butylenammonium moiety rather than the propylenammonium one.[107a]

This penchant was confirmed also for the **98**·H/Spmd pair by ^{1}H NMR data, which showed a preferential (85%) formation of the $H_2N(CH_2)_3NH(CH_2)_4NH_3^+\subset$**98**$^-$ *endo*-cavity complex over the other topoisomer (**Fig. 71**).

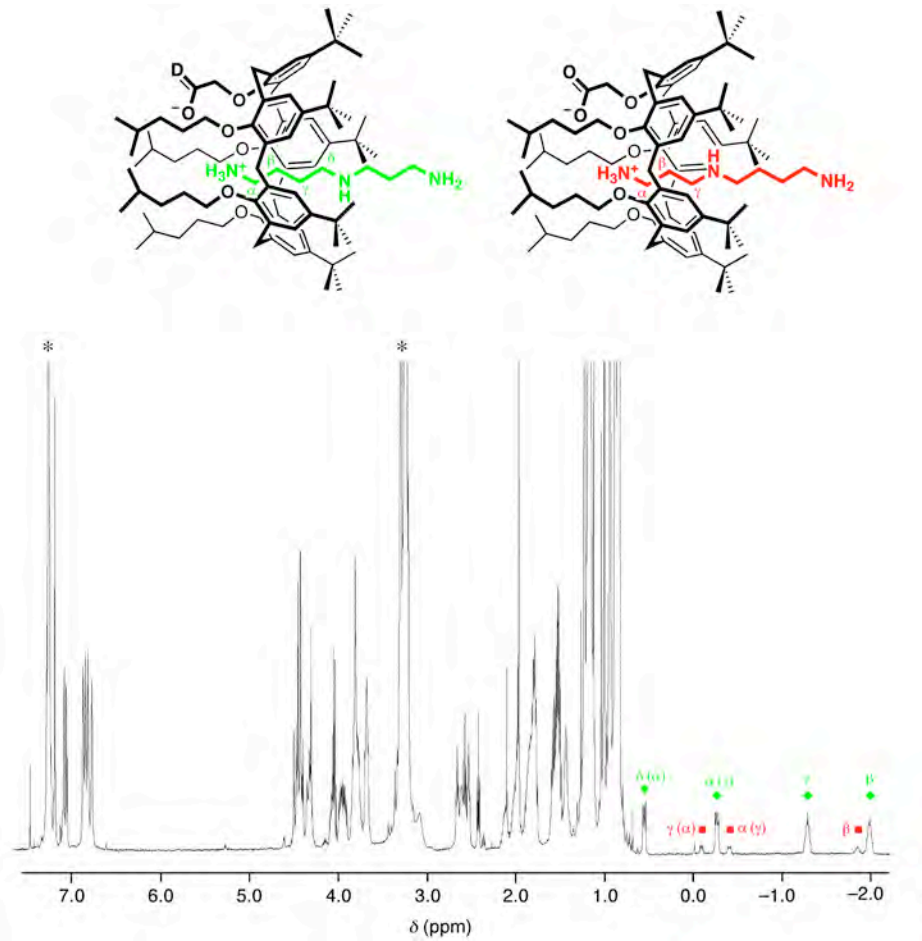

Figure 71. ^{1}H NMR spectrum (500 MHz, 25 °C, $CDCl_3/CD_3OD$ 9:1, v/v) of: [**98**·H] = 1 mM and [Spmd] = 1.25 mM. * Residual solvent peaks.

It was then clear why encapsulation of Spm and Nspm (both of them carrying short propylenamine end-groups) proceeded less effectively than that of α,ω-diamines of equal length. Most likely, solvation of the secondary amino/ammonium group hinders the formation of the minor topoisomer. Contrary to the low affinity seen in solution, solid-state structure analyses of the two complexes revealed an altogether different picture. Single crystals of the capsular complexes were grown by slow evaporation of a $CHCl_3$/trifluoroethanol (TFE) (20% v/v) mixture containing **98**·H (5.5 mM) and Spm or Nspm in a 2:1 molar ratio. The structure of the norspermine capsular complex (**98**$^-$⊃Nspm·2H$^+$⊂**98**$^-$), in line with predictions (see the analogous **98**$^-$⊃$^+H_3N(CH_2)_{11}NH_3^+$⊂**98**$^-$),[119] shows that encapsulation of the dicationic form of the guest –within two facing carboxylatecalix[5]arene cavities – takes place as a result of an initial acid-base host-to-guest proton transfer (**Fig. 72**).

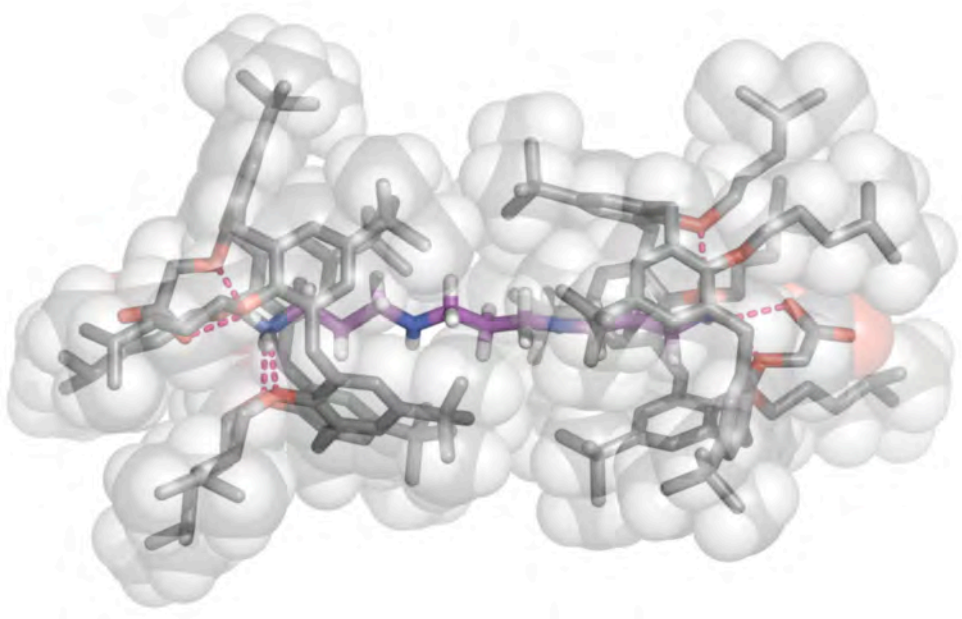

Figure 72. Solid-state structure of the **98**$^-$⊃Nspm·2H$^+$⊂**98**$^-$capsular complex.

Remarkably, the transfer of the two protons proceeds regioselectively, with the exclusive protonation of the primary (and more basic)[120] amino groups, leaving the *intra*-chain secondary amino ones unaltered.

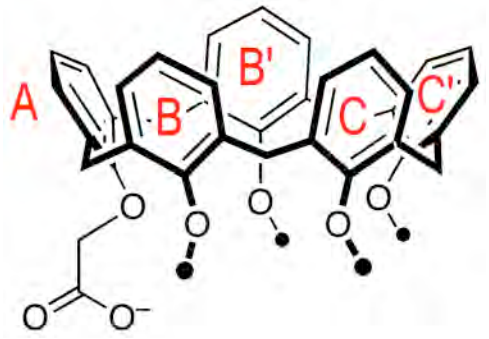

Figure 73. Labelling of aromatic rings of **98**$^{-}$.

The two calix[5]arene molecules, as generally seen in the case of alkylammonium *endo*-cavity inclusion complexes in the solid state, are arranged in a typical (approximately C_S-symmetric) *cone-out* conformation, with the carboxylate-bearing phenolic residue (ring A) adopting the widest tilting angle (θ = 137.4(1)°) with respect to the bridging methylene mean plane. The two facing macrocycles are seen offset by 5.4 Å, while their bridging methylene mean planes lie at a distance of 14.2 Å from each other. The norspermine guest is seen in a helically twisted extended conformation (**Fig. 74**), with torsion angles, between adjacent bonds, in the 162–171° range, and thus considerably smaller than those expected (180°) for a fully stretched linear structure. Topologically, this twist produces a mutual rotation of the two ammonium end-groups, best described by the N6a–C6b–C6b'–N6a' dihedral angle (143.5°). This marked deviation from the theoretical value (0°) –anticipated for an odd-numbered atom linear polyamine adopting an extended zig-zag conformation–

likely reflects the best trade-off between efficient formation of a sealed capsule and the dimension of the guest encapsulated within.

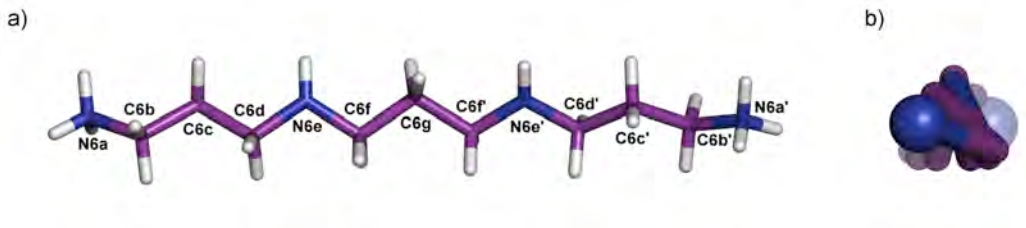

Figure 74. a) Side and b) front (from N6a) views of the dication guest encapsulated within **98**$^{-}$⊃Nspm·2H^{+}⊂**98**$^{-}$. Torsion angles, between adjacent bonds, in the 162–171° range. Torsion angle between the two ammonium end-groups (N6a–C6b——C6b'–N6a') 143.5°.

The ammonium end-groups are involved in four hydrogen bonds, three with the phenolic oxygen atoms of rings A, C and C', and the fourth with the carboxylate oxygen atom, giving rise to an internal salt-bridge interaction (**Table 12**).

Table 12 Hydrogen bonds, C-H···π and van der Waals interactions in the **98**$^{-}$⊃Nspm·2H^{+}⊂**98**$^{-}$ capsular complex.

***d*(N···O)**	**Å**	***d*(C···Cg)**	**Å**	**C(CH$_3$)$_3$···C(CH$_3$)$_3$**	**Å**
N(6a)-H(6a2)···O(1l)	2.798(6)	C(6b)-H(6b1)···Cg(E)	3.490(5)	C(3q)···C(2q)[a]	3.85(1)
N(6a)-H(6a1)···O(3g)	2.766(6)	C(6b)-H(6b2)···Cg(B)	3.528(5)	C(2q)···C(3q)[a]	3.85(1)
N(6a)-H(6a2)···O(1g)	2.794(6)	C(6c)-H(6c2)···Cg(C)	3.608(5)	C(3r) ···C(3r)[a]	4.10(1)
N(6a)-H(6a3)···O4(g)	2.837(7)	C(6c)-H(6c1)···Cg(D)	3.702(5)		

[a] symmetry operation: *x*, *-y*, ½-*z*

In addition, four CH···π interactions (between the α- and β-CH_2 of the guest and the calixarene B, B', C and C' rings) per hemicapsule contribute to the stabilization of the overall assembly. The primary nitrogen atom lies 0.861(5) Å above the mean plane described by the five phenolic oxygen atoms. Furthermore, van der Waals interactions between the wide rim t-butyl substituents of the two calixarene units ensure a supramolecular seal between the two hemicapsules.

A similar picture is seen for the solid-state structure of the spermine capsular complex (**98**$^{-}$⊃Spm·2H^{+}⊂**98**$^{-}$, **Fig. 75**). Again, regioselective acid-base proton-transfer generates a three-component salt-bridged supramolecular complex very similar to the one just described.

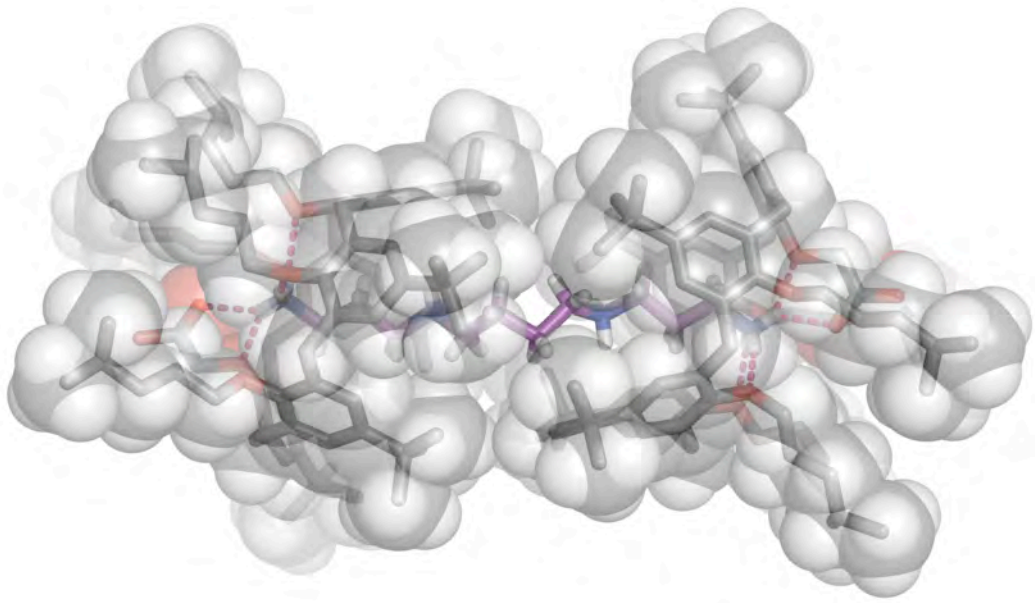

Figure 75. Solid-state structure of the **98**$^{-}$⊃Spm·2H^{+}⊂**98**$^{-}$ capsular complex.

Both calix[5]arenes adopt a *cone-out* conformation, where ring A (**Fig.73**) leans outward the most with respect to the bridging methylene mean plane (θ= 134.9(1)°).

The two opposite calix[5]arene units are offset by 4.9 Å and their methylene mean planes are 14.1 Å apart.

Unlike norspermine, encapsulated spermine molecules are not helically twisted. However, to fit within the capsular hollow, they are forced to curl up in the middle, adopting a "bulged" conformation that in the end produces a significant shrinkage of the chain extension (**Fig. 76**).

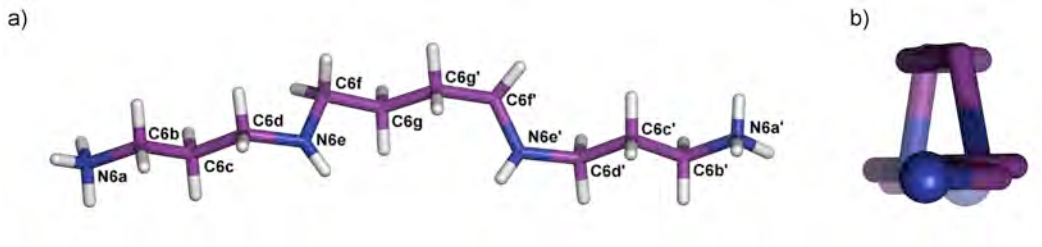

Figure 76. a) Side and b) front (from N6a) views of the dication guest (conformation A) encapsulated within **98**$^{-}$⊃Nspm·2H^{+}⊂**98**$^{-}$; N6e-C6f-C6g-C6g' torsion angle –92.1°.

As a result, the N6a-N6a' distance decreases from 16.4 Å –calculated for an ideal fully extended zig-zag conformation– to 15.2 Å. Interestingly, the two spermine ammonium end-groups retain an overall antiperiplanar orientation expected for linear polyamines containing an even number of atoms. Also in this case, each hemicapsule is stabilized by a carboxylate-ammonium salt bridge, three additional hydrogen bonds (between the NH_3^+ group of the guest and the phenolic oxygen atoms of rings A, C and C' of **1**$^{-}$) and four CH···π interactions (between the propylenammonium α- and β-CH_2 groups and rings B, B', C and C', **Table 13**).

The ammonium nitrogen atom lies slightly closer to the phenolic oxygen mean plane (0.568(6) Å). Surprisingly, capsular sealing is provided, in this case also, by attractive van der Waals interactions between the upper rim substituents of the two calixarene units, despite the increased length of the guest. This was rather unexpected, given that

in the aforementioned *quasi*-capsule 1,12-dodecanediamine case reported earlier,[111e] the guest was deemed too long to allow for the 'bayonet-mount' capsule locking operated by the *t*-butyl groups.[119]

Table 13 Hydrogen bonds, C-H···π and van der Waals interactions in the **98**$^{-}$⊃Spm·2H^{+}⊂**98**$^{-}$ capsular complex.

***d*(N···O)**	**Å**	***d*(C···Cg)**	**Å**	**C(*C*H$_3$)$_3$···C(*C*H$_3$)$_3$**	**Å**
N(6a)-H(6a2)···O(1l)	2.746(7)	C(6b)-H(6b2)···Cg(E)	3.583(5)	C(2r)···C(3q)[a]	3.83(1)
N(6a)-H(6a2)···O(1g)	2.833(4)	C(6b)-H(6b1)···Cg(B)	3.597(4)	C(3ss)···C(3ss)[a]	4.030(8)
N(6a)-H(6a1)···O(3g)	2.800(4)	C(6c)-H(6c4)···Cg(D)	3.622(6)	C(4q)···C(5s)[a]	4.15(1)
N(6a)-H(6a3)···O(4g)	2.891(5)	C(6c)-H(6c3)···Cg(C)	3.861(6)		

[a] symmetry operation: *x*, *-y*, ½-*z*

A closer look at the Nspm and Spm capsules reveals that the two facing calixarene macrocycles adopt an 'eclipsed' conformation (**Fig. 77**), mandatory for *t*-butyl groups to establish efficient van der Waals contacts, whereas in the 1,2-dodecanediamine *quasi*-capsule, studied earlier, the two macrocycles were seen in a 'staggered' orientation with respect to each other.[119]

Further interesting observations on the capsules formed here can be drawn from an analysis of their packing coefficients (PC). As postulated by Rebek and Mecozzi,[116] PC in solid-state encapsulation complexes should reach, when the fit between the guest and the container is close to ideal, values as high as *ca*. 70%. In the cases under investigation here, the space available inside the two capsules is occupied up to the theoretical maximum (**Table 14**), with PC higher than those measured for the corresponding α,ω-diamines:[119] 72% *vs.* 62% for the analogous norspermine/1,11-diaminoundecane capsules and 70% *vs.* 62% for the spermine capsule/1,12-diaminododecane *quasi*-capsule pair (in the latter case, the capsule is not sealed). These

PC differences may be explained by looking at the actual volume occupied by the guest. Spermine takes up a volume (216 Å^3) intermediate between those occupied by 1,12-diaminododecane and 1,11-diaminoundecane (223 and 209 Å^3, respectively).

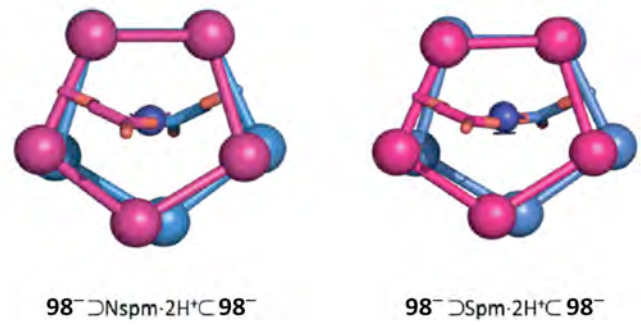

Figure 77. Schematic representation of the solid-state capsular structures displaying the relative orientation of the polygons formed by the five phenolic oxygen atoms belonging to the two calix[5]arene units.

Table 14 Calculated volumes of the guest ($\mathbf{V_G}$), the capsular inner space ($\mathbf{V_C}$) and packing coefficients (**PC**) of the capsular complexes **98**$^-$⊃Nspm·2H$^+$⊂**98**$^-$ and **98**$^-$⊃Spm·2H$^+$⊂**98**$^-$.

	V_G (Å^3)	V_C (Å^3)	*PC* (%)
98$^-$⊃Nspm·2H$^+$⊂**98**$^-$	204	284	72
98$^-$⊃Spm·2H$^+$⊂**98**$^-$	216	310	70

In other words, replacement of two CH_2s with two NH groups and, as a result, a reduced atom size and bond length (1.44 *vs.* 1.53 Å for C–N and C–C) causes the tetraamino guests under investigation to fit better within the capsules than their diamino counterparts, allowing both for higher PC and for the unexpected sealing of the spermine capsular complex.

Inspection of the inner space profiles of the Nspm and Spm capsules (**Fig. 78**) and comparison with those previously observed for the α,ω-diamine-containing complexes, confirms the better fit of biogenic amines within self-assembled carboxyl-calix[5]arene **98**·H capsules.

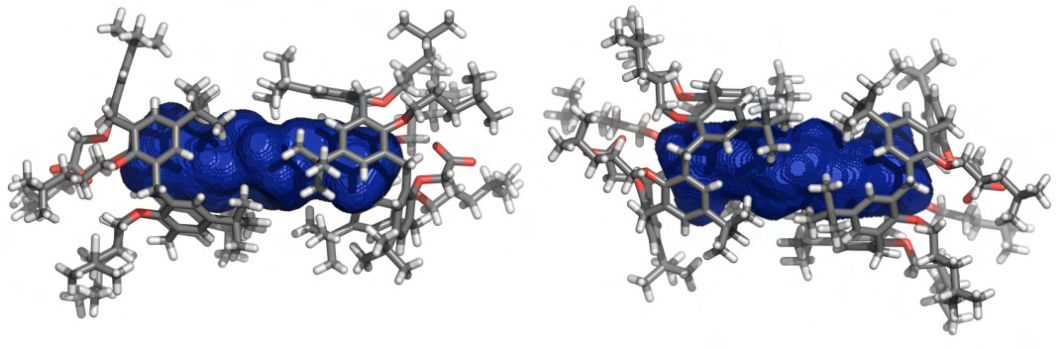

Figure 78. Surfaces of the inner space available in the solid-state structures of the **98**$^{-}$⊃Nspm·2H^{+}⊂**98**$^{-}$ and **98**$^{-}$⊃Spm·2H^{+}⊂**98**$^{-}$ capsular complexes.

Our data seem to indicate that any time two facing calix[5]arenes are able to adopt an eclipsed conformation, as a result of additional van der Waals contacts between t-butyl groups (bayonet-mount fastening[119]), the hollow of the capsule is cylindrically preorganized to best fit linear guests, whereas the lack of such a supramolecular seal generates quasi-capsular assemblies with a Z-shaped interior (e.g. **98**$^{-}$⊃$^{+}$H$_3$N(CH$_2$)$_{12}$NH$_3^{+}$⊂**98**$^{-}$).

The guests discussed herein fit snugly within the capsular assemblies –much better than their non-natural counterparts, validating the efficiency of our supramolecular design. In addition, the evidence that these biogenic amines are not significantly encapsulated in solution, opens up an entire range of possibilities in terms of delivery-and-release of these species. Investigations into the possible biological application of these encapsulation complexes are currently in progress.

2.2.5. From capsular to polycapsular systems

As shown in the past, covalently connecting two calixarene units via their lower rim may result in the evolution of capsular complexes into polycapsular assemblies: the following Chapter will deal with the formation of self-assembled, internally-ion-paired AABB-type supramolecular polymers. A combination of DOSY NMR, DLS and AFM techniques will reveal that bis-calix[5]arene-bis-carboxylic acids, upon exposure to α,ω-diaminoalkanes give rise to cyclic oligomeric assemblies, whose morphology (i.e., cyclic vs. linear) can be controlled by means of external chemical stimuli.

Bis-calix[5]arene-dicarboxylic acids **106**·2H**–108**·2H, featuring differently-sized linkers, were synthesized starting from the known penta-*tert*-butyl-tetrakis-(4-methylpentyloxy)calix[5]arene **109**, as depicted in **Scheme 19.**

As the linkers, *meso*-dibromodiesters **113–115** were selected (8, 9 and 12 carbon atoms), and they were in turn prepared by the three-step, one-pot reaction of α,ω-dicarboxylic acid **116–118** and $SOCl_2$, Br_2 and MeOH (**Scheme 20**).[121] This reaction, a HVZ-type α-halogenation, proceeds with exclusive formation of the *meso*-dibromodiester.[121] Reaction of the bromoesters with calix[5]arene **109**, using potassium carbonate as the base, in refluxing acetonitrile, led to the isolation of bis-calix[5]arene-dimethyl esters **110–112** (89, 21 and 46%, respectively). The ester groups were finally hydrolysed under mild conditions (LiOH, THF/H_2O), to give the desired diacids **106–108** (97, 58 and 57%, respectively).

The three bis-calixarenes-diacids were then preliminarily screened for their amine recognition abilities and self-assembling proclivity. Given the ultimate goal of producing AABB-type supramolecular polymers, that is, aggregates composed of complementary homoditopic pairs of monomers, and drawing on the observations

gathered from the studies on the assembly of the capsular complexes described above, compounds **106**·2H–**108**·2H were tested against 1,12-diaminododecane (henceforth referred to as $NC_{12}N$).

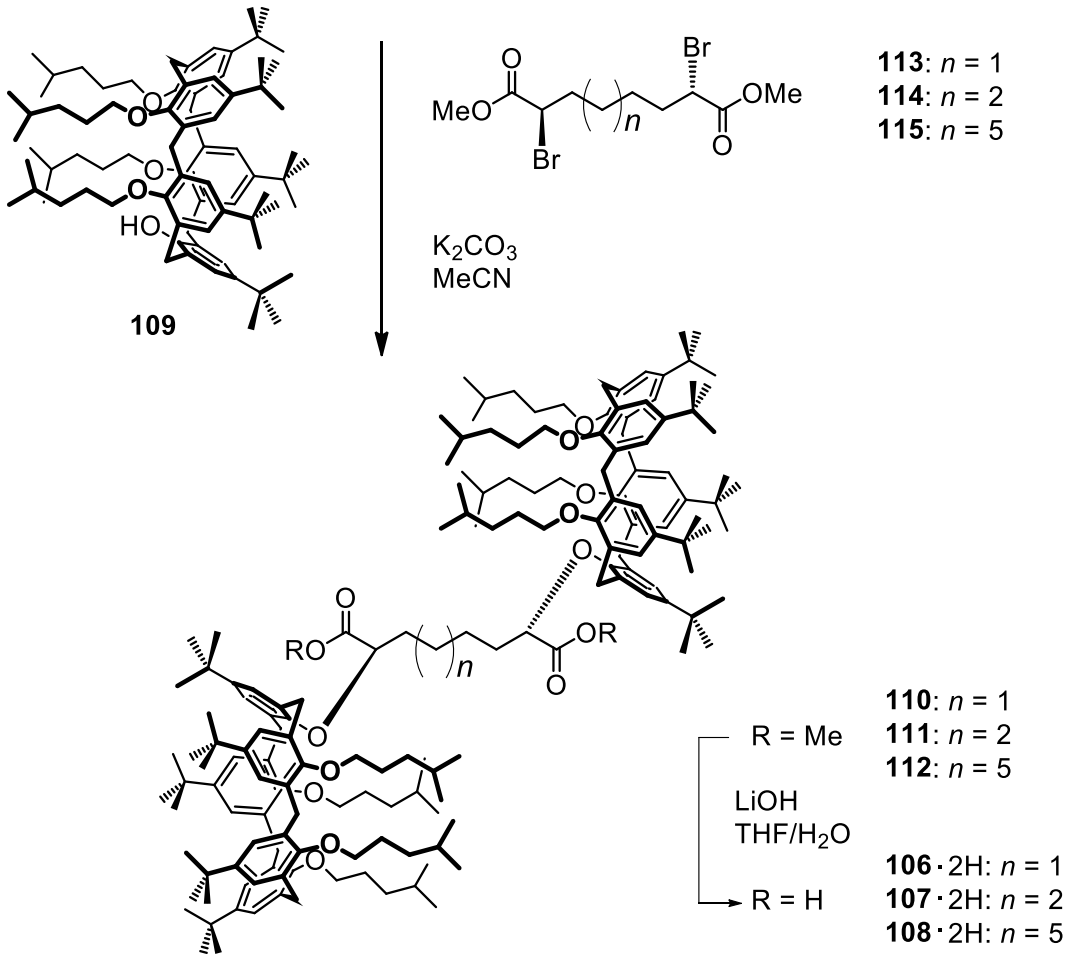

Scheme 19. Synthesis of calix[5]arenes **106–108**: a) K_2CO_3, CH_3CN; b) LiOH, THF/H_2O.

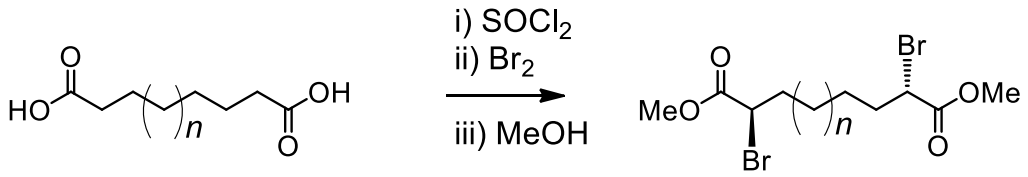

116: *n* = 1
117: *n* = 2
118: *n* = 5

113: *n* = 1
114: *n* = 2
115: *n* = 5

Scheme 20. Synthesis of the *meso*-dibromodiesters **113–115**.

Upon addition of 1 equiv. of the amine to a 3 mM solution (CD_2Cl_2/CF_3CD_2OD,[†††] 9:1, v/v) of the bis-calixarenes, appearance of resonances in the δ = 0 to –2 ppm spectral range for the methylene groups of the diaminododecane revealed that proton-transfer-mediated complexation had taken place (see **Fig. 79** for **106**·2H).

In fact, evidence that the alkyl chains of the diamino guest resonate at very high fields confirms that they are immersed in the shielding cones of the aromatic cavity walls. In addition, the highly symmetric sets of resonances (six instead of twelve) reveals that complexation of both ammonium heads in a capsular fashion has taken place. As it is generally the case for calix[5]arene/alkylammonium complexation, exchange was found to be slow on the NMR timescale.

Formation of large aggregates was also demonstrated by DOSY NMR experiments (**Fig. 80**). In fact, the self-diffusion coefficients (*D*) – extracted from the decay of the resonances assigned to the aromatic hydrogen atoms of the host and to the *endo*-cavity included methylene groups of the guest – decreased considerably with respect to those measured for the free host.

[†††] Earlier studies showed that protic solvents stabilize charge-separated ammonium-carboxylatocalixarene complexes, thus facilitating host-to-guest proton transfer.

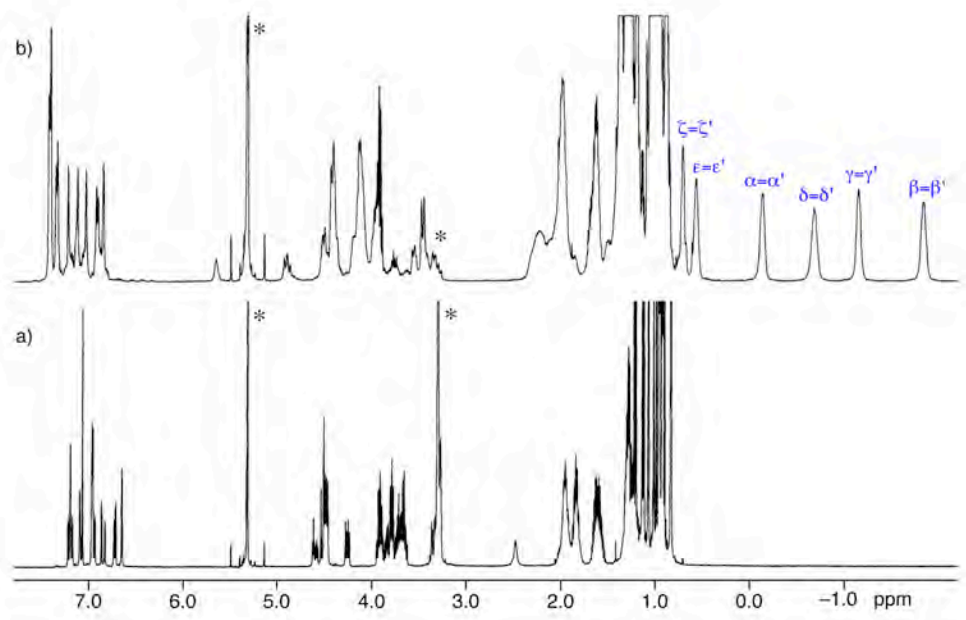

Figure 79. ^{1}H NMR spectra (500 MHz, CD_2Cl_2/CF_3CD_2OD 9:1 v/v, 298 K) of: a) [**106**·2H] = 2.0 mM and b) [**106**·2H] = [$NC_{12}N$] = 2.0 mM.

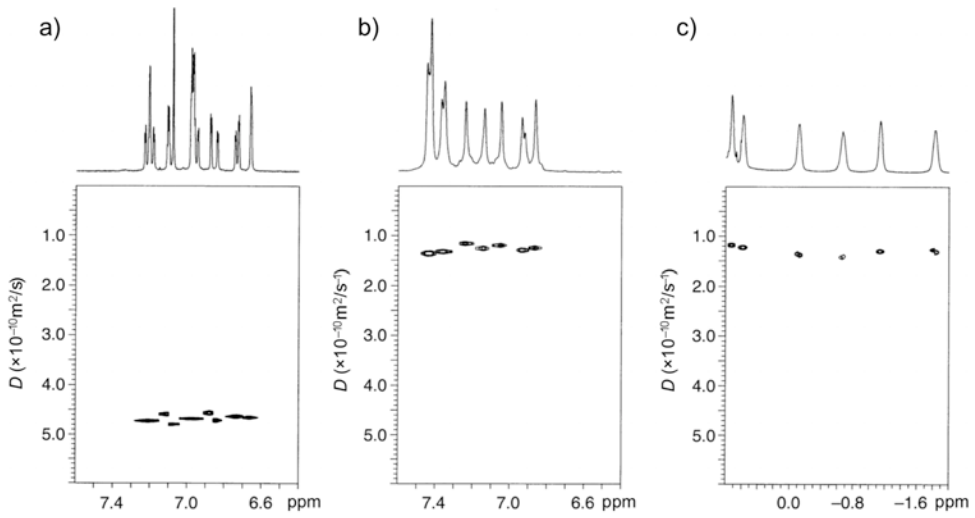

Figure 80. Sections of the DOSY spectra (500 MHz, CD_2Cl_2/CF_3CD_2OD 9:1 v/v, 298 K) of: a) [**106**·2H] = 3.0 mM; b) and c) [**106**·2H] = [$NC_{12}N$] = 3.0 mM.

Remarkably, complexation of the amino (ammonium) moieties of the guest monomer proceeds quantitatively (i.e., no resonances for a free terminal -C*H*$_2$NH$_2$ group in the δ = 2–3 ppm range) in contrast to what was seen for capsule formation in solution, that does not proceed with a similar efficiency. Such a high percentage of complexation prevented the use of direct peak integration to assess the relative efficiency of the three different bis-calixarenes.

Therefore, the solutions were subjected to a DOSY NMR screening to obtain relative information on the efficiency of these self-assembling systems, and to expand the scope of such a preliminary experiments, samples spectra were recorded also after dilution to [host] = [guest] = 0.5 mM. In **Fig. 81** only the high field regions of the spectra (i.e., included guest resonances) are reported for simplicity, whereas **Table 15** contains the self-diffusion coefficients extracted from these spectra. Diffusion data indicates clearly that the aggregates produced by bis-calixarene **108**·2H –the one with the longer, and therefore more flexible linker– are slower that those produced by the other two bis-calixarenes (**106**·2H, **107**·2H). The latter on the other hand yield almost identically-sized aggregates, meaning that even- or odd-numbered spacers behave similarly.

Table 15. Self-diffusion coefficients for the bis-calixarene-diacids/diaminododecane complexes measured in CD_2Cl_2/CF_3CD_2OD 9:1 v/v at different concentrations.

	D ($\times 10^{-10}$ m^2/sec)	
	0.5 mM	3.0 mM
106·2H + $NC_{12}N$	2.26 ± 0.26	1.26 ± 0.06
107·2H + $NC_{12}N$	2.31 ± 0.20	1.26 ± 0.07
108·2H + $NC_{12}N$	1.62 ± 0.13	0.75 ± 0.02

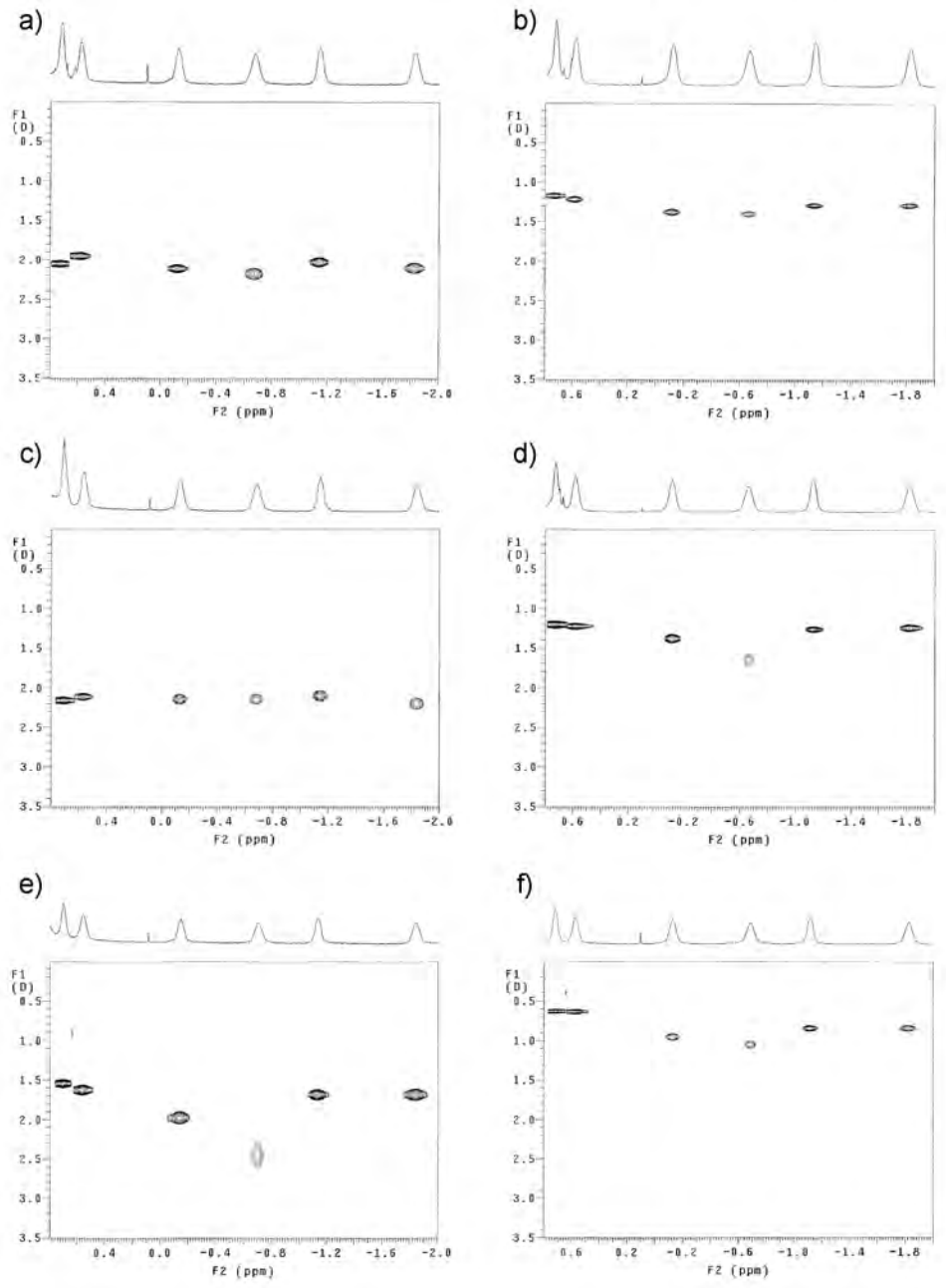

Figure 81. Sections of the DOSY spectra (500 MHz, CD_2Cl_2/CF_3CD_2OD 9:1 v/v, 298 K) of: a) [**106**·2H] = [$NC_{12}N$] = 0.5 mM; b) [**106**·2H] = [$NC_{12}N$] = 3 mM; c) [**107**·2H] = [$NC_{12}N$] = 0.5 mM; d) [**107**·2H] = [$NC_{12}N$] = 3 mM; e) [**108**·2H] = [$NC_{12}N$] = 0.5 mM; f) [**108**·2H] = [$NC_{12}N$] = 3 mM.

The second important evidence is the dependence of the self-diffusion coefficient on the concentration of the monomers, but that will be discussed in detail below.

One last conclusion was drawn from this preliminary screening: the solvent mixture was deemed unsuitable for further studies, because the 9:1 v/v mixture (CD_2Cl_2/CF_3CD_2OD) did not allow to obtain reliable estimates of hydrodynamic radii, given that solvent viscosity is significantly different from neat deuterated dichloromethane viscosity, as shown by the 'unstable' diffusion coefficient of dichloromethane.

Furthermore, the imperfect mixability of chlorinated solvents and trifluoroethanol (i.e., in some cases, droplets separation and/or turbidity was observed upon standing) would impair further studies by light scattering methods. It was therefore decided, after recording some test spectra, to turn to CD_2Cl_2/CF_3CD_2OD 98:2 v/v solvent mixtures, since test spectra showed that a trifluoroethanol content as low as 2% would not affect the diffusion coefficient of dichloromethane (hence making hydrodynamic radii estimation safe by the Stokes-Einstein equation), but it would still be sufficient to stabilize charge-separated complexes. A series of DOSY spectra were then recorded as part of a dilution experiment aimed at clarifying whether the size of these aggregates was concentration-dependent. Experiments were carried out on the **108**·2H/$NC_{12}N$ monomers pair that, giving rise to the largest aggregates among the three bis-calixarenes, were chosen as the best candidate for this study.

Spectra were recorded in the 15 – 0.5 mM range, and the resulting self-diffusion coefficients (extracted from aromatic resonances) are reported in **Table 16**.

The hydrodynamic radii (R_h) were obtained using the Stokes-Einstein equation (eq. (17)):

$$D_{obs} = k_B T/6\pi\eta R_h, \qquad (17)$$

where k_B is the Boltzmann constant, T is the temperature and η is the viscosity of the solvent (0.417×10^{-3} Pa×s).

Table 16. Self-diffusion coefficients and hydrodynamic radii for the bis-calixarene-diacid **108**·2H / diaminododecane aggregates measured in CD_2Cl_2/CF_3CD_2OD 98:2 v/v.

[**108**·2H] = [$NC_{12}N$] (mM)	D ($\times 10^{-10}$ m^2/sec)	R_h (nm)
15	0.74 ± 0.05	7.1
10	0.88 ± 0.04	6.00
6	1.23 ± 0.04	4.3
3	1.43 ± 0.12	3.7
1	2.0 ± 0.10	2.6
0.5	2.41 ± 0.12	2.2

The radii thus obtained shed light on the morphological features of these aggregates. In principle, in a self-assembling AABB-type oligo/polymeric system such as the one under investigation, the degree of polymerization can be described by Carothers' equation (eq. (16), see Introduction 2). Provided that molar ratio r is adjusted to the ideal value of 1 (i.e., equimolar amounts of the two monomers), the equation can be simplified as follows:

$$DP = \frac{1}{1-p}$$

p, as mentioned above represents the degree of 'reaction' of the end-groups, which in the case of self-assembling polymers can be defined as the degree (percentage) of complexation. It follows that, given the quantitative complexation observed for the **108**·2H/$NC_{12}N$ pair, we may expect very high degree of polymerization, and hence the formation of very large aggregates, unless of course aggregation proceeds towards the formation of discrete cyclic species.

DOSY data confirms that **108**·2H/$NC_{12}N$ monomers assemble into medium-sized aggregates (cyclic, as shown above). Furthermore, the size of these cyclic oligomers display some concentration dependence, on going from 2.2 to 7.1 nm (average values) in the 0.5–15 mM concentration range.

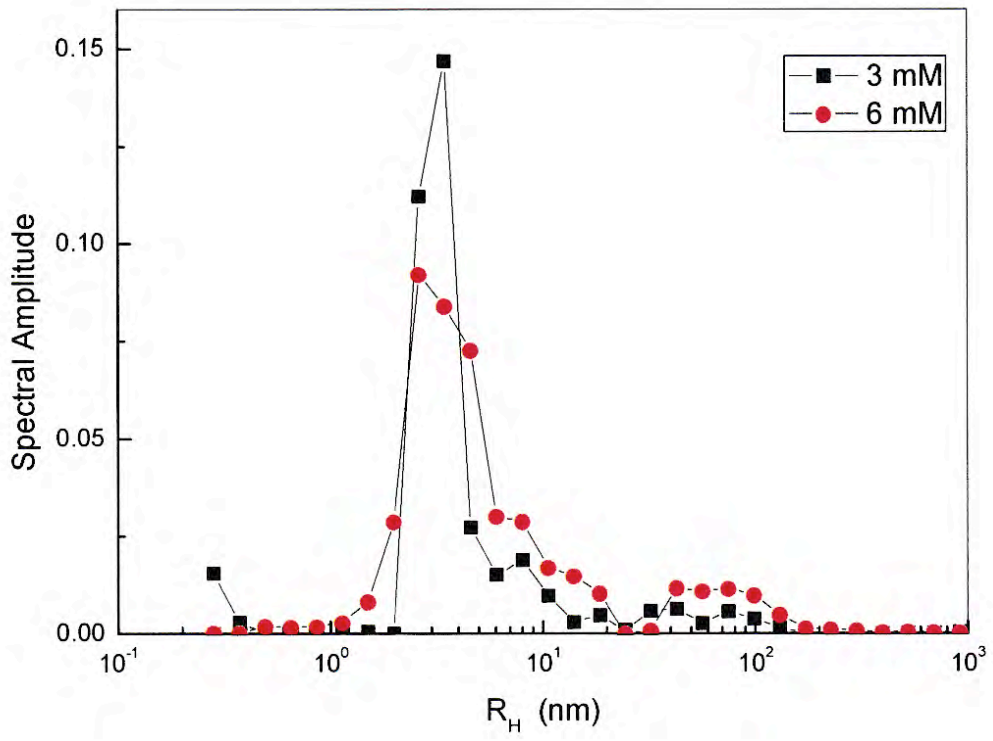

Figure 82. Size distributions of the **108**·2H/$NC_{12}N$ aggregates in a CH_2Cl_2/CF_3CH_2OH 98:2 v/v. (■) [**108**·2H] = [$NC_{12}N$] = 3 mM; (●) [**108**·2H] = [$NC_{12}N$] = 6 mM.

In order to gather further evidence on the behaviour of these cyclic oligomers, DLS analysis was carried out on the 0.5, 3 and 6 mM solutions. Bis-calixarene samples –in the absence of the complementary $NC_{12}N$ monomer– were used as control. No aggregate was seen (nor was expected) in the bis-calixarene alone solutions, where the intensity of scattered light was comparable to that seen for the solvents alone.

Also, no aggregates were visible in the 0.5 mM solution of the **108**·2H/$NC_{12}N$, probably because the concentration was too low. In the 3 an 6 mM solutions, on the other hand, two families of aggregates were seen, the smaller with a R_h = 4 nm, the larger with R_h = 70 nm. Remarkably, the ratio between the two families does not change with concentration, as demonstrated by the observation that the total scattered light increases linearly with the concentration of the samples (**Fig. 83**).

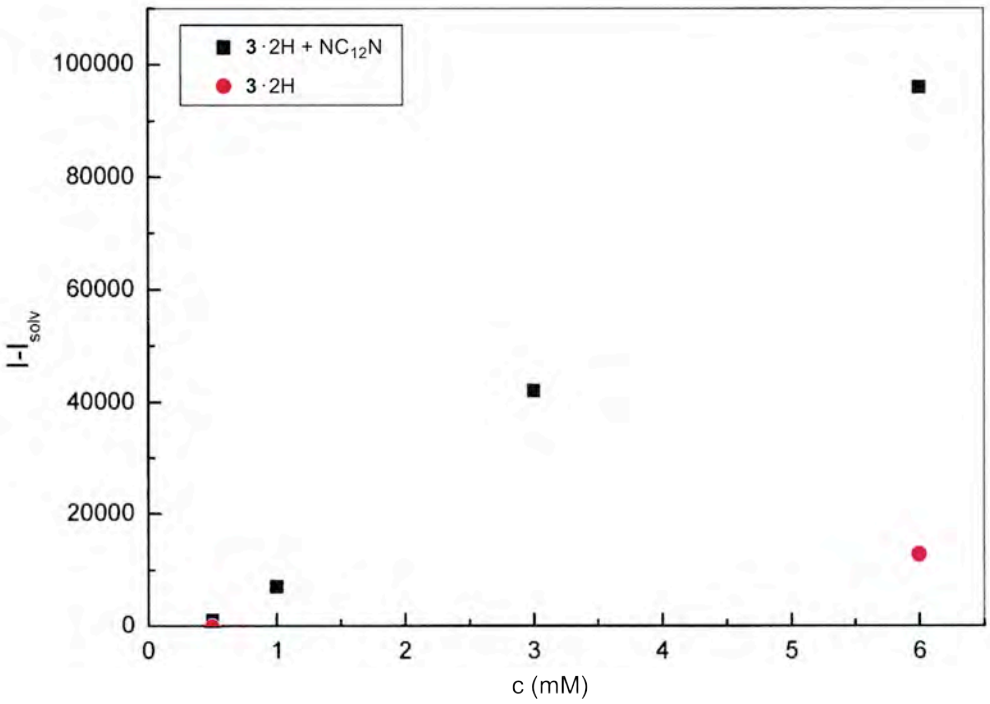

Figure 83. Total scattered light by **108**·2H/$NC_{12}N$ or **108**·2H solutions at different concentrations.

In addition, for the largest aggregate the ratio between the hydrodynamic radius and the radius of gyration indicate that they have a disk or a toroidal shape, rather than a spherical one. Average molecular weight was found to be 55 kDa (*ca*. 20-mer).

The apparent discrepancy of the results on the concentration dependence of the aggregates can be traced back to the fact that light scattered by the *ca*. 70 nm family is so intense that it may cover the contribution provided by even smaller aggregates. DOSY NMR, on the other hand, provides an averaged picture that comprises also the smallest (down to unimers) objects.[122]

Evidence supporting a toroidal organization of the **108**·2H/$NC_{12}N$ pair was also provided by atomic force microscopy studies. The AFM topography image obtained from a 0.5 mM CH_2Cl_2/CF_3CH_2OH 98:2 v/v spin-coated on a silica surface (**Fig. 84**) clearly shows the presence of doughnut-shaped aggregates, with an average diameter of *ca*. 100 nm, in excellent agreement with the value obtained by DLS for the larger objects.

Intrigued by this uncommon morphology,[123] we decided to try to control it the addition of a chain-stopper, e.g. an alkylamine such as *n*-butylamine that, upon filling a single cavity, would stop the growth of the oligo/polymeric aggregate.

Addition of up to 0.2 equiv. of *n*-butylamine to **108**·2H/$NC_{12}N$ solutions (10 and 6 mM in CH_2Cl_2/CF_3CH_2OH 98:2) led to the competitive complexation of the chain-stopper, as shown by the appearance, in the high field region, of the resonances of the *endo*-cavity-included *n*-butyl moiety (**Fig. 85**). DOSY spectra of the same mixtures indicated fragmentation of the aggregates, with both solutions (i.e., the 10 and the 6 mM) returning an average self-diffusion coefficient D of 1.84 ± 0.25 ($\times 10^{-10}$ m^2/sec) for the surviving assembled oligomers.

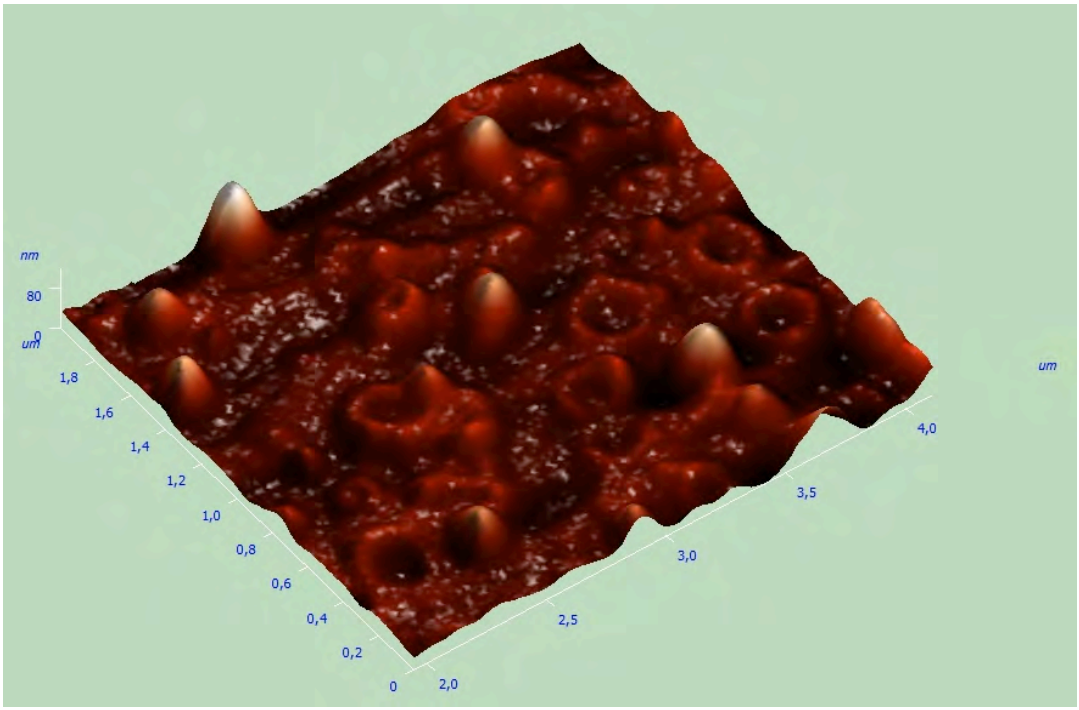

Figure 84. AFM topography image of the **108**·2H/$NC_{12}N$ toroidal aggregates.

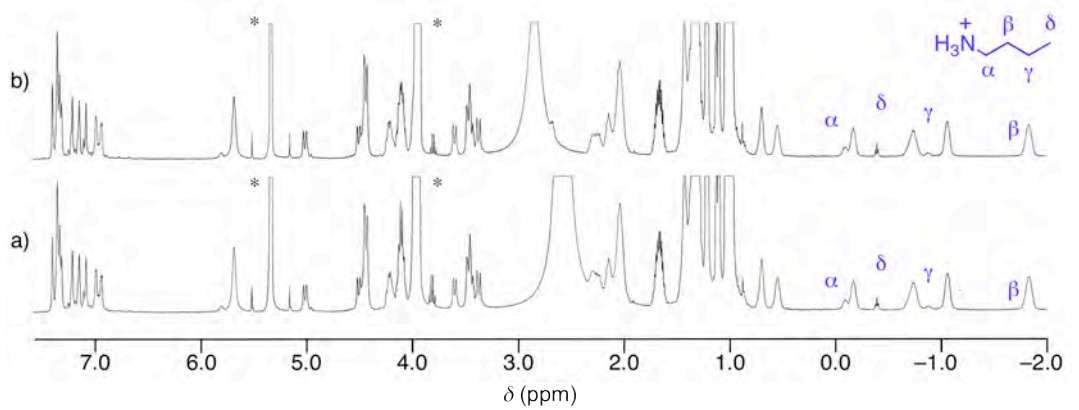

Figure 85. ^{1}H NMR spectra (500 MHz, CD_2Cl_2/CF_3CD_2OD 98:2 v/v, 298 K) of: a) [**108**·2H] = [$NC_{12}N$] = 6 mM, [*n*-$BuNH_2$] = 1.2 mM; b) [**108**·2H] = [$NC_{12}N$] = 10 mM, [*n*-$BuNH_2$] = 1 mM.

Final evidence on the modified morphological features was gather again by AFM analysis. The AFM topography image collected from a 0.5 mM (CH_2Cl_2/CF_3CH_2OH 98:2 v/v) containing 0.2 equiv. of chain stopper (**Fig. 86**) reveals that the doughnut-shaped objects have disappeared, being replaced by a grid structure that indicates the probable presence of linear oligomers.

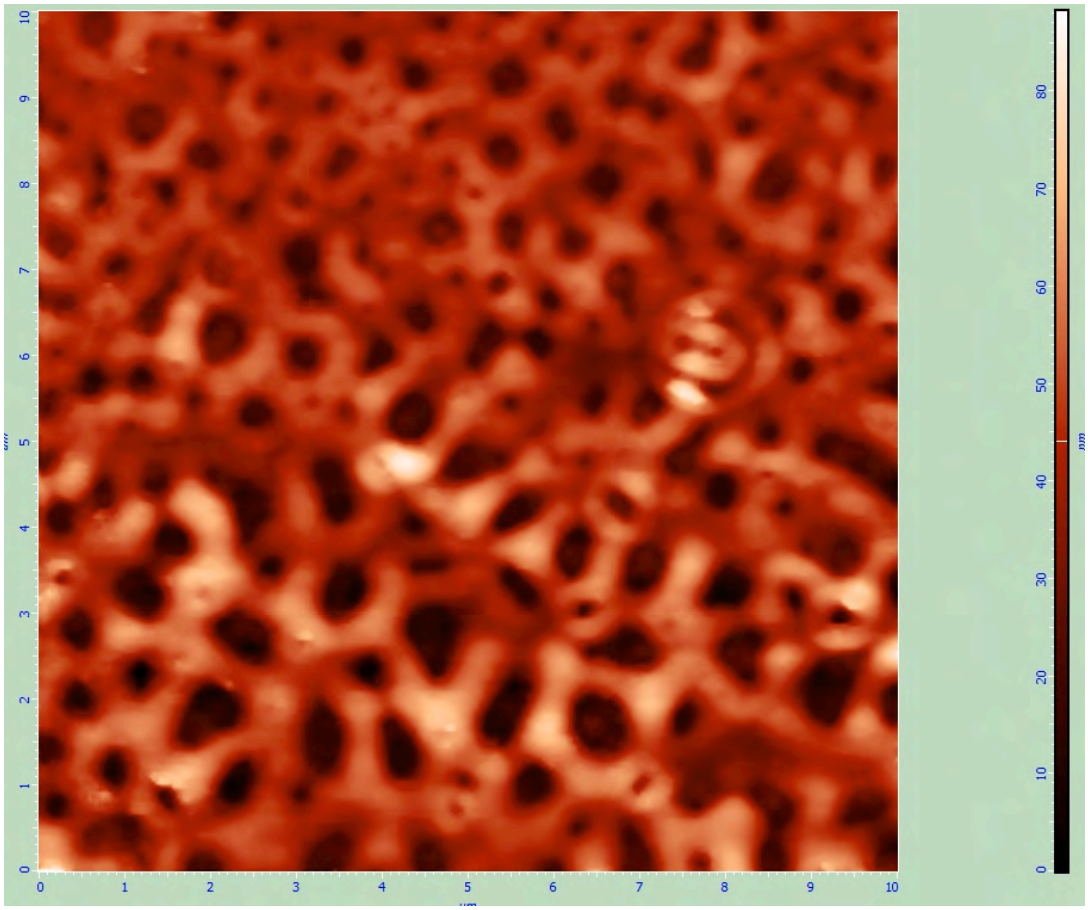

Figure 86. AFM topography image of the grid array obtained by spin coating of a **108**·2H/$NC_{12}N$ + 0.2 equiv. *n*-$BuNH_2$ solution in CH_2Cl_2/CF_3CH_2OH (98:2 v/v).

2.3. Experimental Section

General

Melting points were determined on a Kofler hot stage apparatus and are uncorrected. Unless otherwise stated, ^{1}H and ^{13}C NMR spectra were recorded at 25 °C in $CDCl_3$, at 500 and 125 MHz respectively. Chemical shifts are reported in ppm and are referenced to the residual solvent (∂_H 7.26 ppm and ∂_C 77.0 ppm). Where present, ^{1}H NMR peak assignments follow from COSY experiments. ^{13}C NMR spectra were acquired with the attached proton test (APT) technique. Mass spectra were measured on an ion trap electrospray instrument. Anhydrous solvents were either obtained commercially or dried by standard methods prior to use, while other chemicals were reagent grade, used without further purification. Column chromatography was performed on silica gel (Merck, 230–400 mesh). All reactions were carried out under an argon atmosphere. 5,11,17,23,29-penta-(1,1-dimethylethyl)-31-hydroxy-32,33,34,35-tetra-(4-methylpentyloxy)calix[5]arene (**100**) and 5,11,17,23,29-penta-(1,1-dimethylethyl)-31-benzyloxy-32,33,34,35-tetra-hydroxycalix[5]arene[23] (**102**) were synthesized according to published procedures.

2.3.1. Synthesis

5,11,17,23,29-Penta-(1,1-dimethylethyl)-31-*tert*-butoxycarbonyl-methoxy-32,33,34,35-tetrakis-(4-methylpentyloxy)calix[5]arene (**101**)

A stirred mixture of calix[5]arene **100** (350 mg, 0.305 mmol), *tert*-butyl bromoacetate (135 μL, 0.915 mmol) and K_2CO_3 (126 mg, 0.915 mmol) in CH_3CN (50 mL) was heated to reflux for 24 h. After evaporation of the solvent, the solid residue was partitioned between $CHCl_3$ (50 mL) and aqueous 0.1 M HCl (30 mL). The organic

layer was washed with water (2 × 30 mL), dried over $MgSO_4$ and concentrated under reduced pressure to yield, after recrystallization from $MeOH/CH_2Cl_2$, ester **101** (354 mg, 92%) as a colourless solid. M.p. 177–181 °C; ^1H NMR (500 MHz) ∂ = 6.96 and 6.98 (AB system, *J* =2.3 Hz, ArH, 4H), 6.94 (s, ArH, 2H), 6.79 and 6.84, (AB system, *J* = 2.3 Hz, ArH, 4 H), 4,54 (s, O*CH*$_2$CO, 2 H), 4,53, 4.56, 4.69 (d, *J* = 13.9, 13.6, 14.2 Hz, 2:2:1, $ArCH_2Ar$, 5 H), 3.50–3.72 (m, O*CH*$_2$$CH_2$, 8 H), 3.26, 3.29 (d, *J* = 13.6, 13.9 Hz, 3:2, $ArCH_2Ar$, 5 H), 1.84–1.89 (m, OCH_2CH_2, 8 H), 1.57–1.64 (m, C*H*$(CH_3)_2$, 4 H), 1.44 (s, C(C*H*$_3$)$_3$, 9H), 1.31–1.37 (m, $OCH_2CH_2CH_2$, 8 H), 0.95, 1.07, 1.08 (s, 2:1:2 ratio, C(C*H*$_3$)$_3$, 45 H), 0.94 (d, *J* = 6.6 Hz, CH(C*H*$_3$)$_2$, 24 H) ppm; ^{13}C NMR (500 MHz) ∂ 168.9, 152.8, 152.7, 152.6, 144.8, 144.54, 144.50, 134.0, 133.9, 133.7, 133.41, 133.38, 125.9, 125.4, 125.20, 125.16, 80.8, 74.3, 74.1, 71.0, 35.2, 33.98, 33.96, 33.92, 31.5, 31.4, 31.3, 30.3, 29.53, 29.46, 28.4, 28.3, 28.24, 28.21, 28.1, 22.88, 22.81, 22.80 ppm.

11,17,23,29-Penta-(1,1-dimethylethyl)-31-carboxymethoxy-32,33,34,35-tetrakis-(4-methylpentyloxy)calix[5]arene (98·H)

A solution of derivate **101** (330 mg, 0.262 mmol) was dissolved in $CHCl_3/CF_3CO_2H$ (1:1, v/v, 6 mL,) and stirred under inert atmosphere for 4 h at 25 °C. After evaporation of the solvent, the crude was purified by column chromatography (SiO_2, hexane/ethyl acetate 95:5, v/v). Recrystallization from $MeOH/CH_2Cl_2$ gave product **98**·H (208 mg 66%). M.p. 97–101 °C; ^1H NMR ∂ = 10.2 (br s, COO*H*), 7.27 (s, Ar 2H), 6.82 and 6.91 (AB system, *J* = 2.3 Hz, ArH, 4H), 6.79 and 6.84 (AB system, *J* = 2.3 Hz, ArH, 4 H), 4.41, 4.5 (d, *J* = 13.7, 14.0 Hz, 1:2, $ArCH_2Ar$, 5 H), 3.97 (s, O*CH*$_2$CO, 2 H), 3.84-3.93 (m, O*CH*$_2$$CH_2$, 4 H), 3.76 (t, O*CH*$_2$$CH_2$, 4 H), 3.29 (d, *J* = 14.0 Hz, $ArCH_2Ar$, 5 H), 1.83–1.90 (m, OCH_2CH_2, 8 H), 1.55–1.66 (m, C*H*$(CH_3)_2$, 4 H), 1.20–1.28 (m,$OCH_2CH_2CH_2$, 8 H), 0.91, 1.01, 1.32 (s, 2:2:1

ratio, C(C*H*$_3$)$_3$, 45 H), 0.93 (d, *J* = 6.7 Hz, CH(C*H*$_3$)$_2$, 12 H), 0.91 (d, *J* = 6.5 Hz, CH(C*H*$_3$)$_2$, 12 H) ppm; ^{13}C NMR (500 MHz) ∂ = 170.2, 152.5, 152.1, 150.9, 146.1, 145.4, 145.2, 134.2, 134.1, 133.6, 133.3, 133.1, 126.6, 126.0, 125.5, 125.2, 124.7, 75.6, 75.5, 69.7, 34.92, 34.86, 34.2, 33.9, 31.6, 31.4, 31.2, 30.0, 29.9, 29.3, 28.0, 27.9, 27.81, 27.79, 22.69, 22.67, 22.6 ppm.

5,11,17,23,29-Penta-(1,1-dimethylethyl)-31-benzyloxy-32,33,34,35-tetrakis-(tert-butoxycarbonylmethoxy)calix[5]arene (103)

A mixture of mono-ether **102** (205 mg, 0.228 mmol), *tert*-butyl bromoacetate (404 μL, 2.736 mmol) and K_2CO_3 (378 mg, 2.736 mmol) in CH_3CN (30 mL) was refluxed for 24 h. After cooling, the inorganic salts present in the reaction mixture were collected by filtration, washed with $CHCl_3$ and disposed, while the combined organic layers were evaporated to dryness. The resulting oily residue was treated with petroleum ether (50 mL) and the additional salts precipitate out removed by suction filtration. The filtrate was washed with water (2 × 30 mL), dried over $MgSO_4$ and concentrated under reduced pressure to yield, upon recrystallization from MeOH/$CHCl_3$, tetra-ester **103** (251 mg, 81%). M.p. 187–190 °C; ^{1}H NMR (500 MHz) ∂ = 7.21–7.51 (m, Ph*H*, 5 H), 7.08 (s, ArH, 2 H), 6.99 and 7.13 (AB system, *J* = 2.5 Hz, ArH, 4 H), 6.52 and 6.68 (AB system, *J* = 2.5 Hz, ArH, 4 H), 4.72, 4.75, 4.89 (d, *J* = 14.0, 14.5 and 15.0 Hz, 2:2:1, ArC*H*$_2$Ar, 5 H), 4.35 (s, OC*H*$_2$Ph, 2 H), 4.34 and 4.45 (AB system, *J* =15.5 Hz, OC*H*$_2$CO$_2$*t*Bu, 4H), 4.20 and 4.50 (AB system, *J* =16.0 Hz, OC*H*$_2$CO$_2$*t*Bu, 4H), 3.21, 3.34, 3.42 (d, *J* = 14.0, 14.0 and 15.5 Hz, 2:2:1, ArC*H*$_2$Ar, 5 H), 1.38, 1.48 (s, 1:1, CO$_2$C(C*H*$_3$)$_3$, 36 H), 0.84, 1.14, 1.15 (s, 2:1:2, C(C*H*$_3$)$_3$, 45 H) ppm; ^{13}C NMR (500 MHz) ∂ = 169.2, 168.8, 152.6, 152.2, 152.0, 145.3, 145.2, 145.1, 139.5, 134.0, 133.5, 133.32, 133.26, 133.2, 128.5,

127.6, 126.6, 126.2, 125.7, 125.54, 125.52, 125.49, 81.0, 80.9, 75.2, 71.8, 70.7, 34.03, 34.00, 33.8, 31.5, 31.4, 31.2, 29.4, 28.2, 28.0 ppm.

5,11,17,23,29-Penta-(1,1-dimethylethyl)-31-hydroxy-32,33,34,35-tetrakis-(tert-butoxycarbonylmethoxy)calix[5]arene (104)

A solution of calixarene **103** (198 mg, 0.146 mmol) and Pd/C (35 mg) in AcOEt (22 mL) was stirred at room temperature in presence of H_2 for 5 h. The mixture was filtered through celite and the filtrate was evaporated under reduced pressure to give **104** as a white solid (164 mg, 89%). M.p. 192–194 °C); ^{1}H NMR (500 MHz) ∂ = 7.14 and 7.23 (AB system, *J* = 2.5 Hz, ArH, 4 H), 7.10 (s, ArH, 2 H), 6.47 (s, ArO*H*, 1 H), 6.40 and 6.60 (AB system, *J* = 2.0 Hz, ArH, 4 H), 4.61, 4.71, 4.92 (d, *J* = 14.0, 14.0 and 15.5 Hz, 2:2:1, $ArCH_2Ar$, 5 H), 4.32 and 4.73 (AX, *J* = 16.0 Hz, OCH_2CO_2tBu, 4 H), 4.32 and 4.73 (AX, *J* = 16.0 Hz, OCH_2CO_2tBu, 4 H), 3.22, 3.34, 3.42 (d, *J* = 14.5, 14.0 and 15.0 Hz, 1:2:2, $ArCH_2Ar$, 5 H), 1.50, 1.53 (s, 1:1, $CO_2C(CH_3)_3$, 36 H), 0.65, 1.23, 1.29 (s, 2:1:2, , $C(CH_3)_3$, 45 H) ppm; ^{13}C NMR (500 MHz) ∂ = 169.2, 168.8, 152.6, 152.2, 152.0, 145.3, 145.2, 145.1, 139.5, 134.0, 133.5, 133.32, 133.26, 133.2, 128.5, 127.6, 126.6, 126.2, 125.7, 125.54, 125.52, 125.49, 81.0, 80.9, 75.2, 71.8, 70.7, 34.03, 34.00, 33.8, 31.5, 31.4, 31.2, 29.4, 28.2, 28.0 ppm.

5,11,17,23,29-Penta-(1,1-dimethylethyl)-31-(benzyloxycarbonyl-methoxy)-32,33,34,35-tetrakis-(*tert*-butoxycarbonyl-methoxy)-calix[5]arene (**105**).

A stirred mixture of **104** (183 mg, 0.144 mmol), benzyl bromoacetate (68 µL, 0.432 mmol) and K_2CO_3 (60 mg, 0.432 mmol) in CH_3CN (30 mL) was heated at reflux for 24 h. The mixture was allowed to cool, the inorganic salts were filtered, washed with $CHCl_3$ and disposed. The combined organic layers were concentrated under reduced pressure and the residue left, gave a powdery precipitate after addition of CH_3OH.

Crystallization of this solid from MeOH/$CHCl_3$ afforded mixed penta-ester **105** in 80% yield (163 mg). Mp 196–199 °C; ^{1}H NMR (500 MHz) ∂ = 7.27–7.41(m, Ph*H*, 5 H), 6.97 (s, ArH, 2 H), 6.87 and 6.92 (AB system, *J* = 2.5 Hz, ArH, 4 H), 6.73 and 6.79 (AB system, *J* = 2.5 Hz, ArH, 4 H), 4.74, 4.80, 4.82 (d, *J* = 14.5, 15.0 and 14.5 Hz, 2:1:2, $ArCH_2Ar$, 5 H), 4.65 (s, O*CH*$_2$$CO_2$Ph), 4.58 (s, OCH_2CO_2*t*Bu), 4.46 and 4.53 (AB system, *J* = 15.5 Hz, OC*H*$_2$$CO_2$*t*Bu, 4H), 3.29, 3.35, 3.38 (d, *J* = 14.5, 14.5 and 15.0 Hz, 2:2:1, $ArCH_2Ar$, 5 H), 1.41, 1.44 (s, 1:1, $CO_2C(CH_3)_3$, 36 H), 0.94, 1.03, 1.93 (s, 2:2:1, $C(CH_3)_3$, 45 H) ppm; ^{13}C NMR (500 MHz) ∂ = 170.0, 169.2, 169.0, 152.3, 151.9, 151.8, 145.44, 145.36, 145.35, 136.0, 133.7, 133.4, 133.3, 133.2, 133.1, 128.4, 128.3, 128.0, 126.0, 125.9, 125.7, 125.64, 125.56, 80.98, 80.96, 72.33, 71.27, 70.4, 66.1, 34.0, 33.9, 33.8, 31.4, 31.33, 31.28, 31.2, 30.2, 28.12, 28.09 ppm.

5,11,17,23,29-Penta-(1,1-dimethylethyl)-31-carboxymethoxy-32,33,34,35-tetrakis-(*tert*-butoxycarbonylmethoxy)calix[5]arene (99·H).

A solution of **105** (150 mg, 0.106 mmol) and 5% Pd/C (28 mg) in AcOEt (20 mL) was stirred at room temperature in the presence of H_2 for 6 h. The suspension was filtered through celite and the filtrate was evaporated under reduced pressure to give calixarene **99**·H as a colorless crystalline solid (132 mg, 94%). Mp 125–128 °C; ^{1}H NMR (500 MHz) ∂ = 7.21 (s, ArH, 2 H), 10.5 (s,br, COO*H*), 6.99 and 7.12 (AB system, *J* = 2.5 Hz, ArH, 4 H), 6.45 and 6.65 (AB system, *J* = 2.5 Hz, ArH, 4 H), 4.69, 4.86, 5.01 (d, *J* = 15.5, 14.5 and 14.0 Hz, 1:2:2, $ArCH_2Ar$, 5 H), 4.44 and 4.61 (AB system, *J* = 15.5 Hz, OC*H*$_2$$CO_2$*t*Bu, 4 H), 4.28 and 4.82 (AX, *J* = 16.0 Hz, OC*H*$_2$$CO_2$*t*Bu, 4 H), 4.08 (s, O*CH*$_2$$CO_2$H), 3.26, 3.37, 3.46 (d, *J* = 13.5, 14.0 and 16.0 Hz, 2:2:1, $ArCH_2Ar$, 5 H), 1.45, 1.50 (s, 1:1, $CO_2C(CH_3)_3$, 36 H), 0.77, 1.14, 1.25 (s, 2:2:1, $C(CH_3)_3$, 45 H) ppm; ^{13}C NMR (500 MHz) ∂ = 169.8, 169.3, 169.2,

153.0, 152.9, 150.5, 146.2, 145.5, 134.1, 133.5, 133.34, 133.28, 132.0, 126.4, 126.0, 125.7, 125.5, 125.4, 81.5, 81.3, 72.0, 71.4, 70.8, 34.1, 34.0, 33.7, 31.5, 31.4, 31.1, 31.8, 31.4, 29.2, 28.2, 28.1 ppm.

Biscalix[5]arene dimethyl ester (110).

A suspension of penta-*tert*-butil-*tetrakis*-(4-metilpentyloxy)calix[5]arene **109** (0.050 g, 0.044 mmol), dimethyl 2,7-dibromooctandioate **113** (7.2 mg, 0.020 mmol) and K_2CO_3 (6.0 mg, 0.044 mmol) in MeCN (15 mL) was refluxed for 1 day under a nitrogen atmosphere. After cooling, the solvent was evaporated under reduced pressure, and the resulting crude mixture was partitioned between CH_2Cl_2 (10 mL) and H_2O (20 mL). The organic layer was washed twice with H_2O (2×20 mL), dried with $MgSO_4$, filtered and evaporated under reduced pressure. The resulting residue was purified by column chromatography (SiO_2, *n*-hexane/AcOEt 8:1 v/v) yielding **110** (86%). ^{1}H NMR (300 MHz, $CDCl_3$) ∂ = 7.16 and 7.25 (ABq, 8H, Ar*H*), 6.83 and 7.02 (ABq, 8H, Ar*H*), 6.34 (s, 4H, Ar*H*), 4.40–4.64 (m, 10H, axial ArC*H*$_2$Ar), 4.28–4.38 (m, 2H, OC*H* (CH_2COOH)), 3.42–3.82 (m, 16H, OC*H*$_2$), 3.69 (s, 6H, OC*H*$_3$), 3.14–3.84 (m, 10H, equatorial ArC*H*$_2$Ar), 1.07–1.36 (m, 90H, C(C*H*$_3$)$_3$), 0.84–1.02 (m, 48H, CH(C*H*$_3$)$_2$) ppm.

Bis-calix[5]arene diacid (106·2H).

Aqueous LiOH (1M, 1 mL) was added to a solution of bis-calix[5]arene **110** (0.011 g, 0.010 mmol) in THF (2.5 mL), and the resulting mixture was stirred overnight at room temperature. H_2O (3 mL) was then adde, and pH was adjusted to 6 with 0.1 M HCl. The solution was extracted with $CHCl_3$ (3×10 mL), and the combined organic layer was dried ($MgSO_4$), filtered and evaporated under reduced pressure to give **106**·2H (97%). ^{1}H NMR (300 MHz, $CDCl_3$) ∂ = 7.23 (2H, Ar*H*), 7.22 (2H, *Ar*H),

7.20 (2H, *Ar*H), 7.03 (2H, *Ar*H), 6.98 (2H, *Ar*H), 6.94 (2H, *Ar*H), 6.86 (2H, *Ar*H), 6.77 (2H, *Ar*H), 6.66 (2H, *Ar*H), 6.54 (2H, *Ar*H), 3.54–4.02 (m, 16H, OCH_2), 4.40–4.58 (m, 10H, axial A*r*CH_2Ar), 3.18–3.40 (m, 10H, equatorial A*r*CH_2Ar), 0.88–0.98 (m, 90, C$(CH_3)_3$), 0.81, 0.87 (d, 48H, CH$(CH_3)_2$) ppm.

Dimethyl 2,8-dibromononanedioate (113).

$SOCl_2$ (5.5 mL, 0.075 mol) was added to nonandioic acid **116** (5.65 g, 0.03 mol) and the resulting mixture was refluxed until HCl e SO_2 vapour evolution (trapped by bubbling through 5M NaOH) stopped. Temperature was then kept at 85 °C, and Br_2 (3.9 mL, 0.076 mmol)was added dropwise over 6 h. After an additional 3 h, th mixture was poured over cold MeOH (50 mL), and left under stirring overnight. Crushed ice (50 mL) was added, and the resulting solution was extracted with CH_2Cl_2 (30 mL). The organic layer was washed with 5% aqueous $NaHCO_3$ (20 mL)and H_2O (20 mL), dried ($MgSO_4$), filtered and evaporated under reduced pressure. Crystallization from MeOH gave **113** (9.45 g, 84.1 %).

Biscalix[5]arene dimethyl ester (111).

A suspension of penta-*tert*-butil-*tetrakis*-(4-metilpentyloxy)calix[5]arene **109** (0.130 g, 0.113 mmol), dimethyl 2,8-dibromononandioate **114** (20 mg, 0.051 mmol) and K_2CO_3 (32 mg, 0.23 mmol) in MeCN (30 mL) was refluxed for 1 day under a nitrogen atmosphere. After cooling, the solvent was evaporated under reduced pressure, and the resulting crude mixture was partitioned between CH_2Cl_2 (10 mL) and H_2O (10 mL). The organic layer was washed twice with 1M HCl (2×10 mL), dried with $MgSO_4$, filtered and evaporated under reduced pressure. The resulting residue was purified by preparative TLC (SiO_2, *n*-hexane/AcOEt 35:1 v/v) yielding **111** (61 mg, 21 %). M.p. : 69–72 °C (from CH_2Cl_2). ^{1}H NMR ∂ = 7.25 (dd, *J* = 10.7 Hz, *J* = 2.5 Hz, *Ar*, 4H); 7.16 (t, *J* = 2.4 Hz, *Ar*, 4H); 7.00 (s, *Ar*, 4H); 6.83 (dt, *J* =

20.3 Hz, *J* = 2.4 Hz, *Ar*, 4H); 6.36 (d, *J* = 1.7 Hz, *Ar*, 4H); 4.63–4.44 and 3.34–3.17 (2 × m, ArC*H*$_2$Ar, 2 x 10H); 4.45 and 3.32 (2 × d, ArC*H*$_2$Ar, 4H); 4.32 (td, *J* = 7.45, *J* = 2.5, C*H*(C9), 2H); 3.80–3.66 (m, O-C*H*$_2$-(CH$_2$)$_2$-CH(CH$_3$)$_2$, 8H); 3.68 (s, -CO$_2$*Me*, 6H), 3.63–3.49 (m, O-C*H*$_2$-(CH$_2$)$_2$-CH(CH$_3$)$_2$, 4H); 2.10–2-16 (m, -C*H*$_2$-C(O)O$_2$Me, 4H); 1.95–1.80 (m, O-CH$_2$-C*H*$_2$-CH$_2$-CH(CH$_3$)$_2$, 16H); 1.68–1.58 (m,-C*H*$_2$-, 16H); 1.45-1.22 (m, -C*H*$_2$-CH$_2$-C(O)O$_2$Me, 8H; -C*H*$_2$-CH(CH$_3$)$_2$, 16H; 2H); 1.32 (s, 2 × *tert*-butyl-Ar, 36H); 1.08 (s, *tert*-butyl-Ar, 18H); 0.92-0.98 (m, *tert*-butyl-Ar, 18H; CH(C*H*$_3$)$_2$, 48H); 0.52 (s, *tert*-butyl-Ar, 18H) ppm. ^{13}C NMR ∂ = 171.95; 171.14; 153.4; 152.7; 152.4; 150.7; 144.9; 144.5; 144.47; 144.43; 144.40; 134.7; 134.6; 134.1; 133.99; 133.95; 133.7; 133.4; 133.3; 132.6; 126.8; 126.6; 126.0; 125.4; 124.9; 124.8; 124.5; 124.3; 124.2; 82.4; 82.3; 74.8; 74.7; 74.1; 72.9; 60.4; 51.6; 35.4; 35.2; 35.0; 34.1; 33.98; 33.90; 33.7; 32.9; 31.7; 31.6; 31.5; 31.3; 30.8; 30.6; 30.4; 29.2; 29.1; 28.5; 28.4; 28.38; 28.31; 28.2; 28.1; 25.1; 23.1; 23.0; 22.9; 22.8; 22.73; 22.71; 22.69; 22.65; 21.0; 14.2 ppm.

Bis-calix[5]arene diacid (107·2H).

Aqueous LiOH (1M, 1 mL) was added to a solution of bis-calix[5]arene **111** (0.052 g, 0.021 mmol) in THF (10 mL), and the resulting mixture was stirred overnight at room temperature. H$_2$O (3 mL) was then adde, and pH was adjusted to 6 with 0.1 M HCl. The solution was extracted with CHCl$_3$ (3×10 mL), and the combined organic layer was dried (MgSO$_4$), filtered and evaporated under reduced pressure to give **2**·2H (35 mg, 58%). M.p. : 75–78 °C (da CH$_2$Cl$_2$). ^{1}H NMR ∂ = 7.26–7.19 (m, *Ar*, 2H), 7.0–6.98 (m, *Ar*, 1H), 6.94–6.91 (m, *Ar*, 2H), 6.88–6.86 (m, *Ar*, 1H), 6.78-6.73 (m, *Ar*, 2H), 6.68–6.63 (m, *Ar*, 2H), 4.54–4.46 e 3.23–3.33 (2 x m, sistema AX, ArC*H*$_2$Ar, 10H); 4.26 (d, *J* = 13.8, C*H*(C9), 2H); 3.97–3.93 (m, O-C*H*$_2$-(CH$_2$)$_2$-CH(CH$_3$)$_2$, 2H); 3.81–3.82 (m, O-C*H*$_2$-(CH$_2$)$_2$-CH(CH$_3$)$_2$, 12H); 3.63–3.58 (m, O-

C*H*$_2$-(CH$_2$)$_2$-CH(CH$_3$)$_2$, 2H); 1.98–1.82 (m, -C*H*$_2$-C(O)O$_2$H, 4H; O-CH$_2$-C*H*$_2$-CH$_2$-CH(CH$_3$)$_2$, 16H); 1.66–1.55 (m, -C*H*$_2$-, 16H); 1.30–1.19 (m, -C*H*$_2$-CH$_2$-C(O)O$_2$OH, 8H; -C*H*$_2$-CH(CH$_3$)$_2$, 16H; -C*H*$_2$-, 2H); 1.25 (s, *tert*-butyl-Ar, 18H); 1.06 (s, *tert*-butyl-Ar, 18H); 1.04 (s, *tert*-butyl-Ar, 18H); 0.96–0.90 (m, CH(C*H*$_3$)$_2$, 48H); 0.88 (s, *tert*-butyl-Ar, 18H); 0.87 (s, *tert*-butyl-Ar, 18H) ppm. ^{13}C NMR ∂ = 173.2; 152.9; 152.8; 152.5; 149.7; 149.6; 145.4; 145.36; 145.30; 145.1; 144.4; 134.3; 133.7; 133.6; 133.5; 133.4; 133.1; 132.29; 132.27; 126.8; 126.0; 125.65; 125.61; 125.57; 125.53; 125.3; 125.2; 125.0; 124.9; 124.6; 124.5; 81.5; 81.4; 75.53; 75.51; 75.4; 75.1; 74.82; 74.80; 67.9; 35.1; 34.99; 34.96; 34.8; 34.1; 34.0; 33.9; 33.8; 33.6; 31.5; 31.4; 31.2; 30.34; 30.29; 30.1; 29.8; 29.7; 29.2; 29.17; 28.1; 28.0; 27.99; 27.94; 27.93; 27.91; 27.87; 27.64; 27.63; 25.7; 25.6; 25.5; 22.8; 22.76; 22.75; 22.74; 22.70; 22.68 ppm.

Dimethyl 2,11-dibromododecanedioate (115).

$SOCl_2$ (5.5 mL, 0.075 mol) was added to dodecandioic acid **118** (6.9 g, 0.03 mol) and the resulting mixture was refluxed until HCl e SO_2 vapour evolution (trapped by bubbling through 5M NaOH) stopped. Temperature was then kept at 85 °C, and Br_2 (3.9 mL, 0.076 mmol)was added dropwise over 6 h. After an additional 3 h, th mixture was poured over cold MeOH (50 mL), and left under stirring overnight. Crushed ice (50 mL) was added, and the resulting solution was extracted with CH_2Cl_2 (30 mL). The organic layer was washed with 5% aqueous $NaHCO_3$ (20 mL)and H_2O (20 mL), dried ($MgSO_4$), filtered and evaporated under reduced pressure. Crystallization from MeOH gave **115** (10.67 g, 85 %).

Bis-calix[5]arene dimethyl estere (112).

A suspension of penta-*tert*-butil-*tetrakis*-(4-metilpentyloxy)calix[5]arene **109** (0.130 g, 0.113 mmol), dimethyl 2,8-dibromododecandioate **115** (22 mg, 0.051 mmol) and K_2CO_3 (32 mg, 0.23 mmol) in MeCN (30 mL) was refluxed for 1 day under a nitrogen atmosphere. After cooling, the solvent was evaporated under reduced pressure, and the resulting crude mixture was partitioned between CH_2Cl_2 (10 mL) and H_2O (10 mL). The organic layer was washed twice with 1M HCl (2×10 mL), dried with $MgSO_4$, filtered and evaporated under reduced pressure. The resulting residue was purified by preparative TLC (SiO_2, *n*-hexane/AcOEt 35:1 v/v) yielding **112** (64 mg, 46 %). M.p. : 62–65 °C (da CH_2Cl_2). ^{1}H NMR ∂ = 7.24 (dd, *J* = 17.8 Hz, *J* = 2.7 Hz, *Ar*, 4H); 7.15 (dd, *J* = 6.6 Hz, *J* = 2.5, *Ar*, 4H); 7.00 (s, *Ar*, 4H); 6.83 (dd, *J* = 19.8 Hz, *J* = 2.5 Hz, *Ar*, 4H); 6.40 (s, *Ar*, 4H); 4.67-4.44 e 3.35-3.19 (2 × m, ArC*H*$_2$Ar, 2 × 10H); 4.45 and 3.34 (*J* = 14.2 Hz, ArC*H*$_2$Ar, 4H); 4.36 (t, *J* = 6.8, C*H*(C12), 2H); 3.80–3.61 (m, O-C*H*$_2$-$(CH_2)_2$-$CH(CH_3)_2$, 8H); 3.68 (s, -CO_2*Me*, 6H), 3.55–3.48 (m, O-C*H*$_2$-$(CH_2)_2$-$CH(CH_3)_2$, 4H); 2.18-2.10 (m, -C*H*$_2$-C(O)O_2Me, 4H); 1.96-1.82 (m, O-CH_2-C*H*$_2$-CH_2-$CH(CH_3)_2$, 16H); 1.68-1.57 (m, -C*H*$_2$, 16H); 1.43-1.24 (m, -C*H*$_2$-CH_2-C(O)O_2Me, 8H; -C*H*$_2$-CH_2-CH_2-C(O)O_2Me, 8H; -C*H*$_2$-$CH(CH_3)_2$, 16H; -C*H*$_2$-, 4H); 1.31 (s, *tert*-butyl-Ar, 18H); 1.30 (s, *tert*-butyl-Ar, 18H), 1.09 (s, *tert*-butyl-Ar, 18H); 0.92-0.98 (m, *tert*-butyl-Ar, 18H; CH(C*H*$_3$)$_2$, 48H); 0.55 (s, *tert*-butyl-Ar, 18H) ppm. ^{13}C NMR ∂ = 172.1; 153.3; 153.0; 152.7; 152.4; 150.8; 144.9; 144.5; 144.48; 144.42; 144.40; 134.8; 134.6; 134.0; 133.97; 133.94; 133.7; 133.5; 133.4; 133.3; 132.5; 126.7; 126.6; 126.0; 125.4; 124.9; 124.8; 124.5; 124.3; 124.2; 82.4; 74.8; 74.7; 74.1; 73.0; 51.6; 35.4; 35.2; 35.03; 35.02; 34.1; 34.0; 33.9; 33.7; 33.1; 31.7; 31.6; 31.5; 31.3; 30.9; 30.6; 30.3; 29.8; 29.7; 29.3; 29.2; 28.5; 28.42; 28.40; 28.3; 28.2; 28.5; 26.9; 25.1; 23.1; 23.0; 22.9; 22.8; 22.74; 22.72; 22.69; 22.66 ppm.

Bis-calix[5]arene dia*cid* (108·2H*).*

Aqueous LiOH (1M, 1 mL) was added to a solution of bis-calix[5]arene **112** (0.068 g, 0.027 mmol) in THF (10 mL), and the resulting mixture was stirred overnight at room temperature. H_2O (3 mL) was then adde, and pH was adjusted to 6 with 0.1 M HCl. The solution was extracted with $CHCl_3$ (3×10 mL), and the combined organic layer was dried ($MgSO_4$), filtered and evaporated under reduced pressure to give **108**·2H (40 mg, 59.4%). M.p. : 64–67 °C (from CH_2Cl_2). ^{1}H NMR ∂ = 7.22 (dd, *J* = 10.5 Hz, *J* = 2.4 Hz, *Ar*, 4H); 6.94 (dd, *J* = 4.3 Hz, *J* = 2.0, *Ar*, 4H); 6.89 (dd, *J* = 4.9 Hz, *J* = 2.2, *Ar*, 4H); 6.76 (dd, *J* = 5.7 Hz, *J* = 2.4 Hz, *Ar*, 4H); 6.67 (dd, *J* = 5..7 Hz, *J* = 2.5, *Ar*, 4H); 4.57–4.44 and 3.34–3.25 (2 x m, system AX, ArC*H*$_2$*A*r, 2 x 10H); 4.28 (d, *J* = 14.2, C*H*(C12), 2H); 3.97-3.91 (*m*, O-C*H*$_2$-$(CH_2)_2$-$CH(CH_3)_2$, 2H); 3.82-3.74 (m, O-C*H*$_2$-$(CH_2)_2$-$CH(CH_3)_2$, 12H); 3.62-3.58 (m, O-C*H*$_2$-$(CH_2)_2$-$CH(CH_3)_2$, 2H); 3.34-3.25 (m, O-C*H*$_2$-$(CH_2)_2$-$CH(CH_3)_2$, *2*H); 2.60-*1*.82 (m, -C*H*$_2$-C(O)O_2H, 4H; O-C*H*$_2$-C*H*$_2$-CH_2-$CH(CH_3)_2$, 16H); 1.67-1.54 (*m,* -C*H*$_2$-, 16H); 1.42-1.14 *(m*, -C*H*$_2$-CH_2-C(O)O_2H, 8H; -C*H*$_2$-CH_2-CH_2-C(*O)*O_2H, 8H; -C*H*$_2$-$CH(CH_3)_2$, 16H; -C*H*$_2$-, 4*H)*; 1.27 (s, *tert*-butyl-Ar, 18H); 1.06 *(s*, *tert*-butyl-Ar, 18H), 1.03 (s, *tert*-butyl-Ar, 18H); 0.91-0.86 (m, $CH(CH_3)_2$, 48H); 0.89 (s, *tert*-butyl-Ar, 18H); 0.87 (s, *tert*-butyl-Ar, 18H) ppm. ^{13}C NMR ∂ = 173.3; 152.9; 152.8; 152.3; 149.8; 145.4; 145.38; 145.32; 145.1; 144.4; 134.3; 134.2; 133.7; 133.6; 133.5; 133.4; 133.1; 132.4; 132.3; 126.9; 126.1; 125.7; 125.6; 125; 125.3; 125.1; 125.0; 124.9; 124.5; 81.6; 75.5; 75.4; 75.1; 74.9; 35.1; 35.0; 34.95; 34.91; 34.1; 33.9; 33.8; 32.3; 31.5; 31.4; 31.3; 31.2; 30.3; 30.27; 30.24; 29.91; 29.89; 29.81; 29.6; 29.2; 28.1; 28.0; 27.95; 27.94; 27.92; 27.89; 27.6; 25.5; 22.8; 22.76; 22.74; 22.72; 22.67 ppm.

2.3.2. Crystal structure determination

$99^{-}\supset{}^{+}H_3N(CH_2)_nNH_3^{+}\subset 99^{-}$ (n = 10, 11, 12), $98^{-}\supset$Nspm·$2H^{+}\subset 98^{-}$ and $98^{-}\supset$Spm·$2H^{+}\subset 98^{-}$.

Crystals of all the capsular complexes were of small dimensions and data collection was carried out using synchrotron radiation at the X-ray diffraction beam-line of the Elettra Synchrotron, (Trieste, Italy) employing the rotating-crystal method with the cryo-cooling technique. Routinely, the crystal, dipped in Paratone as cryo-protectant, was mounted in a loop and flash frozen to 100 K with liquid nitrogen. Diffraction data for $99^{-}\supset{}^{+}H_3N(CH_2)_{10}NH_3^{+}\subset 99^{-}$, $99^{-}\supset{}^{+}H_3N(CH_2)_{11}NH_3^{+}\subset 99^{-}$ and $98^{-}\supset$Nspm·$2H^{+}\subset 98^{-}$ were indexed and integrated using the XDS package,[124] while MOSFLM[125] was used for $99^{-}\supset{}^{+}H_3N(CH_2)_{12}NH_3^{+}\subset 99^{-}$ and $98^{-}\supset$Spm·$2H^{+}\subset 98^{-}$. Scaling was carried out with AIMLESS[126,127] for datasets collected from crystals of $99^{-}\supset{}^{+}H_3N(CH_2)_{10}NH_3^{+}\subset 99^{-}$, $99^{-}\supset{}^{+}H_3N(CH_2)_{12}NH_3^{+}\subset 99^{-}$ and $98^{-}\supset$Nspm·$2H^{+}\subset$**98** whereas XSCALE[124] was used for those collected from crystals of $99^{-}\supset{}^{+}H_3N(CH_2)_{11}NH_3^{+}\subset 99^{-}$and $98^{-}\supset$Spm·$2H^{+}\subset 98^{-}$. The structures were solved by direct methods using SIR2011.[128] Non-hydrogen atoms at full occupancy, or with population equal to or higher than 0.5 were anisotropically refined (H atoms at the calculated positions) by full-matrix least-squares methods on F^2 using SHELXL-13.[129] Crystal data and refinement details are reported in **Table 17** for $99^{-}\supset{}^{+}H_3N(CH_2)_nNH_3^{+}\subset 99^{-}$ and in **Table 18** for $98^{-}\supset$Nspm·$2H^{+}\subset 98^{-}$ and $98^{-}\supset$Spm·$2H^{+}\subset 98^{-}$. A detailed description of the treatment of disorder in each crystallographic model is provided in the following section.

Table 17. Crystal data and structure refinement for **99**$^{-}\supset{}^{+}H_3N(CH_2)_{10}NH_3^{+}\subset$**99**$^{-}$, **99**$^{-}\supset{}^{+}H_3N(CH_2)_{11}NH_3^{+}\subset$**99**$^{-}$ and **99**$^{-}\supset{}^{+}H_3N(CH_2)_{12}NH_3^{+}\subset$**99**$^{-}$.

	99$^{-}\supset{}^{+}H_3N(CH_2)_{10}NH_3^{+}\subset$**99**$^{-}$	**99**$^{-}\supset{}^{+}H_3N(CH_2)_{11}NH_3^{+}\subset$**99**$^{-}$	**99**$^{-}\supset{}^{+}H_3N(CH_2)_{12}NH_3^{+}\subset$**99**$^{-}$
Empirical formula	2(C_{81} H_{111} O_{15}), C_{10} H_{26} N_2, 8.8 (C_2 H_3 F_3 O)	2(C_{81} H_{111} O_{15}), C_{11} H_{28} N_2, 2.6 (C_2 H_3 F_3 O), 0.2 K	2(C_{81} H_{111} O_{15}), C_{12} H_{30} N_2, 5.5 (C_2 H_3 F_3 O)
Formula weight	3704.05	3105.66	3403.02
T (K)	100(2)	100(2)	100(2)
λ (Å)	0.900	0.800	0.8856
Crystal system	Orthorhombic	Orthorhombic	Monoclinic
Space group	*P*can	*P*bcn	$P2_1/a$
Unit cell dimensions (Å, °)	a = 22.92(1), α = 90	a = 22.509(1), α = 90	a = 22.59(1), α = 90
	b = 23.62(1), β = 90	b = 22.972(2), β = 90	b = 16.93(1), β = 92.54(4)
	c = 36.17(2), γ = 90	c = 35.249(2), γ = 90	c = 25.77(2), γ = 90
V (Å^3)	19581(16)	18226(2)	9846(11)
Z	8	8	4
$\rho_{(calc)}$ (g/mm^3)	1.256	1.132	1.148
μ (mm^{-1})	0.085	0.068	0.148
F(000)	7889	6635	3650
Resolution range (Å)	36.08-1.15	50.00-0.88	25.80-0.91
Reflections collected	39363	67897	29484
Independent reflections	7517	13881	13054
Data / restraints / parameters	7517 / 81 / 936	12628 / 226 / 1126	12638 / 74 / 1170
GooF	1.026	0.974	1.037
R_1, wR_2 [I>2σ(I)]	0.1118, 0.2035	0.1251, 0.3275	0.1187, 0.3095
R_1, wR_2 (all data)	0.1537, 0.2162	0.1579, 0.3592	0.1462, 0.3476
CCDC code number	1037220	1039436	1038992

Table 18. Crystal data and structure refinement for **98**$^{-}$⊃Nspm·2H^{+}⊂**98**$^{-}$ and **98**$^{-}$⊃Spm·2H^{+}⊂**98**$^{-}$

	98^{-}⊃Nspm·2H^{+}⊂**98**$^{-}$	**98**$^{-}$⊃Spm·2H^{+}⊂**98**$^{-}$
Empirical formula	2(C_{81} H_{119} O_7), C_9 H_{26} N_4, 4.4(C_2 H_3 F_3 O)	2(C_{81} H_{119} O_7), C_{10} H_{28} N_4, 2.5 (C_2 H_3 F_3 O)
Formula weight	3040.04	2863.91
T (K)	100(2)	100(2)
λ (Å)	0.7000	0.6525
Crystal system	Orthorhombic	Orthorhombic
Space group	*P*can	*P*bcn
Unit cell dimensions (Å, °)	a = 23.22(1), α = 90	a = 23.45(1), α = 90
	b = 24.47(2), β = 90	b = 23.02(1), β = 90
	c = 32.46(1), γ = 90	c = 32.88(2), γ = 90
V (Å^3)	18444(18)	17749(15)
Z	4	4
$\rho_{(calc)}$ (g/mm^3)	1.095	0.978
μ (mm^{-1})	0.074	0.051
F(000)	6600	5814.5
Resolution range (Å)	11.69-0.85	11.01-0.80
Reflections collected	39363	77945
Independent reflections	16926	19078
Data / restraints / parameters	16926 / 23 / 1046	16955 / 224 / 971
GooF	1.437	1.049
R_1, wR_2 [I>2σ(I)]	0.1298, 0.3666	0.1128, 0.3043
R_1, wR_2 (all data)	0.1831, 0.4113	0.1338, 0.3384
CCDC code number	1432426	1452078

2.3.3. Treatment of the disorder

$99^{-}\supset{}^{+}H_3N(CH_2)_{10}NH_3^{+}\subset 99^{-}$

The structure of capsule **$99^{-}\supset{}^{+}H_3N(CH_2)_{10}NH_3^{+}\subset 99^{-}$** was solved and refined in the non-standard space group *P*can (n° 60). By applying the transformation matrix [0 1 0, 1 0 0, 0 0 -1] to the cell parameters (a = 22.92(1), b = 23.62(1), c = 36.17(2) Å), the **abc** axes can be transformed into the **ba-c** standard settings of the *P*bcn (a = 23.62(1), b = 22.92(1), c = 36.17(2) Å) space group.

The crystal structure of the **$99^{-}\supset{}^{+}H_3N(CH_2)_{10}NH_3^{+}\subset 99^{-}$** capsular complex showed two disordered orientations for one *tert*-butyl group at the upper rim, that were refined at 0.8/0.2 of partial occupancy.

The cell contained severely disordered solvent molecules with partial occupancy, that were not modelled but taken into account using the SQUEEZE/PLATON[130] procedure. The residual electron density of 1753 electrons/cell found in the inner space of **$99^{-}\supset{}^{+}H_3N(CH_2)_{10}NH_3^{+}\subset 99^{-}$** (corresponding to about 23% of the cell volume) was attributed to 35 trifluoroethanol (TFE) solvent molecules. A refinement using reflections modified by the SQUEEZE procedure gave good results and the *R*-factor was reduced from 26.2 to 17.7%.

$99^{-}\supset{}^{+}H_3N(CH_2)_{11}NH_3^{+}\subset 99^{-}$

The structure of the **$99^{-}\supset{}^{+}H_3N(CH_2)_{11}NH_3^{+}\subset 99^{-}$** capsular complex showed both the guest and the pendant substituents, at the calixarene lower rim, to be severely disordered.

Three of these *tert*-butyloxycarbonylmethyl chains were found to be disordered over two positions and refined at 0.85/0.15, 0.6/0.4, 0.55/0.45 of partial occupancy,

respectively. In addition, the carboxylate group was seen disordered over three positions refined at 0.5/0.4/0.1 of partial occupancy. One *tert*-butyl group at the upper rim was also found to be disordered over two positions refined at 0.65/0.35 of partial occupancy. Two orientations of equal population were found for the undecanediammonium guest. In **Figure 87** all the orientations of the disordered moieties with lower occupancy are depicted in blue.

Restraints on geometrical parameters for all the disordered fragments were introduced during the refinement cycles, by using the DFIX, DANG and SADI cards, as well as restraints on anisotropic thermal parameters for carbon atoms by using the card SIMU.

The cell contained severely disordered solvent molecules with partial occupancy, which could be modelled. The SQUEEZE/PLATON procedure was used to correct the structure factors of these disordered solvent molecules. The residual electron density of 512 electrons/cell found in the inner space of $\mathbf{99}^{-}\supset{}^{+}H_3N(CH_2)_{11}NH_3^{+}\subset\mathbf{99}^{-}$ (15% of the cell volume) corresponded to about 10 TFE molecules (1.3 molecules in the asymmetric unit). A refinement using reflections modified by the SQUEEZE[130] procedure gave good results and the *R*-factor was reduced from 20.7 to 16.5%.

The difference Fourier electron density map showed a residual positive peak of 1.3 e/Å^3 very close to the nitrogen atom of the guest (distance to the nitrogen atom: 1.5 Å), located almost at the centre of the calixarene cavity (distance to the oxygen atoms: 2.5–3.3 Å). Given that this type of interactions has been previously observed in the crystal structure of the $\mathbf{99}^{-}\subset K^{+}$ complex (crystal structure deposited in the CCDC with the code 1056976, **Figure 88**), this residual peak was tentatively assigned to a K^{+} ion with very low occupancy factor (0.1).

a) b)

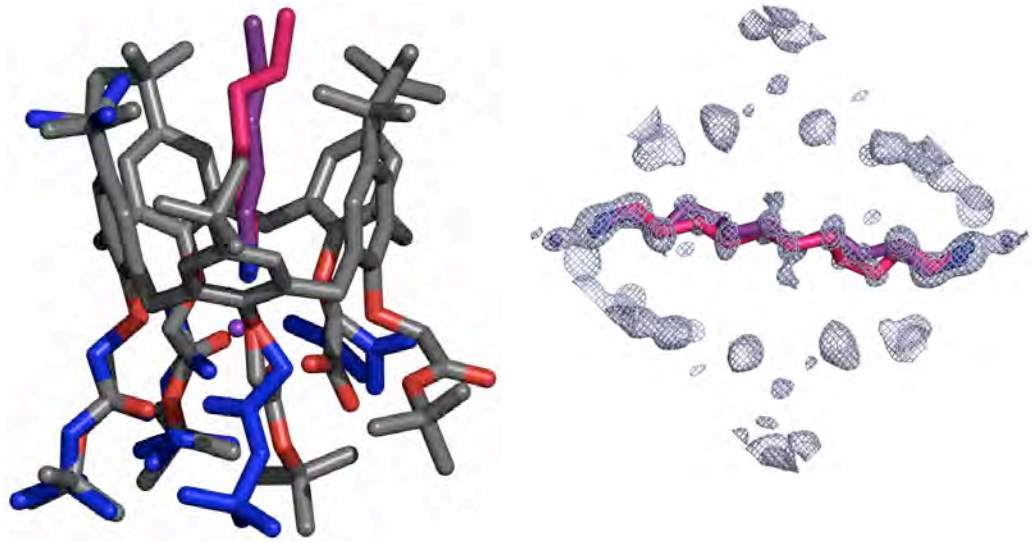

Figure 87. a) Side view of the solid-state structure of the **99**$^{-}\supset{}^{+}H_3N(CH_2)_{11}NH_3^{+}\subset$**99**$^{-}$ capsular complex. The orientations of the disordered calixarene moieties with lower occupancy are shown in blue, whereas the two orientations of the guest having equal occupancy are depicted in violet and magenta. The sphere in violet, seen inside the calixarene cavity, indicates a K^+ ion present in the crystal lattice with 0.1 of partial occupancy. b) Section of the electron density map (2Fo – Fc, contour level 0.8 σ) observed for the undecanediammonium guest disordered over two positions.

99$^{-}\supset{}^{+}$**H$_3$N(CH$_2$)$_{12}$NH$_3^{+}\subset$99**$^{-}$

In the asymmetric unit of the **99**$^{-}\supset{}^{+}H_3N(CH_2)_{12}NH_3^{+}\subset$**99**$^{-}$ *quasi*-capsular complex four TFE solvent molecules were detected and refined at 0.80, 0.75, 0.60, and 0.6 of partial occupancy. In the crystallographic model of **99**$^{-}\supset{}^{+}H_3N(CH_2)_{12}NH_3^{+}\subset$**99**$^{-}$ one pendant substituent was found disordered over two positions and refined at 0.65/0.35 of partial occupancy. For the geometrical parameters of this fragment restraints were applied on bond lengths and angles (using the cards DFIX, DANG and SADI). In

addition, the thermal parameters of the atoms present in this fragment were restrained to be similar (using the card SIMU).

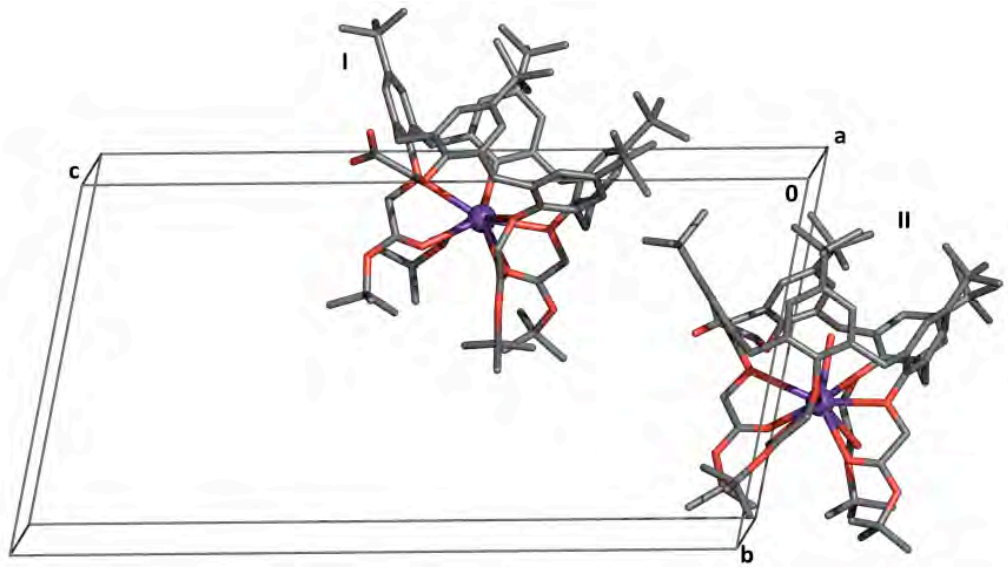

Figure 88. Crystallographic structure of the **99**$^{-}$⊂K^{+} complex. In the asymmetric unit of the complex two crystallographic independent complexes **99**$^{-}$⊂K^{+} (I and II) were found together with six trifluoroethanol molecules. The key crystallographic data for **99**$^{-}$⊂K^{+} are: triclinic space group *P* 1, FW 3189.76, *a* 12.02(1), *b* 14.68(1), *c* 27.57(2) Å, α 77.97(3), β 89.64(4), γ 84.28(2)°; *V* 4734(6) Å^3; R_1 0.1100, wR_2 0.3151, R_1(all) 0.1331, wR_2(all) 0.3504. K^{+}···O$_{Phenol}$ bond distances: 2.641(6) – 3.285(6) Å (I), and 2.650(6) – 3.204(7) Å (II), K^{+}···O$_{Ester}$ bond distances: 2.557(7) – 2.904(6) Å (I), 2.551(6) – 3.303(6) Å (II). K^{+}···O$_{Water}$ bond distance: 2.51(2) Å (II).

98^{-}⊃Nspm·2H^{+}⊂98^{-} and 98^{-}⊃Spm·2H^{+}⊂98^{-}

In the crystallographic model of **98**$^{-}$⊃Nspm·2H^{+}⊂**98**$^{-}$ two 4-methylpentyloxy chains at the narrow rim were found to be disordered over two orientations and were refined at 0.5/0.5 and 0.75/0.25 of partial occupancy. Two molecules of co-crystallization solvent (TFE) were refined at 0.75 of partial occupancy and a third one at 0.7.

Likewise, in the crystallographic model of the **98**$^{-}$⊃Spm·2H^{+}⊂**98**$^{-}$ capsular complex two disordered 4-methylpentyloxy moieties were refined at 0.5/0.5 and 0.4/0.6 of partial occupancy. A terminal methyl group of one of these moieties was also found to be disordered over two positions and refined at 0.4/0.6 of partial occupancy. The internal N-C-C group of the guest was also found to be disordered around a two-fold symmetry axis. The two orientations were refined at equal occupancy and, as a result, the structure of the encapsulated Spm·2H^{+} dication is compatible with either of the two conformations (A and B) reported in **Fig 89**. Restraints on geometrical parameters for all the disordered fragments were introduced during the refinement cycles by using the DFIX, DANG and SAME cards, as were restraints on anisotropic thermal parameters for carbon atoms by using the SIMU card. The cell contained severely disordered solvent molecules with partial occupancy that were not modelled, but were taken into account using the SQUEEZE/PLATON procedure.

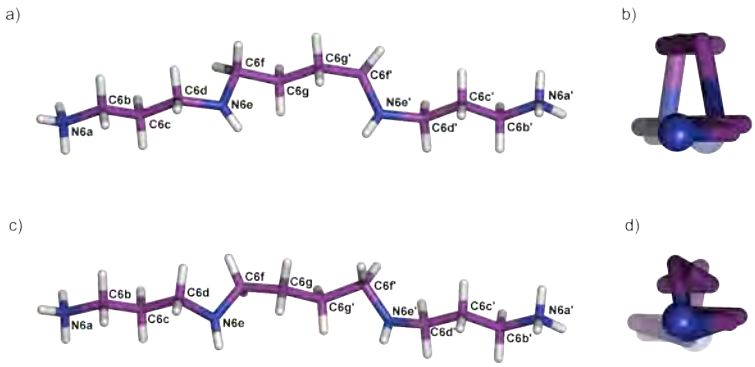

Figure 89. a) Side and b) front (from N6a) views of the solid-state structure of the dication guest (conformation A) encapsulated within **98**$^{-}$⊃Nspm·2H^{+}⊂**98**$^{-}$; N6e-C6f-C6g-C6g' torsion angle –92.1°. c) Side and d) front (from N6a) views of the dication guest (conformation B) encapsulated within **98**$^{-}$⊃Nspm·2H^{+}⊂**98**$^{-}$; N6e-C6f-C6g-C6g' torsion angle 120.4°.

The residual electron density of 518.7 electrons/cell found in the hollow of the **98**$^{-}$⊃Spm·2H^{+}⊂**98**$^{-}$ capsule (corresponding to approximately 13% of the cell volume) was attributed to 10 TFE solvent molecules. A refinement using reflections modified by the SQUEEZE procedure gave good results and the *R*-factor was reduced from 22.2 to 16.7%.

2.3.4. Calculation of the cavity volume for the capsular assemblies

99^{-}⊃$^{+}$**H$_3$N(CH$_2$)$_n$NH$_3^{+}$**⊂**99**$^{-}$ **and** **98**$^{-}$⊃$^{+}$**H$_3$N(CH$_2$)$_n$NH$_3^{+}$**⊂**98**$^{-}$ **(*n* = 10–12)**

Preliminary calculations of the cavity volume on the new capsular complexes **99**$^{-}$⊃$^{+}$H$_3$N(CH$_2$)$_n$NH$_3^{+}$⊂**99**$^{-}$ were carried out with the default setting parameters of the VOIDOO software, following the same procedure as for the previously reported capsular complexes **98**$^{-}$⊃$^{+}$H$_3$N(CH$_2$)$_n$NH$_3^{+}$⊂**98**$^{-}$. Such calculations, however, gave very high packing coefficients for the new structures: 75%, 80% and 70% for **99**$^{-}$⊃$^{+}$H$_3$N(CH$_2$)$_{10}$NH$_3^{+}$⊂**99**$^{-}$, **99**$^{-}$⊃$^{+}$H$_3$N(CH$_2$)$_{11}$NH$_3^{+}$⊂**99**$^{-}$ and **99**$^{-}$⊃$^{+}$H$_3$N(CH$_2$)$_{12}$NH$_3^{+}$⊂**99**$^{-}$, respectively. These suspicious high values, that to the best of our knowledge have never been reported so far even for solid state structures, prompted us to re-analyse the default parameters of the VOIDOO software. New calculations were then performed on both capsular complexes (**99**$^{-}$⊃$^{+}$H$_3$N(CH$_2$)$_n$NH$_3^{+}$⊂**99**$^{-}$ and **98**$^{-}$⊃$^{+}$H$_3$N(CH$_2$)$_n$NH$_3^{+}$⊂**98**$^{-}$), by setting the atomic radii equivalent to those used by Mecozzi and Rebek: aliphatic carbon = 1.70 Å, aromatic carbon = 1.75 Å, oxygen = 1.60 Å, nitrogen = 1.65 Å, aliphatic hydrogen = 1.20 Å, aromatic hydrogen = 1.00 Å.

Additionally, the following parameters were changed from their default settings:

Primary grid spacing: 0.1

Maximum number of volume-refinement cycles: 30

Grid for plot files: 0.1

A virtual probe with a radius of 1.4 Å was employed for **99**$^{-}\supset{}^{+}H_3N(CH_2)_{10}NH_3^{+}\subset$**99**$^{-}$ **99**$^{-}\supset{}^{+}H_3N(CH_2)_{11}NH_3^{+}\subset$**99**$^{-}$, **98**$^{-}\supset{}^{+}H_3N(CH_2)_{10}NH_3^{+}\subset$**98**$^{-}$ and **98**$^{-}\supset{}^{+}H_3N(CH_2)_{11}NH_3^{+}\subset$**98**$^{-}$, whereas a probe with a lager radius (1.7 Å) was necessary to define the two-host cavity of the *quasi*-capsular aggregates **99**$^{-}\supset{}^{+}H_3N(CH_2)_{12}NH_3^{+}\subset$**99**$^{-}$ and **98**$^{-}\supset{}^{+}H_3N(CH_2)_{12}NH_3^{+}\subset$**98**$^{-}$, the 1.4 Å probe being smaller than the gap present between the two calixarene upper rims. For a comparison of the internal volumes of the capsular cavities and the corresponding packing coefficients of the six complexes with the two probes see **Table 19**.

Table 19. Estimate of the guest volume (V_G), internal volume of the capsular cavity (V_C) and packing coefficient (*PC*) of complexes **99**$^{-}\supset{}^{+}H_3N(CH_2)_nNH_3^{+}\subset$**99**$^{-}$ and **98**$^{-}\supset{}^{+}H_3N(CH_2)_nNH_3^{+}\subset$**98**$^{-}$ (n = 10–12).[a,b]

	V_G (Å^3)	V_C (Å^3)[a]	*PC* (%)[a]	V_C (Å^3)[b]	*PC* (%)[b]
99$^{-}\supset{}^{+}H_3N(CH_2)_{10}NH_3^{+}\subset$**99**$^{-}$	195.3	299.4	65.2	279.9	69.8
99$^{-}\supset{}^{+}H_3N(CH_2)_{11}NH_3^{+}\subset$**99**$^{-}$	211.3	307.3	68.8	278.7	75.8
99$^{-}\supset{}^{+}H_3N(CH_2)_{12}NH_3^{+}\subset$**99**$^{-}$	224.9	–	–	368.4	61.0
98$^{-}\supset{}^{+}H_3N(CH_2)_{10}NH_3^{+}\subset$**98**$^{-}$	196.5	297.2	66.1	267.3	73.5
98$^{-}\supset{}^{+}H_3N(CH_2)_{11}NH_3^{+}\subset$**98**$^{-}$	209.3	338.0	61.9	301.9	69.3
98$^{-}\supset{}^{+}H_3N(CH_2)_{12}NH_3^{+}\subset$**98**$^{-}$	223.0	–	–	358.3	62.2

[a]Values refer to calculations carried out with the 1.4 Å probe; [b]values refer to calculations carried out with the 1.7 Å probe.

Volumes of the three alkanediyldiammonium guests (V_G) were calculated with the same software. Data in **Table 19** indicate that the internal volumes of the capsular cavities assessed with a 1.7 Å radius probe –instead of a 1.4 Å one– are on average 6–10% smaller and, as a result, the corresponding packing coefficients are consistently higher. Accordingly, in the case of the *quasi*-capsular complexes **99**$^-$⊃$^+$H$_3$N(CH$_2$)$_{12}$NH$_3^+$⊂**99**$^-$ and **98**$^-$⊃$^+$H$_3$N(CH$_2$)$_{12}$NH$_3^+$⊂**98**$^-$ –where use of the larger 1.7 Å probe was mandatory to avoid the exit of the rolling probe from the internal cavity– the values of the packing coefficients are likely to be overestimated by about 6–10%.

98$^-$⊃**Nspm·2H**$^+$⊂**98**$^-$ **and 98**$^-$⊃**Spm·2H**$^+$⊂**98**$^-$

Calculations of the capsular internal volumes ($\boldsymbol{V}_G$) of **98**$^-$⊃Nspm·2H$^+$⊂**98**$^-$ and **98**$^-$⊃Spm·2H$^+$⊂**98**$^-$ were carried out with the setting parameters of the VOIDOO software, as previously described by us, using a virtual probe with a 1.4 Å radius. Volumes of the Nspm·2H$^+$ and Spm·2H$^+$ dication guests ($\boldsymbol{V}_G$) were calculated with the same software.

2.3.5. ^{1}H NMR measurements

^{1}H NMR spectra (500 MHz) were recorded at 25 °C in CDCl$_3$/CD$_3$OD 9:1 v/v. Chemical shifts are reported in ppm and are referenced to the residual solvent (δ_H 7.26 ppm). Prior to use, CDCl$_3$ was filtered through neutral aluminium oxide to remove any traces of acid.

Sample solutions were routinely prepared by mixing together appropriate aliquots of CDCl$_3$/CD$_3$OD (9:1, v/v), stock solutions of **98**·H or **99**·H (10 mM) and H$_2$N(CH$_2$)$_n$NH$_2$ or Nspm or Spm (50 mM) to a final volume of 600 μL.

Sample solutions of **106**·2H-**108**·2H/$NC_{12}N$ in CD_2Cl_2/CF_3CD_2OD 9:1 v/v, were prepared by mixing together **106**·2H-**108**·2H and of $NC_{12}Nn$ in 1 to 1 molar ratio (a) [**106**·2H] = [$NC_{12}N$] = 0.5 mM; b) [**106**·2H] = [$NC_{12}N$] = 3 mM; c) [**107**·2H] = [$NC_{12}N$] = 0.5 mM; d) [**107**·2H] = [$NC_{12}N$] = 3 mM; e) [**108**·2H] = [$NC_{12}N$] = 0.5 mM; f) [**108**·2H] = [$NC_{12}N$] = 3 mM.

Same procedure was employed for **108**·2H/$NC_{12}N$ in CD_2Cl_2/CF_3CD_2OD 98:2 v/v. ([**108**·2H] = [$NC_{12}N$] = 15 mM; [**108**·2H] = [$NC_{12}N$] = 10 mM; [**108**·2H] = [$NC_{12}N$] = 6 mM; [**108**·2H] = [$NC_{12}N$] = 3 mM; [**108**·2H] = [$NC_{12}N$] = 1 mM; [**108**·2H] = [$NC_{12}N$] = 0.5 mM.)

2.3.6. Diffusion-ordered spectroscopy studies

DOSY experiments were carried out on a 500 MHz NMR spectrometer equipped with a z-gradient system capable of producing pulse gradients up to 50 gauss·cm^{-1}. All spectra were recorded in CD_2Cl_2/CF_3CD_2OD 98:2 v/v or CD_2Cl_2/CF_3CD_2OD 9:1 v/v at 25 °C, using a gradient stimulated echo with spin-lock and a convection compensation pulse sequence.

2.3.7. Atomic Force Microscopy

Atomic force microscopy was performed using an Ntegra probe NanoLaboratory from NT-MDT working in tapping mode and employing a Vit-p as probe. Sample solutions of the complex containing [**108**·2H] = 0.5 mM, [$NC_{12}N$] = 0.5 mM and [*n*-$BuNH_2$] = M wereμ0.1 dropped on the surface of an electronic grade silicon (100) wafer and then dried in air. No additional treatments were carried out on the resulting sample, thus preserving the morphology of the original nanostructures.

Chapter 3

3.1. Introduction

Dithia[3.3]-paracyclophanes are 14-membered macrocycles that have attracted attention owing to the applications they have found as synthetic intermediates in material science.[131] They have been employed as comonomers in the preparation of a wide range of π-conjugated copolymers,[132] (along with fluorene, bithiophene, acetylene, ethylene, or mixtures thereof), given that their peculiar trans-annular π-π interactions may induce significant modifications of the electronic and optical properties of the resulting materials, such as intense red or blue shifts in the emission spectra and enhanced photoluminescence efficiency. Because of the key role of the planar chirality in imparting properties of cyclophanes, an increasing number of papers have been published on the connection between structure and properties of this family of compounds.[133] As an example, a planar chiral ansa-bridge cyclophane was synthesized and successfully used, to mimic the sterospecificity of hydrogen transfer in biological asymmetric reduction with coenzyme NADH.[134]

Among the synthetic approaches employed to prepare planar chiral cyclophanes and heteracyclophanes, the best way was demonstrated to be the use of suitably and complementary functionalized cyclization pairs of molecules, and introducing at last one substituent on one of the aromatic rings to increase the conformational barrier related to complete rotation of the aromatic moieties (**Scheme 21**).[133d]

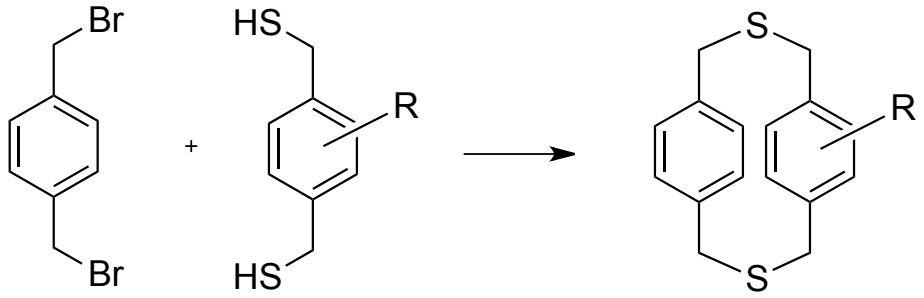

Scheme 21. Synthetic approach to dithia[3.3]paracyclophanes with planar chirality.

An alternative enantioselective route to get a planar chiral dithiacyclophane was reported by Tanaka et al. using a rhodium catalyst,[135] with up to 50% yield.

Also Konamata and co-workers in 2005[136] reported a facile and convenient synthetic method for [*n*]paracyclophanes (*n* = 8-12) by samarium iodide-catalysed intramolecular pinacol coupling and its application to planar-chiral cyclophane synthesis in a preparative scale (yields ranging from 14 to 64%).

Recently, Aversa et al. described an easier fashion strategy to achieve a number of *para*, *meta* and *para,meta*-cyclophanes, obtained from the two-component cyclization reaction of aromatic building blocks containing either two sulfenic acids or two alkynyl substituents – arranged in a *para* or *meta* fashion, through the formation of a suitable transient sulfenic acids in situ (**Scheme 22**).[137]

On that occasion, they observed that in the case of the cyclization reaction of a disulfenic acid with *m*-diethynylbenzene the reaction led to the formation of mixtures of diastereoisomers, whereas when *p*-diethynylbenzene was employed, the cyclization proceeded with complete stereoselection, resulting in the exclusive formation of the *meso*-diastereoisomer. A deeper insight into the reaction mechanism showed that the key step of the synthesis is the thermal *syn*-addition sulfenic acid/carbon-carbon triple bond.

Following the same convenient route, Barattucci and co-workers synthesized a series of dithiacyclophane derivatives with a remarkable planar and central chirality due to the simultaneous presence of chiral sulfinyl groups and two methyl groups on top and bottom of one of the aromatic ring.[138]

In detail, 2,5-dimethyl-1,4-benzenedimethanethiol **119** was employed as electrophilic component in the nucleophilic *syn*-addition of two equivalent of methyl acrylate, leading to a disulfide **120** that underwent controlled oxidation, generating disulfoxide derivative **121**. Subsequent thermolysis afforded the transient sulfenic acid that reacting with a *meta*- and *para*- diethynylbenzene, produce the dithiacyclophane *S*,*S*′-dioxides **122–124**. Again, when *para*-diethynylbenzene is used as nucleophilic partner, the reaction proceeds with a complete stereo and regioselectivity, providing exclusively the *meso*-(*R*,*S*)-diastereoisomer **122**. Moreover, under these reaction conditions, the bis-vinylsulfoxide-bridged paracyclophane, was obtained in a much higher yield (70% *vs.* 30%) than under the conditions previously reported.[137]

3.2. Dithiaparacyclophanes

3.2.1. A deeper insight into the reaction mechanism

Intrigued by the complete stereoselection of the reaction above described,[138] we decided to undertake a theoretical study on the mechanism underlying the formation of this cyclophane. In the previous paper[138] we demonstrated that, given the slow generation of the sulfenic acid moieties, the cyclization reaction proceeds in four distinct steps: i) formation of a first sulfenic acid function, ii) addition to the triple bond, to give a vinyl sulfoxide-containing intermediate, iii) generation of the second

sulfenic acid function, iv) cyclization via intramolecular addition to the second triple bond of the diethynylbenzene to generate the second vinyl sulfoxide bridging unit.

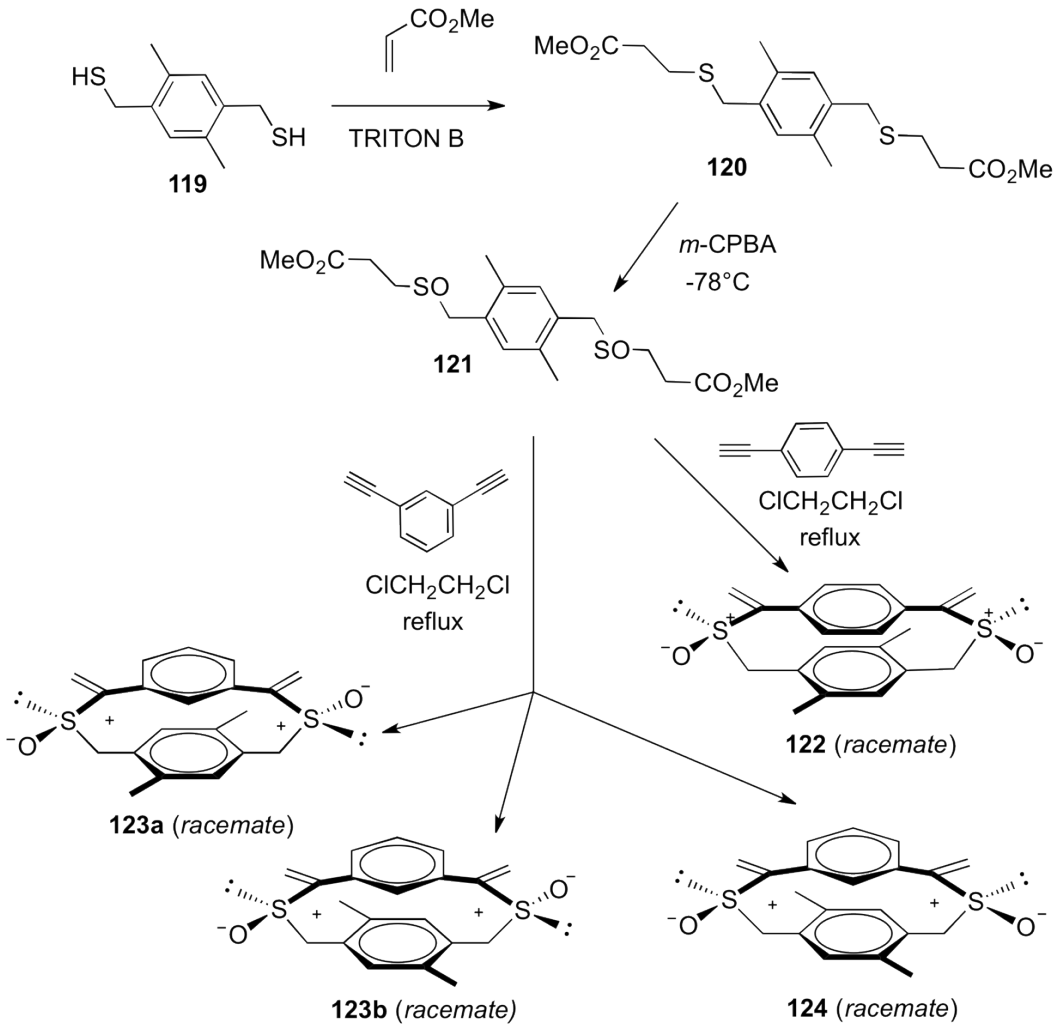

Scheme 22. Synthetic procedure to dithiacyclophane *S,S'*-dioxides with planar and central chirality.

Because of the persistence of the stereoselection, even when different starting materials (with respect to the precursor used in the previously described case[138]) were used in *ex*

novo synthesis of (*R,S*)-**125** (**Scheme 23**), it was reasonable to think that the stereochemical outcome is not determined in the earlier steps. Therefore, a density functional study on the last step was carried out, to examine the pathways that could lead to (*R,S*)-**125** or to the diastereomeric racemic mixture (*R,R*)/(*S,S*)-**125**.

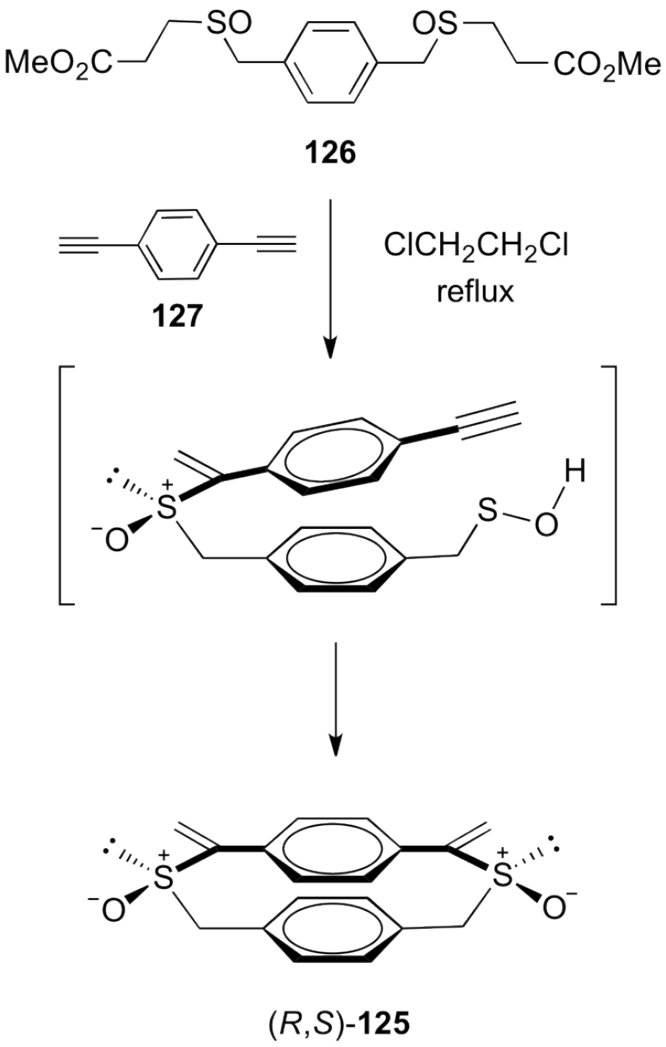

Scheme 23. Synthesis of (*R,S*)-**125**.

Driving from previous theoretical studies on the mechanism of sulfenic acid addition to 1-alkynes,[137] we decided to subject the open-chain precursor (prec-*S*) the cyclic products ((*R*,*S*)-**125**, and the 'hypothetical' (*S*,*S*)-**125**, henceforth referred to as cyc-*SR* and cyc-*SS*, respectively) and the transition states (TS-*SR*, TS-*SS*) to density functional calculation at the B3LYP/6-311+G(d,p) level of theory.[53] As for the choice of the *S* stereogenic centre, it should be noted that the formation of the open-chain intermediate resulting from the first sulfenic acid addition proceeds without stereoselection. We therefore arbitrarily assigned a *S* configuration to the chiral sulfoxide, and studied the formation of the *meso*-(*S*,*R*)-**125** and chiral (*S*,*S*)-**125** deriving from it.

In **Fig**. **90-92** we report the conformational minima turned out after a refined calculation process at the density functional level of theory, while in **Fig. 93**, is showed the energetic profiles of the two reaction pathways, derived from the energy values reported in **Table 20**.

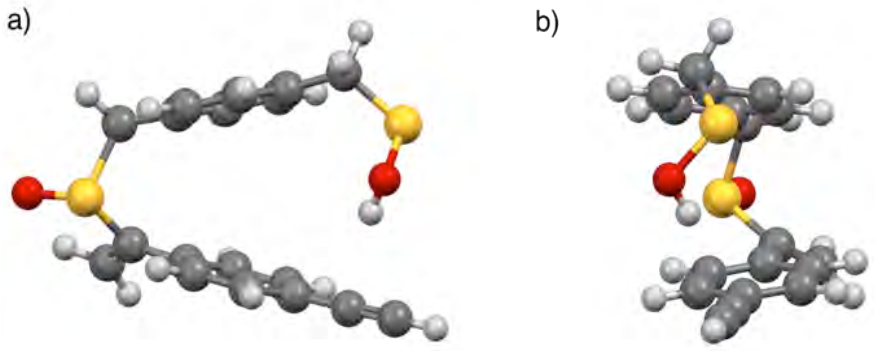

Figure 90. Side (a) and front (b) views of the optimized geometry (B3LYP/6-311+G(d,p)) of the open-chain precursor prec-*S*.

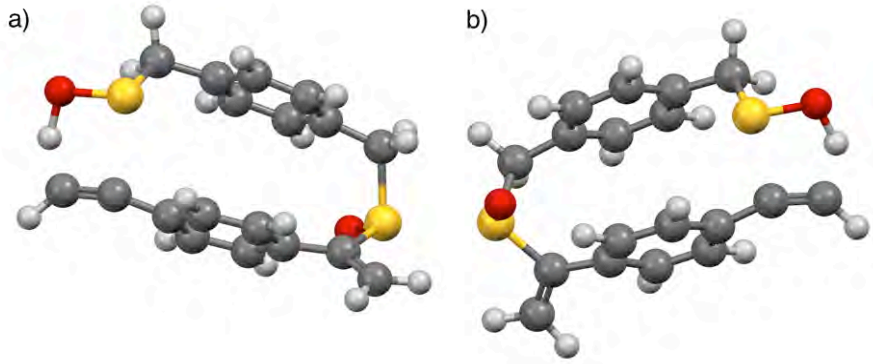

Figure 91. Side views of the optimized geometries (B3LYP/6-311+G(d,p)) of the possible transition states (a) TS-*SR*, (b) TS-*SS*.

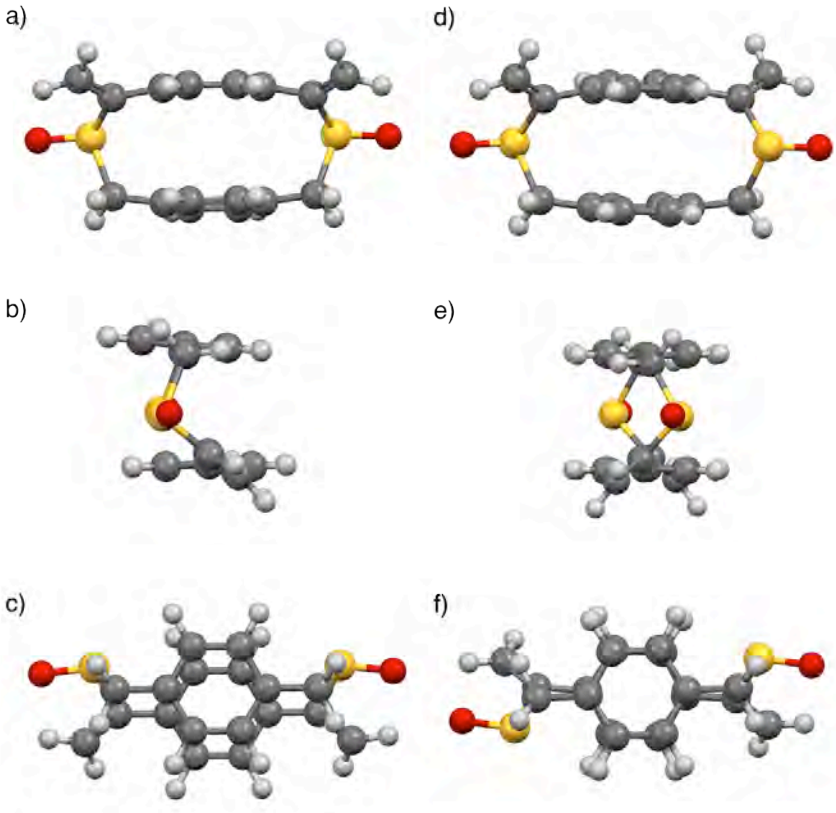

Figure 92. Side (a), front (b) and (c) top views of the optimized geometry (B3LYP/6-311+G(d,p)) of the paracyclophanes cyc-*SR* (a–c) and cyc-*SS* (d–f).

Table 20. DFT B3LYP/6-311+G(d,p) calculated energies (a.u.)

	Energy (a.u.)
prec-*S*	–1642.50333
TS-*SR*	–1642.45883
TS-*SS*	–1642.44932
cyc-*SR*	–1642.51415
cyc-*SS*	–1642.51196

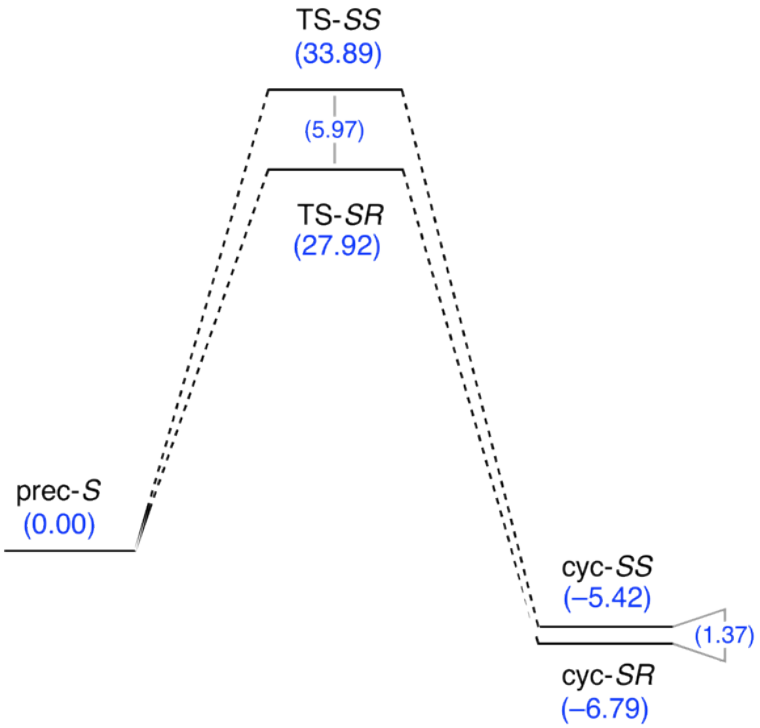

Figure 93. Representation of the potential energy surfaces for the two macrocyclization pathways of prec-*S*. Activation and reaction energy differences are reported (in blue) in kcal/mol.

The cyclic diastereoisomers cyc-*SR* and cyc-*SS* yielded highly symmetric conformation. The *meso*-cyc-*SR* possesses a C_s symmetry, with the two aromatic rings facing each other in an almost parallel arrangement[139,140] (interplanar angle: 5.1°, centroid-to-centroid distance: 3.43 Å), offset by 0.98 Å. The vinyl sulfoxide moieties adopt an s-*cis* conformation, with the C=C–S–O atoms virtually coplanar (dihedral angle: 0.8°). The chiral cyc-*SS* adopts a C_2-symmetric conformation, with perfectly parallel aromatic rings (centroid-to-centroid distance: 3.44 Å) that show no offset but are rotated with respect to each other by 6.8°. Also in this case the C=C–S–O atoms lie on the same plane. The open-chain precursor prec-*S* adopts a highly preorganized folded conformation, where the aromatic rings are seen super-imposed in a paracyclophane-like conformation at a 26.3° angle with respect of each other already in π–π stacking distance.[‡‡‡] The sulfenic acid moiety is already in close proximity of the alkynyl group, at 2.57 Å from the carbon that will be attacked. As expected, the formation of both cyclic compounds was found to be exergonic (**Fig. 93**, $\Delta E_{cyc\text{-}SR}$ = –6.79 kcal/mol, $\Delta E_{cyc\text{-}SS}$ = –5.42 kcal/mol), but the very small energy difference between the two diastereoisomers ($\Delta\Delta E$ = 1.37 kcal/mol) leads away from the hypothesis that stereoselection is thermodynamically controlled. Conversely, the transition states of the two possible reaction pathways provided strong evidence that cyc-*SR* exclusive formation takes place under kinetic control (**Fig. 94**).

In the present case, the geometry of the two transition states shows a marked difference: in TS-*SR* the H atom is 'already' in close proximity to the C–H carbon (O–H···C–H distance: 1.35 Å), while the S atom is still 2.53 Å away from the C–Ar. In TS-*SS* the picture is reversed: the S atom is anticipating the attack to the C–Ar

[‡‡‡] The high preorgazion of prec-*S* may explain why the reaction proceeds to the exclusive formation of the cyclic product (with respect to linear oligomers) even though it is not carried out under high dilution conditions.

(S···C–Ar distance: 2.28 Å), whereas the sulfenic acid H atom transfer appears to be slightly delayed (O–H···C–H distance: 1.48 Å). Furthermore, closer inspection of the TS geometries (**Fig. 94**, bottom row) shows that in TS-*SR* the plane of the 5-membered transition state describes a 58.0° angle with respect to the one defined by the phenylene ring, whereas in TS-*SS* the attack to the Ar–C≡C–H is coming from a more acute angle (46.7°).

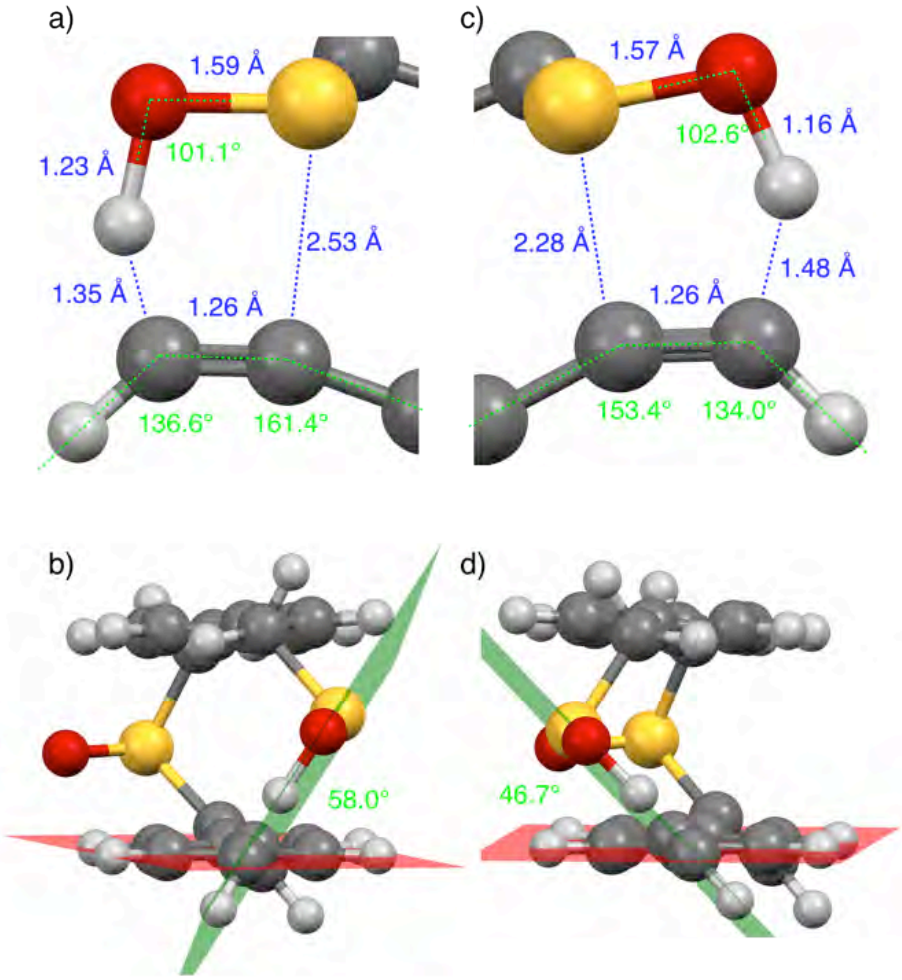

Figure 94. Views of the five-membered transition states TS-*SR* (a,b) and TS-*SS* (c,d) for the *syn*-addition of the sulfenic acid to the alkynyl group leading to cyc-*SR* and cyc-*SS*, respectively. Blue: distances, green: relevant angles.

These different structural features, taken together, may help to explain the different activation energies calculated for the two transition states ($\Delta E^{\ddagger}_{TS\text{-}SR}$ = 27.92 kcal/mol, $\Delta E^{\ddagger}_{TS\text{-}SS}$ = 33.89 kcal/mol, $\Delta\Delta E^{\ddagger}$ = 5.97 kcal/mol). It may be postulated that, owing to the presence of the sulfoxide stereogenic sulfur between the two rigid aromatic moieties, the prec-*S* reactant may comfortably reach only one of the two possible TSs (*i.e.*, TS-*SR*).

The TS-*SS* transition state leading to cyc-*SS* displays two potential drawbacks which may be responsible for the increased activation barrier: i) the anticipated attack of the sulfur atom that has been associated to the formation of the *anti*-Markovnikov-like regioisomer (while in the present case both cyc-*SR* and cyc-*SS* diastereoisomers are Markovnikov-like regioisomers), and ii) the unfavourable angle of attack on the triple bond, which may suffer from increased steric hindrance from the *ortho*-H atom of the ethynylphenylene moiety. Hence, it may be safely assumed that the exclusive formation of the cyc-*SR* diastereoisomer (*meso*-(*S*,*R*)-**125**) proceeds under kinetic rather than thermodynamic control.

The fact that the formation of cyc-*SR* proceeds under kinetic control is further confirmed by two additional pieces of indirect evidence: i) the retro-addition reaction of vinyl sulfoxides usually takes place at higher temperatures than those we employ for sulfenic acid generation,[141] and therefore it is unlikely that the formation of the paracyclophane is reversible, and ii) ^{1}H NMR monitoring of the 5-days reaction showed the exclusive (and progressive) formation of cyc-*SR*.

3.3. Experimental section

*3.3.1. Synthesis of (R,S)-***125**

A solution of disulfoxide **126** (0.15 g, 0.40 mmol) and *p*-diethynylbenzene **127** (0.05 g, 0.40 mmol) in DCE (40 mL) under nitrogen was heated to reflux for five days. The solvent was then removed under reduced pressure and the crude mixture was purified by column chromatography (SiO_2, EtOAc/light petroleum 9:1 v/v) to yield **125** (0.09 g, 70%) as a white solid. All spectroscopic data are in agreement with those previously reported.[137] Selected data: ^{1}H NMR (300 MHz, $CDCl_3$) δ = 7.29 and 6.79 (two split d, $^4J_{meta}$ = 2.3 Hz, 4H, H-14,-15,17,18), 7.14 and 6.46 (two split d, $^4J_{meta}$ = 2.2 Hz, 4H, H-5,6,8,9), 6.17 and 6.16 (two d, $^2J_{gem}$ = 1.0 Hz, 4H, 2 × =CH_2), 4.60 and 3.76 (AB system, $^2J_{gem}$ = 11.6 Hz, 4H, H2-3,10) ppm. ^{13}C NMR (75 MHz, $CDCl_3$) δ = 152.6 (C-1,12), 136.1 and 129.8 (C-4,7,13,16), 133.3, 128.8, 127.2, and 127.1 (C-5,6,8,9,14,15,17,18), 115.3 (2 × =CH_2), 65.0 (C-3,10) ppm.

3.3.2. Molecular modelling

Conformational analysis of the precursors and of the cyclic structures was carried out in the gas phase with the classical molecular mechanics force field using the Monte Carlo method to randomly sample the conformational space. The equilibrium geometries were refined at the density functional level of theory (DFT, B3LYP functional) using the 6-31G(d) basis set, and the resulting geometries were used as input for the calculations at the density functional level of theory (DFT, B3LYP functional) using the 6-311+G(d,p) basis set. The transition states where direct optimized at the B3LYP/6-31G(d) level, and then refined by using the 6-311+G(d,p)

basis set. Vibrational frequencies were computed at the same level of theory to define optimized geometries as minima (no imaginary frequencies) or transition states (a single imaginary frequency corresponding to the vibrational stretching of the forming/breaking bonds) All quantum mechanical calculations were performed using Spartan'10.[53]

References

[1] Lindsey, J. S. *New J. Chem*., **1991**, *15*, 153–180.

[2] Glink, P.T; Schiavo, C.; Stoddart, J.F; Williams, D.J. *Chemm.Commun*., **1996**, 1483–1490.

[3] Pedersen, C. J. *Angew. Chem., Int. Ed. Engl*.**1988**, 27, 1021–1027.

[4] Lehn, J.-M. *Angew. Chem*., *Int. Ed. Engl*. **1988**, *27*, 89–112.

[5] a) Easton, C.J. and Lincoln, S.F. *Modified Cyclodextrins- Scaffolds and Templates for supramolecular Chemistry*, Imperial college Press., London, **1999**; b) *Encyclopedia of Supramolecular Chemistry*; Atwood, J.L. and Steed J.W., Ed.; Marcel Dekker: New York, **2004**.

[6] Cram, D.J. *Angew.Chem.*,*Int. Ed. Engl.* **1988**, *27*, 1009–1020.

[7] *Comprehensive Supramolecular Chemistry*; Atwood, J.L.; Davies, J.E.D.; MacNicol, D.D.; Vogtle, F.; Lehn, J.-M., Ed.; Elsevier: The Netherlands, **1996**.

[8] a) Gutshe, C.D. *Calixarenes*, The Royal Society of Chemistry: Cambridge, **1989**; b) Gutshe, C.D. *Calixarenes Revisited*, The Royal Society of Chemistry: Cambridge, **1998**; c) Gutsche, C. D. *Calixarenes – An Introduction*; Stoddart, J. F., Ed.; Monographs in Supramolecular Chemistry, 2nd Ed.; The Royal Society of Chemistry: Cambridge, **2008**; Vol. 6.

[9] For reviews concerning heterocalix(hetero)arenas, see: a) König, B.; Fonseca, M. H. *Eur. J. Inorg. Chem*. **2000**, 2303–2310; b) Vysotsky, M.; Saadioui, M.; Böhmer, V. in *Calixarenes 2001*; Asfari, Z., Böhmer, V., Harrowfield, J., Vicens, J., Eds.; Kluwer Academic Publishers: Dordrecht, **2001**; p 250; c)Lhotak, P. *Eur. J. Org. Chem*. **2004**, 1675–1692; d) Morohashi, N.; Narumi, F.; Iki, N.; Hattori, T.; Miyano, S. *Chem. Rev*. **2006**, *106*, 5291–5316; e) Wang, M.-X. *Chem. Commun*. **2008**, 4541–4551. For tetraazamacrocycles with alternating meta-para linkages, see: f) Hauck, S. I.; Lakshmi, K. V.; Hartwig, J. F. *Org. Lett*. **1999**, *1*, 2057–2060; g)

Ito, A.; Yamagishi, Y.; Fukui, K.; Inoue, S.; Hirao, Y.; Furukawa, K.; Kato, T.; Tanaka, K. *Chem. Commun*. **2008**, 6573–6575.

[10] a) Gale, P.A.; Anzenbacher, P.; Sessler J.L. *Coord. Chem. Rev*. **2001**, *222*, 57–102; b) Kumar, S.; Paul, D.; Singh, H.; *Adv.Heterocycl. Chem*. **2005**, *89*, 65–124; c) Jain, V.K.; Mandalia, H.C. *Heterocycles* **2007**, *71*, 1261–1314; d) Konig, B.; Fonseca, M.H. *Eur. J. Inorg. Chem*. **2000**, 2303–2310.

[11] *Calixarenes In Action* , Mandolini, L.; Ungaro, R. Ed.; Imperial College Press.: London, **2000**.

[12] a) Lhotak, P. *Eur. J. Org. Chem*. **2004**, 1675–1692; b) Morohaschi, N.; Narumi, F.; Iki, N.; Hattori, T.; Miyano, S. *Chem. Rev*. **2006**, *106*, 5291–5316.

[13] Sommer, N.; Staab, H.A. *Tetrahedron Lett*. **1966**, 2837–2841.

[14] a) Mehta, V.; Panchal, M.; Modi, K.; Kongor, A.; Panchal, U.; Jain, V. K. *Curr. Org. Chem*. **2015**, *19*, 1077–1096; b) Maes, W.; Dehaen,W. *Chem. Soc. Rev*. **2008**, *37*, 2393–2402; c) Pappalardo, S.; Parisi, M. F. In *Comprehensive Heterocyclic Chemistry III*, Katritzky, A. R., Ramsden, C. A., Scriven, E. F. V., Taylor, R. J. K., Eds.; Elsevier: Oxford, **2008**; Vol. 14, p 667.

[15] Lehmann, F.P.A. *Tetrahedron*, **1974**, *30*, 727–733.

[16] Wang, M.-X.; Zhang, X.-H.; Zheng, Q.-Y. *Angew. Chem., Int. Ed*. **2004**, *43*, 838–842.

[17] Gong, H.-Y.; Zhang, X.-H.; Wang, D.-X.; Ma, H.-W.; Zheng, Q.-Y.; Wang, M.-X. *Chem.-Eur. J*. **2006**, *12*, 9262–9275.

[18] Zheng, E.-X; Wang, D.-X.; Zheng, Q.-Y.; Wang, M.-X. *Chem. Commun*. **2008**, *10*, 2565–2568.

[19] Katz, J. L.; Feldman, M. B.; Conry, R. R. *Org. Lett.* **2005**, *7*, 91–94

[20] a) Rowan, S.J.; Cantrill, S.J.; Cousins, G.R.L.; Sanders, J.K.M.; Stoddart, J.F. *Angew. Chem., Int. Ed.* **2002**, *41*, 898–952; b) Konishi, H.; Tanaka, K.; Teshima, Y.; Mita, T.; Morikawa, O.; Kobayashi, K.; *Tetrahedron Lett.*, **2006**, *47*, 4041–4044.

[21] Hao, E.; Fronczek, F.R.; Vincente, M.G.H. *J. Org. Chem*. **2006**, *71*, 1233–1236.

[22] Jiao, L.; Hao, E.; Fronczek, F.r.; Smith, K.M.; Vincente, M.G.H. *Tetrahedron* **2007**, *63*, 4011–4017.

[23] Zhang, C.; Chen, C.-F. *J. Org. Chem*. **2007**, *72*, 3880–3888.

[24] Yang, F.; Yan, L.; Ma, K.; Yang, L.; Li, J.; Chen, L.; You, J. *Eur. J. Org. Chem.* **2006**, 1109–1112.

[25] a) Chambers, R. D.; Hoskin, P. R.; Khalil, A.; Richmond, P.; Sandford, G.; Yufit, D. S.; Howard, J.A.K. *J. Fluorine Chem*. **2002**, *116*, 19–22; b) Chambers, R. D.; Hoskin, P.R.; Kenwright, A.R.; Khalil, A.; Richmond, P.; Sandford, G.; Yufit, D. S.; Howard, J. A. K. *Org. Biomol. Chem* **2003**, *1*, 2137–2147; c) Chambers, R. D.; Khalil, A.; Richmond, P.; Sandford, G.; Yufit, D. S.; Howard, J.A.K. *J. Fluorine Chem.* **2004**, *125*, 715–720.

[26] Katz, J. L.; Selby, K. J.; Conry, R. R. *Org. Lett*. **2005**, *7*, 3505–3507.

[27] Wang, M.-X.; Yang, H.-B. *J.Am. Chem. Soc.* **2004**, *126*, 15412–15422.

[28] Wang, L.-X.; Wang, D.-X.; Huang, Z.-T.; Wang, M.-X. *J. Org. Chem.* **2010**, *75*, 741–747.

[29] a) Mathias, J.P.; Simanek, E.E.; Whitesides, G.M. *J. Am. Chem. Soc*. **1994**, *116*, 4326–4340; b) Prins, L.J.; Huskens, J.; De Jong, F.; Timmerman, P.; Reinhoudt, D.N. *Nature* **2000**, *408*, 181–184; c) Kawasaki, T.; Tokuhiro, M.; Kimizuka, N.; Kunikate, T. *J. Am. Chem. Soc.* **2001**, *123*, 6792–6800.

[30] Hou, B.-Y.; Wang, D.-X.; Yang, H.-B.; Zheng, Q.-Y.; Wang, M.-X. *J. Org. Chem*. **2007**, *72*, 5218–5226.

[31] Hou, B.-Y.; Zheng, Q.-Y.; Wang, D.-X.; Wang, M.-X. *Tetrahedron*, **2007**, *63*, 10801–10808.

[32] Katz, J. L.; Geller, B. J.; Conry, R. R. *Org. Lett*. **2006**, *8*, 2755–2758

[33] Van Rossom, W.; Maes, W.; Kishore, L.;.Van Heeke, L.; Van Merveelt, L.; Dehaen, W. *Org. Lett.*, **2006**, *8,* 4161–4164.

[34] Van Rossom, W.; Maes, W.; Kishore, L.; Ovaere, M.; Van Merveelt, L.; Dehaen, W. *Org. Lett.*, **2008**, *10*, 585–588.

[35] Li, X.; Upton, T. G.; Gibb, C. L. D.; Gibb, B. C. *J. Am. Chem. Soc*. **2003**, *125*, 650–651.

[36] a) Andreetti, G. D.; Ungaro, R.; Pochini, A. *J. Chem. Soc., Chem. Commun*. **1979**, 1005–1007; b) Andreetti, G. D.; Ungaro, R.; Pochini, A. *J. Chem. Soc., Perkin Trans*. 2, **1983**, 1773–1779.

[37] Wang, M.-X. *Acc. Chem. Res*. **2012**, *45*, 182–195.

[38] Konishi, H.; Tanaka, K.; Teshima, Y.; Mita, T.; Morikava, O.; Kobayashi, K. *Tetrahedron Lett.* **2006**, *47*, 4041–4044.

[39] Wang, Q.-Q.; Wang, D.-X.; Zheng, Q.-Y.; Wang, M.-X. *Org. Lett*. **2007**, *9*, 2847–2850.

[40] a) Kong, L.; Ma, M.; Zhao, X.; Liu, Y.; Mi, X.; Jiang, B.; Wen, K. *Chin. J. Chem*. **2013**, *31*, 684–688; b) Van Rossom, W.; Caers, J.; Robeyns, K.; Van Meervelt, L.; Maes, W.; Dehaen, W. *J. Org. Chem*. **2012**, *77*, 2791–2797; c) Hu, S.-Z.; Chen, C.-F. *Org. Biomol. Chem*. **2011**, *9*, 5838–5844; d) Kleyn, A.; Jacobs, T.; Barbour, L. J. *Cryst. Eng. Commun*. **2011**, *13*, 3175–3180; e) Van Rossom, W.; Kundrát, O.; Ngo, T. H.; Lhoták, P.; Dehaen, W.; Maes, W. *Tetrahedron Lett*. **2010**, *51*, 2423–2426; f) Sobransingh, D.; Dewal, M. B.; Hiller, J.; Smith, M. D.; Shimizu, L. S. *New J. Chem*. **2008**, *32*, 24–27; g) Katz, J. L.; Geller, B. J.; Foster, P. D. *Chem. Commun*. **2007**, 1026–1028.

[41] Csokai, V.; Kulik, B.; Bitter, I. *Supramol. Chem*. **2006**, *18*, 111–115.

[42] Yang, H.-B.; Wang, D.-X.; Wang, Q.-Q.; Wang, M.-X. *J.Org. Chem* **2007**, *72*, 3757–3763.

[43] Katz, J.L; Geller, B.J.; Foster, P. D. *Chem. Commun* **2007**, 1026–1028.

[44] Zhang, E.-X.; Wang, D.-X.; Zheng, Q.-Y.; Wang, M.-X. *Org.Lett*. **2008**, *10*, 2565–2568.

[45] He, Q.; Huang, Z.-T.; Wang, D.-X. *Chem. Commun*. **2014**, *50*, 12985–12988.

[46] Capici, C.; Garozzo, D.; Gattuso, G.; Messina, A.; Notti, A.; Parisi, M. F.; Pisagatti, I.; Pappalardo, S. *ARKIVOC* **2009**, *viii*, 199–211.

[47] Hehre, W. J.; Radom, L.; Schleyer, P. R.; Pople, J. A. *Ab Initio Molecular Orbital Theory*; Wiley: New York, **1985**. Calculations performed with Spartan'06, Wavefunction, Inc.: Irvine, CA, 2006; http://www.wavefun.com/.

[48] Capici, C.; Gattuso, G.; Notti, A.; Parisi, M. F.; Bruno, G.; Nicolò, F.; Pappalardo, S. *Tetrahedron Lett*. **2011**, *52*, 1351–1353.

[49] a) Westheimer, F. H. In *Steric Effects in Organic Chemistry*; Newman, M. S., Ed.; John Wiley and Sons: New York, **1956**. Chapter 12; b) Schlosser, M.; Cottet, F.; Heiss, C.; Lefebvre, O.; Marull, M.; Masson, E.; Scopelliti, R. *Eur. J. Org. Chem*. **2006**, 729–734; c) Lunazzi, L.; Mancinelli, M.; Mazzanti, A. *J. Org. Chem*. **2008**, *73*, 2198–2205.

[50] Aromatic transetherification, catalyzed by nucleophiles (such as fluoride ions), is a reversible process that has been used in dynamic covalent chemistry. For a review, see: Rowan, S. J.; Cantrill, S. J.; Cousins, G. R. L.; Sanders, J. K. M.; Stoddart, J. F. *Angew. Chem., Int. Ed.* **2002**, *41*, 898–952.

[51] Gargiulli, C.; Gattuso, G.; Notti, A.; Pappalardo, S.; Parisi, M. F.; Puntoriero F.; *Tetrahedron Lett*. **2012,** *53***,** 616-619**.**

[52] a)Puntoriero, F.; Ceroni, P.; Balzani, V.; Bergamini, G.; Vögtle, F. *J. Am. Chem. Soc*. **2007**, *129*, 10714–10719; b) Jousselme, B.; Blanchard, P.; Gallego-Planas, N.; Delaunay, J.; Allain, M.; Richomme, P.; Levillain, E.; Roncalli, J. *J. Am. Chem. Soc*. **2003**, *125*, 2888–2889; c) Norikane, Y.; Kitamoto, K.; Tamaoki, N. *J. Org. Chem*. **2003**, *68*, 8291–8304.

[53] Spartan'10, Wavefunction, Inc., Irvine, CA. See: Shao, Y.; Molnar, L. F.; Jung, Y.; Kussmann, J.; Ochsenfeld, C.; Brown, S. T.; Gilbert, A. T. B.; Slipchenko, L. V.; Levchenko, S. V.; O'Neill, D. P.; DiStasio, Jr., R. A.; Lochan, R. C.; Wang, T.; Beran, G. J. O.; Besley, N. A.; Herbert, J. M.; Lin, C. Y.; Van Voorhis, T.; Chien, S. H.; Sodt, A.; Steele, R. P.;

Rassolov, V. A.; Maslen, P. E.; Korambath, P. P.; Adamson, R. D.; Austin, B.; Baker, J.; Byrd, E. F. C.; Dachsel, H.; Doerksen, R. J.; Dreuw, A.; Dunietz, B. D.; Dutoi, A. D.; Furlani, T. R.; Gwaltney, S. R.; Heyden, A.; Hirata, S.; Hsu, C.-P.; Kedziora, G.; Khalliulin, R. Z.; Klunzinger, P.; Lee, A. M.; Lee, M. S.; Liang, W. Z.; Lotan, I.; Nair, N.; Peters, B.; Proynov, E. I.; Pieniazek, P. A.; Rhee, Y. M.; Ritchie, J.; Rosta, E.; Sherrill, C. D.; Simmonett, A. C.; Subotnik, J. E.; Woodcock III, H. L.; Zhang, W.; Bell, A. T.; Chakraborty, A. K.; Chipman, D. M.; Keil, F. J.; Warshel, A.; Hehre, W. J.; Schaefer III, H. F.; Kong, J.; Krylov, A. I.; Gilla,P. M. W.; Head-Gordon, M. *Phys. Chem. Chem. Phys*. **2006**, *8*, 3172–3191.

[54] a) Gattuso, G.; Notti, A.; Parisi, M. F.; Pisagatti, I.; Amato, M. E.; Pappalardo, A.; Pappalardo, S. *Chem.-Eur. J*. **2010**, *16*, 2381–2385; b) Gargiulli, C.; Gattuso, G.; Notti, A.; Pappalardo, S.; Parisi, M. F. *Supramol. Chem*. **2010**, *22*, 358–364

[55] F. Bottino, S. Foti and S. Pappalardo, *Tetrahedron*, **1976**, *32*, 2567–2570.

[56] C. Bretti, F. Crea, C. De Stefano, S. Sammartano and G. Vianelli, *J. Chem. Eng. Data*, **2012**, *57*, 1851–1859.

[57] Gangs, P.; Sabatini, A.; Vacca, A. *Ann. Chim*. **1999**, *89*, 45-49.

[58] Alderighi, L.; Gans, P.; Ienco, A.; Peters, D.; Sabatini, A.; Vacca, A.; *Coord. Chem. Rev*. **1999**, *184*, 311-318.

[59] Frassineti, C.; Ghelli, S.; Gans, P.; Sabatini, A.; Moruzzi, M.S.; Vacca, A. *Anal. Biochem*. **1995**, *23*1, 374-382.

[60] De Stefano, C.; Sammartano, S.; Mineo, P.; Rigano, C. in *Computer Tools for the Speciation of Natural Fluids in Marine Chemistry - An Enviromental Analytical Chemistry Approach*, Gianguzza, A.; Pelizzetti, E.; Sammartano, S. ed. Kluwer Academic Publishers: Amsterdam **1997**, pp. 71-83.

[61] Friel, C.J.; Lu, M.C. In *Wilson and Gisvold's Textbook of Organic Medicinal and Pharmaceutical Chemistry*; Beale, J.M., Block J.H., Eds.; Lippincott Williams & Wilkins:Philadelphia, PA, **2011**; Chapter 24.

[62] Southall, N.T.; Dill, K.A.; Haymet, A.D.J. J. *Phys. Chem. B* **2002**, *106*, 521–533.

[63] Smithrud, D.B.; Sanford, E.M.; Chao, I.; Ferguson, S.B.; Carcanague, D.R.; Evanseck, J.D.; Houk, K.N.; Diederich, F. *Pure Appl. Chem*. **1990**, *62*, 2227–2236.

[64] Manganaro, N.; Lando, G.; Gargiulli, C.; Pisagatti, I.; Notti, A.; Pappalardo, S.; Parisi, M. F.; Gattuso, G. *Chem. Commun*. **2015**, *51*, 12657–12660.

[65] Wang, D.-X.; Wang, Q.-Q.; Han, Y.; Wang, Y.; Huang, Z.-T.; Wang, M.-X *Chem.–Eur. J*. **2010**, *16*, 13053-13057.

[66] Naseer, M. M.; Wang, D.-X.; Zhao, L.; Huang, Z.-T.; Wang, M.-X. *J. Org. Chem*. **2011**, *76,* 1804-1813.

[67] Evans, R.; Deng, Z.; Rogerson, A. K.; McLachlan, A. S.; Richards, J. J.;Nilsson, M.; Morris, G. A. *Angew. Chem. Int. Ed*. **2013**, *52*, 3199-3202.

[68] Perrin, D. D.; Armarego, W. L. F.,*Purification of Laboratory Chemicals*, Pergamon Press: Oxford, 1989.

[69] a) Bretti, C.; Cigala, R. M.; De Stefano, C.; Lando, G.; Sammartano, S. *J. Chem. Eng. Data*, **2016,** *61*, 2040–2051; b) Bretti, C.; Cigala, R. M.; De Stefano, C.; Lando, G.; Sammartano, S. *Chemosphere* **2016**, *150*, 341–356.

[70] a) Sgarlata, C.; Zito, V.; Arena, G. *Anal. Bioanal. Chem.*, **2012**, *405*, 1085–1094; b) Arena, G.; Pappalardo, A.; Pappalardo, S.; Gattuso, G.; Notti, A.; Parisi, M.; Pisagatti, I.; Sgarlata, C. J. Therm. Anal. Calorim., **2015**, *121*, 1073–1079.

[71] *Supramolecular Polymers*; Ciferri, A., Ed.; 2nd ed.; CRC Press: Boca Raton, FL, **2005**.

[72] a) Yan, X.; Wang, F.; Zheng B.; Huang, F. *Chem. Soc. Rev.*, **2012**, *41*, 6042–6065; b) Ma, X.; He, T. *Acc. Chem. Res.*, **2014**, *47*, 1971–1981.

[73] Seiffert, S.; Sprakel, J.; *Chem. Soc. Rev*., **2012**, *41*, 909-930.

[74] Fouquey, C.; Lehn, J.-M.; Levelut, A.-M. *Adv. Mater*., **1990**, *2*, 254–257.

[75] Elias, H.-G. *An Introduction to Polymer Science*; VCH: Weinheim, **1997**.

[76] a) Yang, S. K.; Ambadec A. V.; Weck, M. *Chem. Soc. Rev.*, **2011**, *40*, 129–137; b) Li, S.-H.; Xiao, T.; Lin, C.; Wang, L. *Chem. Soc. Rev.*, **2012**, *41*, 5950–5968.

[77] a) Zheng, B.; Wang, F.; Dong, S.; Huang, F. *Chem. Soc. Rev.*, **2012**, *41*, 1621-1636; b) Harada, A.; Takashima, Y.; Yamaguchi, H. *Chem. Soc. Rev.*, **2009**, *38*, 875-882; c) Zayed, J. M.; Nouvel, N.; Rauwald, U.; Scherman, O. A. *Chem. Soc. Rev.*, **2010**, *39*, 2806-2816; d) Liu, Y.; Yu, Y.; Gao, J.; Wang, Z.; Zhang, X. *Angew. Chem., Int. Ed.*, **2010**, *49*, 6576-6579.

[78] Zinke, A.; Ziegler, E. Ber. **1944**, *77*, 264.

[79] a) Gutsche, C. D.; Iqbal, M. *Org. Synth*. **1990**, *68,* 234-237.

[80] a) Böhmer, V.; Merkel, L.; Kunz, U. *J. Chem. Soc. Chem. Commun*. **1987**, 896-897; b) de Mendoza, J.; Nieto, M. P.; Prados, P.; Sànchez, C. *Tetraehdron* **1990**, *46*, 671-682

[81] Gutsche, C. D.; Bauer, L. J. *J. Am. Chem. Soc*. **1985**, *107*, 6063-6069.

[82] Coruzzi, M.; Andreetti, G. D.; Bocchi, V.; Pochini, A.; Ungaro, R. *J. Chem. Soc.*, *Perkin Trans. 2*, **1982**,1133

[83] Talotta, C.; Gaeta, C.; Neri, P. In *Reference Module in Chemistry, Molecular Sciences and Chemical Engineering;* Talotta, C., Gaeta, C., Neri, P., Eds.; Elsevier: Waltham, MA, **2015**, 1–27 ,

[84] Gutsche, C. D. Calixarenes - An Introduction; Stoddart, J. F., Ed.; *Monographs in Supramolecular Chemistry*, 2nd ed.; The Royal Society of Chemistry: Cambridge, U.K., **2008**; Vol. 6.

[85] Atwood, J. L.; Koutsantonis, G. A.; Raston, C. L. *Nature*, **1994**, *368*, 229–231.

[86] Suzuki, T.; Nakashima, K.; Shinkai, S. *Chem. Lett.*, **1994**, 699–702.

[87] Raston, C. L.; Atwood, J. L.; Nichols, P. J.; Sudria, I. B. N. Chem. Commun., **1996**, 2615–2616.

[88] Gallagher, J. F.; Ferguson, G.; Bohmer, V.; Kraft, D. *Acta Cryst. C (Cr. Str. Comm.)*, **1994**, *50*, 73–77.

[89] Haino, T.; Yanase M.; Fukazawa, Y. *Angew. Chem., Int. Ed. Engl.*, **1997**, *36*, 259–260.

[90] Haino, T.; Yanase M.; Fukazawa, Y. *Tetrahedron Lett.*, **1997**, *38*, 3739–3742.

[91] a) Ping, G.; Dalgarno, S.J.; Atwood, J.L. *Coord. Chem. Rev.*, **2010**, *254*, 1760-1760; b) Dalgarno, S.J.; Pwer, N.P.; Atwood, J.L. *Coord. Chem. Rev.*, **2008**, *252*, 825-841.

[92] a) Haino, T.; Yanase, M.; Fukazawa, Y. *Angew. Chem., Int. Ed. Engl.*, **1998**, *37*, 997–998; b) Haino, T.; Yanase M.; Fukunaga, C.; Fukazawa, Y. *Tetrahedron*, **2006**, *62*, 2025–2035.

[93] Haino, T.; Matsumoto, Y.; Fukazawa, Y. *J. Am. Chem. Soc.*, **2005**, *127*, 8936–8937.

[94] Haino, T.; Hirai, E.; Fujiwara, Y.; Kashihara, K. *Angew. Chem. Int. Ed.*, **2010**, *49*, 7899–7903.

[95] Hirao, T.; Masatoshi, M.; Yamago, S.; Haino, T. *Chem. – Eur. J.*, **2014**, *20*, 16138–16146.

[96] Haino, T.; Yanase M.; Fukazawa, Y. *Tetrahedron Lett.*, **2005**, *46*, 1411–1414.

[97] Su, X.; Guo, D.-S.; Liu, Y. *CrystEngComm*, **2010**, *12*, 947–952.

[98] Guo, D.-S.; Chen, K.; Zhang, H.-Q.; Liu, Y. *Chem. Asian J.*, **2009**, *4*, 436–445.

[99] Guo, D.-S.; Jiang, B.-P.; Wang, X.; Liu, Y. *Org. Biomol. Chem.*, **2012**, **10**, 720-723.

[100] Wang, K.; Guo, D.-S.; Liu, Y. *Chem. – Eur. J.*, **2012**, *18*, 8758–8764.

[101] Stewart, D. R.; Krawiec, M.; Kashyap, R. P.; Watson W. H.; Gutsche, C. D. *J. Am. Chem. Soc.*, **1995**, *117*, 586–601.

[102] a) Arnaud-Neu, F.; Fuangswasdi, S.; Notti, A.; Pappalardo, S.; Parisi, M. F. *Angew. Chem., Int. Ed. Engl.*, **1998**, *37*, 112–114; b) Ferguson, G.; Notti, A.; Pappalardo, S.; Parisi, M. F.; Spek, A. L. *Tetrahedron Lett.*, **1998**, *39*, 1965–1968.

[103] a) Gattuso, G.; Notti, A.; Pappalardo, S.; Parisi, M. F.; Pilati, T.; Resnati G.; Terraneo, G. *CrystEngComm*, **2009**, *11*, 1204–1206; b) Gattuso, G.; Notti, A.; Pappalardo, S.; Parisi, M.

F.; Pilati. T.; Terraneo. G. *CrystEngComm*, **2012**, *14*, 2621–2625; c) Capici, C.; Gattuso, G.; Notti, A.; Parisi, M. F.; Pappalardo, S.; Brancatelli, G.; Geremia, S. *J. Org. Chem*., **2012**, *77*, 9668–9675.

[104] Pappalardo, S.; Villari, V.; Slovak, S.; Cohen, Y.; Gattuso, G.; Notti, A.; Pappalardo, A.; Pisagatti, I.; Parisi, M. F. *Chem. – Eur. J*., **2007**, *13*, 8164–8173.

[105] Hofmeister, F. *Arch. Exp. Pathol. Pharmakol*., **1888**, *24*, 247–260.

[106] Gargiulli, C.; Gattuso, G.; Notti. A.; Pappalardo. S.; Parisi, M. F. *Tetrahedron Lett*., **2011**, *52*, 6460–6464.

[107] a) Ballistreri, F. P.; Notti, A.; Pappalardo, S.; Parisi, M. F.; Pisagatti, I. *Org. Lett*., **2003**, *5*, 1071–1074; b) Garozzo, D.; Gattuso, G.: Notti, A.; Pappalardo, A.; Pappalardo, S.; Parisi, M. F.; Perez, M.; Pisagatti I. *Angew. Chem. Int. Ed*., **2005**, *44*, 4892–4896; c) Gargiulli, C; Gattuso, G.; Liotta, C.; Notti, A.; Parisi, M. F.; Pisagatti, I.; Pappalardo, S. *J. Org. Chem*., **2009**, *74*, 4350–4353; d) Capici, C.; De Zorzi, R.; Gargiulli, C.; Gattuso, G.; Geremia, S.; Notti, A.; Pappalardo, S.; Parisi, M. F.; Puntoriero, F. *Tetrahedron*, **2010**, *66*, 4987–4993.

[108] Capici, C.; Cohen, Y.; D'Urso, A.; Gattuso, G.; Notti, A.; Pappalardo, A.; Pappalardo, S.; Parisi, M. F.; Purrello, R.; Slovak, S.; Villari, V. *Angew. Chem. Int. Ed*., **2011**, *50*, 11956–11961.

[109] Villari, V.; Gattuso, G.; Notti, A.; Pappalardo, A.; Micali, N. *J. Phys. Chem. B*, **2012**, *116*, 5537–5541.

[110] a) Brancatelli, G.; Pappalardo, S.; Gattuso, G.; Notti, A.; Pisagatti, I.; Parisi, M. F.; Geremia, S. *CrystEngComm,* **2014**, *16*, 89–93; b) Brancatelli, G.; Gattuso, G.; Geremia, S.; Notti, A.; Pappalardo, S.; Parisi, M. F.; Pisagatti, I. *Org. Lett*., **2014**, *16*, 2354–2357.

[111] Garozzo, D.; Gattuso, G.; Kohnke, F. H.; Malvagna, P.; Notti, A.; Occhipinti, S.; Pappalardo, S.; Parisi M. F.; Pisagatti, I. *Tetrahedron Lett*., **2002**, *43*, 7663–7667.

[112] a) Garozzo, D.; Gattuso, G.; Kohnke, F.H.; Notti, A.; Pappalardo, S.; Parisi, M.F.; Pisagatti, I.; White, A. J. P.; Williams, D. J. *Org. Lett*., **2003**, *5*, 4025–4028; b) Gattuso, G.;

Notti, A.; Pappalardo, A.; Parisi, M. F.; Pisagatti, I.; Pappalardo, S.; Garozzo, D.; Messina, A.; Cohen, Y.; Slovak, S. *J. Org. Chem.*, **2008**, *73*, 7280–7289.

[113] a) Gargiulli, C.; Gattuso, G.; Notti. A.; Pappalardo. S.; Parisi, M. F. *Tetrahedron Lett.*, **2011**, *52*, 7116–7120; b) Gattuso, G.; Liotta, C.; Notti, A.; Pappalardo, S.; Parisi, M. F. *Tetrahedron Lett.*, **2008**, *49*, 7146–7148.

[114] Pappalardo, A.; Ballistreri, F. P.; Li Destri, G.; Mineo, P. G.; Tomaselli, G. A.; Toscano, R. M.; Trusso Sfrazzetto, G. *Macromolecules*, **2012**, *45*, 7549–7556.

[115] De Salvo, G.; Gattuso, G.; Notti, A.; Parisi, M. F.; Pappalardo, S. *J. Org. Chem*. **2002**, *67*, 684–692.

[116] S. Mecozzi and J. Rebek, Jr. *Chem. Eur. J.*, **1998**, *4*, 1016–1022.

[117] G. Gattuso, A. Notti, M. F. Parisi, I. Pisagatti, M. E. Amato, A. Pappalardo and S. Pappalardo, *Chem. Eur. J.*, **2010**, *16*, 2381–2385.

[118] Fuell, K. A. Elliott, C. C. Hanfrey, M. Franceschetti and A. J. Michael, *Plant. Physiol. Biochem.*, **2010**, *48*, 513–520.

[119] Brancatelli, G.; Gattuso, G; Geremia, S; Manganaro, N; Notti, A.; Pappalardo, S.; Parisi, M. F.; Pisagatti, I. *CrystEngComm*, **2015**, *17*, 7915–7921

[120] Takeda, Y.; Samjima, K.; Nagano, K.; Watanabe, M.; Sugeta, H.; Kyogoku, Y. *Eur. J. Biochem.* **1983***, 130,* 383–389.

[121] Zhang, C.; Ling, J.; Wang, Q. *Macromolecules*, **2011**, *44*, 8739–8743.

[122] a) Zhuang, L.-H.; Yu, K.-H.; Wang, G.-W.; Yao, C. *J. Colloid Interface Sci.*, **2007**, *408*, 94–100. b) Barbera, L.; Gattuso, G.; Kohnke, F. H.; Notti, A.; Pappalardo, S.; Parisi, M. F.; Pisagatti, I.; Patanè, S.; Micali, N.; Villari, V. *Org. Biomol. Chem.*, **2015**, *13*, 6468–6473.

[123] Qian, H.; Guo, D.-S.; Liu, Y. Chem. Eur. J., **2012**, *18*, 5087–5095.

[124] Kabsch, W. *Acta Crystallogr.*, **2010**, *D66*, 125–132.

[125] Battye, G. G.; Kontogiannis, L.; Johnson, O.; Powell H. R.; Leslie, A. G. W.; *Acta Crystallogr.*, **2011,** *D67*, 271–281.

[126] Evans, P. R. *Acta Crystallogr.*, **2006**, *D62*, 72–82.

[127] Winn, M. D.; Ballard, C. C.; Cowtan, K. D.; Dodson, E. J.; Emsley, P.; Evans, P. R.; Keegan, R. M.; Krissinel, E. B.; Leslie, A. G. W.; McCoy, a; McNicholas, S. J.; Murshudov, G. N.; Pannu, N. S.; Potterton, E. A.; Powell, H. R.; Read, R. J.; Vagin, A.; Wilson, K. S. *Acta. Crystallogr.*, **2011**, *D67*, 235–242.

[128] Burla, M. C.; Caliandro, R.; Camalli, M.; Carrozzini, B.; Cascarano, G. L.; De Caro, L.; Giacovazzo, C.; Polidori, G.; Siliqi, D.; Spagna, R. *J. Appl. Crystallogr.*, **2007**, *40*, 609–613.

[129] Sheldrick, G. M. *Acta Crystallogr.*, **2008**, *A64*, 112–122.

[130] a) Spek, A. L. *Acta Crystallogr.*, **2015**, *C71*, 9–18; b) Sluis, v.d.; Spek, A. L. *Acta Crystallogr.,* **1990**, *A46*, 194–201.

[131] *Modern Cyclophane Chemistry*; Gleiter, R., Hopf, H., Eds.; Wiley-VCH: Chichester, **2004.**

[132] a) Wang, W.-L.; Xu, J.; Sun, Z.; Zhang, X.; Lu, Y.; Lai, Y.-H. *Macromolecules* **2006**, *39*, 7277–7285; b) Wang, W.; Xu, J.; Lai, Y.-H.; Wang, F. *Macromolecules* **2004**, *37*, 3546–3553; c) Wang, W.; Xu, Jianwei; Lai, Y.-H. *Org. Lett*. **2003**, *5*, 2765–2768.

[133] a) Grimme, S.; Harren, J.; Sobanski, A.; Vogtle, F.; *Eur. J. Org. Chem*. **1998**, 1491-1509; b) Minuti, L.; Marrocchi, A.; Tesei, I.; Gacs-Baitz, E. *Tetrahedron Lett*. **2005**, *46*, 8789-8792; c) Menichetti, S.; Faggi, C.; Lamanna, G.; Marrocchi, A.; Minuti, L.; Taticchi, A. *Tetrahedron*, **2006**, *62*, 5626-5631; d) Xia, L. J.; Liu, S.H.; Cozzi, F.; Mancinelli, M.; Mazzanti, A. *Chem. Eur. J*. **2012**, *18*, 3611-3620.

[134] Kanomata, N.; Nakata, T. *J. Am. Chem. Soc.* **2000**, *122*, 4563-4568.

[135] Tanaka, K.; Hori, T.; Osaka, T.; Noguchi, K.; Hirano, M. *Org. Lett*. **2007**, *72*, 4486-4496.

[136] Ueda, T.; Kanomata, N.; Machida, H.; *Org. Lett.*, **2005**, *7*, 2365-2368.

[137] Aversa, M.C.; Barattucci, A.; Bonaccorsi, P.; Faggi, C.; Papalia, T. *J. Org. Chem.* **2007**, *72*, 4486-4496.

[138] Barattucci, A.; Di Gioia, M.L.; Leggio, A., Minuti, L.; Papalia, T.; Siciliano, C.; Temperini, A.; Bonaccorsi, P. *Eur. J. Org. Chem.* **2014**, 2099-2104.

[139] Xia, J. L.; Liu, S. H.; Cozzi, F.; Mancinelli, M.; Mazzanti, A. *Chem. Eur. J.* **2012**, *18*, 3611–3620;

[140] Annunziata, R.; Benaglia, M.; Cozzi, F.; Mazzanti, A. *Chem. Eur. J.* **2009**, *15*, 4373–4381.

[141] Voronkov, M. G.; Deryagina, É. N.; Sukhomazova, É. N.; Gusarova, N. K.; Efremova, G. G.; Nikol'skii, N. S.; Amosova, S. V.; Trofimov, B. A. B. *Acad. Sci. USSR Ch*. **1982**, *31*, 174–175.